SUPPLEMENTARY INFORMATION FOR

Chemometrics and Genome Mining Reveal an Unprecedented Family of Sugar Acid-Containing Fungal Nonribosomal Cyclodepsipeptides

Chen Wang[a1], Dongliang Xiao[a1], Baoqing Dun[b1], Miaomiao Yin[a], Adigo Setargie Tsega[a], Linan Xie[a], Wenhua Li[a], Qun Yue[a], Sibao Wang[c], Han Gao[c], Min Lin[a], Liwen Zhang[a*], István Molnár[d,e*], and Yuquan Xu[a*]

[a] Biotechnology Research Institute, Chinese Academy of Agricultural Sciences, 12 Zhongguancun South Street, Beijing 100081, P.R. China

[b] The National Key Facility for Crop Gene Resources and Genetic Improvement, Institute of Crop Sciences, Chinese Academy of Agricultural Sciences, 12 Zhongguancun South Street, Beijing 100081, P.R. China

[c] CAS Key Laboratory of Insect Developmental and Evolutionary Biology, CAS Center for Excellence in Molecular Plant Sciences, Shanghai Institute of Plant Physiology and Ecology, Chinese Academy of Sciences (CAS), 300 Feng Lin Road, Shanghai 200032, P.R. China.

[d] Southwest Center for Natural Products Research, University of Arizona, 250 E. Valencia Rd., Tucson, AZ 85706, USA

[e] VTT Technical Research Centre of Finland, P.O. Box 1000, FI-02044 VTT, Espoo, Finland

[1] These authors contribute equally to this work.

* Corresponding authors: Y. Xu (xuyuquan@caas.cn), Tel: +86 (010) 8210-9850; I. Molnár (istvan.molnar@vtt.fi), Tel: +358 (20) 722-5362; L. Zhang (zhangliwen@caas.cn), Tel: +86 (010) 8210-9850.

Contents

1. SI Materials and Methods

1.1. General

All commercial chemical and biological reagents were used as received. Oligonucleotides for polymerase chain reaction (PCR) and quantitative PCR (qPCR) were purchased from Sangon Biotech Co., Ltd. (Shanghai, China). Matrix-Assisted Laser Desorption/Ionization-Time of Flight Mass Spectrometry (MALDI-TOF MS) spectra were recorded on an Autoflex Speed mass spectrometer (Bruker, Billerica, MA, United States). Liquid Chromatography-High Resolution Electrospray Ionization Mass Spectrometry (LC-HRESIMS) spectra were recorded on an Agilent 1290 II Ultra High Performance Liquid Chromatography (UHPLC) coupled with an Agilent 6530 QTOF instrument (Agilent Technologies Inc., Santa Clara, CA, USA) operated in positive ion mode using capillary and cone voltages of 3.6 kV and 40–150 V, respectively. The collision energy was optimized from 15 to 50 eV. For accurate mass measurements the instrument was calibrated each time using a standard calibration mix in the *m/z* range of 150-1900. Routine LC-ESIMS analysis was performed on an Agilent 1290 II UHPLC equipped with an Agilent G6125B single quadrupole mass spectrometer (Agilent Technologies Inc., Santa Clara, CA, USA). Analytical HPLC was performed on a Waters Alliance e2695 system coupled with a Waters 2414 refractive index detector. Optical rotations were measured on an Anton Paar MCP-200 polarimeter (Anton Paar GmbH, Graz, Austria) at 25 °C. UV spectra were recorded on a Shimadzu UV-2450 photometer (Shimadzu Corporation, Kyoto, Japan). ^{1}H, ^{13}C and 2D NMR experiments were carried out on an Agilent DD2 600 MHz NMR spectrometer (Agilent Technologies Inc., Santa Clara, CA, USA). Chemical shift values (δ) are given in parts per million (ppm) and the coupling constants (*J* values) are in Hz. Chemical shifts were referenced to the residual solvent peaks of methanol-d_4, methanol-d_3 or DMSO-d_6. For detection of D-xylose, D-xylono-γ-lactone, D-xylonic acid, and D-xylono-γ-lactone hydrolysate, samples were analyzed by LC-ESIMS or HPLC equipped with a Poroshell 120 HILIC-Z column (Agilent Technologies Inc., Santa Clara, CA, USA), eluting with isocratic 75 % aqueous acetonitrile with 0.1 % formic acid for 10 min at a flow rate of 0.8 mL/min. For column chromatography, macroporous D101 resin (Macklin Biochemical Co. Ltd., Shanghai, China) and Fuji ODS (40–75 μm, Fuji Silysia Chemical Ltd., Osaka, Japan) were used. Semi-preparative HPLC experiments were performed on an Agilent Eclipse XDB-C18 reversed-phase column (5 μm, 9.4 mm × 250 mm) using an Agilent 1260 II HPLC system (Agilent Technologies Inc., Santa Clara, CA, USA). Routine DNA sequencing was performed by Sangon Biotech Co., Ltd. (Shanghai, China).

1.2. MALDI-TOF MS data acquisition and hierarchical cluster analysis

MALDI-TOF MS matrix solution was prepared by dissolving *trans*-2-[3-(4-*tert*-butylphenyl)-2-methyl-

2-propenylidene]malononitrile (Sigma-Aldrich, Saint Louis, MO, United States) at a final concentration of 15 mg/mL in 90 % aqueous methanol solution with 0.1 % formic acid. Small amounts of the fungal mycelia, obtained from 10-14 days old cultures grown on potato dextrose agar (PDA) media, were spotted directly on the stainless steel 384-well target plate and immediately overlaid with 2-5 µL matrix solution. The MALDI-TOF MS spectra were recorded in reflector/positive ion mode, and each sample was ablated 1,000 times within 1 second with a laser energy output of 70 %. A mass-to-charge (*m/z*) window of 500–2,500 was applied to monitor the production of peptide-like secondary metabolites. All mass data were analyzed in the FlexAnalysis software (Bruker, Billerica, MA, United States). The mass peak list of peptide-producing fungal isolates was exported, and all peaks were aligned according to their *m*/*z* values using the Mass Profiler Professional software (Agilent, Santa Clara, CA, United States). Background noise and mass peaks corresponding to non-specific metabolites (ubiquitously present in over 50 % of fungal isolates) were removed. The resulting dataset was subjected to hierarchical clustering and heatmap plotting using imageGP (http://www.ehbio.com/Cloud_Platform/front/#/).

1.3. UHPLC-HRESI-MS/MS data acquisition and molecular network generation

Representative peptide-producing fungal strains were cultivated on PDA medium for 10–14 days, the mycelium was scraped off, and extracted with 90 % aqueous methanol. The resulting extract was concentrated and subjected to full scan UHPLC-HRESI-MS/MS analysis. The obtained tandem LC-MS data were used to generate the initial peptide molecular network using the Global Natural Products Social Molecular Networking (GNPS) server[1] following the well-established protocol[2]. Briefly, the data was filtered by removing all MS/MS fragment ions within +/- 17 Da of the precursor m/z. MS/MS spectra were window filtered by choosing only the top 6 fragment ions in the +/- 50Da window throughout the spectrum. The precursor ion mass tolerance was set to 0.03 Da and a MS/MS fragment ion tolerance of 0.03 Da. A network was then created where edges were filtered to have a cosine score above 0.7 and more than 6 matched peaks. Further, edges between two nodes were kept in the network if and only if each of the nodes appeared in each other's respective top 10 most similar nodes. Finally, the maximum size of a molecular family was set to 100, and the lowest scoring edges were removed from molecular families until the molecular family size was below this threshold. The spectra in the network were then searched against GNPS' spectral libraries. The library spectra were filtered in the same manner as the input data. All matches kept between network spectra and library spectra were required to have a score above 0.7 and at least 6 matched peaks. This initial network was visualized and analyzed in Cytoscape[3]. All precursor ions corresponding to the peptides identified in the earlier MALDI-TOF MS experiments were manually labeled, and the precursor ions that did not show a relationship with these labeled ions (ions corresponding to

metabolites unrelated to the peptides of interest) were removed to reduce complexity and generate the final peptide-specific network.

1.4. Fungal strains and culture conditions

Paramyrothecium sp. XJ0827 and *Colletotrichum* sp. XJ1040 were isolated from soil samples collected from the northern region of Xinjiang province, China. *Paramyrothecium roridum* NRRL 2183 was purchased from the Agriculture Research Service Culture Collection (Peoria, IL, United States). Other fungal strains listed in Table S1 were acquired from the Agriculture Culture Collection of China (ACCC; Beijing, China) or MoonBiotech (MN; Guangzhou, Guangdong, China). Fungal strains were grown on PDA (potato starch 4 g/L, dextrose 20 g/L, agar 15 g/L) medium at 28 °C for 5 days. The colony surface was gently washed with 5 mL sterile water containing 0.1 % Triton X-100, the resulting spore suspension was filtered through a 40 μm cell strainer (Biologix Group Ltd., Jinan, China), and the filtrate was diluted with sterile water to a spore concentration of 1×10^6/mL. To screen for xylomyrocin congeners from various *Paramyrothecium* and *Colletotrichum* spp., 100 μL of the spore stock was used for the inoculation of each petri dish (90 mm in diameter) containing 20 mL of agar medium. Media included PDA; MMK2 (mannitol 40 g/L, yeast extract 5 g/L, Murashige and Skoog basal salt mixture powder 4.3 g/L, agar 15 g/L, pH 6.8); YM (malt extract 10 g/L, yeast extract 2 g/L, agar 15 g/L); YES (yeast extract 20 g/L, $MgSO_4 \cdot 7H_2O$ 0.5 g/L, sucrose 150 g/L, trace element solution 1 mL/L, agar 15 g/L; where the trace element solution contained $ZnSO_4 \cdot 7H_2O$ 0.1 g/L, $CuSO_4 \cdot 5H_2O$ 0.05 g/L); LSF1 (glycerol 75 g/L, glucose 10 g/L, yeast autolysate 5 g/L, soybean meal 5 g/L, tomato paste 5 g/L, $NaNO_3$ 2 g/L, $(NH_4)_2SO_4$ 2 g/L, agar 15 g/L); MV8 (maltose 75 g/L, V8 juice 200 mL/L, soy flour 1 g/L, L-proline 3 g/L, MES 16 g/L, agar 15 g/L, pH 6.5); or super malt (malt extract 50 g/L, yeast extract 10 g/L, $FeSO_4 \cdot 7H_2O$ 20 mg/L, $ZnSO_4 \cdot 7H_2O$ 7 mg/L, agar 15 g/L) media, respectively. The cultures were incubated at 28 °C for 10–14 days, followed by MALDI-TOF MS to monitor the production of peptides as described in section 1.2 above. For scale-up, 10-16 L of the appropriate culture media (500–800 petri dishes) were inoculated with the spore solution of the peptide-producing fungus, and cultivated under the same conditions used for the small-scale fermentations.

1.5. Isolation and characterization of xylomyrocins

1.5.1. Compounds 1–3

Paramyrothecium sp. XJ0827 was grown on PDA medium (a total of 12 L) for 14 days, the medium with the fungal culture was cut into small pieces (1 cm × 1 cm), and extracted with 90 % aqueous ethanol for three times. The extract was concentrated under vaccum to afford a crude extract of 4.7 g. This crude extract was subjected to macroporous D101 resin and ODS chromatography, and the fraction containing

xylomyrocins A–C (750 mg) was detected by MALDI-TOF MS and LC-ESIMS. This fraction was further purified by semi-preparative HPLC eluting with 65 % aqueous acetonitrile containing 0.1 % formic acid at a flow rate of 2.5 mL/min to afford compounds **1** (51 mg), **2** (13 mg), and **3** (7 mg).

Xylomyrocin A (**1**): white amorphous powder; $[\alpha]_D^{25}$ −130.5 (*c* 0.21, CH_3OH); UV (CH_3OH) λ_{max} (log ε) 205 (4.53) nm; ^1H and ^{13}C NMR data see Table S2.1; HRESIMS *m/z* 1120.6295 $[M + H]^+$ (calcd for $C_{54}H_{90}N_9O_{16}$, 1120.6500).

Xylomyrocin B (**2**): white amorphous powder; $[\alpha]_D^{25}$ −196.2 (*c* 0.29, CH_3OH); UV (CH_3OH) λ_{max} (log ε) 205 (4.41) nm; ^1H and ^{13}C NMR data see Table S2.1; HRESIMS *m/z* 1120.6294 $[M + H]^+$ (calcd for $C_{54}H_{90}N_9O_{16}$, 1120.6500).

Xylomyrocin C (**3**): white amorphous powder; $[\alpha]_D^{25}$ −176.6 (*c* 0.59, CH_3OH); UV (CH_3OH) λ_{max} (log ε) 205 (4.54) nm; ^1H and ^{13}C NMR data see Table S2.1; HRESIMS *m/z* 1120.6288 $[M + H]^+$ (calcd for $C_{54}H_{90}N_9O_{16}$, 1120.6500).

The $[M + H]^+$ ion found at *m/z* 1120.6288 in the positive mode HRESIMS (Fig. S17.3), together with the presence of 54 resonance signals in the ^{13}C NMR spectrum (Table S2.1) gave a molecular formula of $C_{54}H_{89}N_9O_{16}$ for **3**, requiring 15 degrees of unsaturation. Multiple carbonyl carbon signals at δ_C 171.2–176.1, and heteroatom-bound carbon signals at δ_C 54.8–74.8 in the ^{13}C NMR spectrum (Table S2.1) strongly indicated that **3** is a peptide natural product. Three significantly deshielded methyl singlets (δ_H 3.39, 3.29, and 2.84) found in the ^1H NMR spectrum suggested the presence of three oxygenated or nitrogenated CH_3 functionalities in **3**, while a series of methyl doublets and triplets found at δ_H 0.91–1.13 (Table S2.1) are characteristic of aliphatic amino acids, such as leucine (Leu), isoleucine (Ile), and valine (Val). A comprehensive analysis of the ^1H, ^{13}C, COSY, TOCSY, HSQC, and HMBC spectra (Fig. S2) revealed that **3** consisted of a noncanonical 2,3,4,5-tetrahydroxypentanoic acid moiety (THP) and nine amino acid residues, including glycine (Gly), Ile, Leu (2×), *N*-methylated phenylalanine (MePhe), *N*-methylated threonine (MeThr), *N*-methylated valine (MeVal), serine (Ser), and Val. Next, a detailed examination of HMBC correlations from the α-proton(s)/*N*-methyl protons to the amide carbonyl carbons (Fig. S2) established a primary sequence of THP_1–Leu_2–$MeThr_3$–Val_4–$MePhe_5$–Gly_6–Ile_7–Ser_8–Leu_9–$MeVal_{10}$ for **3**. All functionalities presented in this linear sequence accounted for 14 of the 15 degrees of unsaturation, indicating that **3** adopts a macrocyclic structure, probably via an ester linkage between one of the OH groups of THP_1, $MeThr_3$, or Ser_8, and the free carbonyl group of $MeVal_{10}$. Indeed, HMBC correlation between the δ-protons of THP_1 (δ_H 4.41, 4.09) and the carbonyl carbon (δ_C 171.87) of $MeVal_{10}$ confirmed the connecting site between THP_1 and $MeVal_{10}$, and fully established the planar structure of **3** (Fig. S2).

De novo sequencing of **3** by analyzing the tandem mass spectrum was inconclusive due to the

complex fragmentation pattern resulting from random ring opening of the cyclodepsipeptide backbone during collision-induced dissociation (CID). To avoid such complexity, **3** was first linearized by methanolysis upon treatment with CH_3ONa/CH_3OH, and the resulting methoxy-substituted derivative (**19**) was subjected to tandem mass analysis (Fig. S1.1). Fragmentation of the $[M + H]^+$ ion of **19** at *m*/*z* 1152.6684 generated a series of b- and y-type fragment ions. The appearance of b-type ions at *m*/*z* 1007.5607, 894.4920, 807.4440, 694.3611, 637.3404, 476.2543, 377.1910, and 262.1277 corresponded to the consecutive loss of methoxy-substituted $MeVal_{10}$, Leu_9, Ser_8, Ile_7, Gly_6, $MePhe_5$, Val_4, and $MeThr_3$ from the *C*-termini of the precursor ion (Fig. S1.1). On the other hand, the presence of y-type ions at *m*/*z* 1004.6305, 891.5493, 776.4872, and 677.4191 was consistent with the successive loss of THP_1, Leu_2, $MeThr_3$, and Val_4 from the *N*-termini of the precursor ion (Fig. S1.1). In summary, the peptide sequence deduced from these MS/MS fragmentation data was in complete agreement with that elucidated by NMR spectrometry, thus further supporting the established planar structure of **3**.

1 and **2** were found to have the same molecular formula ($C_{54}H_{89}N_9O_{16}$) as **3** upon analyzing their HRESIMS (Fig. S17.1 and S17.2) and ^{13}C NMR spectra (Table S2.1). Interpretation of the one- and two-dimensional (1D and 2D) NMR spectra (Fig. S2) revealed that **1** and **2** share the identical linear sequence of THP_1–Leu_2–$MeThr_3$–Val_4–$MePhe_5$–Gly_6–Ile_7–Ser_8–Leu_9–$MeVal_{10}$ with **3**, and this was further supported by the tandem mass data (Fig. S1.2 and S1.3) of the linearized **1** and **2** (**17** and **18**). However, moderate to significant chemical shift variations were observed for the THP_1 protons and carbons (Table S2.1), indicating that **1** and **2** may have different connecting sites between THP_1 and $MeVal_{10}$ as compared to **3**. Clear HMBC correlation was observed for the α-proton of THP_1 (δ_H 5.08) and the carbonyl carbon (δ_C 170.65) of $MeVal_{10}$ for **1** (Fig. S2), confirming the macrocyclic ring was formed via an ester linkage connecting the α-OH of THP_1 and the C=O of $MeVal_{10}$. Noteworthily, formation of ester bound causes considerable deshielding of the OH-donating carbon ($\Delta\delta_C$ +4.5 ppm for the α-C of THP_1 when comparing **1** to **3**; $\Delta\delta_C$ +2.4 ppm for the δ-C of THP_1 when comparing **3** to **1**) and shielding of the immediately adjacent carbon(s) ($\Delta\delta_C$ −1.4 ppm for the β-C of THP_1 when comparing **1** to **3**; $\Delta\delta_C$ −2.9 ppm for the γ-C of THP_1 when comparing **3** to **1**). A general downfield shift is also observed for both the proton(s) on the OH-donating carbon and those on the vicinal carbon ($\Delta\delta_H$ +0.93 and +0.13 ppm for the α-H and β-H of THP_1, respectively, when comparing **1** to **3**; $\Delta\delta_H$ +0.86, +0.60, and +0.37 ppm for the δ-H_a, δ-H_b and γ-H of THP_1, respectively, when comparing **3** to **1**). Such "acylation effect" has long been noted for acyl substituted monosaccharides, and was used to identify the acylation site on the sugar.[4-5] In contrast to **1** and **3**, significant downfield shift was observed for the γ-C of THP_1 in **2** (δ_C 78.02), while the resonance of β-C (δ_C 68.70) and δ-C (δ_C 60.53) of THP_1 largely shifted to upfield. Moreover, the proton on the γ-carbon of THP_1

in **2** (δ_H 4.84) was significantly deshielded as well (Table S2.1). Based on this, an ester linkage between the γ-OH of THP_1 and the carbonyl carbon of $MeVal_{10}$ was expected to establish the macrolactone ring of **2** according to the "acylation rule".

Subsequently, the advanced Marfey's method[6] was applied to assign the absolute configuration of each amino acid residue after acidic hydrolysis of **1**. All of the nine amino acids were determined to have L-configuration after comparative LC-ESIMS analysis of the 1-fluoro-2,4-dinitrophenyl-5-L-leucinamide (L-FDLA) and D/L-FDLA derivatives of the acidic hydrolysate (Fig. S15.1). A single-crystal X-ray diffraction analysis of a sample recrystallized from the acetonitrile solution of **3** (Table S18 and main text Fig. 2B) unequivocally confirmed that all of the nine amino acids were L-configured, and the remaining THP unit adopts a (2*R*,3*S*,4*R*)-configuration which is consistent with that of D-xylonic acid (Xyl). Since all three xylomyrocins were biosynthesized by the same NRPS machinery, the absolute configuration of the THP moiety in **1** and **2** was postulated in analogy with that of **3**.

1.5.2. Compounds 4, M1, and M2

Paramyrothecium roridum NRRL 2183 was grown on MMK2 medium (a total of 24 L) for 14 days, and the resulting culture was processed as described for *Paramyrothecium* sp. XJ0827. The fraction containing putative xylomyrocins (970 mg out of 8.7 g crude extract) was purified by semi-preparative HPLC eluting with 75 % aqueous methanol containing 0.1 % formic acid at a flow rate of 2.5 mL/min to yield compound **4** (11 mg), and two isomeric mixtures **M1** (59 mg), and **M2** (190 mg). Attempts to separate the isomers present in **M1** and **M2** on various conventional and chiral HPLC columns were unsuccessful.

Xylomyrocin D (**4**): white amorphous powder; $[\alpha]_D^{25}$ −198.6 (*c* 0.29, CH_3OH); UV (CH_3OH) λ_{max} (log ε) 205 (4.40) nm; ^1H and ^{13}C NMR data see Table S2.2; HRESIMS *m/z* 1084.6676 $[M + H]^+$ (calcd for $C_{52}H_{94}N_9O_{15}$, 1084.6863).

Xylomyrocins mixutre 1 (**M1**): white amorphous powder; UV (CH_3OH) λ_{max} (log ε) 205 (4.24) nm; HRESIMS *m/z* 1084.6674 $[M + H]^+$ (calcd for $C_{52}H_{94}N_9O_{15}$, 1084.6863).

Xylomyrocins mixutre 2 (**M2**): white amorphous powder; UV (CH_3OH) λ_{max} (log ε) 205 (4.35) nm; HRESIMS *m/z* 1098.6817 $[M + H]^+$ (calcd for $C_{53}H_{96}N_9O_{15}$, 1098.7020).

The molecular formula of **4** was determined as $C_{52}H_{93}N_9O_{15}$, requiring 11 degrees of unsaturation, by analyzing the HRESIMS (Fig. S17.4) and ^{13}C NMR spectroscopic data (Table S2.2). A comprehensive analysis of the 1D and 2D NMR spectra (Fig. S2) suggested that the structure of **4** consists of one glutamine (Gln), one Ile, two Leu, one *N*-methylleucin (MeLeu), one MeThr, two MeVal, and one THP moiety. Further interpretation of the HMBC and ROESY correlations (Fig. S2) established the connectivity between each constitutional unit, and gave a peptide sequence of THP_1-Leu_2-$MeThr_3$-Ile_4-$MeVal_5$-Leu_6-Gln_7-$MeLeu_8$-

MeVal$_9$ for **4**. This sequence was in complete agreement with that deduced from the HRESIMS/MS data of **20**, the methoxy-substituted derivative of **4** (Fig. S1.4). This linear sequence accounted for only 10 of the 11 degrees of unsaturation, suggesting a cyclic structure for **4**. HMBC interaction from the β-proton of THP$_1$ (δ_H 5.14) to the carbonyl carbon of the terminal MeVal$_9$ (δ_C 170.62) was indicative for an ester linkage between the β-OH of THP$_1$ and the carbonyl carbon of MeVal$_9$ (Fig. S2). Thus, the planar structure of **4** was determined as cyclo(THP$_1$-Leu$_2$-MeThr$_3$-Ile$_4$-MeVal$_5$-Leu$_6$-Gln$_7$-MeLeu$_8$-MeVal$_9$).

The positive mode HRESIMS spectrum of **M1** displayed an $[M + H]^+$ ion at *m/z* 1084.6674 (Fig. S17.5), indicating the same molecular formula of $C_{52}H_{93}N_9O_{15}$ as observed for **4**. **M1** was eluted as a broad single chromatographic peak during HPLC analysis, and its ^{1}H NMR spectrum was quite complicated, showing a similar overall resonating pattern yet far more resonance signals as compared to that of **4**. Such complexity of the ^{1}H NMR spectrum indicated that **M1** is a mixture of multiple xylomyrocin congeners, and thus rendered NMR-based structure characterization arduous and error-prone. In this case, tandem mass spectrometry was used to elucidate the peptide sequence of **M1** after methanolysis-mediated linearization. The methanolysis of **M1** gave two major products (**21** and **22**) both showing $[M + H]^+$ ions at *m/z* 1116.7 during LC-HRESIMS analysis. The fragmentation profile of protonated **21** (Fig. S1.5) was identical to that of protonated **20** (Fig. S1.4), indicating they share the same *C*-terminal modified peptide sequence of THP$_1$-Leu$_2$-MeThr$_3$-Ile$_4$-MeVal$_5$-Leu$_6$-Gln$_7$-MeLeu$_8$-MeVal$_9$-OMe. Meanwhile, amongst the b-/b*-type ions generated from the dissociation of protonated **22**, b2/b2*, b7/b7* and b8/b8* were identical to those of protonated **20**, while a mass shift of −14 Da was observed for b3/b3*–b6/b6* (Fig. S1.6). Similarly, y2, y7 and y8 ions from the fragmentation of protonated **22** were identical to those of protonated **20**, yet a mass difference of +14 Da was found for y3, y5 and y6 ions (Fig. S1.6). Both evidences suggested that there is a methyl functionality exchange between the 3rd and 7th amino acid residues in **22** as compared to **20**. Based on this, the amino acid sequence of **22** was deduced as THP$_1$-Leu$_2$-Thr$_3$-Ile$_4$-MeVal$_5$-Leu$_6$-MeGln$_7$-MeLeu$_8$-MeVal$_9$-OMe. Accordingly, **M1** was postulated to be the isomeric mixture of cyclo(THP$_1$-Leu$_2$-MeThr$_3$-Ile$_4$-MeVal$_5$-Leu$_6$-Gln$_7$-MeLeu$_8$-MeVal$_9$) and cyclo(THP$_1$-Leu$_2$-Thr$_3$-Ile$_4$-MeVal$_5$-Leu$_6$-MeGln$_7$-MeLeu$_8$-MeVal$_9$) with a variable macrocyclization site at one of the α-, β-, γ- or δ-carbon of the THP unit.

The HRESIMS-determined molecular weight of **M2** (Fig. S17.6) is 14 Da larger than that of **4**, corresponding to the addition of an extra methyl functionality in the structure as compared to **4**. Similar to **M1**, the ^{1}H NMR spectrum of **M2** displayed resonance signals characteristic for a mixture of multiple xylomyrocin congeners despite of being eluted as a broad single chromatographic peak during HPLC analysis. Therefore, **M2** was subjected to HRESIMS/MS-based *de novo* sequencing after methanolysis-

mediated linearization. The methanolysis of **M2** resulted in a major product (**23**) that displayed an $[M+H]^+$ ion at *m*/*z* 1130.7167. All b-/b*-type fragment ions generated from dissociation of this precursor ion (Fig. S1.7) were identical to those observed for protonated **20** (Fig. S1.4) except for b7/b7* and b8/b8*, which exhibited a mass difference of +14 Da each. Moreover, the detected y3 and y5–y8 ions for protonated **23** (Fig. S1.7) also showed a mass shift of +14 Da each as compared to those found for protonated **20** (Fig. S1.4). Assignment of these b-/b*- and y-type ions indicated that **23** has an additional methyl functionality on the 7th residue as compared to **20**, and thus the peptide sequence of **23** was deduced as THP_1-Leu_2-$MeThr_3$-Ile_4-$MeVal_5$-Leu_6-$MeGln_7$-$MeLeu_8$-$MeVal_9$-OMe. The abundancy of isolated **M2** allowed large scale methanolysis and subsequent purification of **23** for 1D and 2D NMR experiments. To our surprise, the ^{1}H and ^{13}C NMR spectra of purified **23** still exhibited resonance signals for two xylomyrocin-like substances (**23a** and **23b**) with a molar ratio of 5:2 (Table S2.2). A comprehensive analysis of the COSY, TOCSY, HSQC, HMBC, and ROESY data successfully established identical planar structures for both compounds (Fig. S2) and proved that they have an identical peptide sequence which is in complete agreement with that deduced from tandem mass spectrometry. Due to the partial double-bound character of peptide bond, both cyclic and linear peptides are known to have conformational isomers originating from *cis*/*trans*-isomerization of specific peptide bond(s).[7-8] Although the *trans*-peptide bond is thermodynamically favored in unmodified peptides, the *cis*-configuration is frequently observed in *N*-methylated peptides because the energy difference between the *cis*- and *trans*-conformations with *N*-substituted amino acids is significantly reduced.[9] Most of the *cis*- and *trans*-isomers of a specific peptide are difficult to separate by HPLC, yet they could be differentiated by NMR spectrometry.[7-8] In light of this, a detailed analysis of the 2D-ROSEY data of **23a** and **23b** was carried out to see if they are *cis*/*trans*-conformational isomers. Satisfactorily, strong ROESY correlations were observed for *N*-CH_3 protons of each of the five *N*-methylated amino acids with the α-proton of the preceding amino acid in **23a**, indicating *trans*-configured peptide bonds between Leu_2 and $MeThr_3$; Ile_4 and $MeVal_5$; Leu_6 and $MeGln_7$; $MeGln_7$ and $MeLeu_8$; and $MeLeu_8$ and $MeVal_9$ (Fig. S2). Similarly, *trans*-configured peptide bonds for Ile_4-$MeVal_5$, Leu_6-$MeGln_7$, and $MeGln_7$-$MeLeu_8$ in **23b** were evident by the presence of clear ROESY correlations between the corresponding *N*-CH_3 and α-protons. However, the observed ROESY correlations between the α-protons of Leu_2 and $MeThr_3$, and $MeLeu_8$ and $MeVal_9$ strongly suggested *cis*-configured peptide bonds for Leu_2-$MeThr_3$, and $MeLeu_8$-$MeVal_9$ (Fig. S2). Since methanolysis of **M2** resulted in a single peptide (**23**) with significantly simplified and interpretable 1D NMR spectra, **M2** was postulated to be the isomeric mixture of cyclo(THP_1-Leu_2-$MeThr_3$-Ile_4-$MeVal_5$-Leu_6-$MeGln_7$-$MeLeu_8$-$MeVal_9$) with a variable macrocyclization site at one of the α-, β-, γ- or δ-carbon of the THP unit. Whether *cis*/*trans*-isomerization at Leu_2-$MeThr_3$ and $MeLeu_8$-$MeVal_9$

exists in the macrocyclized **M2** was not clear due to the extreme complexity of the NMR spectra of **M2**.

LC-ESIMS analysis of the L- and D/L-FDLA derivatives of the acidic hydrolysate of **4** confirmed that all amino acid components of **4** are L-configured (Fig. S15.2). GC-EIMS analysis revealed that the THP residue of **4** is xylonic acid by comparing the retention time and mass spectrum of the trimethylsilyl (TMS)-derivative of THP with that of the TMS-derivative of an authentic xylonic acid standard (Fig. S16). Considering that the biosyntheses of **4**, **M1** and **M2** are carried out by the same NRPS, the absolute configurations of the amino and hydroxy acid residues in **M1** and **M2** were postulated in analogy with that of **4**.

1.5.3. Compounds 5–10

Paramyrothecium roridum MN113194 was grown on PDA medium (a total of 14 L) for 14 days, and the resulting culture was processed as described for *Paramyrothecium* sp. XJ0827. The fraction containing putative xylomyrocins (180 mg out of 1.5 g crude extract) was repeatedly purified by semi-preparative HPLC eluting with 65 % and 55 % aqueous acetonitrile containing 0.1 % formic acid at a flow rate of 2.5 mL/min to yield compounds **6** (8 mg), **7** (3 mg), **8** (3 mg), **9** (3 mg), and the mixture of **5** and **10** (5 mg).

Xylomyrocin E (**5**): white amorphous powder; UV (CH_3OH) λ_{max} (log ε) 205 (4.40) nm; ^1H and ^{13}C NMR data see Table S2.3; HRESIMS *m/z* 1100.5845 $[M + Na]^+$ (calcd for $C_{51}H_{83}N_9O_{16}Na$, 1100.5850).

Xylomyrocin F (**6**): white amorphous powder; $[\alpha]_D^{25}$ −167.8 (*c* 0.78, CH_3OH); UV (CH_3OH) λ_{max} (log ε) 205 (4.53) nm; ^1H and ^{13}C NMR data see Table S2.3; HRESIMS *m/z* 1114.6050 $[M + Na]^+$ (calcd for $C_{52}H_{85}N_9O_{16}Na$, 1114.6006).

Xylomyrocin G (**7**): white amorphous powder; $[\alpha]_D^{25}$ −185.7 (*c* 0.30, CH_3OH); UV (CH_3OH) λ_{max} (log ε) 205 (4.34) nm; ^1H and ^{13}C NMR data see Table S2.3; HRESIMS *m/z* 1114.6044 $[M + Na]^+$ (calcd for $C_{52}H_{85}N_9O_{16}Na$, 1114.6006).

Xylomyrocin H (**8**): white amorphous powder; $[\alpha]_D^{25}$ −201.5 (*c* 0.26, CH_3OH); UV (CH_3OH) λ_{max} (log ε) 205 (4.46) nm; ^1H and ^{13}C NMR data see Table S2.4; HRESIMS *m/z* 1128.6219 $[M + Na]^+$ (calcd for $C_{53}H_{87}N_9O_{16}Na$, 1128.6163).

Xylomyrocin I (**9**): white amorphous powder; $[\alpha]_D^{25}$ −191.3 (*c* 0.22, CH_3OH); UV (CH_3OH) λ_{max} (log ε) 205 (4.42) nm; ^1H and ^{13}C NMR data see Table S2.4; HRESIMS *m/z* 1114.6055 $[M + Na]^+$ (calcd for $C_{52}H_{85}N_9O_{16}Na$, 1114.6006).

Xylomyrocin J (**10**): white amorphous powder; UV (CH_3OH) λ_{max} (log ε) 205 (4.40) nm; ^1H and ^{13}C NMR data see Table S2.4; HRESIMS *m/z* 1128.6173 $[M + Na]^+$ (calcd for $C_{53}H_{87}N_9O_{16}Na$, 1128.6163).

The positive mode HRESIMS spectrum of **6** showed an $[M + Na]^+$ ion at *m/z* 1114.6050 (Fig. S17.8), and the ^{13}C NMR spectrum displayed resonances for a total of 52 carbons (Table S2.3). Based on these

spectroscopic data, a molecular formula of $C_{52}H_{85}N_9O_{16}$, requiring 15 degrees of unsaturation, was deduced for **6**. An initial examination of the ^1H and ^{13}C NMR spectra of **6** revealed significant similarity to those of previously characterized xylomyrocins (Table S2.3). Structural elucidation of **6** was then carried out through concerted analysis of the 2D NMR spectra. Eleven proton-proton spin systems were identified by interpretation of COSY and TOCSY correlations (Fig. S2), and the carbons to which the protons attach were assigned based on HSQC data. Further analysis of the HMBC and ROESY data (Fig. S2) correlated these spin systems to nine amino acid residues, including Gly, Ile (2×), Leu, *N*-methylalanine (MeAla), MePhe, MeThr, Ser, and Val, and one THP unit, and established a linear peptide sequence of THP_1-Leu_2-$MeThr_3$-Val_4-$MePhe_5$-Gly_6-Ile_7-Ser_8-Ile_9-$MeAla_{10}$. This interpretation was further supported by HRESIMS/MS-based *de novo* sequencing (Fig. S1.9) of the methoxy-substituted derivative of **6** (**25**). Finally, the HMBC correlation between the α-H of THP_1 (δ_H 4.99) and the carbonyl carbon of $MeAla_{10}$ (δ_C 170.17) helped determine the macrocyclization position (Fig. S2), and fully established the planar structure of **6**.

The HRESIMS-determined molecular formulae of **7** and **9** ($C_{52}H_{85}N_9O_{16}$) were identical to that of **6**, and the ^1H and ^{13}C NMR data (Table S2.3 and S2.4) of these three compounds were also remarkably similar to each other. A comprehensive analysis of the COSY, TOCSY, HSQC, HMBC, and ROESY data (Fig. S2) revealed that the only difference between **6** and **7** was the switch of amino acid residues at the 4th and 9th position: **6** adopts Val and Ile as the 4th and 9th residue, respectively, while **7** has Ile and Val instead at the same location. Interpretation of the HRESIMS/MS spectrum of linearized **7** (**26**) (Fig. S1.10) gave a peptide sequence which further confirmed the planar structure of **7** as cyclo(THP_1-Leu_2-$MeThr_3$-Ile_4-$MePhe_5$-Gly_6-Ile_7-Ser_8-Val_9-$MeAla_{10}$). On the other hand, elucidation of the NMR spectroscopic data (Fig. S2) indicated that the identity and sequential order of the amino/hydroxy acid residues of **6** and **9** were exactly the same, yet the macrocyclization site in these two compounds was different: instead of the α-OH, **9** utilizes the δ-OH of THP_1 to form the cyclodepsipeptide ring. A molecular formula of $C_{53}H_{87}N_9O_{16}$ was deduced for **8** based on the $[M + Na]^+$ ion at *m*/*z* 1128.6219 in the positive mode HRESIMS spectrum (Fig. S17.10), indicating the addition of a CH_3 group in **8** as compared to **6**, **7**, and **9**. Indeed, a thorough interpretation of the 2D NMR data (Fig. S2) confirmed that the planar structure of **8** was almost identical to those of **6** and **7**, except that the 4th and 9th residues were both Ile.

Compounds **5** and **10** were eluted together during HPLC, and displayed $[M + Na]^+$ ions at *m*/*z* 1100.5845 and 1128.6173, respectively, in their positive mode HRESIMS spectra (Fig. S17.7). The molecular formula deduced for **5** ($C_{51}H_{83}N_9O_{16}$) was one CH_2 unit less than that of **6**, **7**, and **9**, indicating **5** is the demethylated derivative of these xylomyrocins. On the other hand, the molecular formula determined for **10** ($C_{53}H_{87}N_9O_{16}$) was identical to that of **8**, suggesting they are regio- or stereo-isomers.

The ^{1}H and ^{13}C NMR spectra of the mixture of **5** and **10** were relatively complex, yet all resonances could be clearly differentiated and assigned to **5** and **10** by detailed analysis of the 2D NMR data (Table S2.3 and S2.4). The molar ratio between **5** and **10** was inferred as 1:1 by comparing the integrals of the ^{1}H NMR signals corresponding to these two compounds. Careful interpretation of COSY, TOCSY, HSQC, HMBC, and ROESY correlations (Fig. S2), along with detailed analysis of the tandem mass spectra of the linearized **5** (**24**) and **10** (**27**) (Fig. S1.8 and S1.11), revealed that the planar structure of **5** closely resembles those of **6** and **7**, except that **5** has Val at both 4th and 9th positions. In contrast, the peptide sequence established for **10** was exactly the same as that of **8**, yet a different -OH donor (δ-OH of THP) was used to construct the macrolactone ring in **10**.

To determine the absolute configuration of the amino acid residues present in **5**-**10**, the relatively abundant **6** was selected for acidic hydrolysis and Marfey's analysis. The LC-ESIMS result showed that all chiral amino acids found in **6** were L-configured (Fig. S15.3). GC-EIMS analysis confirmed that the THP residue of **6** is xylonic acid by comparing the retention time and mass spectrum of the TMS-derivative of THP with that of the TMS-derivative of an authentic xylonic acid standard (Fig. S16). Since all xylomyrocins produced by *Paramyrothecium roridum* MN113194 share the same biosynthetic origin, the amino/hydroxy acid residues in **5** and **7**–**10** were postulated in analogy with that of **6**.

1.5.4. Compounds 11 and 12

Colletotrichum sp. XJ1040 was grown on MMK2 medium (a total of 12 L) for 14 days, and the resulting culture was processed as described for *Paramyrothecium* sp. XJ0827. The fraction containing putative xylomyrocins (750 mg out of 2.6 g crude extract) was purified by semi-preparative HPLC eluting with 75 % aqueous acetonitrile containing 0.1 % formic acid at a flow rate of 2.5 mL/min to give compounds **11** (26 mg) and **12** (2 mg).

Xylomyrocin K (**11**): white amorphous powder; $[\alpha]_D^{25}$ −181.3 (*c* 0.68, CH_3OH); UV (CH_3OH) λ_{max} (log ε) 205 (4.43) nm; ^{1}H and ^{13}C NMR data see Table S2.5; HRESIMS *m/z* 1128.7036 $[M + H]^+$ (calcd for $C_{54}H_{98}N_9O_{16}$, 1128.7126).

Xylomyrocin L (**12**): white amorphous powder; $[\alpha]_D^{25}$ −132.2 (*c* 0.18, CH_3OH); UV (CH_3OH) λ_{max} (log ε) 205 (4.62) nm; ^{1}H and ^{13}C NMR data see Table S2.5; HRESIMS *m/z* 1128.7115 $[M + H]^+$ (calcd for $C_{54}H_{98}N_9O_{16}$, 1128.7126).

The molecular formula of **11** was determined as $C_{54}H_{97}N_9O_{16}$, requiring 11 degrees of unsaturation, based on the $[M + H]^+$ ion found in the positive mode HRESIMS spectrum (Fig. S17.12). The ^{1}H and ^{13}C NMR spectra of **11** (Table S2.5) exhibited characteristic resonances for a peptidic structure, e.g. six amide protons resonating at 7.31–8.85 ppm, 10 carbonyl carbons resonating at 167.7–172.8 ppm, and 15

heteroatom-bearing carbons resonating at 51.6–75.3 ppm. The absence of ^{13}C NMR signals in the range of 100–160 ppm indicated the lack of aromatic amino acid residues in the structure of **11**. A detailed analysis of the 2D NMR data (Fig. S2) revealed that **11** consisted of seven aliphatic amino acids, including Ile (3×), MeLeu, MeVal, and Val (2×), two hydroxylic amino acids including MeThr and Ser, and one THP unit. Ten carbonyl functionalities of these amino/hydroxy acid residues accounted for 10 of the 11 degrees of unsaturation in **11**, leaving the remaining one degree of unsaturation for a cyclic structure. Careful interpretation of the HMBC and ROESY correlations (Fig. S2), along with detailed analysis of the tandem mass spectrum of linearized **11** (**28**) (Fig. S1.12) successfully established the connectivities of the 10 residues and established the planar structure of **11**.

A comprehensive analysis of the HRESIMS and NMR spectroscoic data (Fig. S17.13 and Table S2.5) suggested that **12** was a cyclic decadepsipeptide with the sequence of cyclo(THP_1-Val_2-$MeThr_3$-Ile_4-$MeVal_5$-Val_6-Ile_7-Ser_8-Ile_9-$MeLeu_{10}$). The deshielded γ-CH of THP moiety in **12** (δ_H 5.00, δ_C 76.53) strongly indicated that the γ-OH of THP_1 was used to form the macrolactone ring with the carbonyl carbon of $MeLeu_{10}$. Thus, the planar structure of **12** was determined as shown in Fig. S2.

LC-ESIMS analysis of the L- and D/L-FDLA derivatives of the acidic hydrolysate of **11** confirmed that all amino acid residues of **11** are L-configured (Fig. S15.4), while GC-EIMS analysis of the TMS-derivatives of the acidic hydrolysate of **11** demonstrated that the THP moiety is xylonic acid (Fig. S16). Considering that **11** and **12** are biosynthesized by the same NRPS, the absolute configurations of the amino/hydroxy acid residues in **12** were postulated in analogy with that of **11**.

1.6. Advanced Marfey's analysis

500 µg of the appropriate xylomyrocin congener was hydrolyzed in 6 N HCl at 115 °C for 18 hrs. The hydrolysate was dried under vacuum, and dissolved in 100 µL H_2O. An 50 µL aliquot of this solution was treated with 20 µL of 1 M $NaHCO_3$ and 100 µL of 1 % 1-fluoro-2,4-dinitrophenyl-5-L-leucinamide (L-FDLA) in acetone, while the other 50 µL aliquot was treated with 20 µL of 1 M $NaHCO_3$ and 100 µL of D/L-FDLA. The reaction mixtures were heated at 45 °C for 2 hrs. After cooling to room temperature, the reactions were quenched with 10 µL of 2 N HCl. Then, the resulting residues were diluted with 1 mL of 50 % aqueous CH_3CN for subsequent LC-ESIMS analysis. The FDLA-derivative of each amino acid (AA) residue was identified in the extracted ion chromatogram based on the corresponding *m*/*z* value. The absolute configurations of constituent AA residues were determined by comparing the retention times of AA-L-FDLA with those of AA-D/L-FDLA derivative, and by applying the empirical rule that the L-AA-L-FDLA / D-AA-D-FDLA derivatives are always eluted earlier from the reverse phase C18 column than the L-AA-D-FDLA / D-AA-L-FDLA derivatives.[6] The LC-ESIMS spectra of the AA-L-FDLA and AA-D/L-FDLA derivatives are shown

in Figure S15.

1.7. X-ray crystallographic analysis

X-ray crystallographic data of **3** were collected on an XtaLAB Synergy R, HyPix diffractometer (Rigaku Corporation, Tokyo, Japan) using Cu Kα radiation. The crystal was kept at 100 K during data collection. The structure was solved in Olex2[10] with the ShelXT[11] structure solution program using Intrinsic Phasing and refined with the ShelXL[11] refinement package using Least Squares minimisation. The X-ray crystallographic data has been deposited in the Cambridge Crystallographic Data Centre with the deposition number CCDC 2119453. Copies of these data can be obtained free of charge via www.ccdc.cam.ac.uk/data_request/cif, or by emailing data_request@ccdc.cam.ac.uk, or by contacting the Cambridge Crystallographic Data Centre, 12, Union Road, Cambridge CB2 1EZ, UK; fax: (+44) 1223-336-033.

1.8. GC-EIMS analysis

Gas Chromatography-Electron Impact Mass Spectrometry (GC-EIMS) analysis was carried out on an Agilent 7890A GC system coupled with an Agilent 7000B tripe quadrupole mass spectrometer (Agilent Technologies Inc., Santa Clara, CA, USA). The GC-EIMS instrument was equipped with an Agilent HP-5 capillary column (30 mm × 0.25 mm × 0.25 µm). The sample was injected in a common splitless mode with an inlet temperature of 280 °C, and the flow rate was set to 1 mL/min using helium as the constant carrier gas. The initial column temperature was 100 °C, raised to 150 °C at the rate of 20 °C/min and then to 310 °C at the rate of 5 °C/min, and finally maintained at 310 °C for an additional 10 min. For the EIMS detection, the ion source temperature was set to 250 °C, and mass data acquisition was operated in full scan mode (m/z 50–900). The acid hydrolysate of the appropriate xylomyrocin congener was dried under vacuum, and the residue was dissolved in 500 µL anhydrous pyridine (Sigma-Aldrich, Saint Louis, MO, United States). An 80 µL aliquot of this solution was mixed with 80 µL *N*,*O*-bis(trimethylsilyl)trifluoroacetamide (BSTFA) + 1 % trimethylchlorosilane (TMCS) (Sigma-Aldrich, Saint Louis, MO, United States). The silylation reaction was carried out at 70 °C for 90 min, and 1 µL of the reaction mixture was used for GC-EIMS analysis.

1.9. Genomic DNA preparation

Paramyrothecium sp. XJ0827 was grown in potato dextrose broth (PDB; potato starch 4 g/L, dextrose 20 g/L) at 28 °C with shaking at 220 rpm for 5 days. The mycelium was collected by filtration, washed with water, and dried with paper towels. The dried mycelia were frozen in liquid nitrogen and ground in a mortar. The resulting powder was suspended in Lysis buffer (solution A 370 ml/L, solution B 370 ml/L, solution C 148 ml/L, 0.1 % polyvinylpyrrolidone 100 ml/L, proteinase K 7 ml/L. Solution A: 0.35 M sorbitol, 0.1 M Tris-HCl pH 9, 5 mM EDTA pH 8; solution B: 0.2 M Tris-HCl pH 9, 50 mM EDTA pH 8, 2 M NaCl, 2 %

cetyltrimethylammonium bromide [CTAB]; solution C: 5 % N-laroylsarcosine sodium salt), and incubated at 65 °C for 30 min. Next, 0.33 volume of 5 M potassium acetate was added to the suspension. After incubation on ice for 30 min, the suspension was centrifuged at 10,000 × g, 4 °C for 20 min. To the supernatant was added 1 volume of chloroform:isoamylalcohol (24:1), vortexed for 15 sec, and centrifuged at 10,000 × g, 4 °C for 10 min. The aqueous phase was treated with RNAse A at 37 °C for 90 min, followed by addition of 0.1 volume of 3 M sodium acetate and 1 volume of isopropanol. After incubation at room temperature for 5 min, the genomic DNA was recovered by centrifugation at 10,000 × g, 4 °C for 30 min. The pellet was washed with 70 % aqueous ethanol and allowed to dry at room temperature for 5 min. The isolated DNA was resuspended in TE buffer (10 mM Tris-HCl pH 8, 1 mM EDTA), and stored at −20 °C until further use.

1.10. Genome sequencing and annotation

The genome of *Paramyrothecium* sp. XJ0827 was sequenced using a combination of Illumina NovaSeq and Oxford Nanopore technologies. For Illumina sequencing, genomic DNA was extracted and randomly fragmented, and DNA fragments with the required lengths were isolated by electrophoresis. After ligation with adapters, DNA fragments were sequenced. For Nanopore sequencing, DNA samples were sheared using a G-tube, the fragments were end-repaired, and both ends of the DNA fragments were ligated with adapters to generate the sequencing library. Quality control was performed at each stage of the sample preparation and sequencing. The obtained nanopore subreads were corrected and then assembled using canu.[12] Single base errors in the assembly were further corrected with Illumina NovaSeq data using GATK.[13-14] Contigs were linked to scaffolds with long insert size pair-end reads using SSPACE_Basic_v2.0.[15] The gaps were filled using pbjelly2.[16] The predicted proteins were compared to various databases using blastp, and the highest quality alignments were chosen. The databases and versions were: Gene Ontology (GO), release_2017-09-08; Kyoto Encyclopedia of Genes and Genomes (KEGG), version 81; Cluster of Orthologous Groups of proteins (COG), version 2014-11-10; Swiss-Prot, release 2017-07; Trembl, release-2017-09; NR, version 2017-10-10; EggNOG, version 4.5.

1.11. Accession numbers

The genome assembly of *Paramyrothecium* sp. XJ0827 has been deposited in the NCBI GenBank as BioProject: PRJNA770833 with the accession number JAJFPB000000000. Accession numbers for the proteins encoded by the *Paramyrothecium* sp. XJ0827 and the *P. roridum* NRRL 2183 *xmc* biosynthetic gene clusters are shown in Tables S8 and S15, respectively. Accession numbers for the additional putative xylose metabolic enzymes from both fungi, and putative xylan degradation enzymes from

Paramyrothecium sp. XJ0827 are listed in Tables S9 and S10, respectively.

1.12. Total RNA extraction and cDNA synthesis

Paramyrothecium sp. XJ0827 was cultured in liquid M-100 medium (D-glucose 10 g/L, KNO_3 3 g/L, salt solution 62.5 mL/L. Salt solution: KH_2PO_4 16 g/L, Na_2SO_4 4 g/L, KCl 8 g/L, $MgSO_4 \cdot 7H_2O$ 2 g/L, $CaCl_2$ 1 g/L, trace element solution 8 mL/L; trace element solution: H_3BO_3 60 mg/L, $MnCl_2 \cdot 4H_2O$ 140 mg/L, $Na_2MoO_4 \cdot 2H_2O$ 400 mg/L, $FeCl_3 \cdot 6H_2O$ 100 mg/L, $CuSO_4 \cdot 5H_2O$ 400 mg/L) with shaking at 28 °C, 220 rpm for 5 days (start of the accumulation of compounds **1**–**3**); 7 days (the active production phase for **1**–**3**); or 9 days (late production phase for **1**–**3**). The mycelium was collected by filtration, washed with water, and dried with a paper towel. The dried mycelia were frozen in liquid nitrogen and ground into a fine powder. The resulting powder was suspended in Trizol (Thermo Fisher Scientific, Wilmington, DE, United States) and mixed by vortexing. The suspension was kept at room temperature for 15 min, then centrifuged at 10,000 × g, 4 °C for 10 min. The supernatant was transferred to a clean Eppendorf tube, mixed with chloroform by gently inverting the tube, and kept at room temperature for 15 min. After centrifugation at 10,000 × g, 4 °C for 10 min, the aqueous phase was collected, and the RNA was precipitated with isopropanol. The RNA was collected by centrifugation at 10,000 × g, 4 °C for 10 min, and the pellet was washed with 70 % aqueous ethanol and air dried at room temperature. The isolated total RNA was resuspended in diethylpyrocarbonate (DEPC)-treated sterile water. RNA concentration and purity were estimated from the optical density ratio at A_{260}/A_{280} and A_{260}/A_{230} using a NanoDrop 2000 spectrophotometer (Thermo Fisher Scientific, Wilmington, DE, United States). The integrity of the RNA was evaluated by electrophoresis. cDNA was prepared from the total RNA using the PrimeScript RT kit (Takara Bio Inc., Shiga, Japan), and stored at −20 °C for further use.

1.13. Reverse transcription - quantitative PCR (RT-qPCR) analysis.

RT-qPCR was performed using the ABI Prism 7500 real-time PCR system (Applied Biosystems, Foster City, CA, United States), in a final reaction volume of 20 µL containing cDNA, Power SYBR Green PCR master mix (Thermo Fisher Scientific, Wilmington, DE, United States), and the appropriate primers (final concentration: 200 nM each) listed in Table S17. PCR amplification was conducted with an initial denaturation cycle of 30 sec at 95 °C; 40 cycles of 5 sec at 95 °C for denaturation, 30 sec at 60 °C for primer annealing and extension; and a melt-curve stage consisting of 15 sec at 95 °C, 1 min at 60 °C, 30 sec at 95 °C, and finally 15 sec at 60 °C. The tubulin-encoding gene was used as the reference gene, and the relative expression fold-change was calculated using the comparative threshold cycle $2^{-\Delta\Delta CT}$ method. Three biological replicates were analyzed, and for each sample, three technical replicates for each targeted gene

were performed.

1.14. Knockout of the *pxxmc* biosynthetic genes

The flanking regions of the target genes were amplified from the genomic DNA of *Paramyrothecium* sp. XJ0827 using appropriate primers that also included specific cloning end regions that are complementary to the 5'- or 3'-ends of the linearized pJET1.2 vector and those of the hygromycin B phosphotransferase gene (*hph*) cassette (Table S17). The resulting targeting arms were fused with the hygromycin resistance cassette and cloned into the pJET1.2 vector using the ClonExpress MultiS one step cloning kit (Vazyme Biotech Co., Ltd., Nanjing, Jiangsu, China) to generate the gene deletion plasmids. The linear gene deletion cassettes were amplified from these plasmids and transformed into *Paramyrothecium* sp. XJ0827 protoplasts using PEG-mediated transformation as described for *Aspergillus nidulans*[17], with slight modifications. Briefly, protoplasts were generated from germlings using osmotic buffer (1.2 M $MgSO_4 \cdot 7H_2O$, 10 mM PBS adjusted to pH 5.8 with 1 M Na_2HPO_4) containing 5 mg/mL Lysing enzyme (Sigma-Aldrich, Saint Louis, MO, United States) and 2 mg/mL Yatalase (Takara Bio Inc., Shiga, Japan) at 37 °C with gentle shaking at 80 rpm for 6 hrs. The reaction mixture was transferred to a 50 mL OakRidge Makrolon tube and kept on ice. After the addition of trapping buffer (0.6 M sorbitol, 0.1 M Tri-HCl pH 7.0) and centrifugation at 5,000 × g, 4 °C for 15 min, the protoplasts were recovered from the middle layer. The harvested protoplasts were washed with STC solution (1.2 M sorbitol, 10 mM $CaCl_2$, 0.1 M Tri-HCl pH 7.5), centrifuged at 6,000 × g, 4 °C for 8 min, and then resuspended in STC solution. For transformation, 800–1,500 ng linear DNA fragment was added to 100 μL protoplast solution, and incubated on ice for 50 min. After addition of 1.25 mL PEG solution (60 % PEG 4,000, 50 mM $CaCl_2$, 50 mM Tris-HCl pH 7.5), the mixture was kept at room temperature for 20 min. After further dilution with STC solution, the protoplasts were plated on selective medium (M-100 agar medium containing 50 μg/mL hygromycin B) in a 4 mL soft agar overlay. Non-selective medium was used to determine the viability of protoplasts. The cultures were incubated at 28 °C for 5–7 days, hygromycin B resistant colonies were isolated, and gene knockouts were verified by PCR using multiple primers (Table S17; Figure S5).

1.15. Culturing, feeding, and extraction of *Paramyrothecium* sp. XJ0827 with ^{13}C-labeled monosaccharides for MS analysis.

Thirty milliliters of regular or modified M-100 media (in modified M-100 medium, D-glucose-$^{13}C_6$ [Cambridge Isotope Laboratories, Andover, MA, USA] replaces D-glucose as the sole carbon source) were inoculated with the wild type or the Δ*pxxmcE* strains of *Paramyrothecium* sp. XJ0827 and incubated with shaking at 28 °C for nine days. After centrifugation, the liquid media were extracted with equal volume of

EtOAc, while the fungal mycelia were extracted with 15 mL methanol. The organic solutions were combined, concentrated under vaccum, and dissolved in 1 mL methanol for subsequent LC-ESIMS analysis. For the feeding experiment with stable isotope-labeled D-xylose, regular M-100 medium was used to cultivate the wild type or the Δ*pxxmcE* strains of *Paramyrothecium* sp. XJ0827 at 28 °C with shaking. D-xylose-1-^{13}C (Cambridge Isotope Laboratories, Andover, MA, USA) was supplemented to the culture at a final concentration of 17 mM at day 7. Fermentation was continued for another three days to facillitate complete utilization of the supplemented substrate, and the extraction was carried out as described above.

The $[M+H]^+$ ion of **1** extracted from cultures of the WT and the Δ*pxxmcE* strains grown in the modified M-100 medium exhibited a +54 Da mass shift (*m*/*z* 1175.2) as compared to that of **1** extracted from cultures grown in regular M-100 medium (*m*/*z* 1120.8), indicating all carbons in **1** ($C_{54}H_{89}N_9O_{16}$) were isotopically labeled (Fig. S6). This confirmed that D-glucose can be used by the fungus as the sole carbon source to produce xylomyrocins, including the D-xylonic acid unit. On the other hand, supplementation of D-xylose-1-^{13}C to regular M-100 medium resulted in an obvious increment of abundancies of the +1, +2, and +3 Da isotopic peaks of the $[M+H]^+$ ion of **1** at *m*/*z* 1120.8 (Fig. S6). Tandem mass analysis of this ^{13}C-labeled **1** after methanolysis-mediated linearization revealed that the Xyl_1 unit is isotopically labeled, probably at the carbonyl carbon (Fig. S7). This strongly supports that the D-xylonic acid building block in xylomyrocins is directly synthesized from D-xylose via PxXmcE-catalyzed dehydrogenation, while D-xylose could be supplied from either monosaccharide interconversions (endogenous route) or hemicellulose metabolism (exogenous route).

1.16. Cloning and expression of PxXmcG-A_1T_1 and PxXmcG-A_1.

The A_1T_1 di-domain (M265 – Y912) and the A_1 mono-domain (M265 – E819) of PxXmcG were amplified by PCR from the cDNA of *Paramyrothecium* sp. XJ0827 using appropriate primers for expression as *N*-terminally or *C*-terminally His-tagged proteins (Table S17). The PCR products were ligated into pET28a using In-Fusion cloning as *Nde*I-*Xho*I fragments to afford pET28a-N-His-PxXmcG-A_1T_1 and pET28a-N-His-PxXmcG-A_1, and as *Nco*I-*Xho*I fragments to yield pET28a-C-His-PxXmcG-A_1T_1 and pET28a-C-His-PxXmcG-A_1. The cloned genes were validated by sequencing.

Each of the four constructs was then introduced separately into *E*. *coli* BL21 for overexpression. Three independent transformants representing each of the constructs were grown at 37 °C with shaking at 250 rpm until the OD_{600} reached 0.8–1.0. After cooling to 25 °C, 16 °C, or 11 °C, isopropyl β-D-thiogalactopyranoside (1, 0.5, or 0.15 M) was supplemented to the cultures. After continued cultivation with shaking at 25 °C, 16 °C, or 11 °C for 18 hrs or 24 hrs, the cells were harvested by centrifugation at 6,000 rpm for 10 min. The harvested cells were resuspended in disruption buffer (50 mM Tris-HCl, 150

mM NaCl, pH 7.5) and disrupted by sonication on ice. After centrifugation, the cleared lysates and cell pellets were analyzed by SDS-PAGE to monitor the expression of the target protein (Fig. S13).

1.17. Antimicrobial activity evaluation

Plasmodium falciparum strain 3D7 was used in antimalaria tests. Fresh O-type human erythrocytes were obtained from volunteers, with the samples de-identified before they were used in our study. Cultivation of *P. falciparum* was carried out as described previously.[18] *P. falciparum* 3D7 parasites were maintained in RPMI 1640 complete medium with 25 mM HEPES, 50 mg/L hypoxanthine, 2.1 g/L $NaHCO_3$, and 0.5 % AlbuMAX® I Lipid-Rich Bovine Serum Albumin, adjusted to pH7.2-7.4. Synchronous ring-stage *P. falciparum* was generated using 5 % sorbitol, and diluted with complete medium and normal human erythrocytes to a starting 2 % hematocrit and 0.5 % parasitemia. 90 µL of this cell suspension was split into each test well, and wells containing non-parasitized erythrocytes at 4 % hematocrit served as reference controls. Stock solutions of the test compounds (in DMSO) were prepared at a concentration of 10 mM, serially diluted in complete medium, and dispensed into triplicate test wells to give a final well volume of 100 µL with the final concentrations of test compounds ranging from 0 to 10^{-5} M. After 48 hrs of incubation at 37 °C, the widely-adopted fluorescence-based method[18] was used to evaluate the antiprotozoal activity of xylomyrocins against *P. falciparum*. Briefly, 100 µl supernatant was removed in to a 96-well plate and 100 µl SYBR green-I solution with lysis buffer [20 mM Tris, pH 7.5, 5 mM EDTA, 0.008 % (wt/vol) saponin and 0.08 % (vol/vol) Triton X-100] was added to each well. The plates were then incubated for 2 h in the dark at room temperature. All the plates were read using a fluorescence plate reader, with excitation and emission wavelengths of 485 and 535 nm, respectively. The background reading for an empty well was subtracted to yield fluorescence counts for the assessment of parasite viability. The inhibition rate was calculated relative to the parasite-growth-medium negative control (0 % inhibition). Three biological replicates were assayed.

Two strains of the Gram-positive bacteria *Staphylococcus aureus*: subsp. *aureus* Rosebach (ATCC 6538) and methicillin-resistant *S. aureus* (MRSA) 11646, and one Gram-negative bacterium *Escherichia coli* ATCC 25922 were used to evaluate the antibacterial activity of isolated xylomyrocins. Antibacterial assays were carried out utilizing the two-fold serial broth microdilution method with slight modifications.[19] Briefly, each test bacterial strain was inoculated into Luria-Bertani (LB, 10 g/L tryptone, 10 g/L NaCl, 5 g/L yeast extract) broth, and incubated at 37 °C with shaking at 150 rpm for 12 hrs. The bacterial cultures were diluted 1,000-fold with fresh LB medium once the OD_{600} reached 0.8. The stock solutions of test compounds (in DMSO) were diluted with LB medium to give serial two-fold dilutions. The final concentrations of each compound in the wells were 20, 10, 5, 2.5, 1.2, and 0.6, 0.3, 0.15 µg/mL. Kanamycin was used as the positive control.

Negative control wells were treated with DMSO instead of the test compound, and blank control wells contain LB medium only. The plates were incubated at 37 °C for 7 hrs. Finally, 10 μL of CCK-8 solution from the Cell Counting Kit-8 (Dojindo, Shanghai, China) was added to each well and incubated at 37 °C for an additional 1.5 hrs. The absorbance at 450 nm was measured on a FlexStation 3 microplate reader (Molecular Devices, San Jose, CA, USA). MIC values were defined as the lowest concentrations of the test compounds that inhibited bacterial growth.

Antifungal activity was evaluated against two fungal panthogens of high medical relevance, *Cryptococcus neoformans* H99 and *Candida albicans* SC5314 as described previously with slight modifications.[20] Briefly, the MIC was determined with the serial microdilution method in 96-well plates with MOPS buffered RPMI-1640 as the growth medium. The cell suspension was incubated with serial dilutions of various xylomyrocins at a dose range of 20–0.15 μg/mL. Amphotericin B and pneumocandin B_0 were used as positive controls. Cells were incubated at 25 °C (mimicking the enviromental condition) and 37 °C (mimicking the host condition), and 10 μL of CCK-8 were added into each well at 24 hrs for *C. albicans*, and at 48 hrs for *C. neoformans*. Viability was determined with a FlexStation 3 microplate reader (Molecular Devices, San Jose, CA, USA). MIC value was defined as the lowest concentration of the test compound that resulted in a culture with unchanged density (100% inhibition when compared to the growth of the untreated control).

2. SI Tables

Table S1. Taxonomic information on the 182 fungal isolates identified by MALDI-TOF MS to produce peptide-like SMs

Genera	Number of strains		Genera	Number of strains
Acremonium	4		*Lecanicillium*	1
Alternaria	2		*Leptosphaeria*	2
Aspergillus	13		*Mortierella*	8
Auxarthron	1		*Mucor*	1
Beauveria	1		*Myceliophthora*	1
Bionectria	4		*Myrothecium*	5
Camarosporium	1		*Paecilomyces*	1
Cladosporium	1		*Paramyrothecium*	1
Chrysosporium	1		*Penicillium*	13
Clonostachys	9		*Phaeosphaeria*	1
Colletotrichum	1		*Purpureocillium*	11
Coniothyrium	1		*Scopulariopsis*	1
Cordyceps	5		*Scytalidium*	1
Doratomyces	1		*Stachybotrys*	1
Fusarium	59		*Tolypocladium*	1
Gibberella	4		*Trichoderma*	23
Keissleriella	1		*Wojnowiciella*	1

Table S2. ^{1}H NMR and ^{13}C NMR data

Table S2.1. Compounds 1–3[a]

no.	1		2		3	
	δ_C, type	δ_H, mult. *J* in Hz	δ_C, type	δ_H, mult. *J* in Hz	δ_C, type	δ_H, mult. *J* in Hz
Xyl$_1$						
C=O	170.47, C		174.90, C		174.56, C	
α	76.60, CH	5.08, d 2.0	71.60, CH	4.02, m[b]	72.14, CH	4.15, d 2.0
β	73.43, CH	4.04, m[b]	68.70, CH	4.01, m[b]	74.79, CH	3.91, dd 6.5, 2.0
γ	73.62, CH	3.65, m	78.02, CH	4.84, m	70.69, CH	4.02, m
δ	64.18, CH_2	3.55, dd 11.4, 5.2	60.53, CH_2	3.86, dd 12.2, 3.9	66.61, CH_2	4.41, m[b]
		3.49, m[b]		3.78, dd 12.2, 7.6		4.09, dd 11.5, 4.5
Leu$_2$						
NH						
C=O	175.37, C		175.95, C		176.10, C	
α	48.93, CH	5.11, m[b]	49.57, CH	5.02, m[b]	49.07, CH	5.05, m[b]
β	41.92, CH_2	1.90, m	42.56, CH_2	1.64, m	42.63, CH_2	1.60, m
		1.30, m		1.46, m		1.49, m
γ	25.63, CH	1.74, m	25.92, CH	1.75, m	26.05, CH	1.68, m
δ	23.65, CH_3	0.93, m[b]	24.11, CH_3	0.94, m[b]	23.63, CH_3	0.93, m[b]
δ'	21.79, CH_3	0.96, m[b]	22.28, CH_3	0.96, m[b]	22.36, CH_3	0.96, m[b]
MeThr$_3$						
N-CH_3	31.37, CH_3	3.28, s	31.71, CH_3	3.32, s	32.37, CH_3	3.39, s
C=O	171.51, C		171.61, C		171.69, C	
α	62.91, CH	5.45, d 9.9	63.55, CH	5.45, d 9.7	62.91, CH	5.57, d 9.1
β	64.94, CH	4.10, m	65.27, CH	4.08, m	65.98, CH	4.07, m
γ	20.50, CH_3	1.02, d 6.2	20.28, CH_3	1.03, d 6.3	20.05, CH_3	1.01, d 6.2
Val$_4$						
NH						
C=O	173.48, C		173.38, C		173.52, C	
α	54.91, CH	4.66, d 7.8	54.81, CH	4.67, d 7.3	54.84, CH	4.67, d 7.6
β	32.51, CH	2.01, m	32.63, CH	2.01, m	32.51, CH	2.01, m
γ	20.23, CH_3	0.90, m[b]	20.22, CH_3	0.90, m[b]	20.24, CH_3	0.92, m[b]
γ'	18.75, CH_3	0.91, m[b]	18.37, CH_3	0.91, m[b]	18.55, CH_3	0.91, m[b]
MePhe$_5$						
N-CH_3	40.34, CH_3	2.85, s	40.31, CH_3	2.84, s	40.39, CH_3	2.84, s
C=O	172.52, C		172.54, C		172.54, C	
α	68.74, CH	4.02, m[b]	71.06, CH	4.04, m[b]	68.69, CH	4.04, m[b]
β	35.41, CH_2	3.48, m[b]	35.39, CH_2	3.47, m[b]	35.38, CH_2	3.47, m[b]
		3.21, dd 13.4, 11.0		3.22, dd 13.8, 11.2		3.22, dd 13.8, 11.0
1'	139.70, C		139.67, C		139.64, C	
2'	130.50, CH	7.25, m[b]	130.49, CH	7.25, m[b]	130.50, CH	7.25, m[b]
3'	129.67, CH	7.30, m[b]	129.67, CH	7.30, m[b]	129.67, CH	7.30, m[b]
4'	127.82, CH	7.23, m[b]	127.84, CH	7.23, m[b]	127.84, CH	7.23, m[b]
5'	129.67, CH	7.30, m[b]	129.67, CH	7.30, m[b]	129.67, CH	7.30, m[b]
6'	130.50, CH	7.25, m[b]	130.50, CH	7.25, m[b]	130.50, CH	7.25, m[b]
Gly$_6$						
NH						
C=O	171.18, C		171.16, C		171.20, C	
α	44.21, CH_2	4.05, m[b]	44.24, CH_2	4.02, m[b]	44.15, CH_2	4.03, m[b]
		3.44, m[b]		3.48, m[b]		3.48, m[b]
Ile$_7$						
NH						
C=O	173.32, C		173.06, C		173.37, C	
α	58.03, CH	4.49, d 8.0	58.19, CH	4.46, d 8.3	58.19, CH	4.42, m[b]
β	39.27, CH	2.08, m	39.04, CH	2.03, m	38.60, CH	2.08, m
γ	25.62, CH_2	1.65, m	25.65, CH_2	1.67, m	25.76, CH_2	1.67, m

		1.32, m		1.28, m		1.27, m
δ	11.45, CH_3	0.93, m[b]	11.35, CH_3	0.93, m[b]	11.16, CH_3	0.93, m[b]
γ'	16.16, CH_3	0.98, m[b]	15.97, CH_3	0.95, m[b]	15.90, CH_3	0.96, m[b]
Ser_8						
NH						
C=O	172.22, C		172.54, C		171.99, C	
α	56.45, CH	4.93, t 7.3	56.36, CH	5.01, m[b]	56.94, CH	4.92, dd 7.9, 5.7
β	62.32, CH_2	3.75, dd 11.1, 7.2	62.60, CH_2	3.69, dd 11.5, 5.8	62.71, CH_2	3.66, dd 11.3, 5.7
		3.67, dd 10.3, 7.2		3.57, dd 11.4, 7.9		3.60, m[b]
Leu_9						
NH						
C=O	173.94, C		175.54, C		174.65, C	
α	48.39, CH	5.13, m[b]	49.39, CH	5.17, dd 10.7, 3.1	49.57, CH	5.06, m[b]
β	43.48, CH_2	1.74, m	43.53, CH_2	1.72, m	42.79, CH_2	1.72, m
		1.53, m		1.49, m		1.49, m
γ	25.82, CH	1.63, m	25.61, CH	1.79, m	25.76, CH	1.82, m
δ	23.42, CH_3	0.96, m[b]	23.75, CH_3	0.94, m[b]	24.06, CH_3	0.93, m[b]
δ'	23.17, CH_3	0.96, m[b]	22.13, CH_3	0.99, m[b]	21.79, CH_3	0.96, m[b]
$MeVal_{10}$						
N-CH_3	40.77, CH_3	3.34, s	37.80, CH_3	3.33, s	39.28, CH_3	3.29, s
C=O	170.65, C		171.39, C		171.87, C	
α	70.77, CH	3.51, d 8.2	69.08, CH	3.74, d 7.4	71.18, CH	3.59, m[b]
β	30.26, CH	2.56, m	29.83. CH	2.44, m	28.79, CH	2.61, m
γ	21.91, CH_3	1.16, d 6.2	20.90, CH_3	1.12, d 6.5	21.87, CH_3	1.13, d 6.5
γ'	19.70, CH_3	0.94, m[b]	20.28, CH_3	1.02, m[b]	19.85, CH_3	0.92, m[b]

[a] ^1H and ^{13}C NMR spectra were recorded at 600 and 150 MHz, respectively; methanol-d_4 was used as solvent.

[b] Multiplicity due to overlapping.

Table S2.2. Compounds 4, 23a, and 23b[a]

no.	4		23a		23b	
	δ_C, type	δ_H, mult. *J* in Hz	δ_C, type	δ_H, mult. *J* in Hz	δ_C, type	δ_H, mult. *J* in Hz
Xyl$_1$						
C=O	175.83, C	-	174.88, C	-	175.18, C	-
α	74.09, CH	4.05, brs	73.93, CH	4.23, d 2.5	73.94, CH	4.25, d 2.6
β	76.54, CH	5.14, m[b]	73.09, CH	3.89, dd 4.2, 2.5	73.24, CH	3.93, d 4.6, 2.6
γ	73.54, CH	3.71, m	74.10, CH	3.79, m	74.11, CH	3.82, m
δ	61.21, CH_2	3.74, m[b]	63.96, CH_2	3.66, dd 11.2, 4.8	63.96, CH_2	3.68, m[b]
		3.66, m[b]		3.62, m[b]		3.63, m[b]
α-OH	-	5.92, brs	-	-	-	-
β-OH	-	-	-	-	-	-
γ-OH	-	5.16, brs	-	-	-	-
δ-OH	-	5.47, t 6.3	-	-	-	-
Leu$_2$						
NH	-	7.34, brs	-	-	-	-
C=O	175.50, C	-	175.11, C	-	176.02, C	-
α	51.72, CH	4.74, m[b]	49.18, CH	5.01, m[b]	48.88, CH	5.04, m[b]
β	40.18, CH_2	1.52, m	42.65, CH_2	1.59, m	41.35, CH_2	1.75, m
				1.49, m		1.64, m
γ	26.51, CH	1.81, m	25.96, CH	1.70, m	25.96, CH	1.75, m
δ	23.61, CH_3	0.99, d 6.6	23.75, CH_3	0.96, m[b]	23.75, CH_3	0.96, m[b]
δ'	21.06, CH_3	1.02, m[b]	22.09, CH_3	1.00, d 6.7	22.09, CH_3	0.96, m[b]
MeThr$_3$						
N-CH_3	32.39, CH_3	3.30, s	32.43, CH_3	3.21, s	30.15, CH_3	2.84, s
C=O	171.96, C	-	171.61, C	-	170.98, C	-
α	64.98, CH	5.03, m[b]	63.79, CH	4.84, m[b]	67.09, CH	4.64, m[b]
β	65.54, CH	4.21, m	65.46, CH	4.21, m	64.18, CH	4.16, m
γ	21.22, CH_3	1.19, d 6.2	20.60, CH_3	1.14, d 6.2	21.13, CH_3	1.19, d 6.2
Ile$_4$						
NH	-	8.23, d 9.5	-	-	-	-
C=O	173.57, C	-	174.80, C	-	174.76, C	-
α	54.45, CH	4.74, m[b]	54.64, CH	4.65, m[b]	54.85, CH	4.66, m[b]
β	37.46, CH	1.82, m	38.10, CH	1.88, m	37.37, CH	2.02, m
γ	24.81, CH_2	1.38, m	25.96, CH_2	1.55, m	26.00, CH_2	1.54, m
		1.05, m		1.19, m		1.20, m
δ	10.79, CH_3	0.77, t 7.8	11.08, CH_3	0.89, m[b]	10.73, CH_3	0.86, m[b]
γ'	15.99, CH_3	0.86, m[b]	15.46, CH_3	0.88, m[b]	15.28, CH_3	0.87, m[b]
MeVal$_5$						
N-CH_3	42.05, CH_3	3.37, s	31.61, CH_3	3.21, s	31.75, CH_3	3.24, s
C=O	172.01, C	-	172.34, C	-	172.34, C	-
α	75.43, CH	3.24, d 11.5	63.00, CH	4.77, m[b]	62.90, CH	4.79, m[b]
β	27.28, CH	2.81, m	27.89, CH	2.21, m	27.75, CH	2.21, m
γ	21.63, CH_3	1.09, d 6.1	22.27, CH_3	0.94, m[b]	22.27, CH_3	0.94, m[b]
γ'	19.64, CH_3	0.99, d 6.0	19.05, CH_3	0.80, m[b]	19.05, CH_3	0.80, m[b]
Leu$_6$						
NH	-	7.86, d 8.8	-	-	-	-
C=O	174.32, C	-	174.93, C	-	174.80, C	-
α	49.18, CH	4.33, m	50.04, CH	4.72, m[b]	49.86, CH	4.75, m[b]
β	40.61, CH_2	1.81, m	41.14, CH_2	1.63, m	41.19, CH_2	1.62, m
				1.29, m		1.32, m
γ	26.15, CH	1.63, m	26.00, CH	1.68, m	25.96, CH	1.62, m
δ	23.71, CH_3	0.95, d 6.5	23.60, CH_3	0.95, m[b]	23.56, CH_3	0.93, m[b]
δ'	21.06, CH_3	0.92, d 6.5	21.56, CH_3	0.92, m[b]	21.50, CH_3	0.93, m[b]
Gln$_7$/Me Gln$_7$						
NH/*N*-	-	8.42, d 8.0	30.66, CH_3	3.04, s	30.83, CH_3	3.06, s

CH_3						
C=O	173.65, C	-	172.50, C	-	171.40, C	-
α	50.56, CH	4.86, m	54.12, CH	5.52, m[b]	54.03, CH	5.47, m[b]
β	28.32, CH_2	2.19, m	25.42, CH_2	2.16, m	25.83, CH_2	1.99, m
		2.00, m		2.04, m		
γ	32.07, CH_2	2.44, m	32.03, CH_2	2.17, m	32.10, CH_2	2.13, m
$CONH_2$	177.51, C	7.32, brs	177.57, C	-	177.72, C	-
		6.84, brs				
MeLeu$_8$						
N-CH_3	31.06, CH_3	3.05, s	31.10, CH_3	2.95, s	30.47, CH_3	2.77, s
C=O	172.38	-	173.37, C	-	172.44, C	-
α	53.63, CH	5.69, brs	52.94, CH	5.50, m[b]	52.87, CH	5.53, m[b]
β	39.22, CH_2	2.01, m	38.52, CH_2	1.68, m	39.33, CH_2	1.60, m
		1.16, m		1.53, m		
γ	26.01, CH	1.48, m	26.00, CH	1.38, m	25.50, CH	1.33, m
δ	24.08, CH_3	0.87, m[b]	22.71, CH_3	0.94, m[b]	22.28, CH_3	0.93, m[b]
δ'	22.90, CH_3	0.81, d 6.8	19.71, CH_3	0.94, m[b]	19.82, CH_3	0.93, m[b]
MeVal$_9$						
N-CH_3	31.06, CH_3	2.90, s	32.99, CH_3	3.05, s	30.15, CH_3	2.82, s
C=O	170.62	-	172.34, C	-	171.50, C	-
α	63.33, CH	4.95, m[b]	64.53, CH	4.58, d 2.4	65.75, CH	4.19, d 2.5
β	27.11, CH	2.24, m	28.91, CH	2.29, m	28.58, CH	2.28, m
γ	20.17, CH_3	1.04, m[b]	20.45, CH_3	1.02, d 6.6	21.92, CH_3	1.00, d 6.5
γ'	18.87, CH_3	0.85, m[b]	19.45, CH_3	0.85, d 6.6	19.05, CH_3	0.91, m[b]
OCH_3	-	-	52.39, CH_3	3.70, s	53.05, CH_3	3.77, s

[a] ^1H and ^{13}C NMR spectra were recorded at 600 and 150 MHz, respectively; CD_3OH was used as solvent for **4**, and methanol-d_4 was used as solvent for **23a** and **23b**.

[b] Multiplicity due to overlapping.

Table S2.3. Compounds 5–7[a]

no.	5		6		7	
	δ_C, type	δ_H, mult. *J* in Hz	δ_C, type	δ_H, mult. *J* in Hz	δ_C, type	δ_H, mult. *J* in Hz
Xyl$_1$						
C=O	167.44, C	-	167.48, C	-	167.49, C	-
α	74.72, CH	5.01, brs	74.85, CH	4.99, brs	74.75, CH	5.01, brs
β	70.96, CH	3.89, m[b]	71.07, CH	3.88, brs	70.93, CH	3.89, m[b]
γ	72.23, CH	3.47, m	72.21, CH	3.46, m	72.26, CH	3.47, m
δ	62.62, CH_2	3.38, m[b]	62.64, CH_2	3.37, m[b]	62.62, CH_2	3.38, m[b]
		3.24, m[b]		3.24, m[b]		3.24, m[b]
Leu$_2$						
NH	-	7.56, d 9.4	-	7.58, d 9.5	-	7.55, d 9.4
C=O	172.75, C	-	172.78, C	-	172.72, C	-
α	46.47, CH	5.01, m[b]	46.34, CH	5.03, m[b]	46.43, CH	5.02, m[b]
β	40.96, CH_2	1.65, m	41.17, CH_2	1.62, m	41.08, CH_2	1.70, m
		1.17, m		1.22, m		1.14, m
γ	24.04, CH	1.61, m	23.70, CH	1.58, m	23.66, CH	1.61, m
δ	23.18, CH_3	0.83, m[b]	23.15, CH_3	0.82, m[b]	23.27, CH_3	0.84, m[b]
δ'	21.34, CH_3	0.87, m[b]	21.57, CH_3	0.86, m[b]	21.27, CH_3	0.88, m[b]
MeThr$_3$						
N-CH_3	30.57, CH_3	3.16, s	30.61, CH_3	3.16, s	30.46, CH_3	3.14, s
C=O	168.74, C	-	168.87, C	-	168.69, C	-
α	61.66, CH	5.09, m[b]	61.56, CH	5.14, d, 10.0	61.47, CH	5.11, d 10.0
β	62.96, CH	3.90, m	63.00, CH	3.89, m	62.85, CH	3.90, m
γ	20.40, CH_3	0.90, m[b]	20.20, CH_3	0.88, m[b]	20.28, CH_3	0.88, m[b]
Val$_4$/Ile$_4$						
NH	-	8.74, d 9.4	-	8.70, d 9.4	-	8.68, d 9.6
C=O	171.48, C	-	171.40, C	-	171.65, C	-
α	52.81, CH	4.50, m[b]	52.73, CH	4.51, m[b]	51.37, CH	4.60, m[b]
β	30.64, CH	1.89, m	30.61, CH	1.86, m	36.41, CH	1.72, m
γ	19.40, CH_3	0.78, m[b]	19.48, CH_3	0.76, m[b]	23.27, CH_2	1.39, m
						1.00, m
δ	-	-	-	-	10.00, CH_3	0.71, m[b]
γ'	17.52, CH_3	0.73, d 6.2	17.32, CH_3	0.75, m[b]	15.28, CH_3	0.73, m[b]
MePhe$_5$						
N-CH_3	39.44, CH_3	2.77, s	39.35, CH_3	2.75, s	39.58, CH_3	2.81, s
C=O	169.77, C	-	169.85, C	-	169.90, C	-
α	66.60, CH	3.93, m[b]	66.56, CH	3.93, m[b]	66.61, CH	3.96, m[b]
β	33.96, CH_2	3.38, m[b]	33.97, CH_2	3.36, m[b]	33.98, CH_2	3.38, m[b]
		3.01, m[b]		3.01, m[b]		3.01, m[b]
1'	138.91, C	-	138.92, C	-	138.95, C	-
2'	128.23, CH	7.27, m[b]	128.24, CH	7.27, m[b]	128.23, CH	7.27, m[b]
3'	129.20, CH	7.24, m[b]	129.22, CH	7.21, m[b]	129.23, CH	7.24, m[b]
4'	126.29, CH	7.21, m[b]	126.30, CH	7.21, m[b]	126.27, CH	7.21, m[b]
5'	129.20, CH	7.24, m[b]	129.22, CH	7.21, m[b]	129.23, CH	7.24, m[b]
6'	128.23, CH	7.27, m[b]	128.24, CH	7.27, m[b]	128.23, CH	7.27, m[b]
Gly$_6$						
NH	-	7.77, t 5.8	-	7.85, m	-	7.83, t 5.4
C=O	167.63, C	-	167.67, C	-	167.59, C	-
α	43.05, CH_2	3.79, m[b]	43.04, CH_2	3.78, dd 16.5, 5.5	43.09, CH_2	3.77, dd 17.0, 5.3
		3.19, m[b]		3.17, m[b]		3.16, m[b]
Ile$_7$						
NH	-	7.45, d 9.8	-	7.47, d 9.7	-	7.42, d 9.9
C=O	171.69, C	-	171.49, C	-	171.46, C	-
α	54.97, CH	4.47, m[b]	55.09, CH	4.48, m[b]	54.94, CH	4.47, m[b]
β	36.98, CH	1.82, m	37.71, CH	1.81, m	37.54, CH	1.82, m
γ	23.89, CH_2	1.49, m	23.66, CH_2	1.51, m	23.74, CH_2	1.49, m

				1.16, m		1.18, m
δ	10.61, CH_3	0.78, m[b]	10.77, CH_3	0.78, m[b]	10.56, CH_3	0.77, m[b]
γ'	15.04, CH_3	0.82, m[b]	14.99, CH_3	0.82, m[b]	15.02, CH_3	0.81, m[b]
Ser_8						
NH	-	8.56, d 7.2	-	8.60, d 7.5	-	8.58, d 7.3
C=O	169.87, C	-	169.80, C		169.85, C	-
α	51.20, CH	4.68, m[b]	55.16, CH	4.79, m[b]	55.37, CH	4.72, m[b]
β	60.46, CH_2	3.57, m[b]	60.48, CH_2	3.56, m[b]	60.40, CH_2	3.56, m[b]
		3.49, m[b]		3.46, m[b]		3.48, m[b]
Val_9/Ile_9						
NH	-	8.91, d 9.5	-	8.85, d 9.4	-	8.94, d 9.7
C=O	171.48, C	-	171.67, C	-	171.65, C	-
α	53.25, CH	4.55, m[b]	51.67, CH	4.65, m[b]	53.24, CH	4.56, m[b]
β	31.01, CH	2.03, m	37.16, CH	1.84, m	31.01, CH	2.02, m
γ	18.96, CH_3	0.81, m[b]	23.62, CH_2	1.54, m	18.98, CH_3	0.80, m[b]
				1.03, m		
δ			10.62, CH_3	0.77, m[b]	-	-
γ'	18.18, CH_3	0.84, m[b]	14.76, CH_3	0.77, m[b]	18.09, CH_3	0.84, d 6.4
$MeAla_{10}$						
N-CH_3	37.33, CH_3	3.19, s	37.48, CH_3	3.20, s	37.33, CH_3	3.19, s
C=O	170.17, C	-	170.17, C	-	170.19, C	-
α	58.55, CH	3.91, m	58.59, CH	3.91, m[b]	58.56, CH	3.91, m[b]
β	13.53, CH_3	1.33, d 6.2	13.44, CH_3	1.33, d 6.3	13.53, CH_3	1.33, d 6.2

[a] ^1H and ^{13}C NMR spectra were recorded at 600 and 150 MHz, respectively; DMSO-d_6 was used as solvent.

[b] Multiplicity due to overlapping.

Table S2.4. Compounds 8–10[a]

no.	8		9		10	
	δ_C, type	δ_H, mult. *J* in Hz	δ_C, type	δ_H, mult. *J* in Hz	δ_C, type	δ_H, mult. *J* in Hz
Xyl$_1$						
C=O	167.48, C	-	171.44, C	-	171.57, C	-
α	74.91, CH	4.98, brs	70.78, CH	3.87, brs	70.69, CH	3.89, m[b]
β	71.09, CH	3.89, brs	72.69, CH	3.68, brs	72.77, CH	3.68, m[b]
γ	72.19, CH	3.47, m	69.77, CH	3.74, m	69.77, CH	3.76, m
δ	62.65, CH_2	3.38, m[b]	64.77, CH_2	4.55, m[b]	64.75, CH_2	4.58, m[b]
		3.24, m[b]		3.75, m[b]		3.76, m[b]
Leu$_2$						
NH	-	7.61, d 8.7	-	7.74, d 8.8	-	7.74, d 8.8
C=O	172.71, C	-	173.60, C	-	173.62, C	-
α	46.36, CH	5.03, m[b]	46.49, CH	5.06, m[b]	46.50, CH	5.07, m[b]
β	41.30, CH_2	1.67, m	41.44, CH_2	1.45, m	41.41, CH_2	1.50, m
		1.21, m		1.28, m		1.30, m
γ	23.66, CH	1.61, m	24.02, CH	1.59, m	23.67, CH	1.61, m
δ	23.27, CH_3	0.84, m[b]	23.06, CH_3	0.81, m[b]	21.72, CH_3	0.86, m[b]
δ'	20.10, CH_3	0.88, m[b]	21.70, CH_3	0.83, m[b]	21.34, CH_3	0.86, m[b]
MeThr$_3$						
N-CH_3	30.46, CH_3	3.15, s	31.13, CH_3	3.24, s	31.07, CH_3	3.25, s
C=O	168.55, C	-	168.93, C	-	168.74, C	-
α	61.38, CH	5.16, d 9.7	60.99, CH	5.31, d 9.0	60.84, CH	5.34, d 9.2
β	62.88, CH	3.90, m	63.57, CH	3.86, m	63.55, CH	3.86, m
γ	21.51, CH_3	0.88, m[b]	19.90, CH_3	0.86, m[b]	19.76, CH_3	0.88, d 6.3
Val$_4$/Ile$_4$						
NH	-	8.64, d 9.1	-	8.53, d 9.3	-	8.48, d 9.4
C=O	171.51, C	-	171.53, C	-	171.53, C	-
α	51.37, CH	4.60, t 8.1	52.41, CH	4.58, m[b]	55.38, CH	4.69, m[b]
β	36.54, CH	1.70, m	30.77, CH	1.77, m	36.75, CH	1.61, m
γ	23.18, CH_2	1.40, m	19.41, CH_3	0.76, m[b]	23.08, CH	1.42, m
		1.01, m				1.02, m
δ	10.68, CH_3	0.79, m[b]	-	-	10.55, CH_3	0.74, m[b]
γ'	15.40, CH_3	0.73, m[b]	17.21, CH_3	0.76, m[b]	15.33, CH_3	0.75, m[b]
MePhe$_5$						
N-CH_3	39.53, CH_3	2.79, s	39.33, CH_3	2.74, s	39.44, CH_3	2.78, s
C=O	169.86, C	-	169.71, C	-	169.62, C	-
α	66.61, CH	3.96, m[b]	66.39, CH	3.97, m[b]	66.41, CH	4.01, m[b]
β	62.65, CH_2	3.38, m[b]	33.98, CH_2	3.38, m[b]	33.96, CH_2	3.38, m[b]
		3.24, m[b]		3.01, m[b]		3.01, m[b]
1'	138.95, C	-	138.87, C	-	138.87, C	-
2'	128.23, CH	7.27, m[b]	128.23, CH	7.27, m[b]	128.23, CH	7.27, m[b]
3'	129.23, CH	7.24, m[b]	129.20, CH	7.24, m[b]	129.20, CH	7.24, m[b]
4'	126.27, CH	7.21, m[b]	126.29, CH	7.21, m[b]	126.29, CH	7.21, m[b]
5'	129.23, CH	7.24, m[b]	129.20, CH	7.24, m[b]	129.20, CH	7.24, m[b]
6'	128.23, CH	7.27, m[b]	128.23, CH	7.27, m[b]	128.23, CH	7.27, m[b]
Gly$_6$						
NH	-	7.88, brs	-	7.98, brs	-	8.02, t 5.5
C=O	167.63, C	-	167.70, C	-	167.68, C	-
α	43.12, CH_2	3.77, dd 16.8, 4.8	43.03, CH_2	3.77, m[b]	43.05, CH_2	3.77, m[b]
		3.16, m[b]		3.19, m[b]		3.19, m[b]
Ile$_7$						
NH	-	7.45, d 9.8	-	7.52, d 9.5	-	7.52, d 9.7
C=O	171.45, C	-	171.66, C	-	171.69, C	-
α	55.11, CH	4.47, m[b]	55.24, CH	4.43, m[b]	55.26, CH	4.44, m[b]
β	37.62, CH	1.80, m	37.35, CH	1.80, m	37.56, CH	1.82, m
γ	23.74, CH_2	1.51, m	23.87, CH_2	1.50, m	23.74, CH_2	1.49, m

		1.16, m		1.13, m		1.18, m
δ	10.22, CH_3	0.72, m[b]	10.60, CH_3	0.77, m[b]	10.97, CH_3	0.78, m[b]
γ'	14.99, CH_3	0.83, m[b]	14.97, CH_3	0.81, m[b]	14.99, CH_3	0.82, m[b]
Ser_8					-	-
NH	-	8.59, d 7.0	-	8.62, d 7.5	-	8.65, d 7.6
C=O	169.73, C	-	169.66, C	-	168.95, C	-
α	55.10, CH	4.85, m[b]	55.33, CH	4.85, m[b]	55.26, CH	4.89, m[b]
β	60.47, CH_2	3.56, m[b]	61.00, CH_2	3.44, m[b]	61.05, CH_2	3.46, m[b]
		3.48, m[b]		3.41, m[b]		3.42, m[b]
Val_9/Ile_9						
NH	-	8.85, d 9.1	-	8.71, d 8.9	-	8.72, d 8.8
C=O	171.63, C	-	171.60, C	-	171.48, C	-
α	51.53, CH	4.67, t 9.2	52.14, CH	4.84, m[b]	51.96, CH	4.84, m[b]
β	37.24, CH	1.82, m	36.98, CH	1.80, m	37.24, CH	1.82, m
γ	23.71, CH_2	1.51, m	23.25, CH_2	1.33, m	23.08, CH_2	1.37, m
		1.05, m		1.14, m		1.18, m
δ	10.68, CH_3	0.79, m[b]	11.07, CH_3	0.73, m[b]	10.42, CH_3	0.74, m[b]
γ'	14.76, CH_3	0.78, m[b]	14.97, CH_3	0.81, m[b]	14.95, CH_3	0.85, m[b]
$MeAla_{10}$						
N-CH_3	37.51, CH_3	3.21, s	38.11, CH_3	3.19, s	38.06, CH_3	3.21, s
C=O	170.18, C	-	169.82, C	-	169.70, C	-
α	58.58, CH	3.93, m[b]	58.80, CH	3.99, m[b]	58.77, CH	4.02, m[b]
β	13.47, CH_3	1.33, d 6.0	13.07, CH_3	1.36, d 6.3	13.10, CH_3	1.38, d 6.2

[a] ^1H and ^{13}C NMR spectra were recorded at 600 and 150 MHz, respectively; DMSO-d_6 was used as solvent.

[b] Multiplicity due to overlapping.

Table S2.5. Compounds 11 and 12[a]

no.	11		12	
	δ_C, type	δ_H, mult. *J* in Hz	δ_C, type	δ_H, mult. *J* in Hz
Xyl$_1$				
C=O	167.66, C	-	n.a.[b]	-
α	75.09, CH	4.99, brs	70.76, CH	4.11, brs
β	71.14, CH	3.87, m[c]	70.39, CH	4.09, m[c]
γ	72.03, CH	3.48, m	76.53, CH	5.00, m
δ	62.75, CH_2	3.35, m[c]	59.29, CH_2	3.58, m[c]
		3.28, m[c]		
α-OH	-	-	-	5.84, brs
β-OH	-	4.30, brs	-	5.34, brs
γ-OH	-	4.69, m[c]	-	-
δ-OH	-	4.51, m[c]	-	5.00, m[c]
Val$_2$				
NH	-	7.41, d 9.3	-	7.60, d 9.8
C=O	172.79, C	-	171.65, C	-
α	53.20, CH	4.80, m[c]	53.20, CH	4.75, m[c]
β	30.93, CH	2.10, m	30.97, CH	2.14, m
γ	18.40, CH_3	0.80, m[c]	18.76, CH_3	0.82, m[c]
γ'	18.05, CH_3	0.84, m[c]	18.17, CH_3	0.82, m[c]
MeThr$_3$				
N-CH_3	39.04, CH_3	3.25, s	28.62, CH_3	2.67, s
C=O	168.94, C	-	n.a.[b]	-
α	62.23, CH	5.07, m[c]	64.24, CH	4.27, m[c]
β	63.34, CH	3.89, m	62.11, CH	4.00, m
γ	20.05, CH_3	0.84, m[c]	20.27, CH_3	1.03, d 6.3
Ile$_4$				
NH	-	8.84, d 9.8	-	7.42, d 9.3
C=O	171.61, C	-	172.90, C	-
α	52.51, CH	4.50, t 9.7	51.62, CH	4.62, m[c]
β	35.27, CH	1.88, m	34.76, CH	1.76, m
γ	23.68, CH_2	1.42, m	23.36, CH_2	1.44, m
		1.03, m		1.04, m
δ	10.51, CH_3	0.72, t 7.5	11.05, CH_3	0.75, m[c]
γ'	15.76, CH_3	0.79, m[c]	15.26, CH_3	0.84, m[c]
MeVal$_5$				
N-CH_3	41.12, CH_3	3.23, s	30.11, CH_3	3.02, s
C=O	168.65, C	-	n.a.[b]	-
α	75.33, CH	3.20, m[c]	61.17, CH	4.83, m[c]
β	25.68, CH	2.84, m	25.97, CH	2.17, m
γ	20.45, CH_3	0.98, d 6.5	19.39, CH_3	0.82, m[c]
γ'	18.85, CH_3	0.89, m[c]	17.46, CH_3	0.65, d 6.4
Val$_6$				
NH	-	7.32, d 9.5	-	7.34, d 9.6
C=O	169.32, C	-	n.a.[b]	-
α	57.13, CH	4.30, m[c]	56.26, CH	4.52, m[c]
β	29.78, CH	2.45, m	31.41, CH	2.12, m
γ	19.74, CH_3	0.84, m[c]	19.56, CH_3	0.90, m[c]
γ'	16.85, CH_3	0.79, m[c]	17.81, CH_3	0.78, m[c]
Ile$_7$				
NH	-	7.37, d 9.2	-	8.36, d 9.6
C=O	170.86, C	-	n.a.[b]	-
α	55.33, CH	4.70, m[c]	52.56, CH	4.81, m[c]
β	38.35, CH	1.70, m	37.06, CH	1.77, m
γ	23.93, CH_2	1.49, m	24.15, CH_2	1.42, m
		1.20, m		1.03, m

δ	11.18, CH_3	0.79, m[c]	10.99, CH_3	0.80, m[c]
γ'	14.88, CH_3	0.85, m[c]	15.21, CH_3	0.86, m[c]
Ser$_8$				
NH	-	8.70, d 8.7	-	7.78, d 8.0
C=O	169.49, C	-	n.a.[b]	-
α	54.62, CH	5.03, m[c]	62.30, CH	3.99, m[c]
β	61.06, CH_2	3.52, m[c]	60.53, CH_2	3.85, m[c]
		3.36, m[c]		3.64, m[c]
Ile$_9$				
NH	-	8.56, d 9.3	-	7.58, d 9.6
C=O	172.07, C	-	170.98, C	-
α	51.62, CH	4.69, m[c]	52.15, CH	4.58, m[c]
β	37.45, CH	1.76, m	35.18, CH	1.76, m
γ	23.65, CH_2	1.42, m	23.36, CH_2	1.49, m
		1.03, m		1.07, m
δ	10.68, CH_3	0.76, m[c]	10.46, CH_3	0.73, m[c]
γ'	14.83, CH_3	0.76, m[c]	15.53, CH_3	0.82, m[c]
MeLeu$_{10}$				
N-CH_3	31.45, CH_3	3.26, s	30.62, CH_3	2.90, s
C=O	170.14, C	-	n.a.[b]	-
α	61.67, CH	3.87, m[c]	53.37, CH	5.57, m[c]
β	37.45, CH_2	1.85, m	37.14, CH_2	1.74, m
		1.70, m		
γ	24.48, CH	1.58, m	24.45, CH	1.50, m
δ	23.33, CH_3	0.88, m[c]	22.09, CH_3	0.86, m[c]
δ'	21.54, CH_3	0.93, d 6.4	21.79, CH_3	0.90, m[c]

[a] ^1H and ^{13}C NMR spectra were recorded at 600 and 150 MHz, respectively; DMSO-d_6 was used as solvent.

[b] n.a. not assigned.

[c] Muliplicity due to overlapping.

Table S3. Genome assembly statistics for *Paramyrothecium* sp. XJ0827

Illumina Total Data [Mb]	Expected coverage of the genome	GC %	Q20[a]	Q30[a]
5,998	115x	50.82	96.54	90.93

Nanopore Total Data (Mb)	Expected coverage of the genome	Subreads N50 Length (bp)	Subreads N90 Length (bp)	Subreads Average Length (bp)	Subreads Max Length (bp)	Subreads Min Length (bp)	Subreads GC Content (%)
20,095	388x	11,574	2,968	7,197.72	170,586	2,000	51.18

Hybrid Assembly Scaffold Number	Total Length (bp)	N50 Length (bp)	N90 Length (bp)	Max Length (bp)	Min Length (bp)	Gap Number (bp)	GC Content (%)
15	51,769,651	4,590,572	2,170,085	6,525,119	54,848	0	51.23

[a] Percent of total data with base calling accuracy quality score of Q20 and Q30 (probability of a call error for each base is less than 1 % and 1 ‰, respectively).

Table S4. Summary of BGC types in *Paramyrothecium* sp. XJ0827

BGC types[a]	Number
PKS	41
NRPS	11
NRPS-like	15
PKS-NRPS hybrid	15
Terpenoid	9
Meroterpenoid	2
Others	5
Total	98

[a] As defined by antiSMASH 5.0[21]

Table S5. Predicted NRPSs encoded in the *Paramyrothecium* sp. XJ0827 genome

NRPS	Domain organization[a]	Closest homologue in NCBI database (Identity, Coverage)	E value
PxNRPS1.3	A-TD	RYO92480.1 *Monosporascus cannonballus* CBS 609.92 (59 %, 83 %)	0.0
PxNRPS1.7	A-T-TD	KPM42168 *Neonectria ditissima* R09/05 (55 %, 98 %)	0.0
PxNRPS2.4	A-T - C-A-T - C-A-T - C-A-T - C-A-M-T - C-A-T-C_T	TRX91230 *Xylaria fiabelliformis* G536 (55 %, 99 %)	0.0
PxNRPS3.5	A-T	KFA60410 *Stachybotrys chlorohalonata* IBT 40285 (67 %, 99 %)	0.0
PxNRPS3.8	A-T-TD	EMR61501 *Eutypa lata* UCREL1 (91 %, 99 %)	0.0
PxNRPS4.4	A-T-TE	RYP62514 *Monosporascus* sp. 5C6A (53 %, 94 %)	0.0
PxNRPS5.3	A-T-TD	RTE78703 *Fusarium euwallaceae* UCR1854 (78 %, 100 %)	0.0
PxNRPS5.4	A-T-TD	KAF4468798 *Fusarium albosuccineum* NRRL 20459 (68 %, 99 %)	0.0
PxNRPS5.5	A-T	KAF4449115 *Fusarium austroafricanum* NRRL 53441 (96 %, 99 %)	0.0
PxNRPS6.4 (PxXmcG)	A-T - C-A-T - C-A-M-T - C-A-T - C-A-M-T - C-A-T - C-A-T - C-A-T - C-A-T - C-A-M-T-C_T	PKS05731 *Lomentospora prolificans* JHH-5317 (67 %, 99 %)	0.0
PxNRPS6.5	A-T - C-A-T-TD	RFU80400 *Trichoderma arundinaceum* IBT 40837 (43 %, 99 %)	0.0
PxNRPS6.8	A-T - C-A-T-C_T	KFA73725 *Stachybotrys chartarum* IBT 40288 (72 %, 91 %)	0.0
PxNRPS6.9	C-A-T-C_T	KEY70558 *Stachybotrys chartarum* IBT 7711 (58 %, 97 %)	0.0
PxNRPS7.4	A-T-TE	KFA61393 *Stachybotrys chartarum* IBT 40285 (51 %, 98 %)	0.0
PxNRPS7.6	A-C	KAF5012017 *Fusarium decemcellulare* NRRL 13412 (43 %, 98 %)	0.0
PxNRPS7.8	A-T	KKK24685 *Aspergillus rambellii* SRRC1468 (76 %, 99 %)	0.0
PxNRPS8.6	A-T-TD	KAF5011710 *Fusarium decemcellulare* NRRL 13412 (86 %, 100 %)	0.0
PxNRPS8.7	A-T-TD	RYO99767 *Monosporascus cannonballus* CBS 586.93 (83 %,99 %)	0.0
PxNRPS9.1	A-T - C-A-T - C-A-T - C-A-T - C-A-T - C-A-T	KFA47609 *Stachybotrys chartarum* IBT 40293 (52 %, 99 %)	0.0
PxNRPS9.3	A-T-E - C-A-T - C-A-T-E - C-A-T - C-A-T-E - C-A-T-C_T	KPM37793 *Neonectria ditissima* R09/05 (71 %, 99 %)	0.0
PxNRPS9.4	A-T-TD	EQL01287 *Ophiocordyceps sinensis* CO18 (44 %, 99 %)	0.0
PxNRPS10.3	T - C-A-T - C-A-T - C-A-T - C-A-T - C-A-T - C-A-T-TD	XP_024752339 *Trichoderma citrinoviride* TUCIM 6016 (39 %, 98 %)	0.0

PxNRPS11.1	A-T	KFH42337 *Acremonium chrysogenum* ATCC 11550 (65 %, 99 %)	0.0
PxNRPS11.3	C-A-T - C-A-T - C-A-M-T - C-A-T - C-A-M-T - C-A-T - C-A-M-T - C-A-T - C-A-T - C-A-M-T - C-A-T - C-A-T - C-A-T - C-A-M-T-C_T	KZL76007 *Colletorichum tofieldiae* 0861 (67 %, 99 %)	0.0
PxNRPS11.4	A-M	RYP40686 *Monosprascus* sp. MG133 (68 %, 99 %)	0.0
PxNRPS12.4	A-T	AIT18914 *Hirsutella thompsonii* MTCC3556 (41 %, 99 %)	0.0

[a] A: Adenylation domain; C: condensation domain; C_T: terminal condensation domain; E: epimerization domain; M: *N*-methylation domain; T: thiolation domain; TD: uncharacterized terminal domain.

Table S6. Substrate specificity signatures of the A domains of PxXmcG of *Paramyrothecium* sp. XJ0827

Module	34-amino acid and 10-amino acid specificity signature[22-23]	Predicted amino acid / analogue[a]	Amino acid / analogue[a] in xylomyrocins A-C
1	CQFSFGSSLAECTLLSGGEFNSYGQSESATICSA / **G**SATLGSTIK	Val/Leu/Ile/Abu/Iva	Xyl
2	LDNSFDASTWETLLLAGGDFNAYGPTENTVISTI / DAWLLGAVIK	Val/Leu/Ile/Abu/Iva	Leu
3	LNTAFDAATWETMFFASGDINALGHTENTVYSTA / DAWMFSAVYK	Val/Leu/Ile/Abu/Iva	Thr
4	LSDSFDATTWESFFLIGGDCNAYGPTENTTFSAL / DAWFLGATFK	Val/Leu/Ile/Abu/Iva	Val
5	LQSFFDATTLESVFWIGGDYNVYGPTENSNSSTF / DALVWGVNSK	Phe/Trp/Phg/Tyr/Bht	Phe
6	LNSTFDLSTWEAMFLACGEYNTYGPTENSVVSTI / DLWMLCTVVK	Val/Leu/Ile/Abu/Iva	Gly
7	LQTSFDAATWETFFLAGGEYHVYGPTENTTFSTL / DAWFLGVTFK	Val/Leu/Ile/Abu/Iva	Ile
8	LSGSFDNSTWEVMLLAAGDYNAYGPTENTVTSTI / DNWMLAAVTK	Val/Leu/Ile/Abu/Iva	Ser
9	LSTSFDASTWETFVYSGGDFNLYGPTENTVVSSC / DAWFYGLVVK	Val/Leu/Ile/Abu/Iva	Leu
10	LGSSFDASAWEAMLFVAGDYNAYGPTENGVLSTI / DAWMFAAVLK	Val/Leu/Ile/Abu/Iva	Val

[a] Abu, α-aminobutyric acid; Bht, β-hydroxytyrosine; Iva, isovaline; Phg: phenylglycine, Xyl: D-xylonic acid

Table S7. Homologues of PxXmcG-A_1[a] in characterized cyclodepsipeptide synthetases

NRPS	UniProtKB/Swiss-Prot accession number	Organism	Identity	Coverage	E value
KK-1 synthetase	A0A348AXX4	*Curvularia clavata* BAUA-2787	54 %	100 %	0
Enniatin synthetase	A0A0A1EA36	*Fusarium oxysporum* ETH 1536	52 %	99 %	3E-173
Enniatin synthetase	Q00869	*Fusarium equiseti*	52 %	99 %	2E-170
Beauvericin synthetase	S0EN43	*Fusarium fujikuroi* IMI 58289	52 %	99 %	1E-167
Beauvericin synthetase	G3GBU7	*Fusarium proliferatum* LF061	51 %	99 %	2E-167
Bassianolide synthetase	J5JV76	*Beauveria bassiana* ARSEF 2860	50 %	99 %	8E-163
Bassianolide synthetase	D1FVF0	*Beauveria bassiana* ATCC 7159	50 %	99 %	2E-162
Beauvericin synthetase	B6D9A8	*Beauveria bassiana* ATCC 7159	51 %	99 %	1E-159

[a] PxXmcG-A_1: the first adenylation domain of PxXmcG of *Paramyrothecium* sp. XJ0827, proposed to be responsible for the activation and loading of D-xylonic acid.

Table S8. Annotation of the *pxxmc* locus of *Paramyrothecium* sp. XJ0827

Protein / GenBank acession number	Protein length (aa)	Functional annotation / Conserved domain	Closest GenBank homologue (Identity, Quality cover)
PxXmc-3 / OL625655	647	Heterokaryon incompatibility protein / pfam06985	RSL52536 *Fusarium* sp. AF-8 (52 %, 99 %)
PxXmc-2 / OL625654	78	Hypothetical protein / ND	KAB8252745 *Aspergillus flavus* (52 %, 97 %)
PxXmc-1 / OL625653	449	Kynurenine or aspartate aminotransferase / cl18945 (Aspartate aminotransferase superfamily)	RFU73586 *Trichoderma arundinaceum* (72 %, 99 %)
PxXmcA / OL625656	647	Fungal transcription factor / cd12148 (Middle homology region of fungal transcription factors with GAL4-like C6 zinc binuclear cluster DNA-binding domain)	TEA13464 *Colletotrichum sidae* CBS 518.97 (56 %, 85 %)
PxXmcB / OL625657	415	Hypothetical protein / ND	KPM43911 *Neonectria ditissima* R09/05 (49 %, 98 %)
PxXmcC / OL625658	587	Secreted[a] *β*-1,4-xylosidase / cd18833 (Glycoside hydrolase family 43 protein)	KAF6823992 *Colletotrichum musicola* (65 %, 98 %)
PxXmcD / OL625659	576	Secreted[a] GMC oxidoreductase / COG2303 (Choline dehydrogenase or related flavoprotein)	OTA66111 *Hypoxylon* sp. EC38 (70 %, 95 %)
PxXmcE / OL625660	331	NAD^+-dependent oxidoreductase / COG0451 (WcaG nucleoside-diphophate-sugar epimerase)	XP_036586351 *Colletotrichum truncatum* (74 %, 90 %)
PxXmcF / OL625661	1,332	ABC transporter / COG1132 (ABC-type multidrug transport system)	OHX00951 *Colletotrichum incanum* (74 %, 100 %)
PxXmcG / OL625662	12,303	Nonribosomal peptide synthetase	XP_018161716 *Colletotrichum higginsianum* IMI 349063 (66 %, 99 %)
PxXmcH / OL625663	108	Hypothetical protein / pfam03647 (Transmembrane protein 14C)	XP_028491477 *Verticillium nonalfalfae* NRRL 66861 (95 %, 100 %)
PxXmcI / OL625664	113	Hypothetical protein / ND	KAB5539334 *Coniochaeta* sp. 2T2.1 (51 %, 84 %)
PxXmcJ / OL625665	254	Glycoside hydrolase / pfam11790 (Glycosyl hydrolase)	TRX95652 *Xylaria flabelliformis* (74 %, 99 %)
PxXmc+1 / OL625650	645	Heterokaryon incompatibility protein / pfam06985	XP_040789813 *Cucurbitaria berberidis* CBS 394.84 (30 %, 99 %)
PxXmc+2 / OL625651	383	Hypothetical protein / cl21460 (Haloacid dehalogenase-like hydrolases)	KFA64452 *Stachybotrys chlorohalonata* IBT 40285 (57 %, 71 %)
PxXmc+3 / OL625652	1,220	Hypothetical protein / ND	RYC57606 *Xylaria longipes* (44 %, 84 %)

ND: Not detected.

[a] Extracellular localization was predicted with SignalP-5.0 (http://www.cbs.dtu.dk/services/SignalP/).

Table S9. Putative xylose metabolic enzymes in *Paramyrothecium* sp. XJ0827 and *P. roridum* NRRL 2183.

XJ0827 Protein / GenBank accession number	Protein length (aa)	Closest homologue in NRRL 2183 / GenBank accession number (Identity, Quality cover)	Functional annotation / Conserved domain	Closest GenBank homologue (Identity, Quality cover)
PxXyd1[a] / OL625666	391	PrXyd1[b] / OL654441 (90 %, 99 %)	NADP:D-xylose dehydrogenase / COG0673 (Predicted MviM dehydrogenase)	XP_013947251 *Trichoderma atroviride* IMI 206040 (74 %, 99 %)
PxXyd2[a] / OL625667	389	PrXyd2[b] / OL654442 (81 %, 99 %)	NADP:D-xylose dehydrogenase / COG0673 (Predicted MviM dehydrogenase)	XP_028468087 *Sodiomyces alkalinus* F11 (56 %, 98 %)
PxXyrA[c] / OL625668	323	PrXyrA[d] / OL654443 (98 %, 100 %)	NAD(P)H-dependent D-xylose reductase / cd19115 (AKR2D family aldo-keto reductase)	KFH46419 *Acremonium chrysogenum* ATCC 11550 (89 %, 99 %)
PxUxs1[e] / OL625649	320	PrUxs1 / OL654424 (93 %, 99 %)	UDP-glucuronate decarboxylase / cd05230 (UDP-glucuronate decarboxylase)	KAG5665494 *Fusarium avenaceum* (64 %, 97 %)

[a] The *pxxyd1* and *pxxyd2* genes are not part of the *P.* sp. XJ0827 *pxxmc* locus in Scaffold 6. These two genes are located in Scaffold 2 in genomic loci that are ~3.2Mb apart from each other.

[b] The *prxyd1* and *prxyd2* genes are located in contigs PXOD01001614 and PXOD01000303, respectively, and they are not part of the *prxmc* locus of *P. roridum* NRRL 2183 in contigs PXOD01000192 and PXOD01000490.

[c] The *pxxyrA* gene is located in Scaffold 2, and is not a part of the *P.* sp. XJ0827 *pxxmc* locus in Scaffold 6.

[d] The *prxyrA* gene is located in contig PXOD01000131, and is not part of the *prxmc* locus of *P. roridum* NRRL 2183 in contigs PXOD01000192 and PXOD01000490.

[e] The *pxuxs1* gene is located in Scaffold 3, and is not a part of the *P.* sp. XJ0827 *pxxmc* locus in Scaffold 6.

[f] The *pruxs1* gene is located in contig PXOD01000335, and is not part of the *prxmc* locus of *P. roridum* NRRL 2183 in contigs PXOD01000192 and PXOD01000490.

Table S10. Putative xylan degradation enzymes in *Paramyrothecium* sp. XJ0827

GenBank accession number of predicted protein	GenBank homologue	CAZy class	Functional annotation	Identity (%)	E value
OL654480	ATE54694	CE1	acetyl xylan esterase	68	2E-110
OL654468	CEI70467	CE2	acetyl xylan esterase	72	3E-146
OL654455	CCT67685	CE3	acetyl xylan esterase	60	0
OL654458	VBB73025	CE3	acetyl xylan esterase	71	2E-99
OL654459	CEI63671	CE3	acetyl xylan esterase	48	3E-109
OL654460	CCT73237	CE3	acetyl xylan esterase	62	0
OL654462	ANH22672	CE3	acetyl xylan esterase	45	5.2E-53
OL654471	CCT67685	CE3	acetyl xylan esterase	60	0
OL654473	CCT73237	CE3	acetyl xylan esterase	59	0
OL654476	CEF83009	CE3	acetyl xylan esterase	62	3.1E-80
OL654479	VBB73025	CE3	acetyl xylan esterase	76	4E-132
OL654464	APZ43753	CE4	acetyl xylan esterase	46	5.2E-75
OL654456	AGZ41852	GH43	β-xylosidase	68	3E-125
OL654457	ANJ25952	GH43	β-xylosidase	67	6E-119
OL654461	SDT24851	GH43	β-xylosidase	52	8E-142
OL654463	AGT84551	GH43	β-xylosidase	48	1.2E-74
OL654465	ACM26788	GH43	β-xylosidase	59	2E-176
OL654467	ADJ45074	GH43	β-xylosidase	52	4E-150
OL654469	AFS39313	GH43	β-xylosidase	60	6E-111
OL654472	ASB39391	GH43	β-xylosidase	41	1.1E-57
OL654474	BAL88020	GH43	β-xylosidase	41	7.5E-58
OL654475	ACU35804	GH43	β-xylosidase	56	2E-111
OL654478	CCQ33428	GH43	β-xylosidase	40	1.1E-61
OL654482	ADJ45712	GH43	β-xylosidase	48	4.2E-83
OL654466	AAP57293	GH10	endo-1,4-β--xylanase	58	7E-107
OL654470	AAC06114	GH11	endo-β-1,4-xylanase	47	2.2E-48
OL654477	SBT43763	GH11	endo-β-1,4-xylanase	42	5.5E-45
OL654481	ATB44315	GH30	endo-β-1,4-xylanase	47	1E-124

Table S11. Fungal BGCs in GenBank and MycoCosm encoding PxXmcG and PxXmcE homologues

Strain	PxXmcE homologue	PxXmcG homologue
Paramyrothecium roridum NRRL 2183	OL654435[b]	OL654437[b]
Colletotrichum cereale CBS 129662	Colce1/642940[a]	Colce1/576756[a]
Colletotrichum eremochloae CBS 129661	Coler1/602296[a]	Coler1/626878[a]
Colletotrichum falcatum MAFF 306170	Colfa1/701189[a]	Colfa1/585066[a]
Colletotrichum graminicola M1.001	XP_008089346[b]	XP_008089345[b]
Colletotrichum higginsianum IMI 349063	XP_018161714[b]	XP_018161716[b]
Colletotrichum higginsianum MAFF 305635-RFP	TID02370[b]	AFI23568[b]
Colletotrichum incanum MAFF 238704	KZL85774[b]	OHX00952[b]
Colletotrichum navitas CBS 125086	Colna1/666877[a]	Colna1/508102[a]
Colletotrichum shisoi PG-2018a	TQN74157[b]	TQN74151[b]
Colletotrichum spaethianum MAFF 239500	GJC81060[b]	GJC81063[b]
Colletotrichum sublineola TX430BB	KDN70284[b]	KDN70282[b]
Colletotrichum tanaceti BRIP 57314	TKW53031[b]	TKW53032[b]
Colletotrichum tofieldiae 0861	KZL76002[b]	KZL76007[b]
Colletotrichum tofieldiae MAFF 712333	GKT54243[b]	GKT54246[b]
Colletotrichum truncatum CMES1059	XP_036579086[b]	XP_036579089[b]
Colletotrichum zoysiae MAFF 235873	Colzo1/579611[a]	Colzo1/501283[a]
Dactylonectria macrodidyma MPI-CAGE-AT-0147	Dacma1/872502[a]	Dacma1/847184[a]
Dactylonectria estremocensis MPI-CAGE-AT-0021	Daces1/514266[a]	Daces1/514259[a]
Ilyonectria sp. MPI-CAGE-AT-0134	Neora1/560831[a]	Neora1/633922[a]
Phaeoacremonium sp. FL0889	PhaeoFL0889_1/483306[a]	PhaeoFL0889_1/517047[a]

[a] Assembly/Protein ID in JGI MycoCosm.

[b] GenBank Protein ID.

Table S12. Potential xylomyrocin-producing fungal strains screened in this study

Species	Strain		Species	Strain
Colletotrichum acutatum	ACCC 38933		*Paramyrothecium nigrum*	MN12473
Colletotrichum agaves	ACCC 30011		*Paramyrothecium roridum*	MN115828
Colletotrichum alatae	ACCC 39281		*Paramyrothecium roridum*	MN115950
Colletotrichum capsici	ACCC 36172		*Paramyrothecium roridum*	MN19842
Colletotrichum coccodes	ACCC 36067		*Paramyrothecium roridum*	MN19843
Colletotrichum dematium	ACCC 37048		*Paramyrothecium roridum*	MN19850
Colletotrichum frigidum	ACCC 36179		*Paramyrothecium roridum*	MN19887
Colletotrichum fructicola	ACCC 39328		*Paramyrothecium roridum*	MN19946
Colletotrichum gloeosporioides	ACCC 31200		*Paramyrothecium roridum*	MN19979
Colletotrichum glycines	ACCC 36201		*Paramyrothecium roridum*	MN110185
Colletotrichum gossypiii	ACCC 36176		*Paramyrothecium roridum*	MN110364
Colletotrichum graminicola	ACCC 36361		*Paramyrothecium roridum*	MN111032
Colletotrichum hibisci	ACCC 30326		*Paramyrothecium roridum*	MN111047
Colletotrichum higginsianum	ACCC 37053		*Paramyrothecium roridum*	MN113194
Colletotrichum japonicum	ACCC 36182		*Paramyrothecium roridum*	MN113894
Colletotrichum lagenarium	ACCC 30016		*Paramyrothecium roridum*	MN113965
Colletotrichum lindemuthianum	ACCC 36066		*Paramyrothecium roridum*	MN114944
Colletotrichum musae	ACCC 31244		*Paramyrothecium roridum*	MN115048
Colletotrichum orbiculare	ACCC 36065		*Paramyrothecium roridum*	MN115132
Colletotrichum panacicola	ACCC 30017		*Paramyrothecium roridum*	MN115382
Colletotrichum papayae	ACCC 36363		*Paramyrothecium roridum*	MN115948
Colletotrichum sp.	XJ1040		*Paramyrothecium roridum*	MN115978
Colletotrichum tabacum	ACCC 36167		*Paramyrothecium roridum*	MN116117
Colletotrichum trichellum	ACCC 36404		*Paramyrothecium roridum*	NRRL 2183
Colletotrichum truncatum	ACCC 36322		*Paramyrothecium tellicola*	MN12884

ACCC: Agriculture Culture Collection of China (Beijing, China); MN: MoonBiotech (Guangzhou, China).

Table S13. MALDI-TOF MS data for 10 groups of peptides produced by seven representative *Paramyrothecium* and *Colletotrichum* spp.[a]

Strain	Group	MALDI-TOF MS (*m/z*)
Paramyrothecium roridum NRRL 2183	1	$[M+Na]^+$ 858, $[M+K]^+$ 874 $[M+Na]^+$ 872, $[M+K]^+$ 888 $[M+Na]^+$ 900, $[M+K]^+$ 916
	2	$[M+Na]^+$ 1107, $[M+K]^+$ 1123 $[M+Na]^+$ 1121, $[M+K]^+$ 1137
Paramyrothecium roridum MN115382	3	$[M+Na]^+$ 2173 $[M+Na]^+$ 2187 $[M+Na]^+$ 2201
Paramyrothecium nigrum MN12473	4	$[M+Na]^+$ 1024, $[M+K]^+$ 1040 $[M+Na]^+$ 1038, $[M+K]^+$ 1054 $[M+Na]^+$ 1052, $[M+K]^+$ 1068
	5	$[M+Na]^+$ 1189 $[M+Na]^+$ 1205 $[M+Na]^+$ 1221 $[M+Na]^+$ 1237
Paramyrothecium roridum MN110185	6	$[M+Na]^+$ 1542, $[M+K]^+$ 1568
Paramyrothecium roridum MN113194	7	$[M+Na]^+$ 1115, $[M+K]^+$ 1131 $[M+Na]^+$ 1129, $[M+K]^+$ 1145
Paramyrothecium roridum MN19850	8	$[M+Na]^+$ 1190, $[M+K]^+$ 1206
Colletotrichum sp. XJ1040	9	$[M+Na]^+$ 523, $[M+K]^+$ 539 $[M+Na]^+$ 570, $[M+K]^+$ 586
	10	$[M+Na]^+$ 1121, $[M+K]^+$ 1137 $[M+Na]^+$ 1151, $[M+K]^+$ 1167

[a] Peptides subsequently identified as xylomyrocin-type cyclodepsipeptides are shown in red.

Table S14. Substrate specificity signatures of the A domains of PrXmcG of *Paramyrothecium roridum* NRRL 2183

Module	34-amino acid and 10-amino acid specificity signature[22-23]	Predicted amino acid / analogue[a]	Amino acid / analogue[a] in xylomyrocins A-C
1	CQFSFGSSLAECTLLSGGEINSYGQSESSTICGA / **G**SATLGSTIK	Val/Leu/Ile/Abu/Iva	Xyl
2	LQDSFDASIFEFLLVVGGDYNAYGPTENTVVSTF / DAFLVGAVVK	Val/Leu/Ile/Abu/Iva	Leu
3	LNTAFDASTWETMFFASGDINVLGHTENTVYSTA / DAWMFSVVYK	Val/Leu/Ile/Abu/Iva	Thr
4	LNNSFDATTWESFVLTGGECHVYGPTENTTFSTL / DAWFLGVTFK	Val/Leu/Ile/Abu/Iva	Ile
5	LQSSFDASTWESMLFAAGDYNAYGPTENTVLSTI / DAWMFAAVLK	Val/Leu/Ile/Abu/Iva	Val
6	LNTSFDAATWETIFFSGGEYHAYGPSENTTYSTI / DAWIFGATYK	Val/Leu/Ile/Abu/Iva	Leu
7	THRSFDTSVLENMYLCGGDYNSYGPTENSVNSTI / DTLMLGSVNK	Phe/Trp/Phg/Tyr/Bht	Gln
8	LSTSFDAATWEALFYVGGDFNAYGPTENTVMSAI / DAWLYGAVMK	Val/Leu/Ile/Abu/Iva	Leu
9	LNSSFDASTWEAMIFVAGDYNAYGPTENTVLSTV / DAWMFAAVLK	Val/Leu/Ile/Abu/Iva	Val

[a] Abu, α-aminobutyric acid; Bht, β-hydroxytyrosine; Iva, isovaline; Phg: phenylglycine, Xyl: D-xylonic acid

Table S15. Annotation of the *prxmc* locus of *Paramyrothecium roridum* NRRL 2183.

Protein / GenBank acession number	Protein length (aa)	Closest homologue in the *pxxmc* locus of *P.* sp. XJ0827 (Identity, Quality cover)[a]	Functional annotation / Conserved domain	Closest GenBank homologue (Identity, Quality cover)
PrXmc-5 / OL654430	>404	ND[b]	Hypothetical protein / ND	KAF5578726 *Fusarium pseudoanthophilum* (37 %, 92 %)
PrXmc-4 / OL654429	213	ND[b]	Secreted hypothetical protein / cd00118 (LysM peptidoglycan-binding domain)	KAB8252745 *Fusarium longipes* (48 %, 98 %)
PrXmc-1 / OL654428	449	PxXmc-1 (86 %, 99 %)	Kynurenine or aspartate aminotransferase / cI18945 (Aspartate aminotransferase superfamily)	RFU73586 *Trichoderma arundinaceum* (72 %, 99 %)
PrXmcA / OL654431	676	PxXmcA (69 %, 94 %)	Fungal transcription factor / cd12148 (Middle homology region of fungal transcription factors with GAL4-like C6 zinc binuclear cluster DNA-binding domain)	TEA13464 *Colletotrichum sidae* CBS 518.97 (54 %, 81 %)
PrXmcX / OL654440	426	ND[b]	Hypothetical protein / pfam00646 (F-box domain)	*Monosporascus* sp. CRB-8-3 (40 %, 90 %)
PrXmcB / OL654432	411	PxXmcB (81 %, 100 %)	Hypothetical protein / ND	KPM43911 *Neonectria ditissima* (50 %, 98 %)
PrXmcC / OL654433	587	PxXmcC (91 %, 99 %)	Secreted[c] *β*-1,4-xylosidase / cd18833 (Glycosyl hydrolase family 43 protein)	KAF6823992 C*olletotrichum musicola* (69 %, 95 %)
PrXmcD / OL654434	576	PxXmcD (83 %, 100 %)	Secreted[c] GMC oxidoreductase / COG2303 (Choline dehydrogenase or related flavoprotein)	XP_007835811 *Pestalotiopsis fici* W106-1 (68 %, 98 %)
PrXmcG / OL654437	11,225	PxXmcG (63 %, 99 %)	Nonribosomal peptide synthetase	KZL76007 *Colletotrichum tofieldiae* (68 %, 99 %)
PrXmcF / OL654436	1,338	PxXmcF (72 %, 99 %)	ABC transporter / COG1132 (ABC-type multidrug transport system)	KZL76004 *Colletotrichum tofieldiae* (71 %, 98 %)
PrXmcE / OL654435	324	PxXmcE (83 %, 99 %)	NAD^+-dependent oxidoreductase / COG0451 (WcaG nucleoside-diphophate-sugar epimerase)	XP_036586351 *Colletotrichum truncatum* (74 %, 91 %)
PrXmcH[d] / OL654438	108	PxXmcH (95 %, 100 %)	Hypothetical protein / pfam03647 (Transmembrane protein 14C)	KAG7111059 *Verticillium longisporum* NRRL 66861 (95 %, 100 %)
PrXmcJ[d] / OL654439	254	PxXmcJ (91 %, 100 %)	Glycoside hydrolase / pfam11790 (Glycosyl hydrolase)	OTA95937 *Hypoxylon* sp. CO27-5 (78 %, 99 %)
PrXmc+1[d] / OL654425	645	PxXmc+1 (68 %, 100 %)	Heterokaryon incompatibility protein / pfam06985	PMD24880 *Hyaloscypha hepaticicola* (30 %, 99 %)
PrXmc+4[d] / OL654426	481	ND[b]	Calcium-transporting ATPase 2 / COG0474 (Mg-transporting ATPase)	KUI62530 *Valsa mali* var. pyri (33 %, 69 %)
PrXmc+5[d] / OL654427	538	ND[b]	Hypothetical protein / COG0154 (tRNA amidotransferase-related)	KAG6358477 *Diaporthe citri* (62 %, 96 %)

[a] Genes for close homologues of PxXmcI and PxXmc+3 from strain XJ0827 were not detected in the *P. roridum* NRRL 2183 genome assembly (GCA_003012165). Genes for the homologues of PxXmc+2 and

PxXmc-2 of strain XJ0827 are not part of the *prxmc* locus. Instead, they were detected in two additional contigs (PXOD01000044 and PXOD01000112, respectively) in the *P. roridum* NRRL 2183 genome assembly (GenBank: GCA_003012165). A gene for a homologue of PxXmc-3 of strain XJ0827 is present in the same contig (PXOD01000192) as the *prxmc-5* – *prxmcE* part of the *prxmc* locus, but it is located ~22kb downstream from *prxmc-5* in *P. roridum* NRRL 2183.

[b] ND: Not detected in the *pxxmc* locus of *P.* sp. XJ0827.

[c] Extracellular localization was predicted with SignalP-5.0: http://www.cbs.dtu.dk/services/SignalP/

[d] The *prxmc* locus is located in two contigs (*prxmc-5* to *prxmcE*: PXOD01000192; *prxmcH* to *prxmc+5*: PXOD01000490) in the *P. roridum* NRRL 2183 genome assembly (GenBank: GCA_003012165).

Table S16. Minimum inhibitory concentrations (MICs) of xylomyrocin A–C (1–3)

Organism	Compound (MIC; µg/mL)					
	1	**2**	**3**	kanamycin	amphotericin B	pneumocandin B_0
S. aureus ATCC 6538	>20	>20	>20	5	nt	nt
MRSA 11646	>20	>20	>20	>20	nt	nt
E. coli ATCC 25922	>20	>20	>20	>20	nt	nt
C. albicans SC5314	>20	>20	>20	nt	nt	0.2
C. neoformans H99	>20	>20	>20	nt	0.2	nt

nt, Not tested.

Table S17. PCR primers used in this study

Primer name	Sequence (5'–3')	Notes
pxxmcC-KO-UA-F	GTTTTTCAGCAAGATATCCCAGGACGTCGGGTCATCCC	For gene disruption cassette cloning
pxxmcC-KO-UA-R	CTTGGTACCGAGCTCCAGGGATGTTCCTGGTGATGGGCATTTCAATGGAGA	
pxxmcC-KO-DA-F	ATGGTGGCAGGCCCCCTTGGCCCACAGGAACATAGATTCG	For gene disruption cassette cloning
pxxmcC-KO-DA-R	ATCTTCTAGAAAGATATCGCTTCTGTCCCCTAAGCTGCTGATGTA	
HygR-F	GAGCTCGGTACCAAGGCCCGG	For gene disruption cassette cloning
HygR-R	GGGGCCTGCCACCATACCCA	
pxxmcC-KO-seg-F	CCAGGACGTCGGGTCATCCC	For gene disruption cassette amplification
pxxmcC-KO-seg-R	CTTCTGTCCCCTAAGCTGCTGATG	
pxxmcD-KO-UA-F	GTTTTTCAGCAAGATATCTTGAAGAAAGTCGAATTGGTCCCG	For gene disruption cassette cloning
pxxmcD-KO-UA-R	CTTGGTACCGAGCTCCTCTCCTGATGACTGGATCGTCAATG	
pxxmcD-KO-DA-F	ATGGTGGCAGGCCCCCTCATCTTGTGAAAAGGCGCTTACA	For gene disruption cassette cloning
pxxmcD-KO-DA-R	ATCTTCTAGAAAGATATCACATGACCCTGCATGCTGCCCAGCTTCTTCCTGATT	
pxxmcD-KO-seg-F	TTGAAGAAAGTCGAATTGGTCCCG	For gene disruption cassette amplification
pxxmcD-KO-seg-R	ACATGACCCTGCATGCTGCCCAGCTTCTTCCTGATT	
pxxmcE-KO-UA-F	GTTTTTCAGCAAGATATCGAATGAAATCCCAAAACACCGAAGT	For gene disruption cassette cloning
pxxmcE-KO-UA-R	CTTGGTACCGAGCTCGGACTTGTTGTGGAGTAGCTTAGTGGTT	
pxxmcE-KO-DA-F	ATGGTGGCAGGCCCCTTGCCCATAGTGTCAATGTCCCC	For gene disruption cassette cloning
pxxmcE-KO-DA-R	ATCTTCTAGAAAGATATCTTCATTGCACTTGTCGGTCCTTCA	
pxxmcE-KO-seg-F	GAATGAAATCCCAAAACACCGAAGT	For gene disruption cassette amplification
pxxmcE-KO-seg-R	TTCATTGCACTTGTCGGTCCTTCA	
pxxmcG-KO-UA-F	GTTTTTCAGCAAGATATCAAGATGAGATACTCAACAAGGCAGCTTT	For gene disruption cassette cloning
pxxmcG-KO-UA-R	CTTGGTACCGAGCTCGATTCTCAATCAGTCCTGCAGAGTAATGT	
pxxmcG-KO-DA-F	ATGGTGGCAGGCCCCTTGATTCCGGTCACGCCGTGCCTCTATGCTTTGAGA	For gene disruption cassette cloning
pxxmcG-KO-DA-R	ATCTTCTAGAAAGATATCGTAGACGATGATACGTCAATAACACGCA	
pxxmcG-KO-seg-F	AAGATGAGATACTCAACAAGGCAGCTTT	For gene disruption cassette amplification
pxxmcG-KO-seg-R	AGACGATGATACGTCAATAACACGCA	
pxxmcC-KO-verif-p1	GTCACGAATTCAAATGGGACAACG	For gene knockout verification
pxxmcC-KO-verif-p2	TCTGGGGTATCAATGTGAAGACGAA	
pxxmcC-KO-verif-p3	ATACGAGATTCACATGATTGCCAGC	
pxxmcC-KO-verif-p4	AAGTGGCTACGAGGCCGCCAAAGACTGGATAGTGAG	
pxxmcD-KO-verif-p1	GCCGCCAATTGACGAGATCTTT	For gene knockout verification
pxxmcD-KO-verif-p2	TTCAACGGGGTGAGCCCGCTCTTCGCTGGAAATTTC	
pxxmcD-KO-verif-p3	CGGAGGTTGCTTGAGTGGAATTATC	
pxxmcD-KO-verif-p4	TCAAGGTGCCACACGAGACATG	
pxxmcE-KO-verif-p1	CCTCGGCGTCTCGCTTATCAG	For gene knockout verification
pxxmcE-KO-verif-p2	TTACGAGCTTGTGGTGACGATGAA	
pxxmcE-KO-verif-p3	GCAGTTTCGAATTGCCTGCCCGTTTCTCATGGTTCC	
pxxmcE-KO-verif-p4	GTACGGTGGCCGTCTTCTTGC	
pxxmcG-KO-verif-p1	AGAAGACGCGAATGTAATCTTTGAGG	For gene knockout verification
pxxmcG-KO-verif-p2	TTCTGTACACAAACTCTCACTGAACCGT	
pxxmcG-KO-verif-p3	TGGGATACAGACACAACCTCCATGT	
pxxmcG-KO-verif-p4	AAATGCCAAGCTCCCTGCGC	
tubulin-F	GTCTACAATGGCACCTCCGAG	For RT-qPCR analysis
tubulin-R	AAGTTGTCGGGACGGAAGAG	
pxxyd1-F	TGAGCATCAAGATCCGAGAGC	For RT-qPCR analysis
pxxyd1-R	CGTTAAACTGCCATCGTCTGC	
pxxyd2-F	ACACCGCACTCGCACCAT	For RT-qPCR analysis

pxxyd2-R	ATACCTTCTTGTTCAACGGCTG	
pxuxs1_F	GCGAGACTACTTCTAGCGAGC	For RT-qPCR analysis
pxuxs1_R	TTGCCTTCGTCGTAGCATGA	
pxxyrA_F	GCCTACCGTCAAGCTCAACA	For RT-qPCR analysis
pxxyrA_R	TCACCGCACTCCTTCTCATT	
pxxmc-3-F	TGGGCCAGTGGGCTAGAAT	For RT-qPCR analysis
pxxmc-3-R	ATGTGGGCGCAAGATTGTTT	
pxxmc-2-F	CAAGTGCAGCAGAACCGTAG	For RT-qPCR analysis
pxxmc-2-R	CTATCGCCATACTTTCCACAGAT	
pxxmc-1-F	AAGGCAACGTGATCTTGACG	For RT-qPCR analysis
pxxmc-1-R	CGACCAGCATTCAGAAGCGT	
pxxmcA-F	CCTGCAAGCCGTATCAGCAT	For RT-qPCR analysis
pxxmcA-R	TTTTCCAGCGATTGTGGGGT	
pxxmcB-F	ATCGTTTGCGACATGCTCC	For RT-qPCR analysis
pxxmcB-R	TTTCCATGGCCTGAGGATTG	
pxxmcC-F	AATCTGGGTCCTGGCAGTTTAG	For RT-qPCR analysis
pxxmcC-R	CTTGCGTAGCCACATAGACCTT	
pxxmcD-F	GCTGGCTAGAAGGCACAAATC	For RT-qPCR analysis
pxxmcD-R	CAGGCGGCTGGAAGTAAAGA	
pxxmcE-F	AAGGTGCCTGTAAGATGGGTG	For RT-qPCR analysis
pxxmcE-R	AGAGTCAGTTGGGTTACAGTCGG	
pxxmcF-F	CAACTGTTCAGAATGCCGATGT	For RT-qPCR analysis
pxxmcF-R	TCACCTGTCAAGAGCCTGGC	
pxxmcG-F	ATGGTGGAATGGATGCTGTTT	For RT-qPCR analysis
pxxmcG-R	AAGGCAGTAGGTTCTTGAGGCT	
pxxmcH-F	CCGAGCACCCAGCATTCA	For RT-qPCR analysis
pxxmcH-R	CGCCGTTGTCCTTGTTCTT	
pxxmcI-F	CAATCCAATTGTGCGAGAGCC	For RT-qPCR analysis
pxxmcI-R	CGTTGGATCCATCCATGCTG	
pxxmcJ-F	GCAATGCTGCCATCAGGTATC	For RT-qPCR analysis
pxxmcJ-R	GGAAGACAAACAGACCGTACTCG	
pxxmc+1-F	CCCCAATTTTGCAAGCACGA	For RT-qPCR analysis
pxxmc+1-R	GCTTATGGCCTCAGCATCCA	
pxxmc+2-F	CGACAACTTTGACAGCGTCC	For RT-qPCR analysis
pxxmc+2-R	CAACCGAGCTGACTGTGACT	
pxxmc+3-F	CAAGGATGACCTGACGGAAT	For RT-qPCR analysis
pxxmc+3-R	CTTGAGTGCCGCCTAGGTT	
NHisAT-F	CCGCGCGGCAGCCATATGATCACGGAAGAAGACCGTACG	For constructions of pET28a-N-His-PxXmcG-A_1T_1 and pET28a-N-His-PxXmcG-A_1
NHisAT-R	GGTGGTGGTGCTCGAGTTAGTACGGCTTTGGAGTTATGGTGTTGC	For construction of pET28a-N-His-PxXmcG-A_1T_1
NHisA-R	GGTGGTGGTGCTCGAGTTACTCCAAAGAGCTGGCATTTTGATTATG	For construction of pET28a-N-His-PxXmcG-A_1

CHisAT-F	AGGAGATATACCATGATCACGGAAGAAGACCGTACG	For constructions of pET28a-C-His-PxXmcG-A_1T_1 and pET28a-C-His-PxXmcG-A_1
CHisAT-R	GGTGGTGGTGCTCGAGGTACGGCTTTGGAGTTATGGTGTTGC	For constructions of pET28a-C-His-PxXmcG-A_1T_1
CHisA-R	GGTGGTGGTGCTCGAGCTCCAAAGAGCTGGCATTTTGATTATG	For constructions of pET28a-C-His-PxXmcG-A_1

Table S18. Crystal data and structure refinement of compound 3

Identification code	827_ODS90_4_1B
Empirical formula	$C_{54}H_{89}N_9O_{16}$
Formula weight	1120.34
Temperature/K	100
Crystal system	orthorhombic
Space group	$P2_12_12_1$
a/Å	33.8453(6)
b/Å	17.7843(3)
c/Å	10.78100(10)
α/°	90
β/°	90
γ/°	90
Volume/Å^3	6489.25(17)
Z	4
ρ_{calc} g/cm^3	1.147
μ/mm^{-1}	0.699
F(000)	2416.0
Crystal size/mm^3	0.1 × 0.08 × 0.02
Radiation	CuKα (λ = 1.54184)
2Θ range fro data collection/°	7.21 to 133.186
Index ranges	−40 ≤ h ≤ 35, −21 ≤ k ≤ 21, −12 ≤ l ≤ 12
Reflections collected	47100
Independent reflections	11362 [R_{int} = 0.0989, R_{sigma} = 0.0661]
Data/restraints/parameters	11362/0/731
Goodness-of-fit on F^2	1.042
Final R indexes [I >= 2σ(I)]	R_1 = 0.0756, wR_2 = 0.1989
Final R indexes [all data]	R_1 = 0.0816, wR_2 = 0.2034
Largest diff. peak/hole / e Å^{-3}	0.51/−0.32
Flack parameter	−0.02(13)

3. SI Figures

Figure S1. HRESIMS/MS analysis

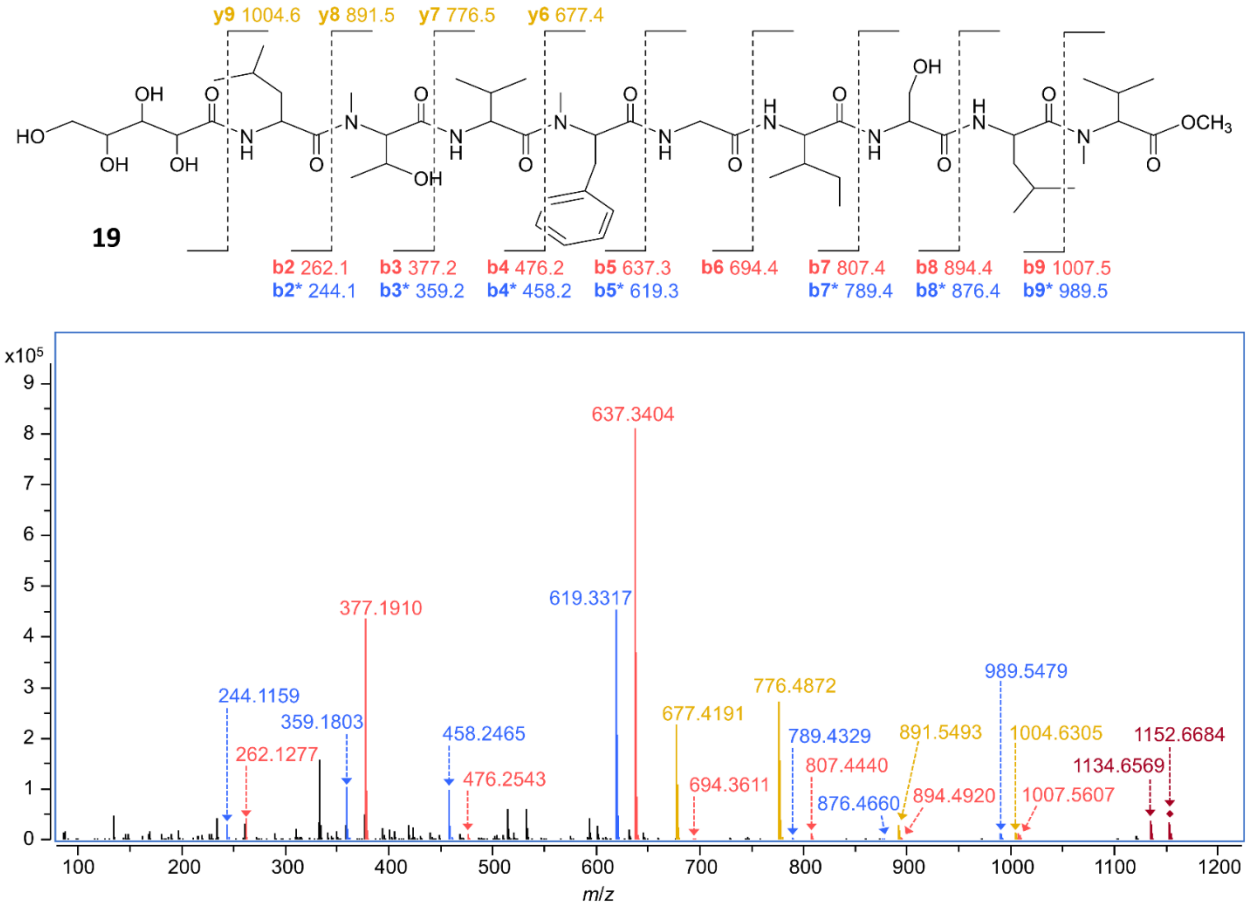

Figure S1.1. Product ion mass spectrum of the $[M + H]^+$ ion of 19 (*m/z* 1152.6684).

Compound **3** was first linearized by methanolysis upon treatment with CH_3ONa/CH_3OH to afford the methoxy-substituted derivative **19**. Fragment ions of the b-, b−H_2O (b*-), and y-type, resulting from collision-induced dissociation of the $[M + H]^+$ ion of **19**, are shown in *red*, *blue* and *yellow* respectively. The $[M+H]^+$ and $[M–H_2O+H]^+$ ions are shown in *maroon*.

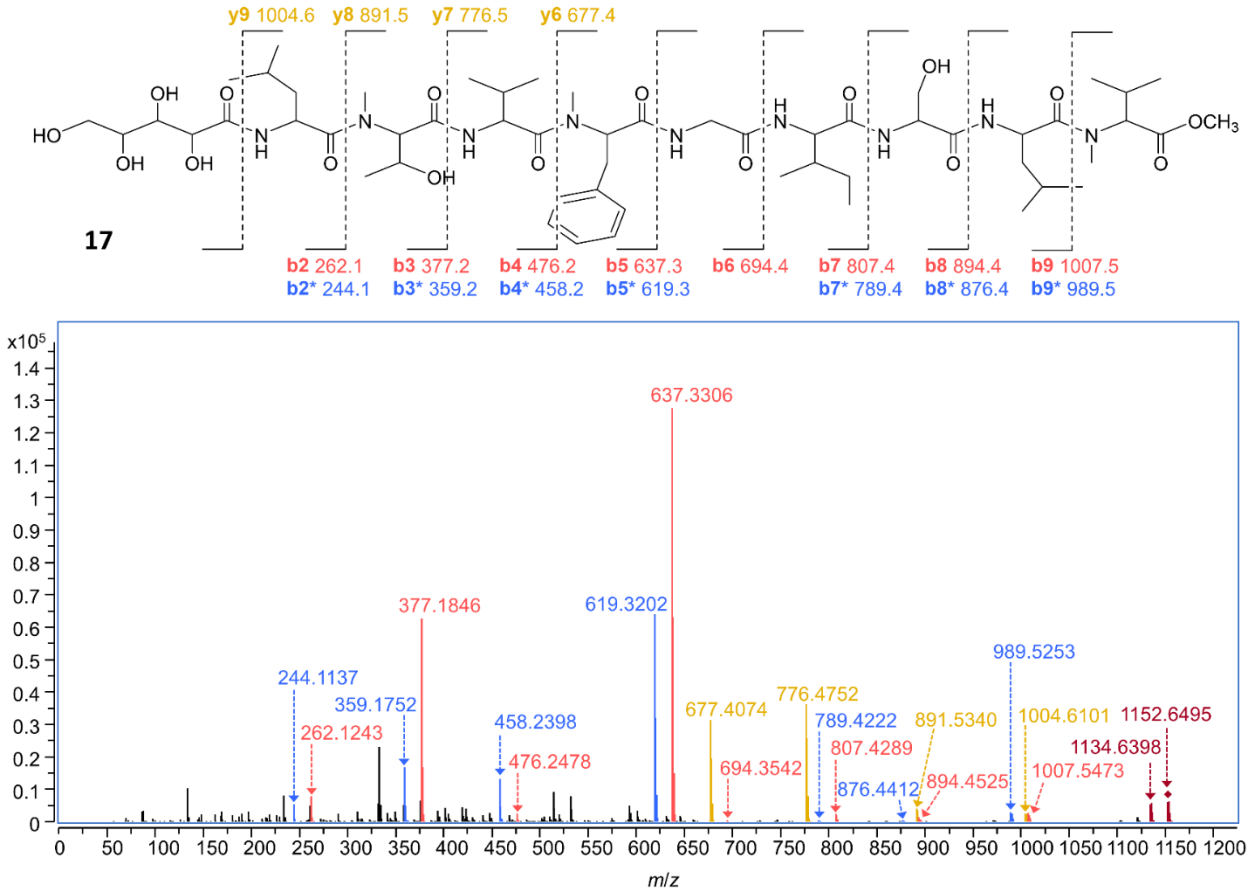

Figure S1.2. Product ion mass spectrum of the $[M + H]^+$ ion of 17 (*m/z* 1152.6495).

Compound **1** was first linearized by methanolysis upon treatment with CH_3ONa/CH_3OH to afford the methoxy-substituted derivative **17**. Fragment ions of the b-, b−H_2O (b*-), and y-type, resulting from collision-induced dissociation of the $[M + H]^+$ ion of **17**, are shown in *red*, *blue* and *yellow* respectively. The $[M+H]^+$ and $[M–H_2O+H]^+$ ions are shown in *maroon*.

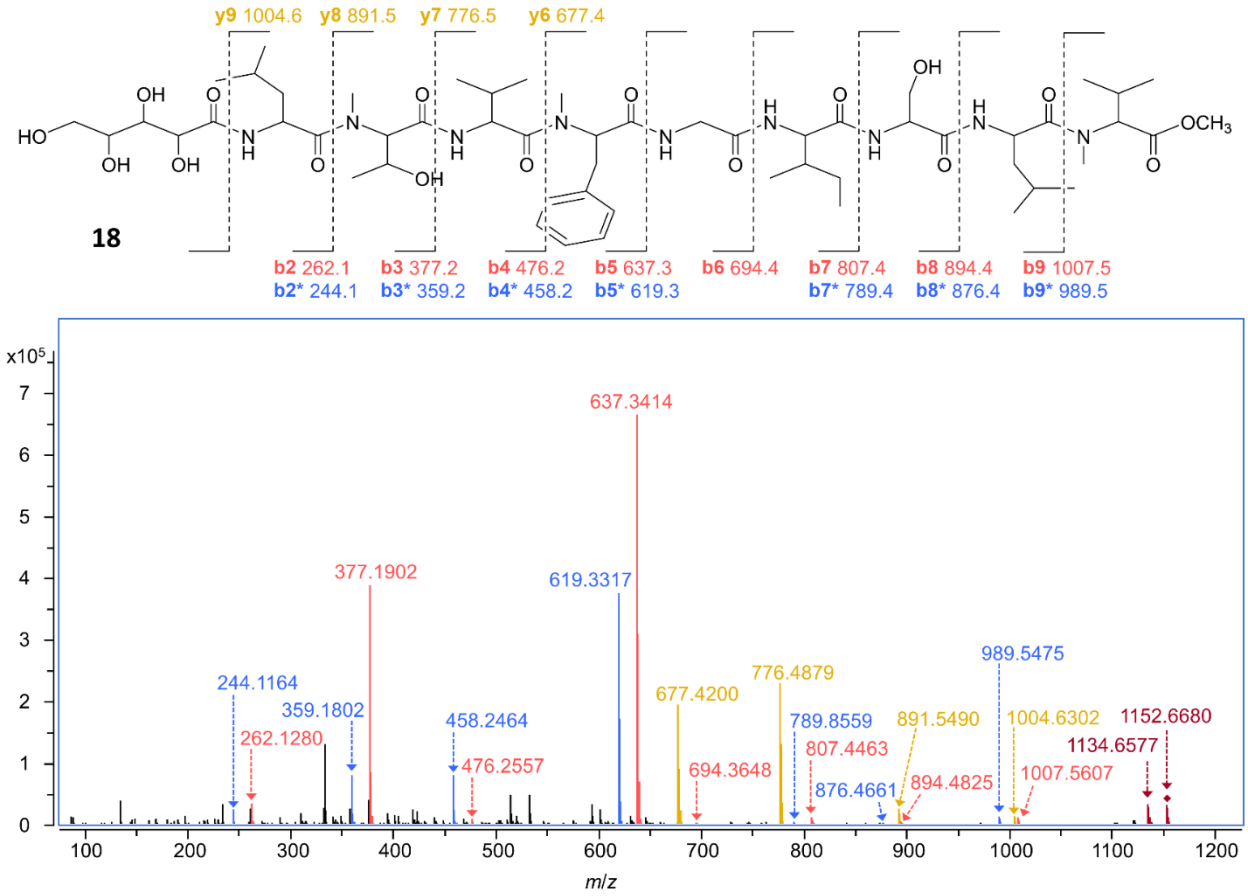

Figure S1.3. Product ion mass spectrum of the $[M + H]^+$ ion of 18 (*m/z* 1152.6680).

Compound **2** was first linearized by methanolysis upon treatment with CH_3ONa/CH_3OH to afford the methoxy-substituted derivative **18**. Fragment ions of the b-, b−H_2O (b*-), and y-type, resulting from collision-induced dissociation of the $[M + H]^+$ ion of **18**, are shown in *red*, *blue* and *yellow* respectively. The $[M+H]^+$ and $[M–H_2O+H]^+$ ions are shown in *maroon*.

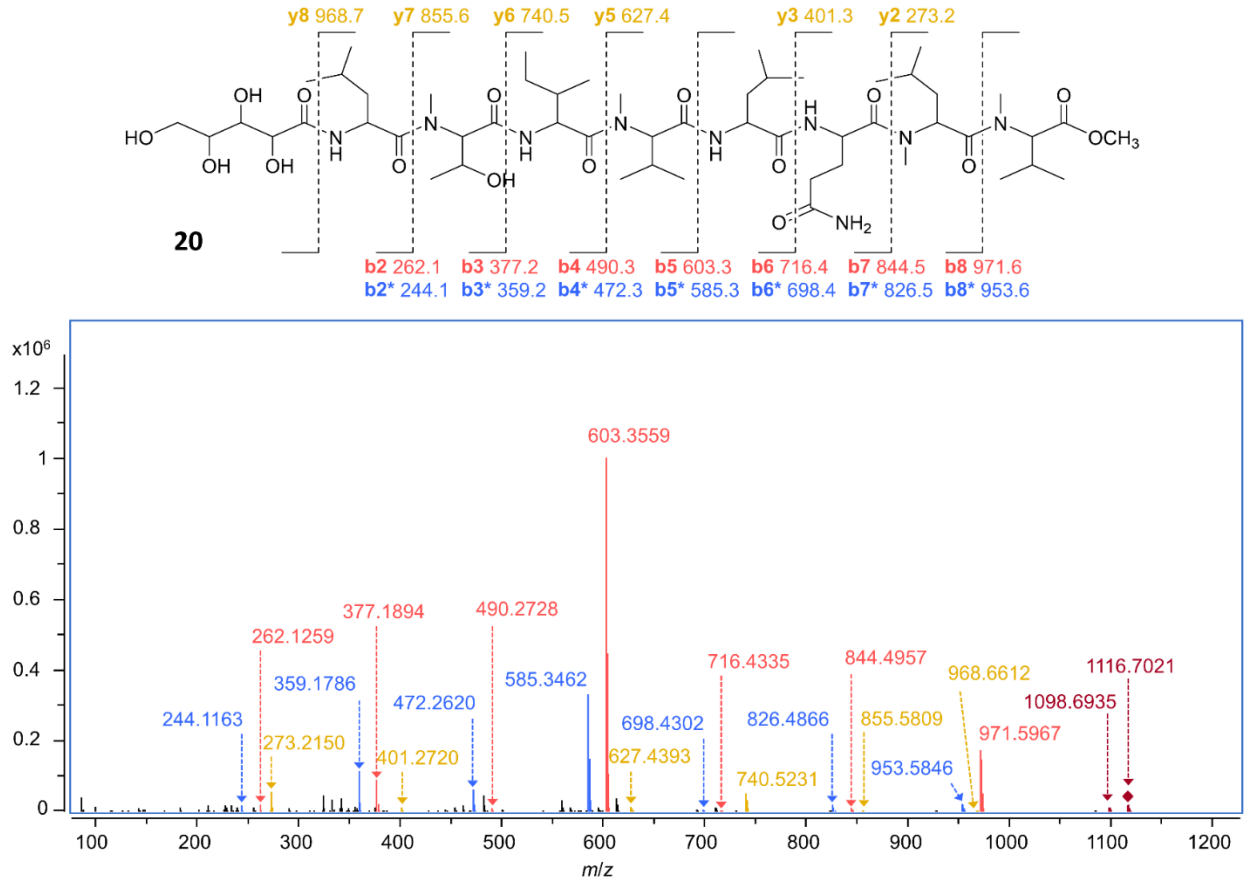

Figure S1.4. Product ion mass spectrum of the $[M + H]^+$ ion of 20 (*m/z* 1116.7021).

Compound **4** was first linearized by methanolysis upon treatment with CH_3ONa/CH_3OH to afford the methoxy-substituted derivative **20**. Fragment ions of the b-, b–H_2O (b*-), and y-type, resulting from collision-induced dissociation of the $[M + H]^+$ ion of **20**, are shown in *red*, *blue* and *yellow* respectively. The $[M+H]^+$ and $[M–H_2O+H]^+$ ions are shown in *maroon*.

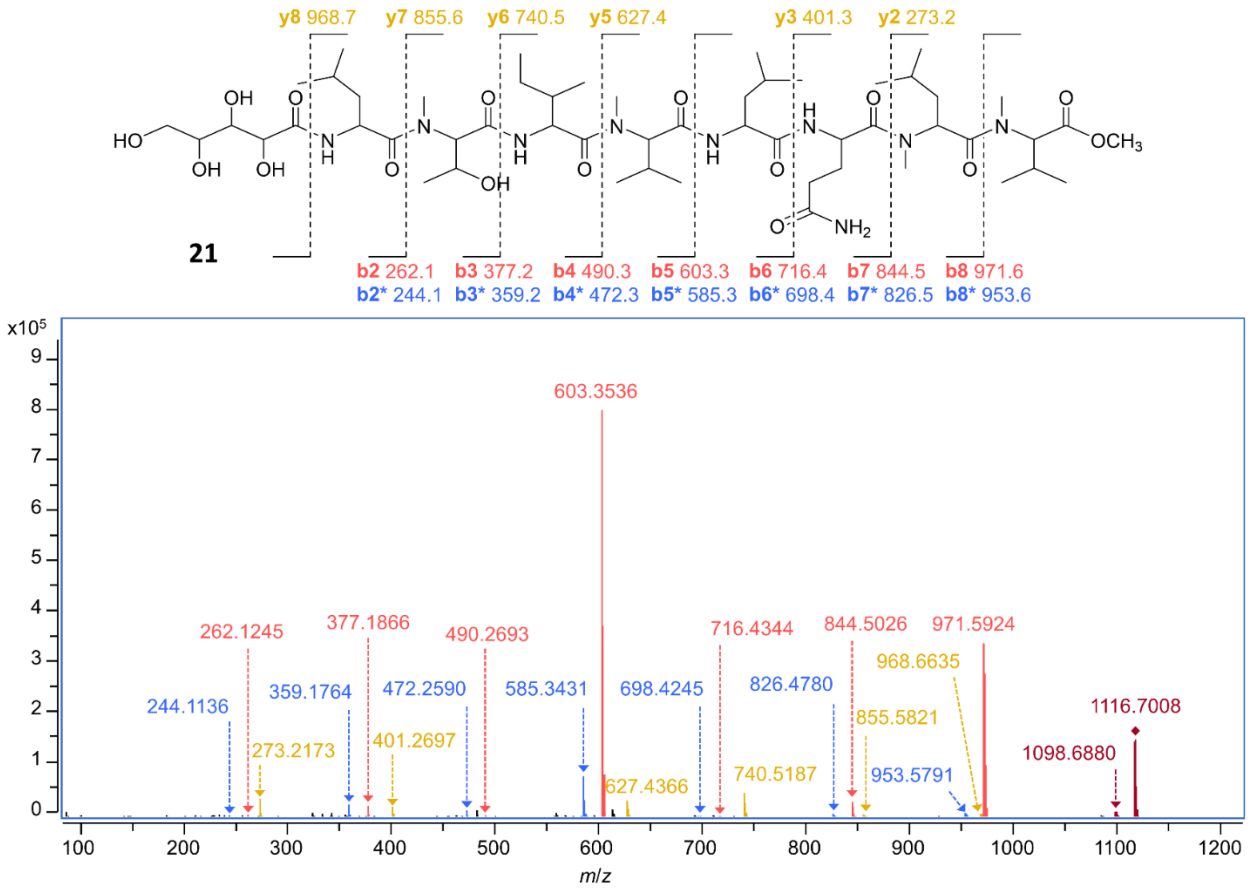

Figure S1.5. Product ion mass spectrum of the $[M + H]^+$ ion of 21 (*m/z* 1116.7008).

Compound **M1** was first linearized by methanolysis upon treatment with CH_3ONa/CH_3OH to afford two methoxy-substituted derivatives **21** and **22**. Fragment ions of the b-, b−H_2O (b*-), and y-type, resulting from collision-induced dissociation of the $[M + H]^+$ ion of **21**, are shown in *red*, *blue* and *yellow* respectively. The $[M+H]^+$ and $[M–H_2O+H]^+$ ions are shown in *maroon*.

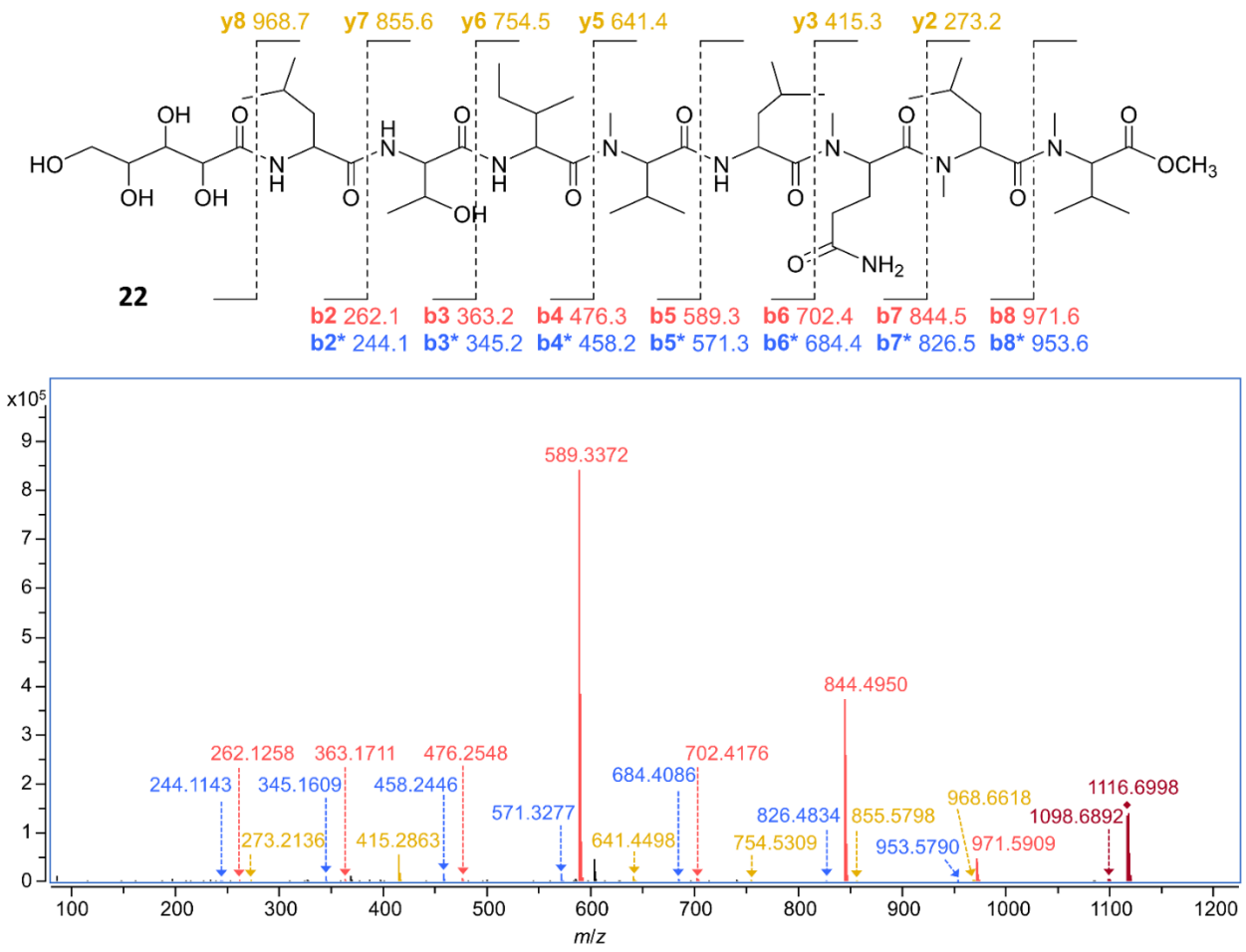

Figure S1.6. Product ion mass spectrum of the $[M + H]^+$ ion of 22 (*m/z* 1116.6998).

Compound **M1** was first linearized by methanolysis upon treatment with CH_3ONa/CH_3OH to afford two methoxy-substituted derivatives **21** and **22**. Fragment ions of the b-, b−H_2O (b*-), and y-type, resulting from collision-induced dissociation of the $[M + H]^+$ ion of **22**, are shown in *red*, *blue* and *yellow* respectively. The $[M+H]^+$ and $[M–H_2O+H]^+$ ions are shown in *maroon*.

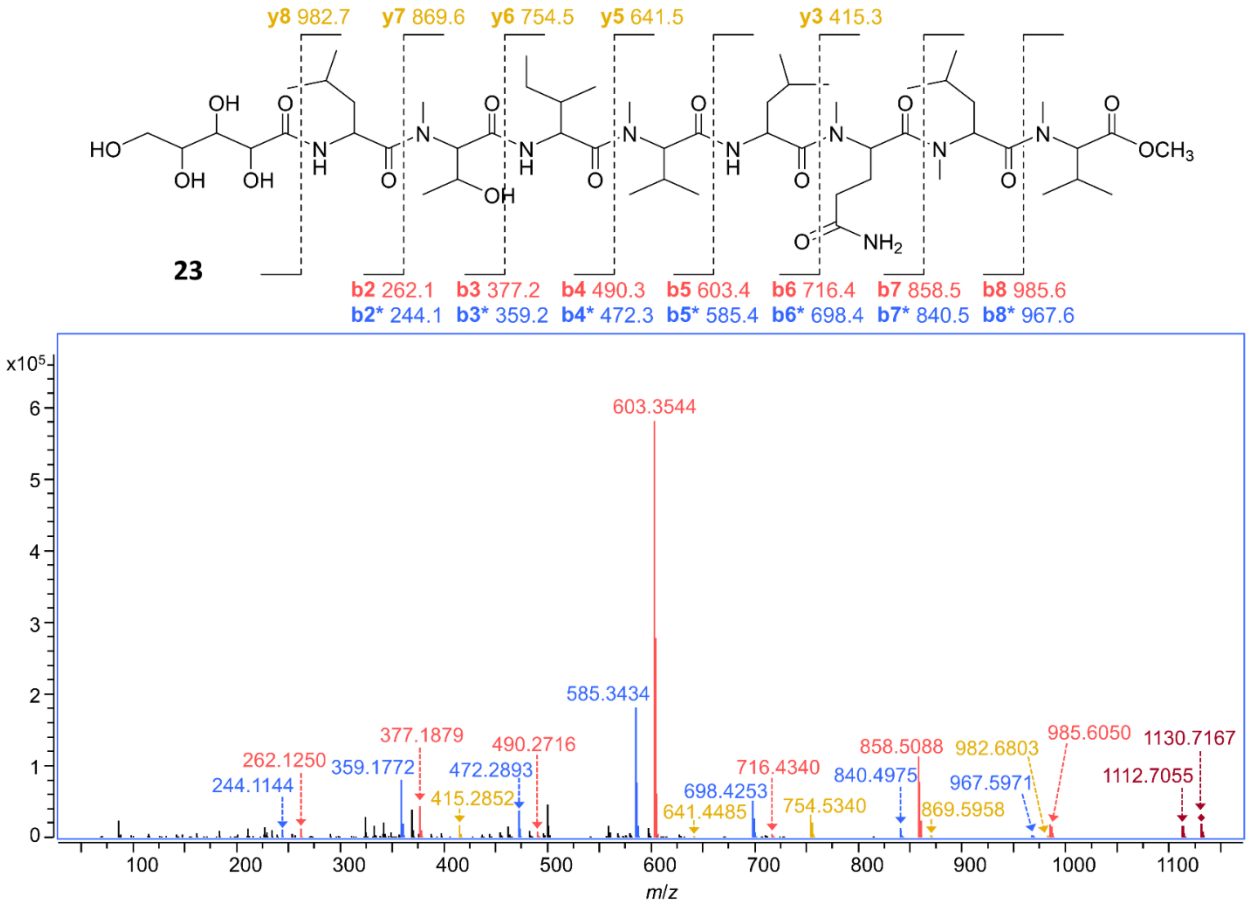

Figure S1.7. Product ion mass spectrum of the $[M + H]^+$ ion of 23 (*m/z* 1130.7167).

Compound **M2** was first linearized by methanolysis upon treatment with CH_3ONa/CH_3OH to afford the methoxy-substituted derivative **23**. Fragment ions of the b-, b–H_2O (b*-), and y-type, resulting from collision-induced dissociation of the $[M + H]^+$ ion of **23**, are shown in *red*, *blue* and *yellow* respectively. The $[M+H]^+$ and $[M–H_2O+H]^+$ ions are shown in *maroon*.

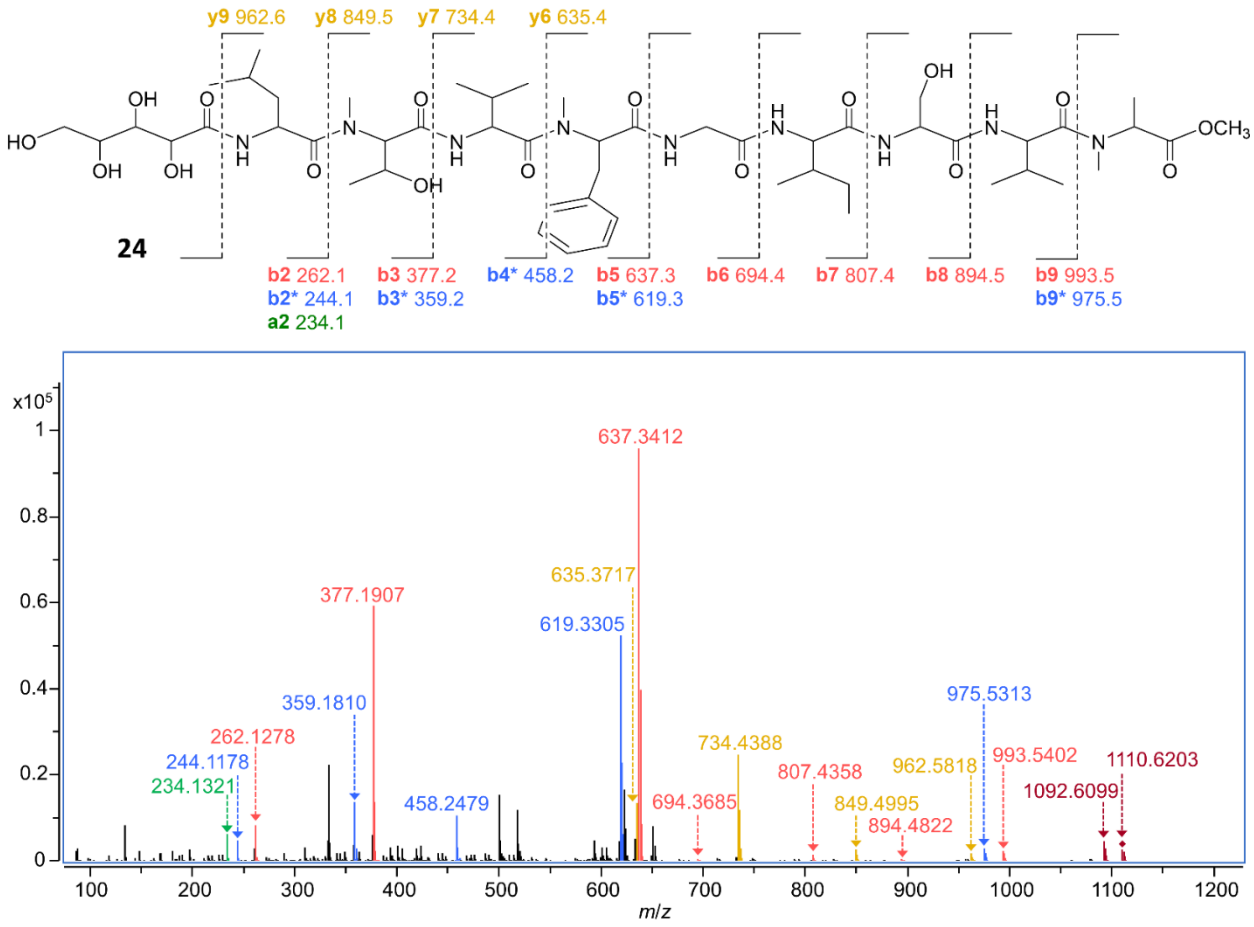

Figure S1.8. Product ion mass spectrum of the $[M + H]^+$ ion of 24 (*m/z* 1110.6203).

Compound **5** was first linearized by methanolysis upon treatment with CH_3ONa/CH_3OH to afford the methoxy-substituted derivative **24**. Fragment ions of the b-, b−H_2O (b*-), and y-type, resulting from collision-induced dissociation of the $[M + H]^+$ ion of **24**, are shown in *red*, *blue* and *yellow* respectively. The $[M+H]^+$ and $[M–H_2O+H]^+$ ions are shown in *maroon*.

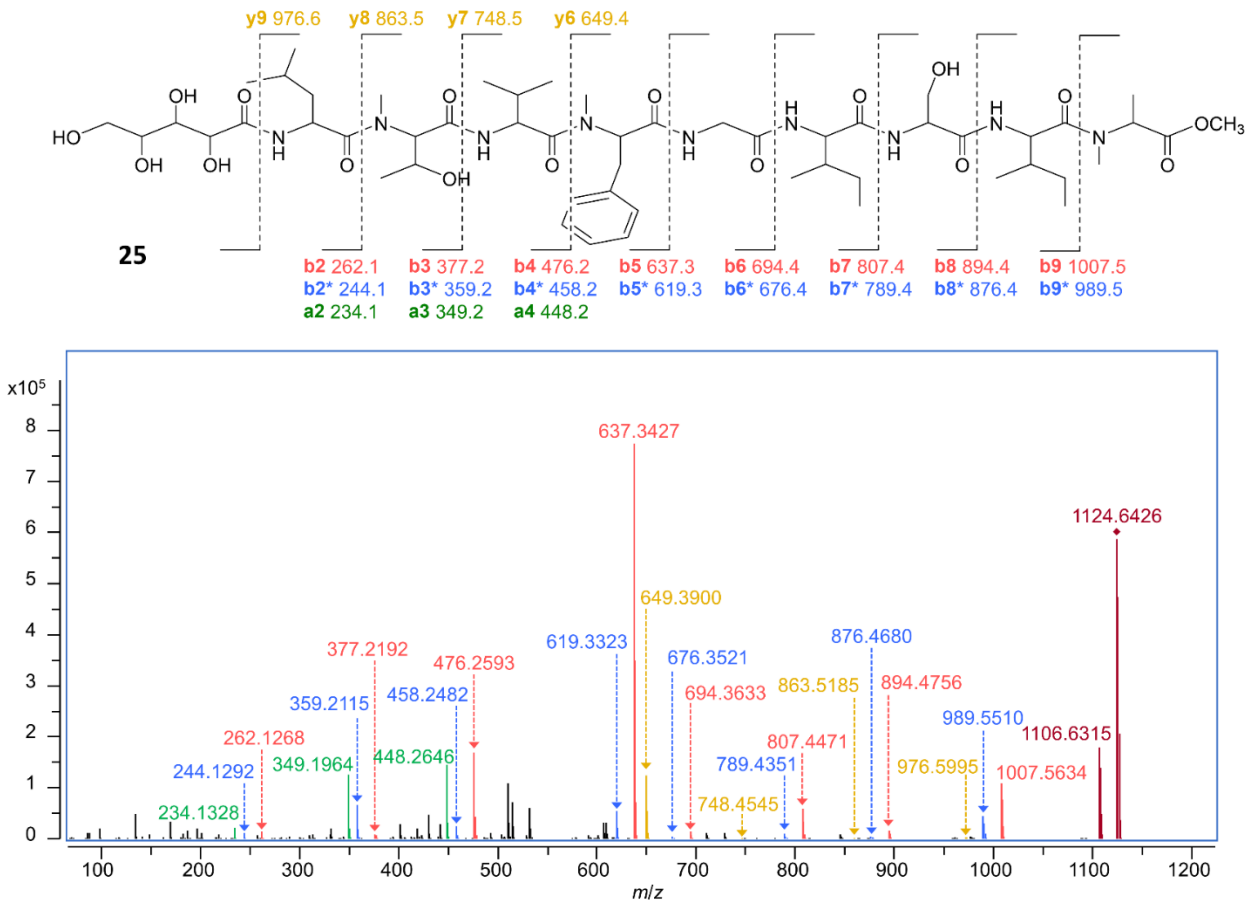

Figure S1.9. Product ion mass spectrum of the $[M + H]^+$ ion of 25 (*m/z* 1124.6426).

Compound **6** was first linearized by methanolysis upon treatment with CH_3ONa/CH_3OH to afford the methoxy-substituted derivative **25**. Fragment ions of the b-, b−H_2O (b*-), and y-type, resulting from collision-induced dissociation of the $[M + H]^+$ ion of **25**, are shown in *red*, *blue* and *yellow* respectively. The $[M+H]^+$ and $[M–H_2O+H]^+$ ions are shown in *maroon*.

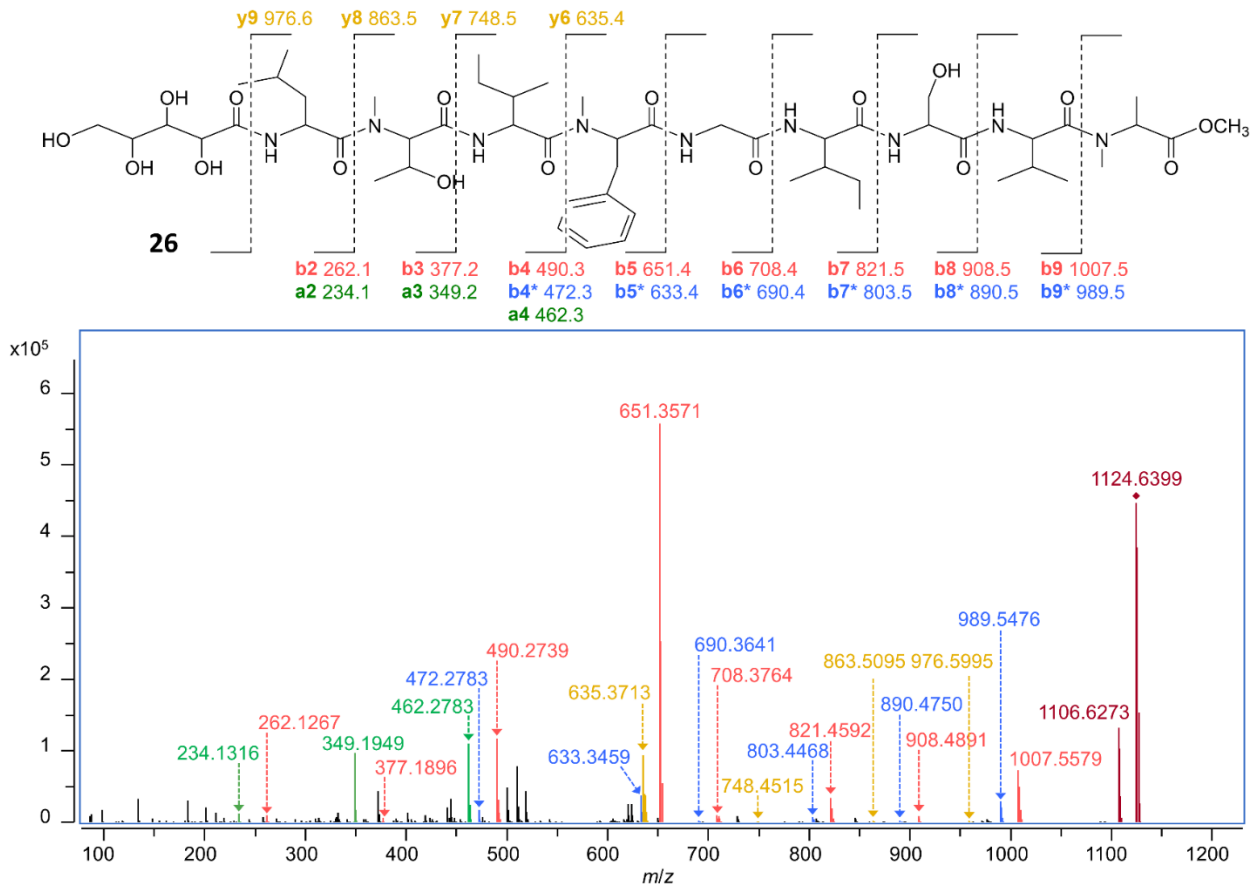

Figure S1.10. Product ion mass spectrum of the $[M + H]^+$ ion of 26 (*m/z* 1124.6399).

Compound **7** was first linearized by methanolysis upon treatment with CH_3ONa/CH_3OH to afford the methoxy-substituted derivative **26**. Fragment ions of the b-, b–H_2O (b*-), and y-type, resulting from collision-induced dissociation of the $[M + H]^+$ ion of **26**, are shown in *red*, *blue* and *yellow* respectively. The $[M+H]^+$ and $[M–H_2O+H]^+$ ions are shown in *maroon*.

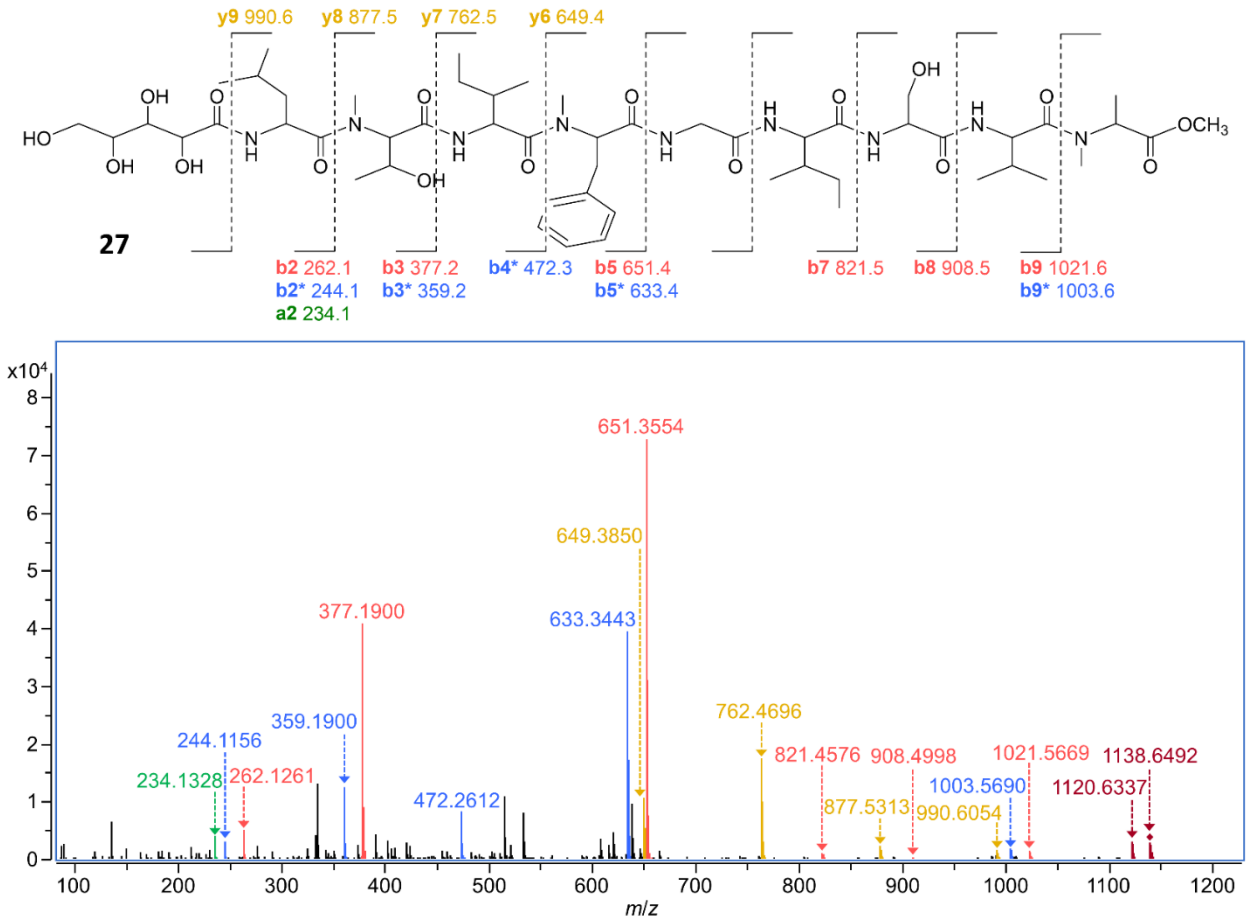

Figure S1.11. Product ion mass spectrum of the $[M + H]^+$ ion of 27 (*m/z* 1138.6492).

Compound **10** was first linearized by methanolysis upon treatment with CH_3ONa/CH_3OH to afford the methoxy-substituted derivative **27**. Fragment ions of the b-, b−H_2O (b*-), and y-type, resulting from collision-induced dissociation of the $[M + H]^+$ ion of **27**, are shown in *red*, *blue* and *yellow* respectively. The $[M+H]^+$ and $[M–H_2O+H]^+$ ions are shown in *maroon*.

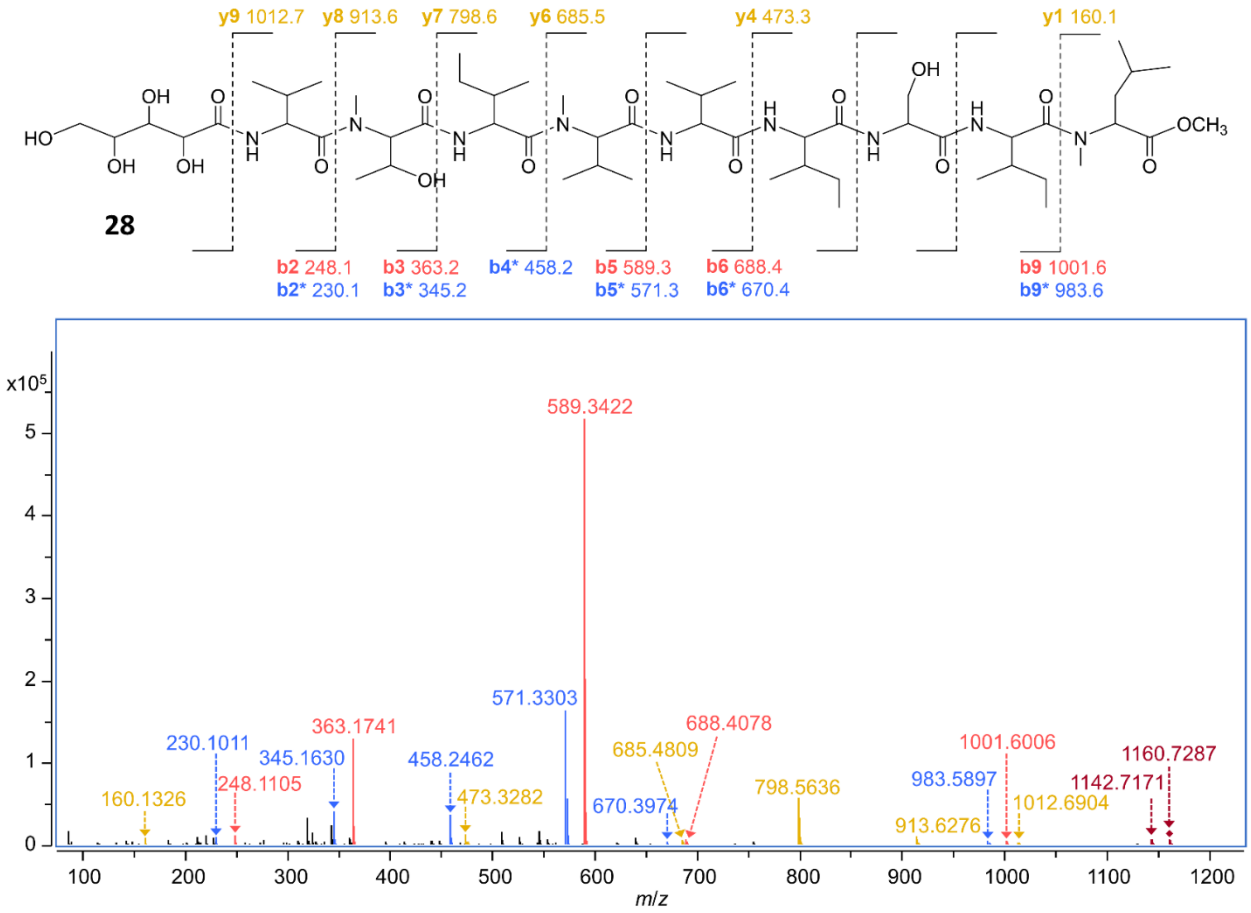

Figure S1.12. Product ion mass spectrum of the $[M + H]^+$ ion of 28 (*m/z* 1160.7287).

Compound **11** was first linearized by methanolysis upon treatment with CH_3ONa/CH_3OH to afford the methoxy-substituted derivative **28**. Fragment ions of the b-, b–H_2O (b*-), and y-type, resulting from collision-induced dissociation of the $[M + H]^+$ ion of **28**, are shown in *red*, *blue* and *yellow* respectively. The $[M+H]^+$ and $[M–H_2O+H]^+$ ions are shown in *maroon*.

Figure S2. Chemical structures and key ^{1}H-^{1}H COSY/TOCSY (bold lines), HMBC (plain arrows) and NOE (dashed arrows) correlations of isolated compounds.

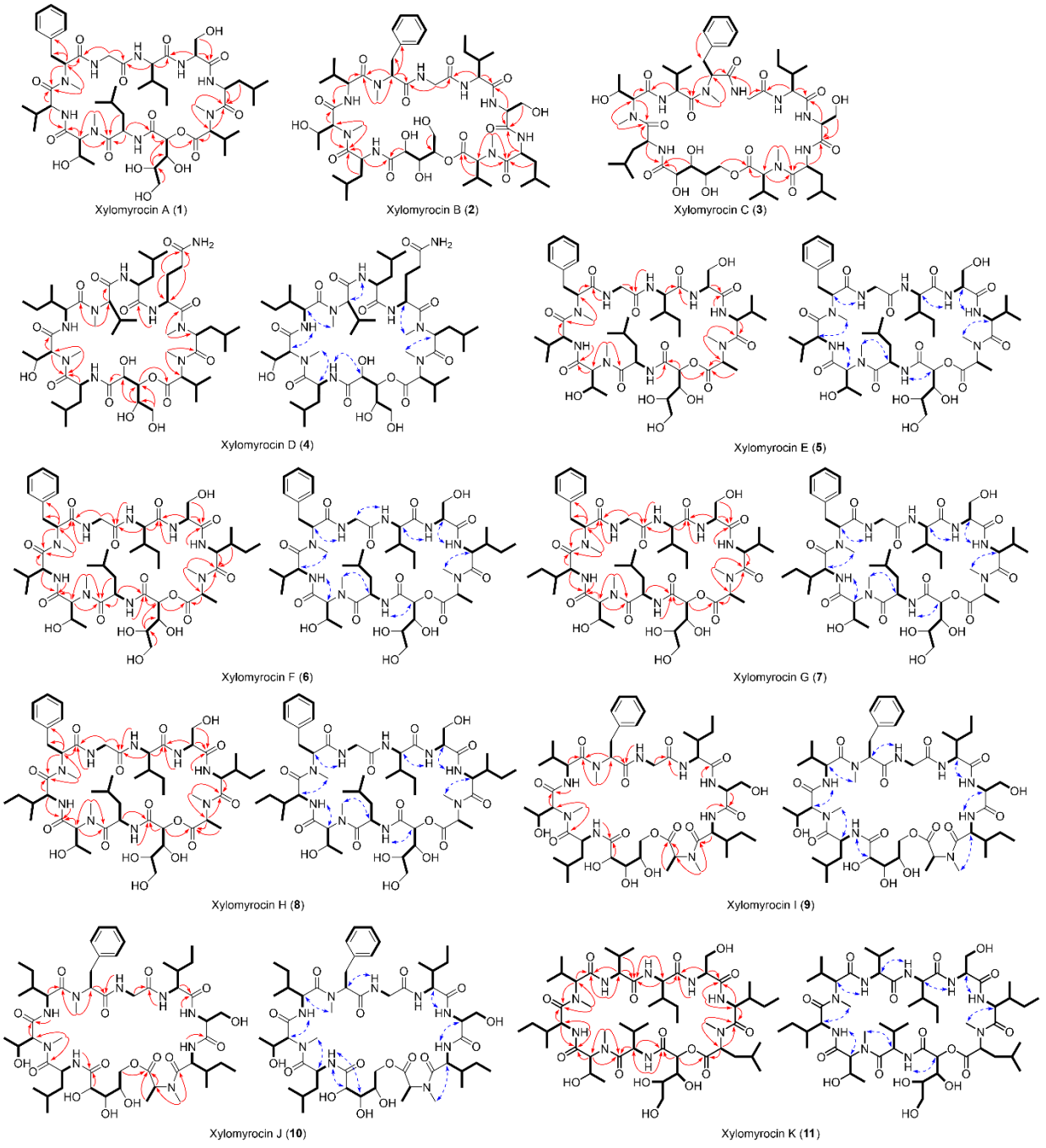

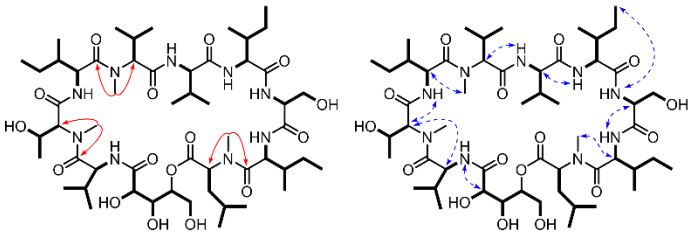

Xylomyrocin L (**12**)

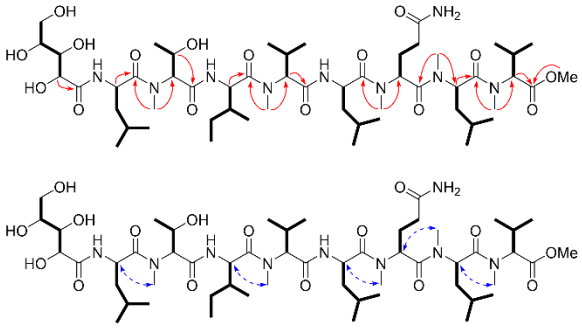

23a

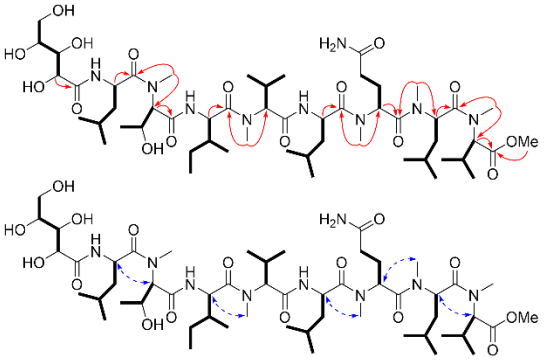

23b

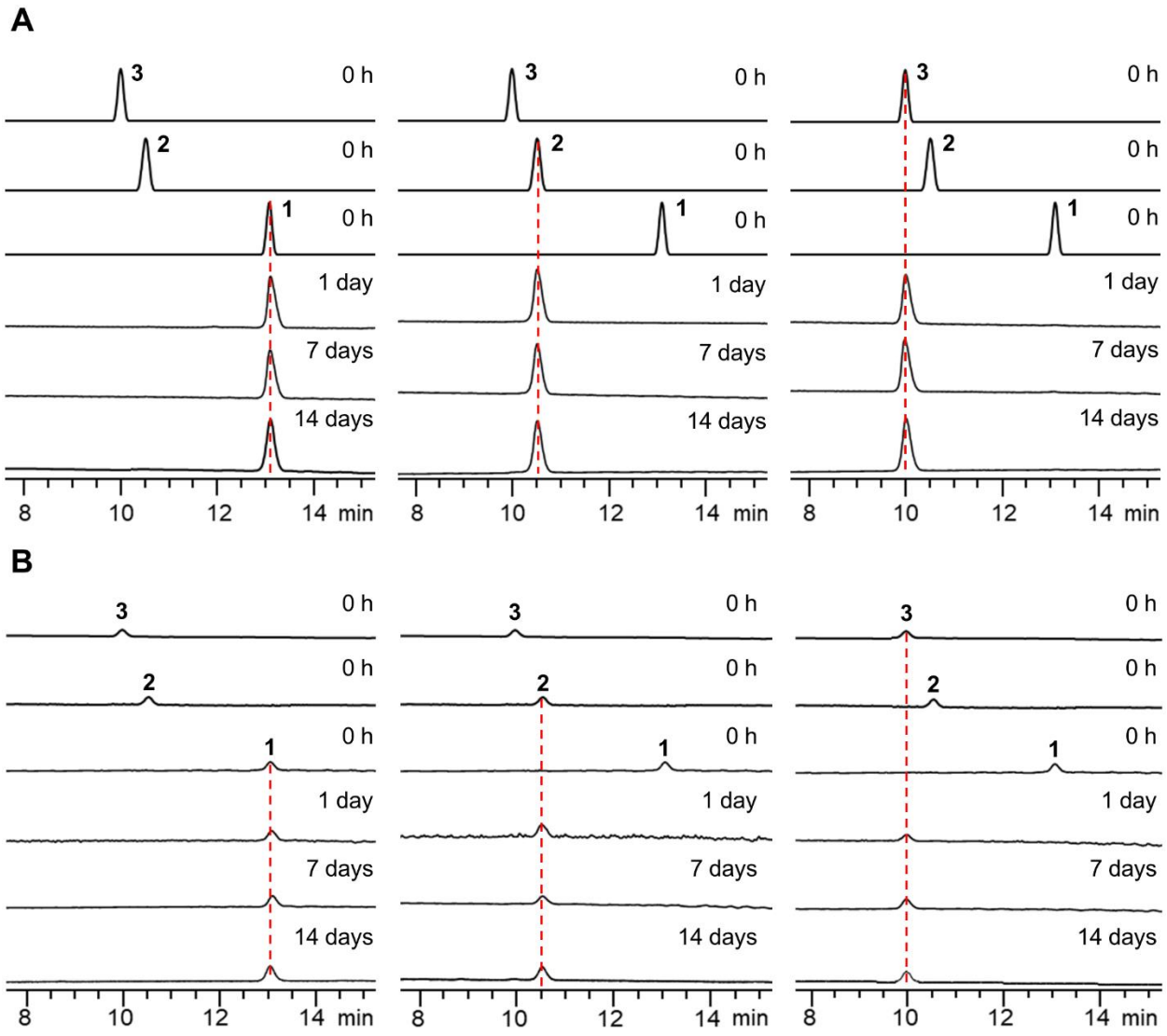

Figure S3. Stability of the ester linkage in xylomyrocins.

HPLC traces of compounds **1**–**3**, monitored at 210 nm, after incubation in **A**. acidic CH_3CN (containing 1% formic acid, pH = 5.5) or **B**. acidic water (containing 1% formic acid, pH = 5.0) for 1, 7, and 14 days.

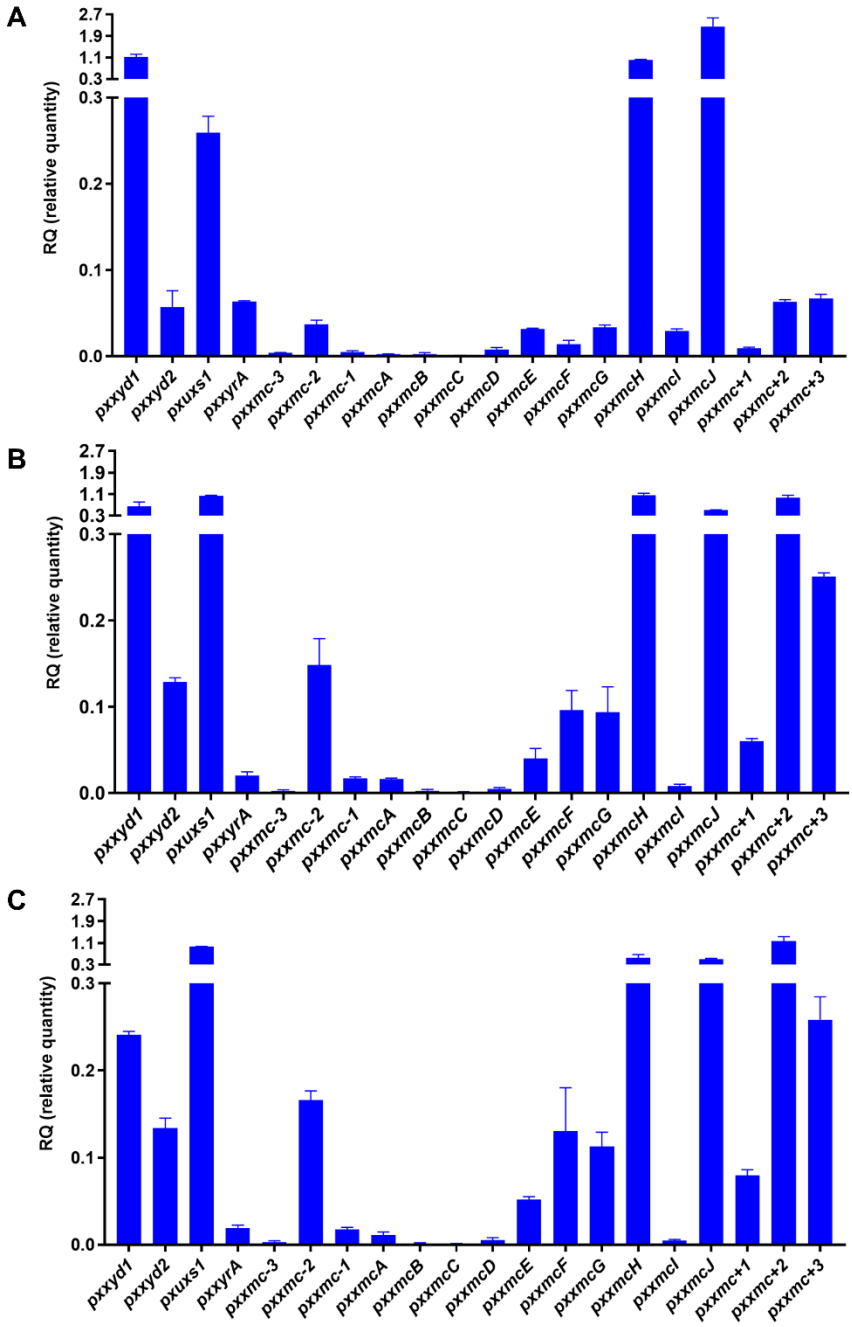

Figure S4. RT-qPCR analysis of *pxxyd1, pxxyd2, pxuxs1*, *pxxyrA*, and genes in the *pxxmc* locus.

Paramyrothecium sp. XJ0827 was grown in liquid M-100 media for: **A**, 5 days; **B**, 7 days; and **C**, 9 days. The β-tubulin-encoding gene was used as the reference gene, and the relative expression fold-change was calculated using the comparative threshold cycle $2^{-\Delta\Delta CT}$ method. Data were collected from three biological replicates measured in three technical replicates each (n = 9). Columns represents the mean ± SE.

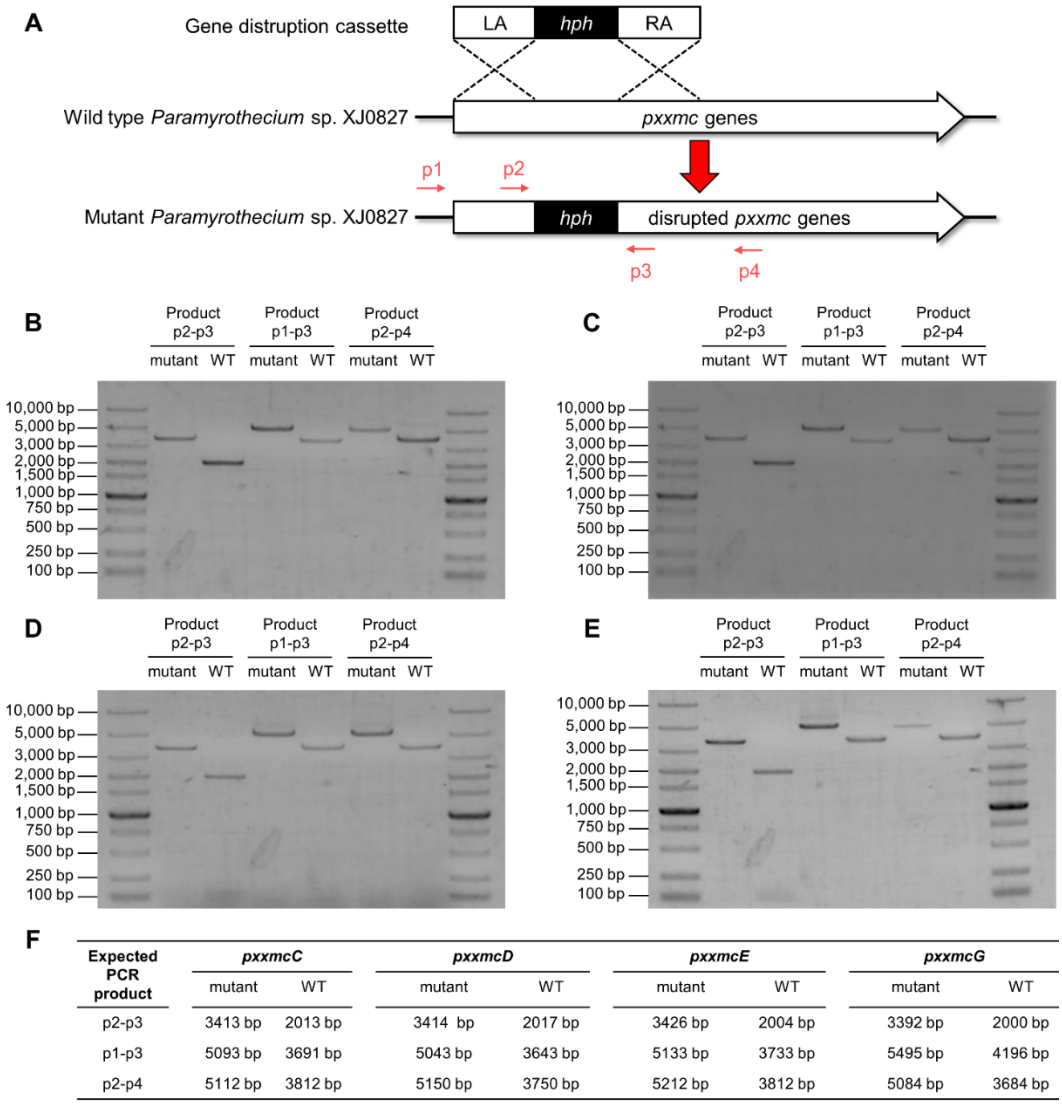

F

Expected PCR product	*pxxmcC*		*pxxmcD*		*pxxmcE*		*pxxmcG*	
	mutant	WT	mutant	WT	mutant	WT	mutant	WT
p2-p3	3413 bp	2013 bp	3414 bp	2017 bp	3426 bp	2004 bp	3392 bp	2000 bp
p1-p3	5093 bp	3691 bp	5043 bp	3643 bp	5133 bp	3733 bp	5495 bp	4196 bp
p2-p4	5112 bp	3812 bp	5150 bp	3750 bp	5212 bp	3812 bp	5084 bp	3684 bp

Figure S5. Targeted disruption of *pxxmc* genes.

A. Scheme for the double homologous recombination between a *pxxmc* gene disruption cassette and the *Paramyrothecium* sp. XJ0827 genome. Primers p1–p4 (red arrows), locating outside (p1 and p4) and inside (p2 and p3) the left or the right targeting arms were used for PCR validation of the hygromycin resistant gene knockout *Paramyrothecium* sp. XJ0827 strains. PCR products for representative isolates of the wild type XJ0827 strain (WT, control) and: **B**. the Δ*pxxmcC* mutant; **C**. the Δ*pxxmcD* mutant; **D**. the Δ*pxxmcE* mutant; and **E**. the Δ*pxxmcG* mutant. **F**. The expected lengths of the PCR products amplified by the appropriate primers using the wild type or the mutant *Paramyrothecium* sp. XJ0827 genomic DNA as the template.

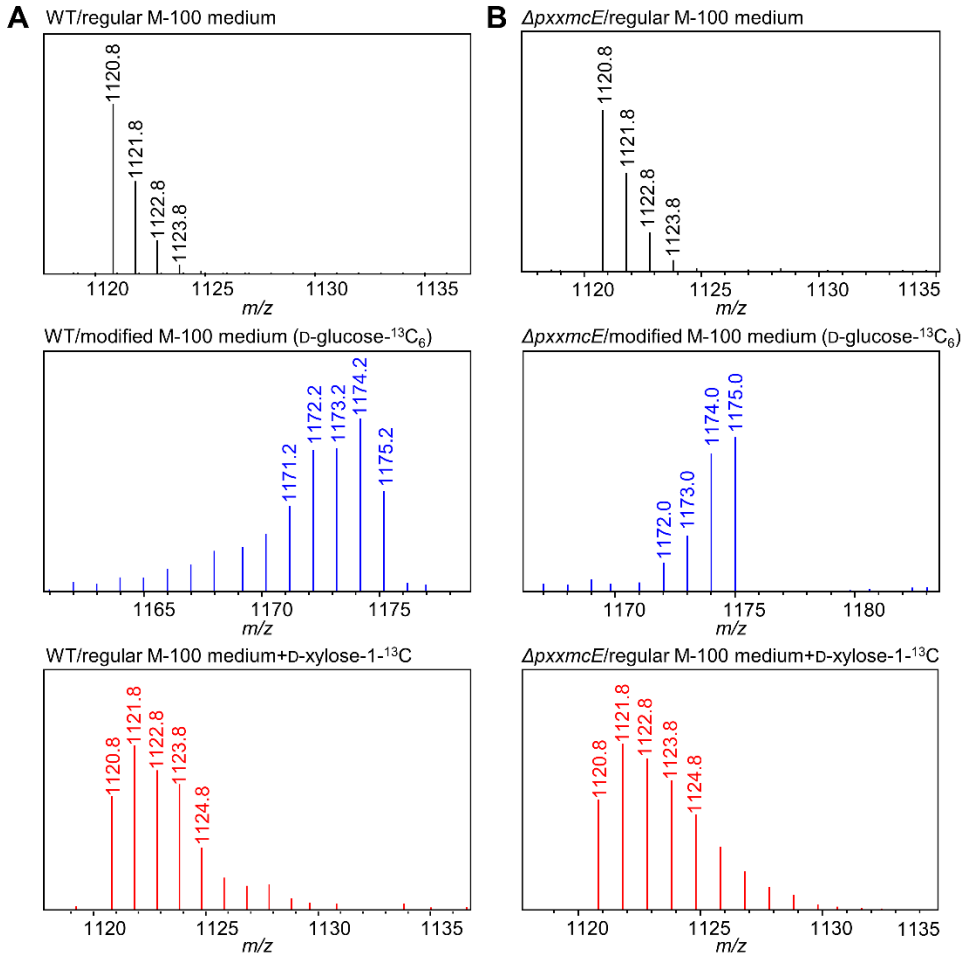

Figure S6. Mass spectra of isotopically labeled xylomyrocin A.

Mass spectra of **1** from culture extract of **A.** the wild type or **B.** the Δ*pxxmcE* strain of *Paramyrothecium* sp. XJ0827 grown in regular M-100 medium (*black*), or modified M-100 medium where D-glucose-$^{13}C_6$ replaces D-glucose as the sole carbon source (*blue*), or regular M-100 medium with the supplementation of D-xylose-1-^{13}C (*red*).

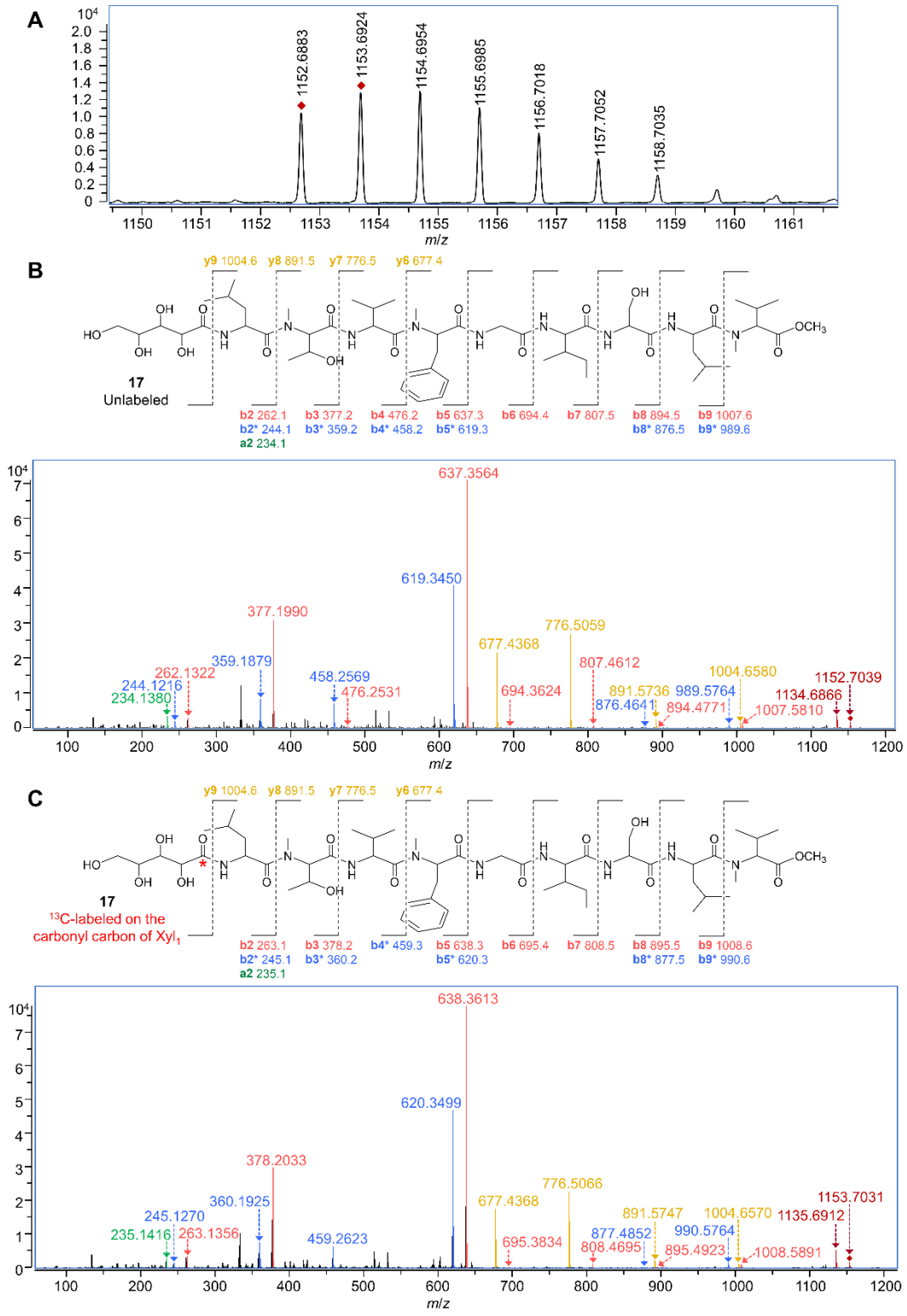

Figure S7. Tandem mass analysis of linearized 1 (17) with isotopical label.

A. Mass spectra of **17** obtained from culture extract of wild type *Paramyrothecium* sp. XJ0827 grown in

regular M-100 medium with the supplementation of D-xylose-1-^{13}C. **B.** Theoretical and experimental MS/MS fragmentation pattern of unlabeled **17**. **C.** Theoretical and experimental MS/MS fragmentation pattern of ^{13}C-labeled **17**. The labeling position is indicated by an asterisk. Fragment ions of the a-, b-, b−H_2O (b*-), and y-type, resulting from collision-induced dissociation are shown in *green*, *red*, *blue* and *yellow* respectively. The $[M+H]^+$ and $[M–H_2O+H]^+$ ions are shown in *maroon*.

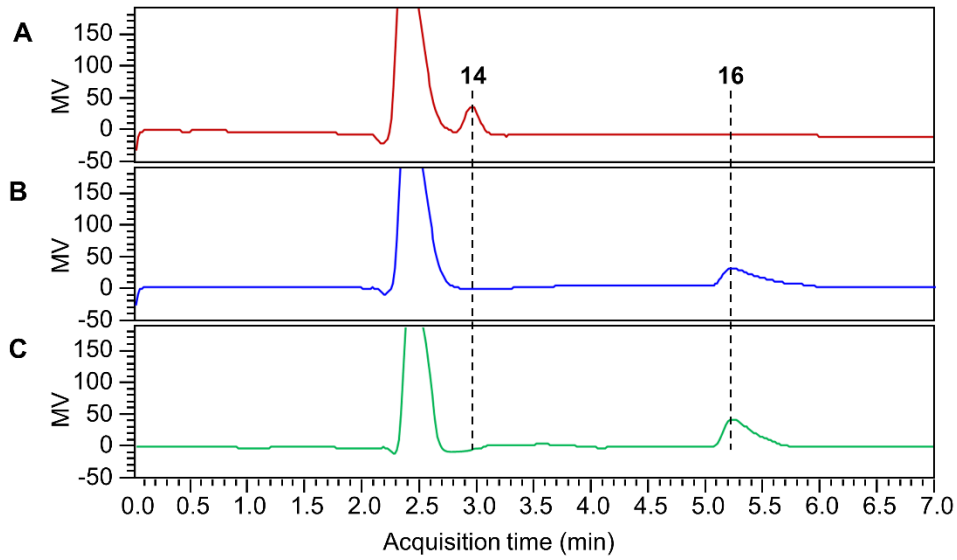

Figure S8. HPLC analysis of the hydrolysis of D-xylono-γ-lactone (14).

A. D-xylono-γ-lactone (**14**), **B.** D-xylonic acid (**16**), and **C.** D-xylono-γ-lactone hydrolysate (**15**).

HPLC was carried out on a Waters Alliance e2695 system coupled with a Waters 2414 refractive index detector. Hydrolysate **15** was prepared by treating **14** with 1 M aqueous NaOH solution.

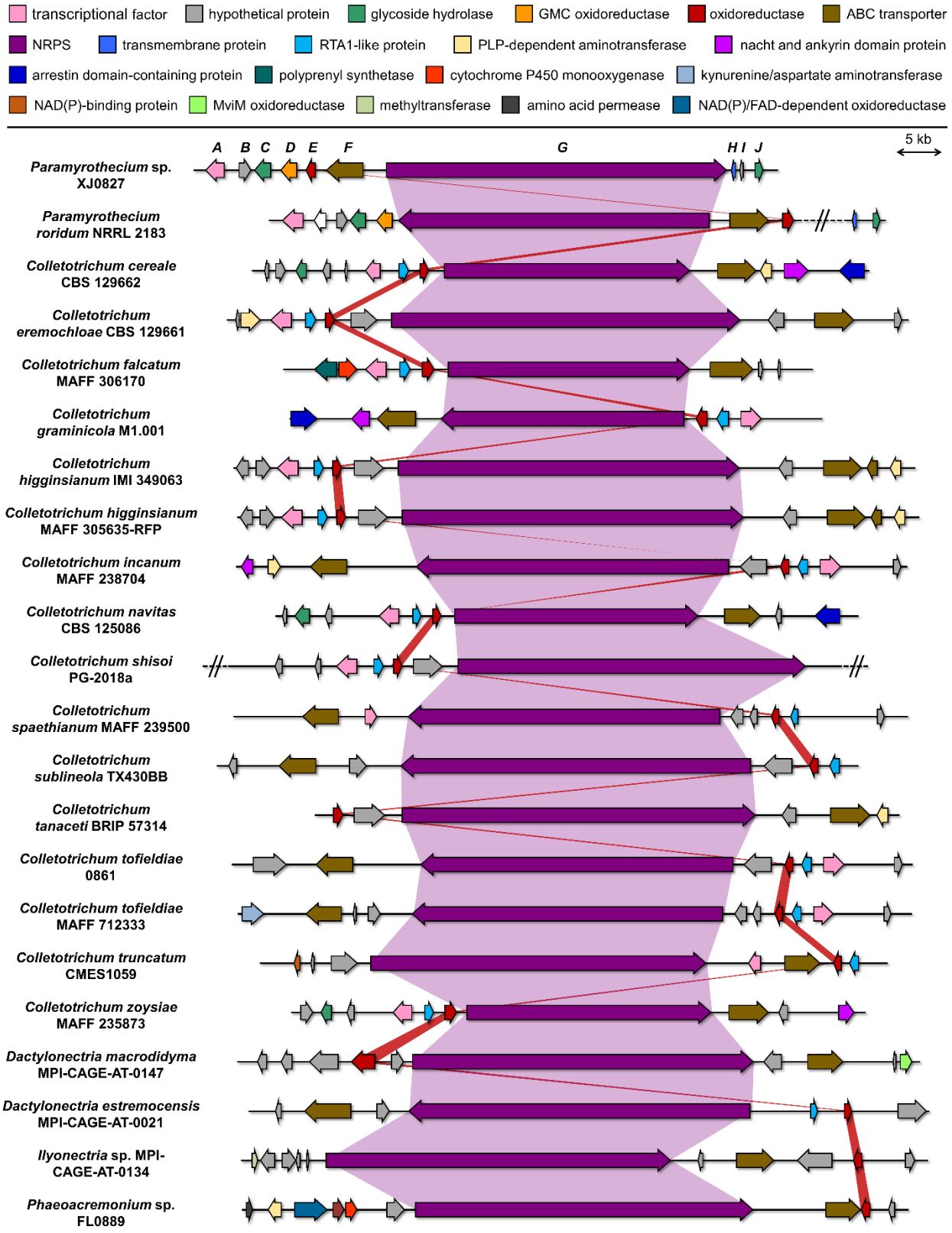

Figure S9. *pxxmc*-like BGCs in fungal genomes.

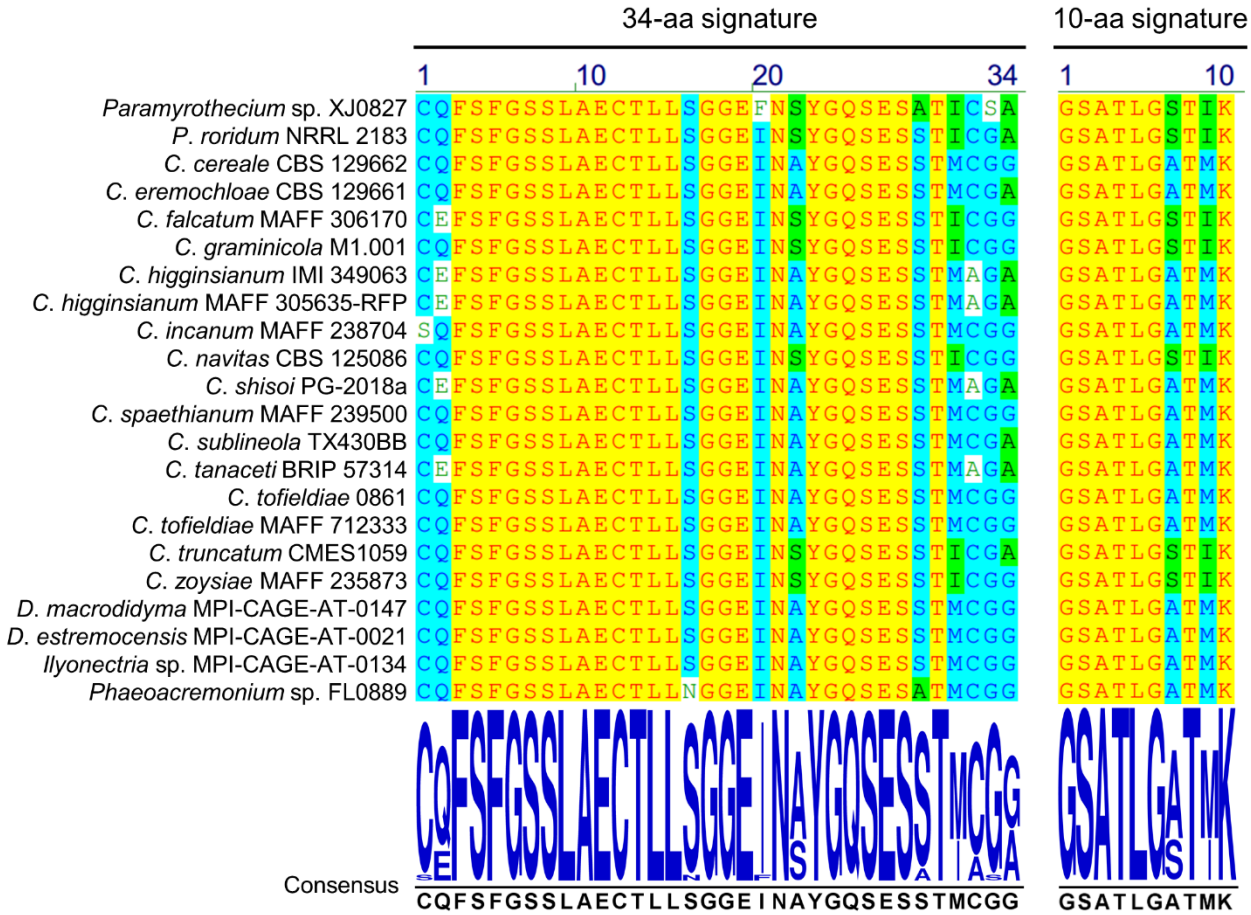

Figure S10. Substrate specificity signatures of the A_1 domains of PxXmcG homologues found in fungal genomes[21-22]

Compound	Producer	Amino Acids/Hydroxy Acids										Lactone Ring
1	*Paramyrothecium* sp. XJ0827	Xyl_1	Leu_2	$MeThr_3$	Val_4	$MePhe_5$	Gly_6	Ile_7	Ser_8	Leu_9	$MeVal_{10}$	α-OH
2	*Paramyrothecium* sp. XJ0827	Xyl_1	Leu_2	$MeThr_3$	Val_4	$MePhe_5$	Gly_6	Ile_7	Ser_8	Leu_9	$MeVal_{10}$	γ-OH
3	*Paramyrothecium* sp. XJ0827	Xyl_1	Leu_2	$MeThr_3$	Val_4	$MePhe_5$	Gly_6	Ile_7	Ser_8	Leu_9	$MeVal_{10}$	δ-OH
4	*P. roridum* NRRL 2183	Xyl_1	Leu_2	$MeThr_3$	Ile_4	$MeVal_5$	-	Leu_6	Gln_7	$MeLeu_8$	$MeVal_9$	α-OH
M1	*P. roridum* NRRL 2183	Xyl_1	Leu_2	Thr_3	Ile_4	$MeVal_5$	-	Leu_6	$MeGln_7$	$MeLeu_8$	$MeVal_9$	nd
M2	*P. roridum* NRRL 2183	Xyl_1	Leu_2	$MeThr_3$	Ile_4	$MeVal_5$	-	Leu_6	$MeGln_7$	$MeLeu_8$	$MeVal_9$	nd
5	*P. roridum* MN131194	Xyl_1	Leu_2	$MeThr_3$	Val_4	$MePhe_5$	Gly_6	Ile_7	Ser_8	Val_9	$MeAla_{10}$	α-OH
6	*P. roridum* MN131194	Xyl_1	Leu_2	$MeThr_3$	Val_4	$MePhe_5$	Gly_6	Ile_7	Ser_8	Ile_9	$MeAla_{10}$	α-OH
7	*P. roridum* MN131194	Xyl_1	Leu_2	$MeThr_3$	Ile_4	$MePhe_5$	Gly_6	Ile_7	Ser_8	Val_9	$MeAla_{10}$	α-OH
8	*P. roridum* MN131194	Xyl_1	Leu_2	$MeThr_3$	Ile_4	$MePhe_5$	Gly_6	Ile_7	Ser_8	Ile_9	$MeAla_{10}$	α-OH
9	*P. roridum* MN131194	Xyl_1	Leu_2	$MeThr_3$	Val_4	$MePhe_5$	Gly_6	Ile_7	Ser_8	Ile_9	$MeAla_{10}$	δ-OH
10	*P. roridum* MN131194	Xyl_1	Leu_2	$MeThr_3$	Ile_4	$MePhe_5$	Gly_6	Ile_7	Ser_8	Ile_9	$MeAla_{10}$	δ-OH
11	*Colletotrichum* sp. XJ1040	Xyl_1	Val_2	$MeThr_3$	Ile_4	$MeVal_5$	Val_6	Ile_7	Ser_8	Ile_9	$MeLeu_{10}$	α-OH
12	*Colletotrichum* sp. XJ1040	Xyl_1	Val_2	$MeThr_3$	Ile_4	$MeVal_5$	Val_6	Ile_7	Ser_8	Ile_9	$MeLeu_{10}$	γ-OH

Figure S11. Sequence alignment of isolated xylomyrocins.

Yellow: identical residues; *blue*: highly conserved residues; *green*: similar residues; *white*: divergent residues; nd: not determined. Gln: L-glutamine; Gly: glycine; Ile: L-isoleucine; Leu: L-leucine; MeAla: *N*-methyl-L-alanine; MeGln: *N*-methyl-L-glutamine; MeLeu: *N*-methyl-L-leucine; MePhe: *N*-methyl-L-phenelalanine; MeThr: *N*-methyl-L-threonine; MeVal: *N*-methyl-L-valine; Ser: L-serine; Thr: L-threonine; Val: L-valine; Xyl: D-xylonic acid.

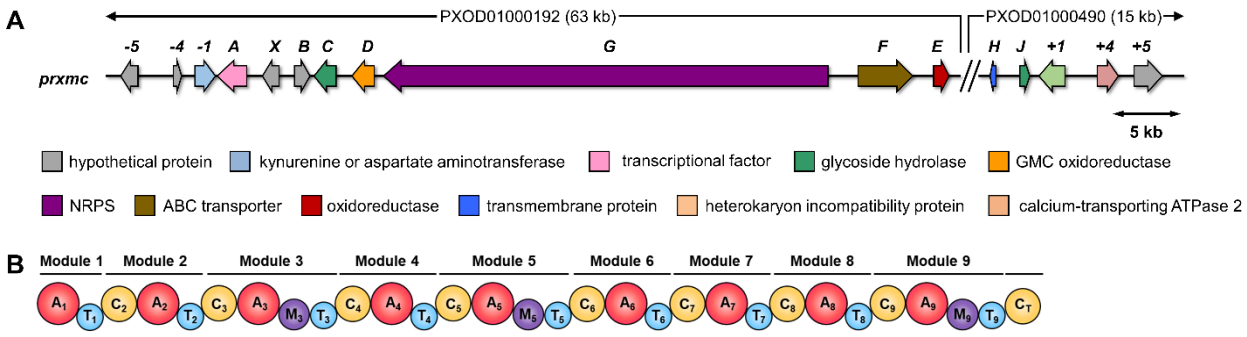

Figure S12. Bioinformatic analysis of the *prxmc* locus in *Paramyrothecium roridum* NRRL 2183.

A. Schematic representation of the *prxmc* locus. **B**. Domain organization of the NRPS PrXmcG.

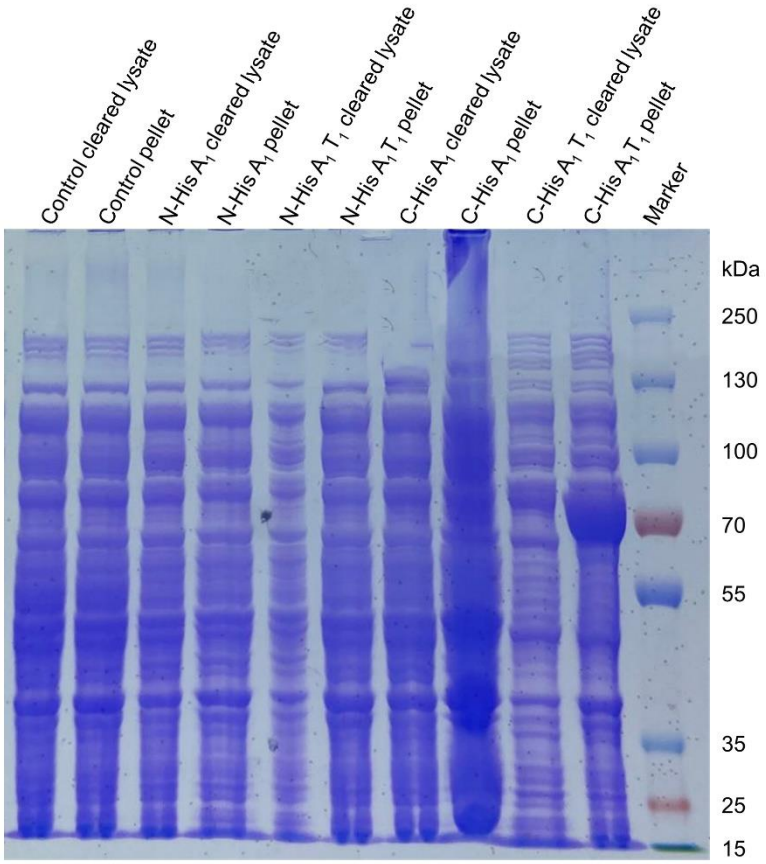

Figure S13. Absence of soluble, dissected recombinant PxXmcG-A_1 and A_1-T_1 in *E. coli* lysates.

SDS-PAGE analysis of the cleared lysate and the pellet of *E*. *coli* BL21 cells carrying pET28a plasmids that encode the *N*-His or *C*-His tagged A_1 mono-domain (c.a. 61.3 kDa) or A_1T_1 di-domain (c.a. 71.6 kDa) of PxXmcG. Expression was induced with 0.5 mM isopropyl β-D-thiogalactopyranoside (IPTG) and the cultures were incubated at 16 °C for 24 hrs with shaking at 250 rpm before the cells were harvested and lysed with sonication. The lysate and pellet of *E*. *coli* BL21 cells containing the empty pET28a vector were used as controls. Attempts to solubilize the putative *C*-His-A1T1 recombinant protein from the lysate pellets were unsuccessful. Induction with different IPTG concentrations (1, 0.5, or 0.15 mM), expression temperatures (25 °C, 16 °C, or 11 °C), and cultivation times (18 hrs or 24 hrs) did not afford soluble recombinant protein either with any of the expression constructs.

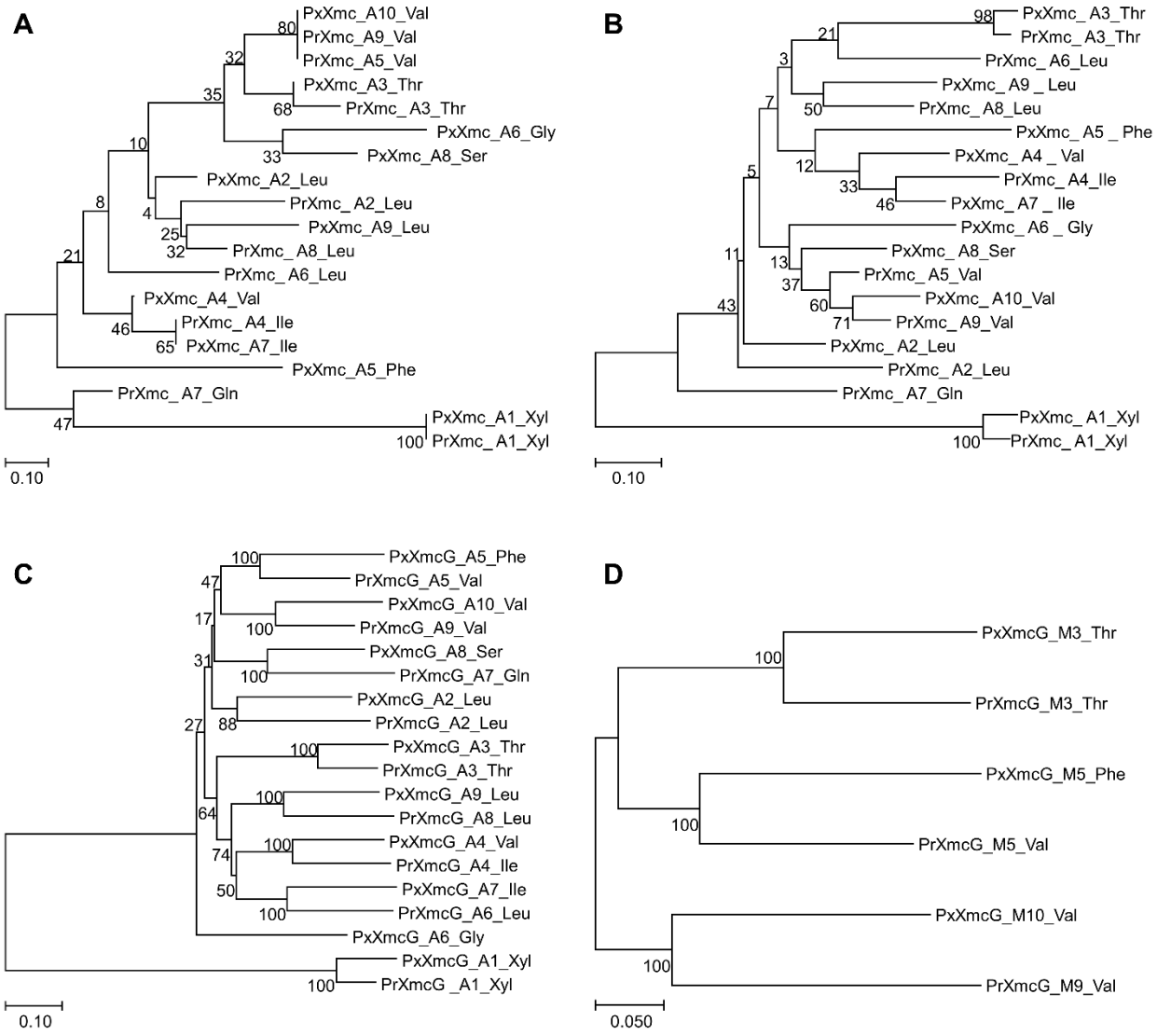

Figure S14. Phylogenetic analysis of A and M domains from PxXmcG and PrXmcG.

A. 10 aa code of A domains; **B.** 34 aa code of A domains; **C.** full length A domains; and **D.** full length M domains. Amino acid sequences were aligned by ClustalW, and phylogenetic analysis was carried out using the neighbor joining method in MEGA 7.

Figure S15. Advanced Marfey's analysis

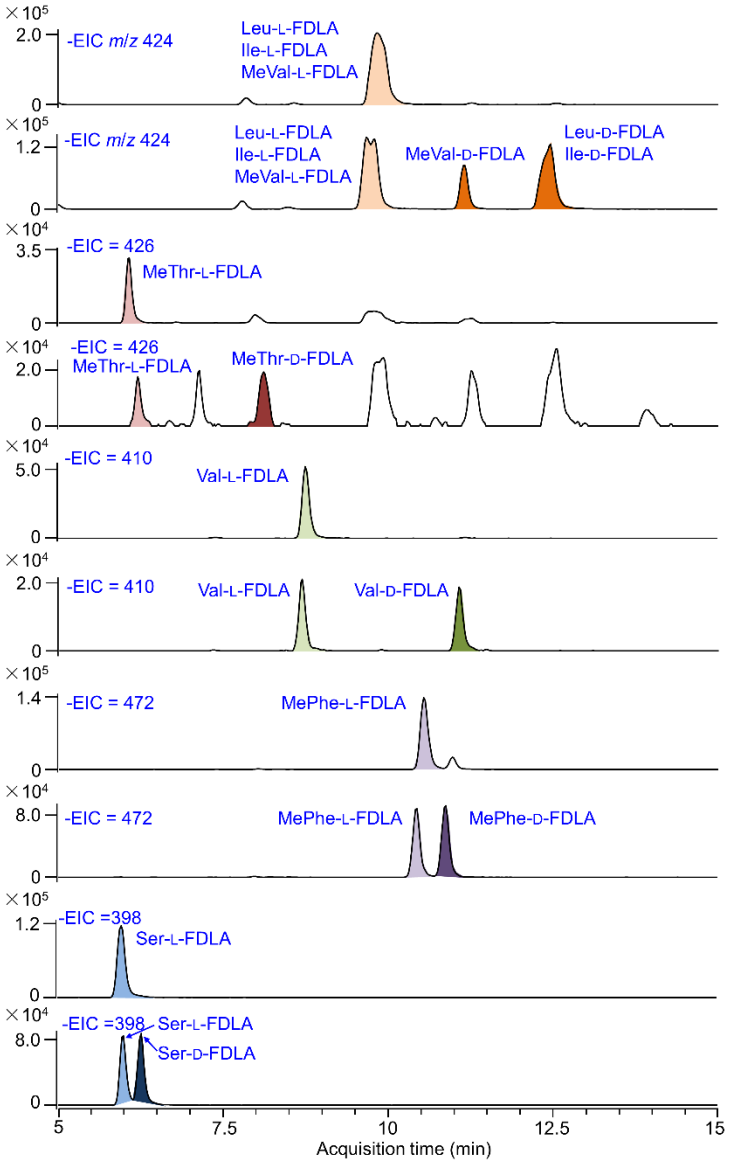

Figure S15.1. Extracted ion chromatograms of L- and D/L-FDLA derivatives of the acid hydrolysate of 1

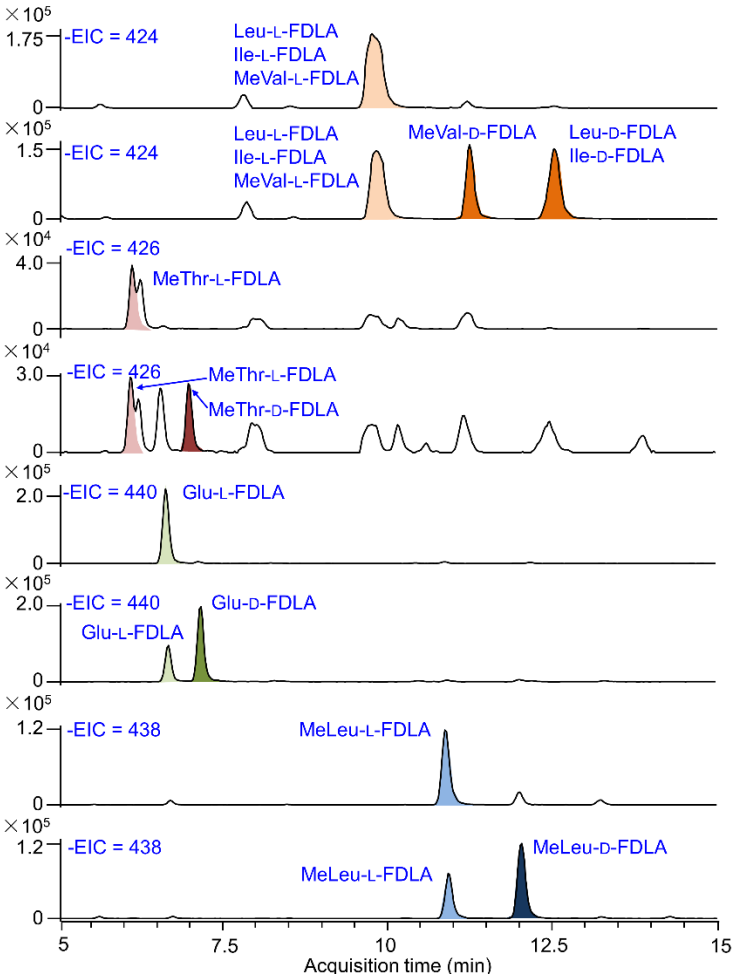

Figure S15.2. Extracted ion chromatograms of L- and D/L-FDLA derivatives of the acid hydrolysate of 4

Glutamine (Gln) was converted to glutamic acid (Glu) after HCl hydrolysis.

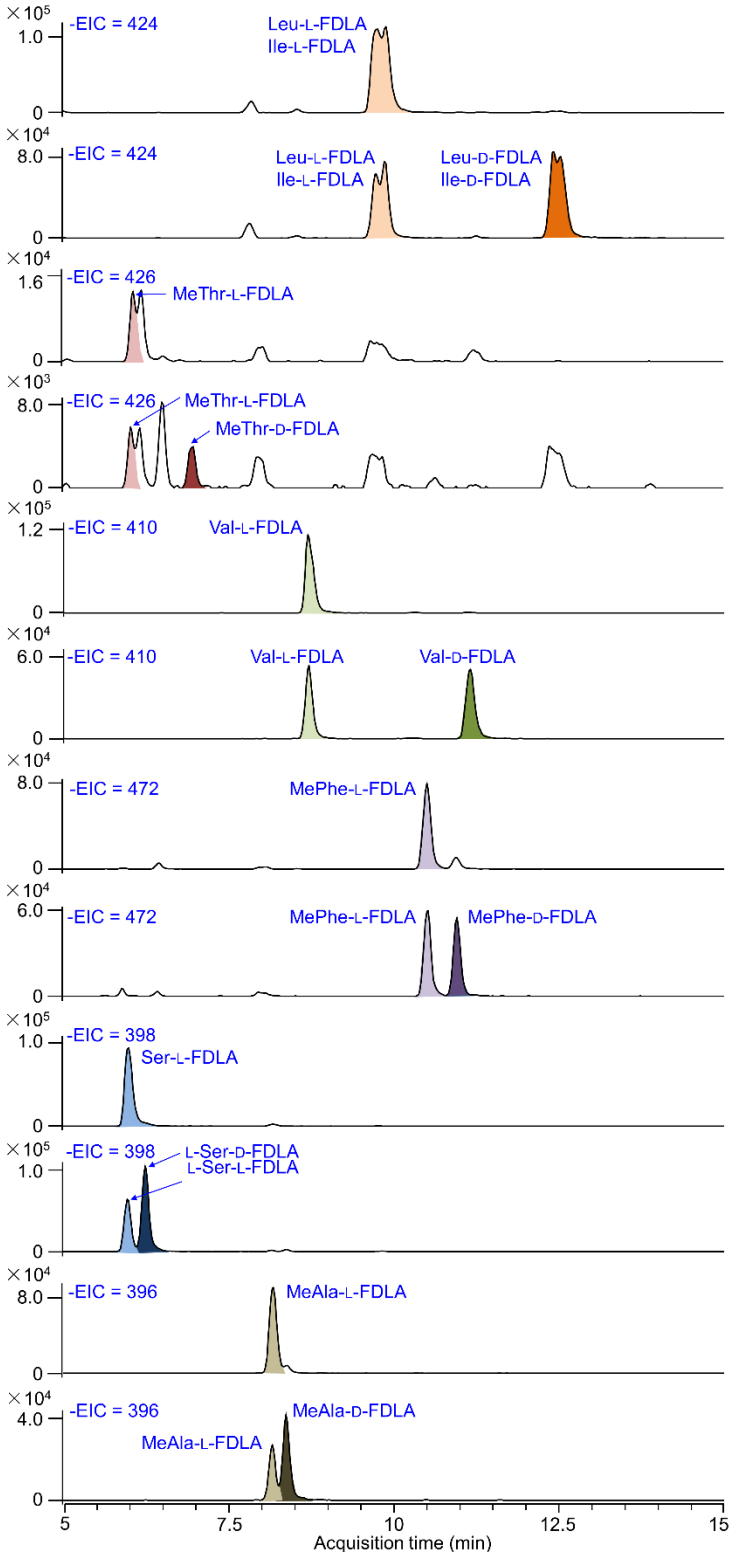

Figure S15.3. Extracted ion chromatograms of L- and D/L-FDLA derivatives of the acid hydrolysate of 6

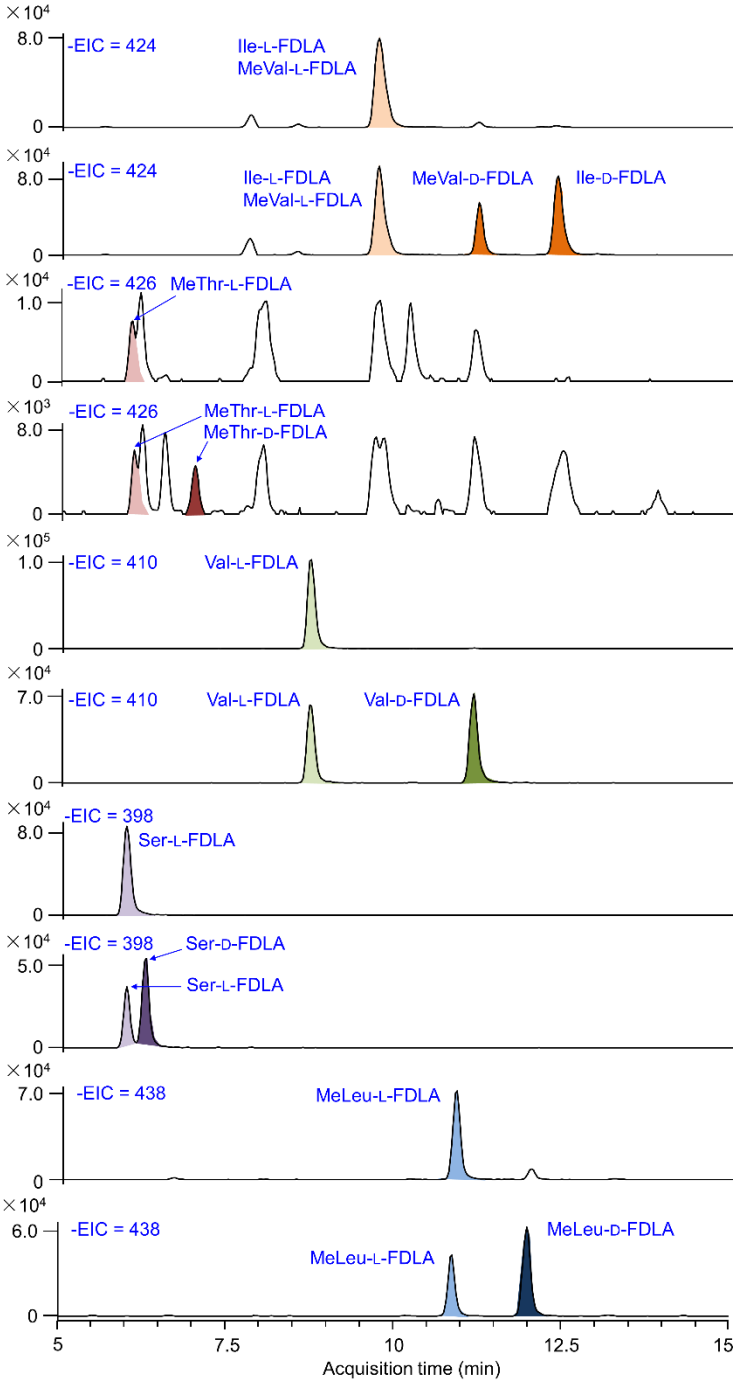

Figure S15.4. Extracted ion chromatograms of L- and D/L-FDLA derivatives of the acid hydrolysate of 11

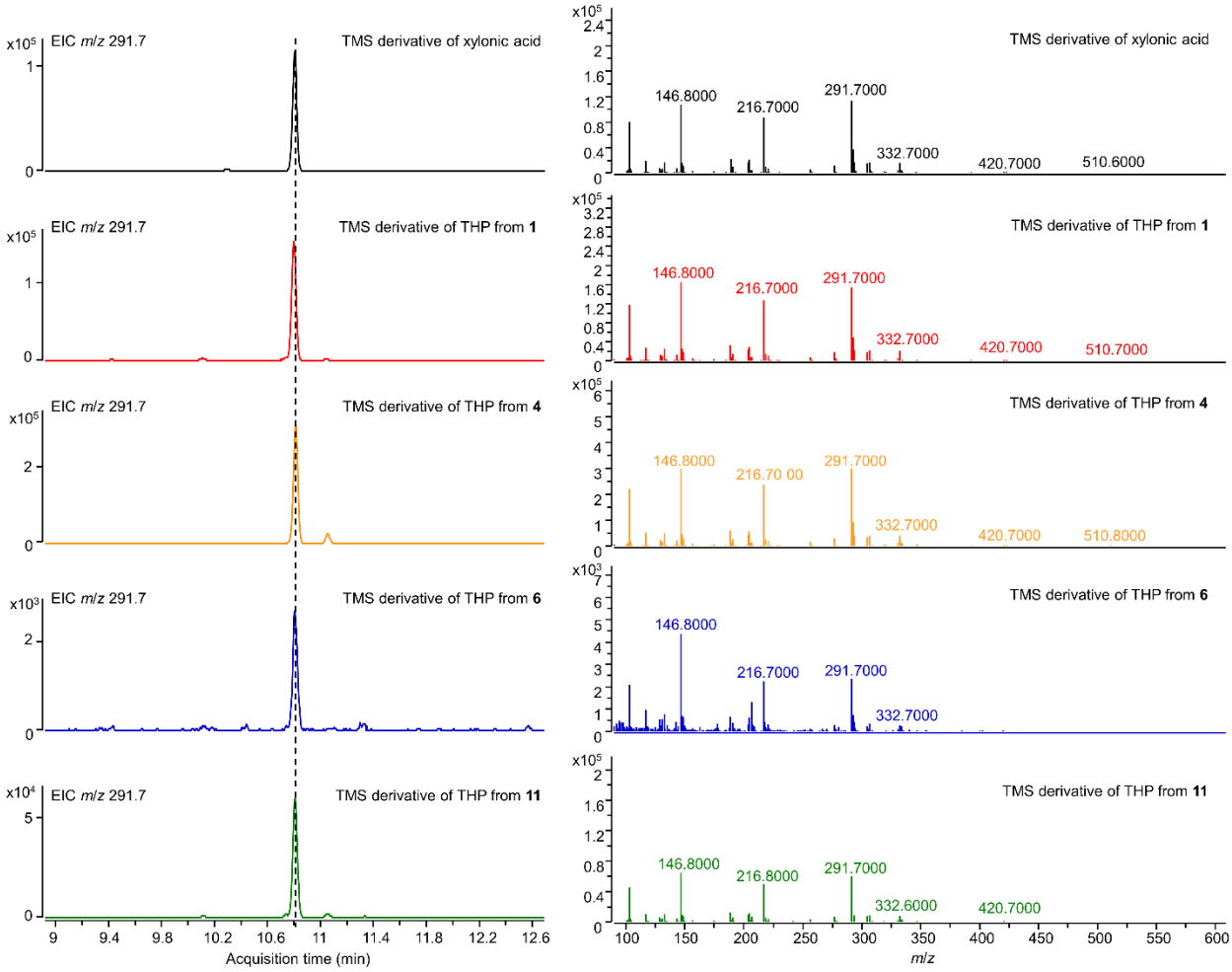

Figure S16. Comparison of the GC-EIMS spectra of the TMS derivative of the xylonic acid standard and the TMS derivatives of the tetrahydroxypentanoic acid (THP) residues of compounds 1, 4, 6, and 11. Left panels: extracted ion chromatograms at *m/z* 291.7 (the most abundant fragment ion of the TMS derivative of authentic xylonic acid standard) recorded in the positive mode; right panels: mass spectra of the selected peaks at 10.8 min.

Figure S17. HRESIMS spectra.

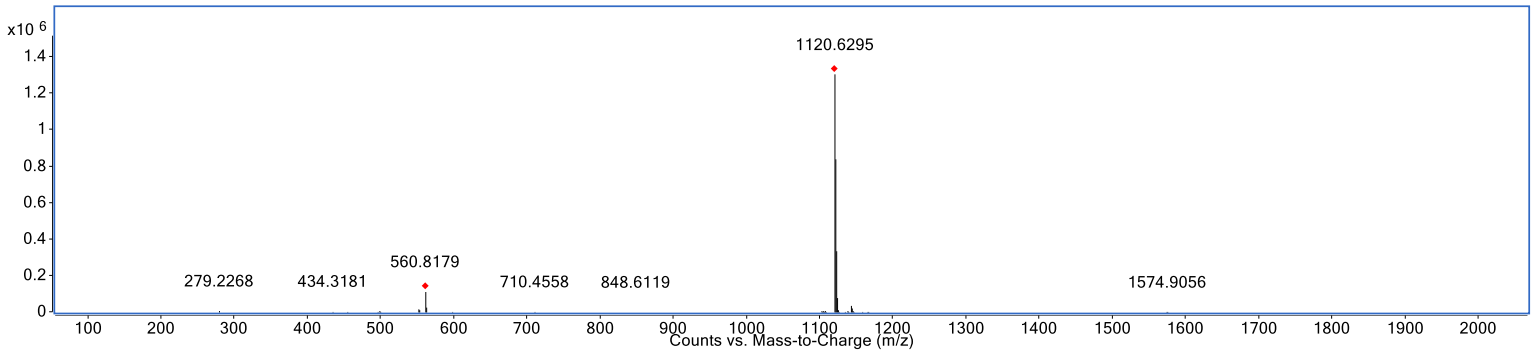

Figure S17.1. (+)-HRESIMS spectrum of 1

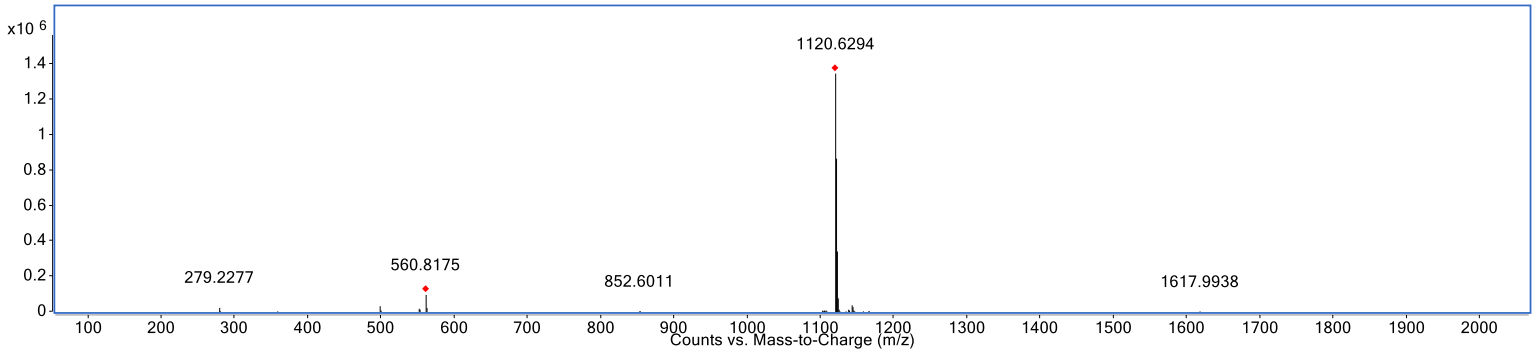

Figure S17.2. (+)-HRESIMS spectrum of 2

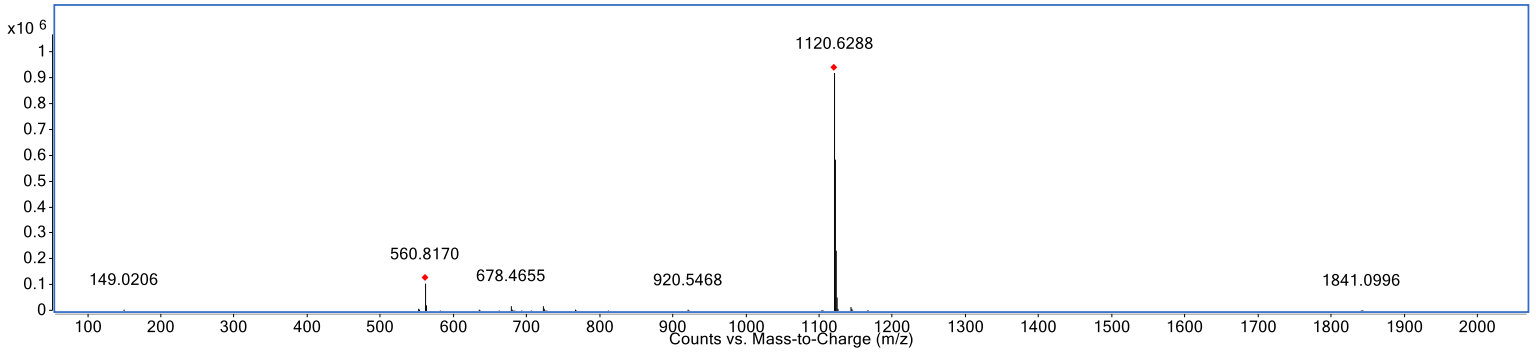

Figure S17.3. (+)-HRESIMS spectrum of 3

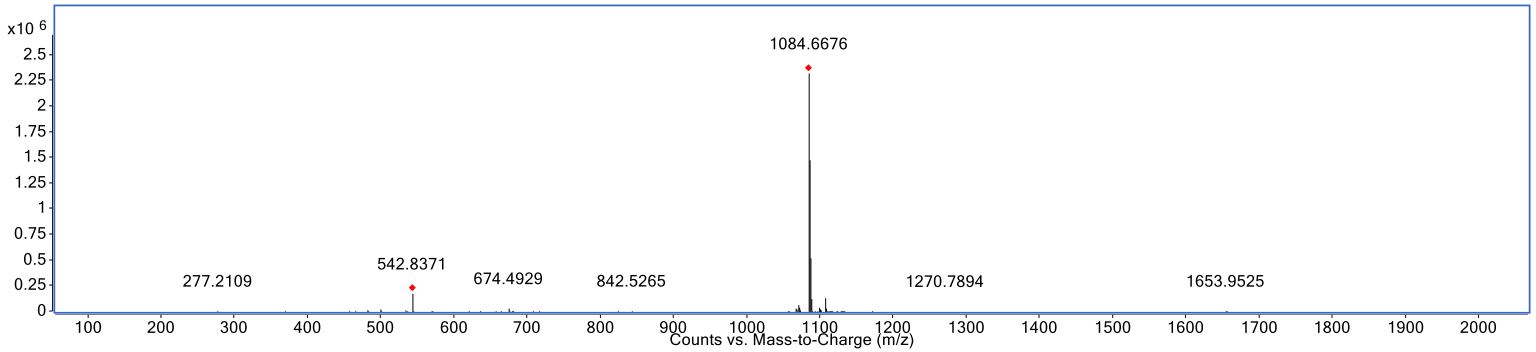

Figure S17.4. (+)-HRESIMS spectrum of 4

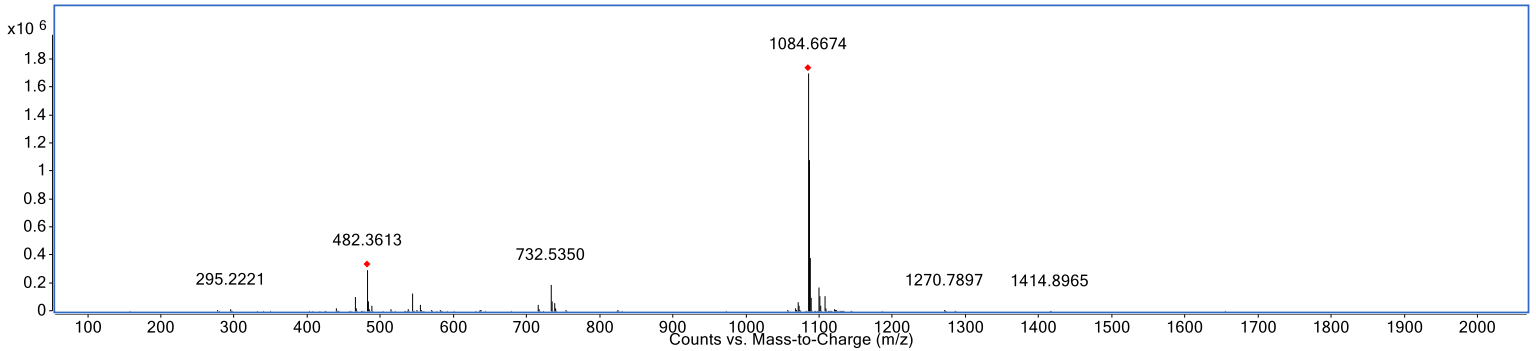

Figure S17.5. (+)-HRESIMS spectrum of M1

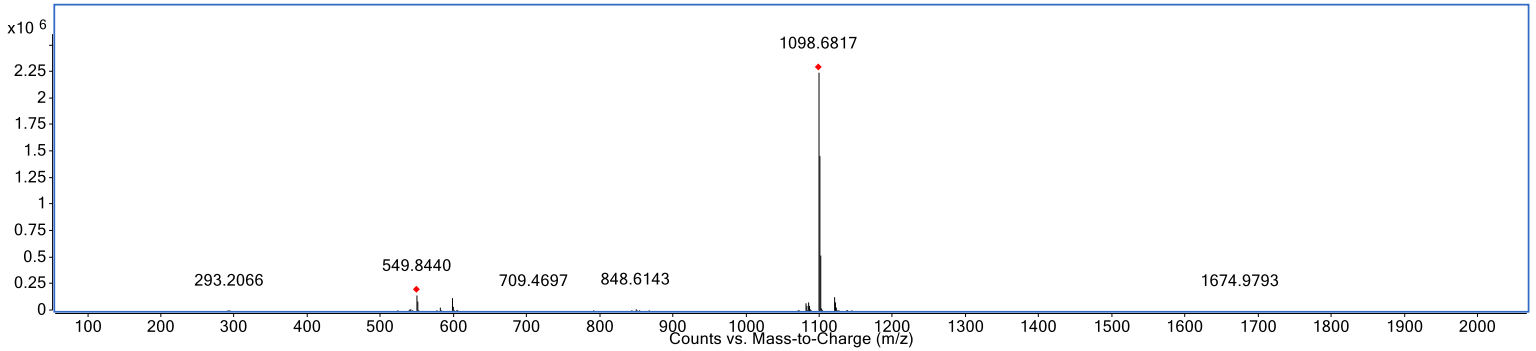

Figure S17.6. (+)-HRESIMS spectrum of M2

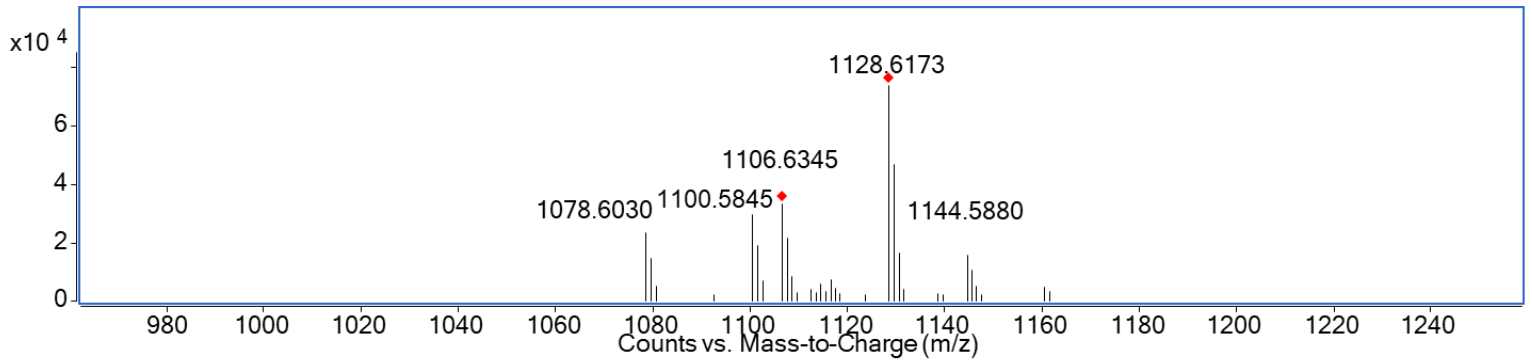

Figure S17.7. (+)-HRESIMS spectrum of the mixture of 5 and 10

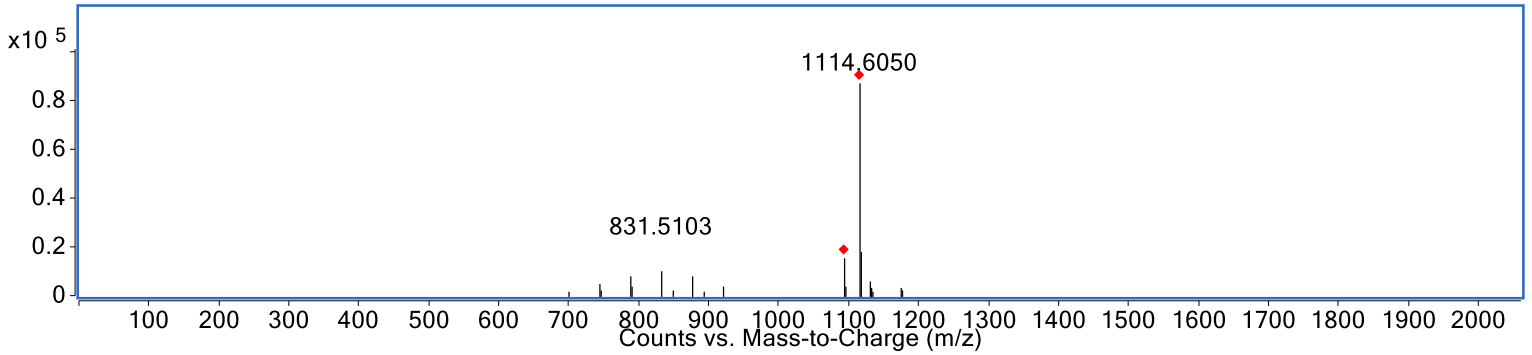

Figure S17.8. (+)-HRESIMS spectrum of 6

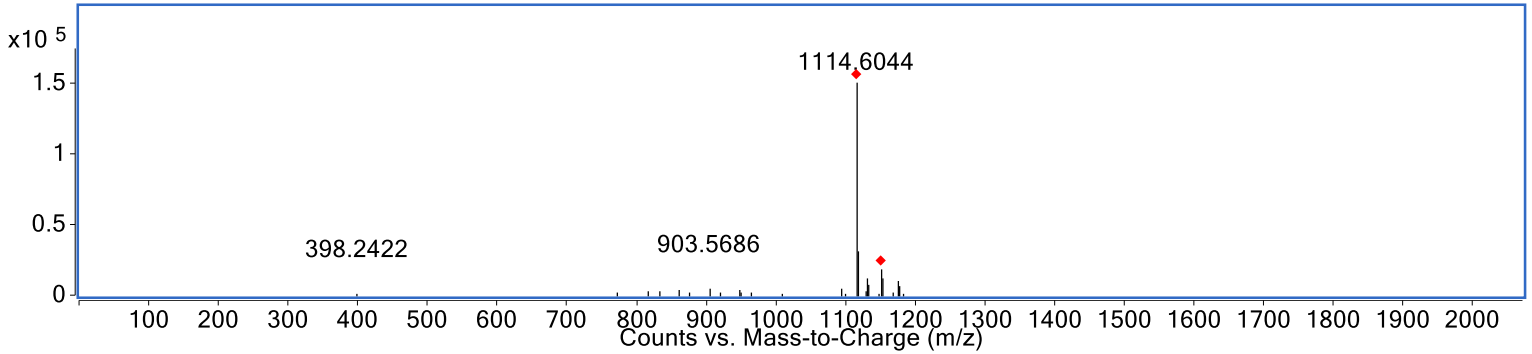

Figure S17.9. (+)-HRESIMS spectrum of 7

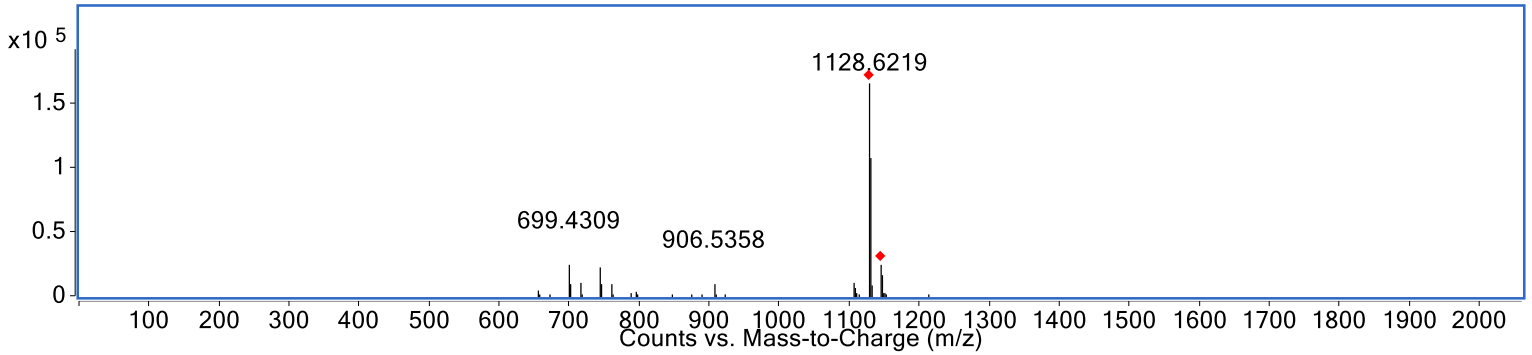

Figure S17.10. (+)-HRESIMS spectrum of 8

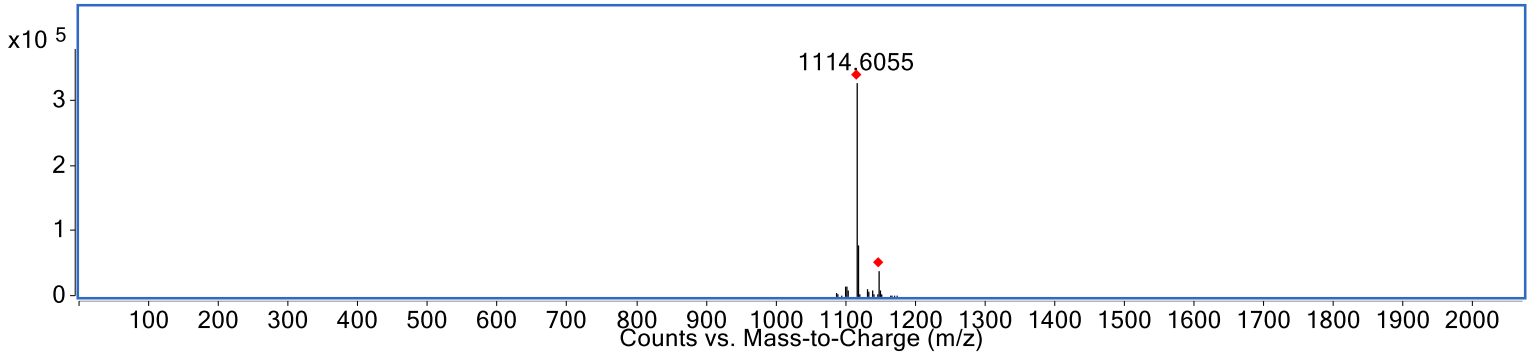

Figure S17.11. (+)-HRESIMS spectrum of 9

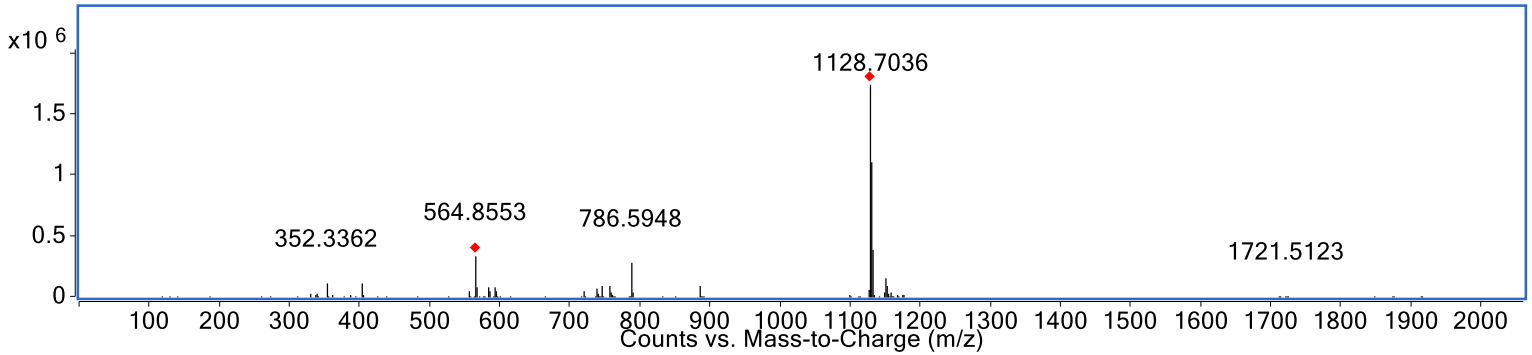

Figure S17.12. (+)-HRESIMS spectrum of 11

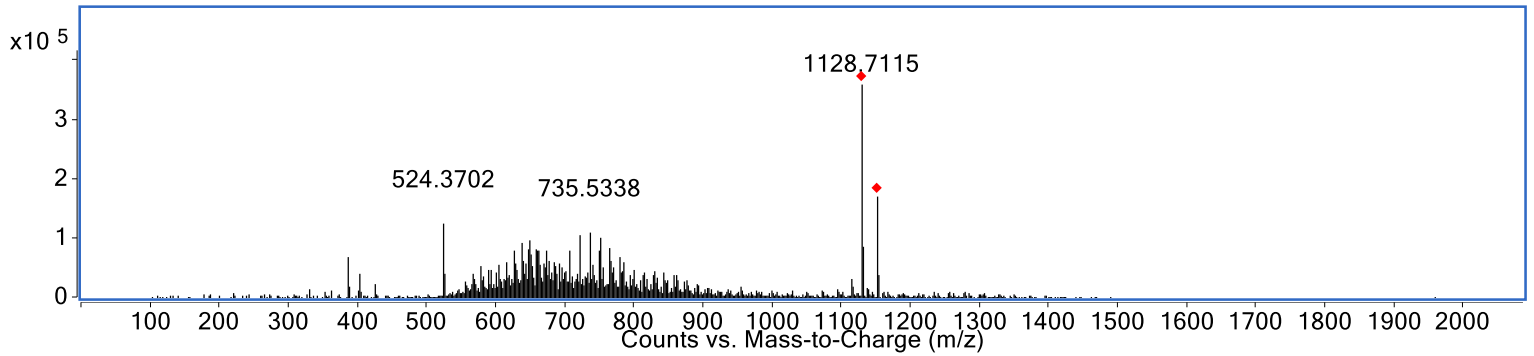

Figure S17.13. (+)-HRESIMS spectrum of 12

Figure S18. NMR spectra

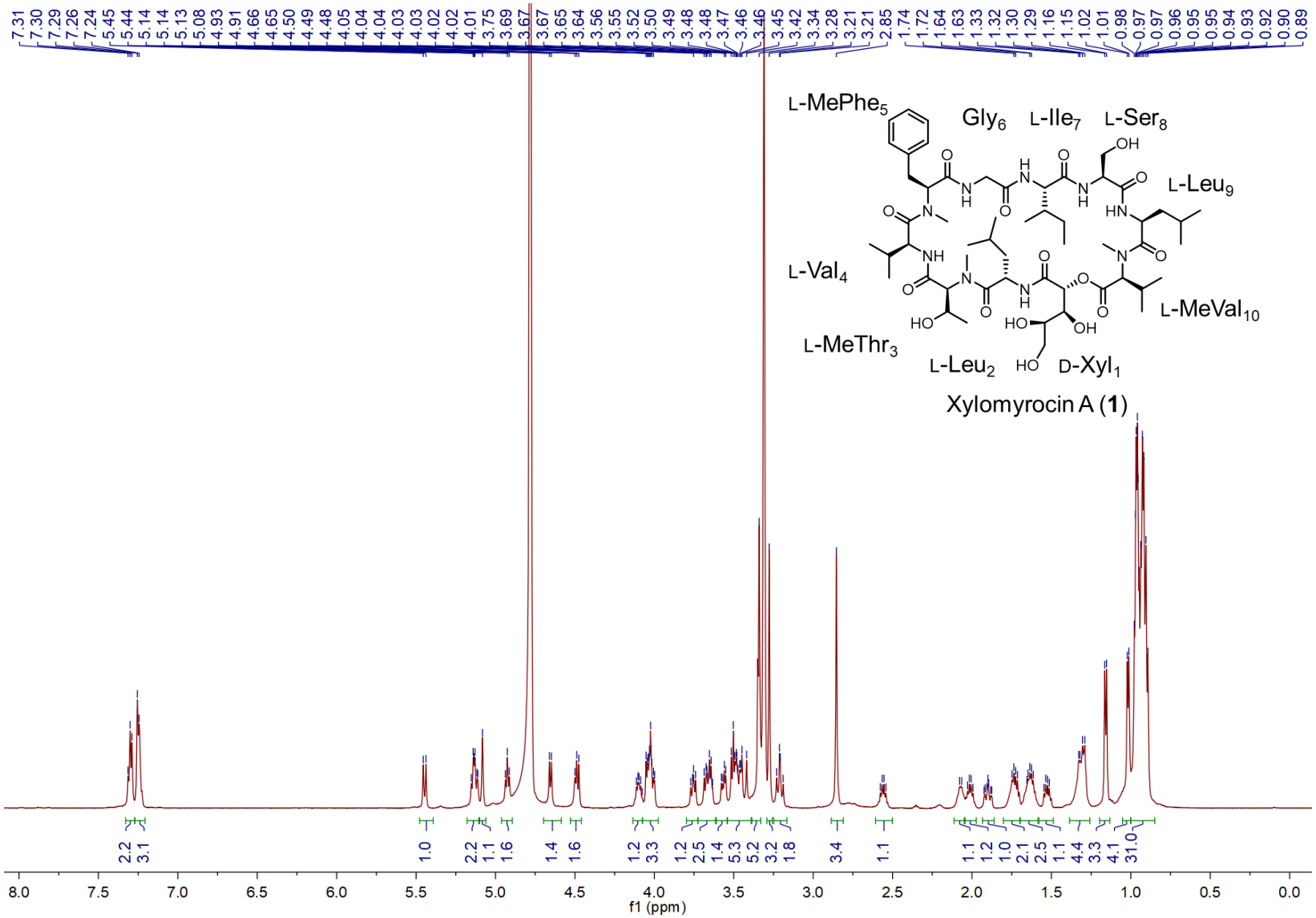

Figure S18.1. ^{1}H NMR spectrum of 1 in methanol-d_4

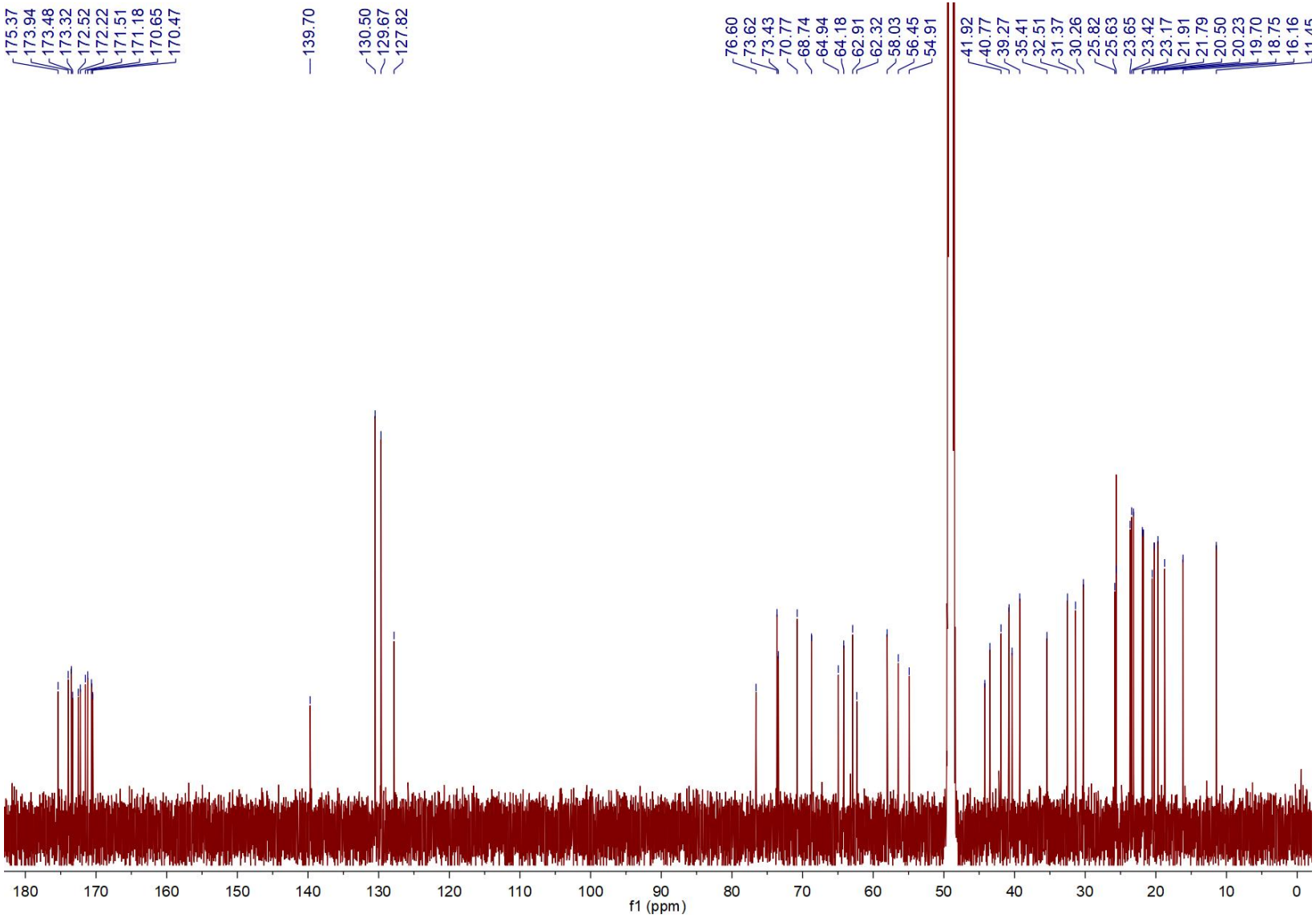

Figure S18.2. ^{13}**C NMR spectrum of 1 in methanol-*d*$_4$**

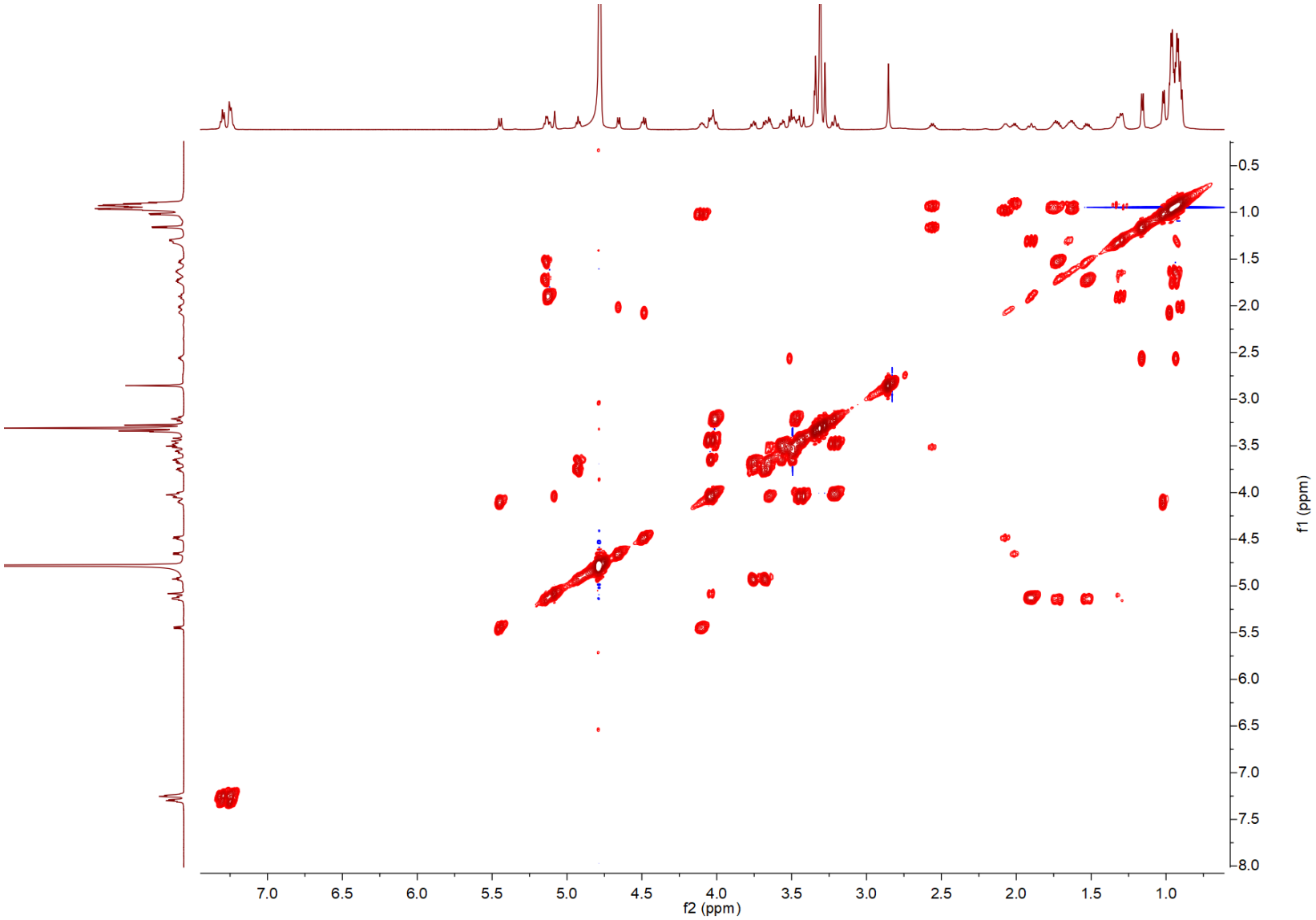

Figure S18.3. ^{1}H-^{1}H COSY spectrum of 1 in methanol-d_4

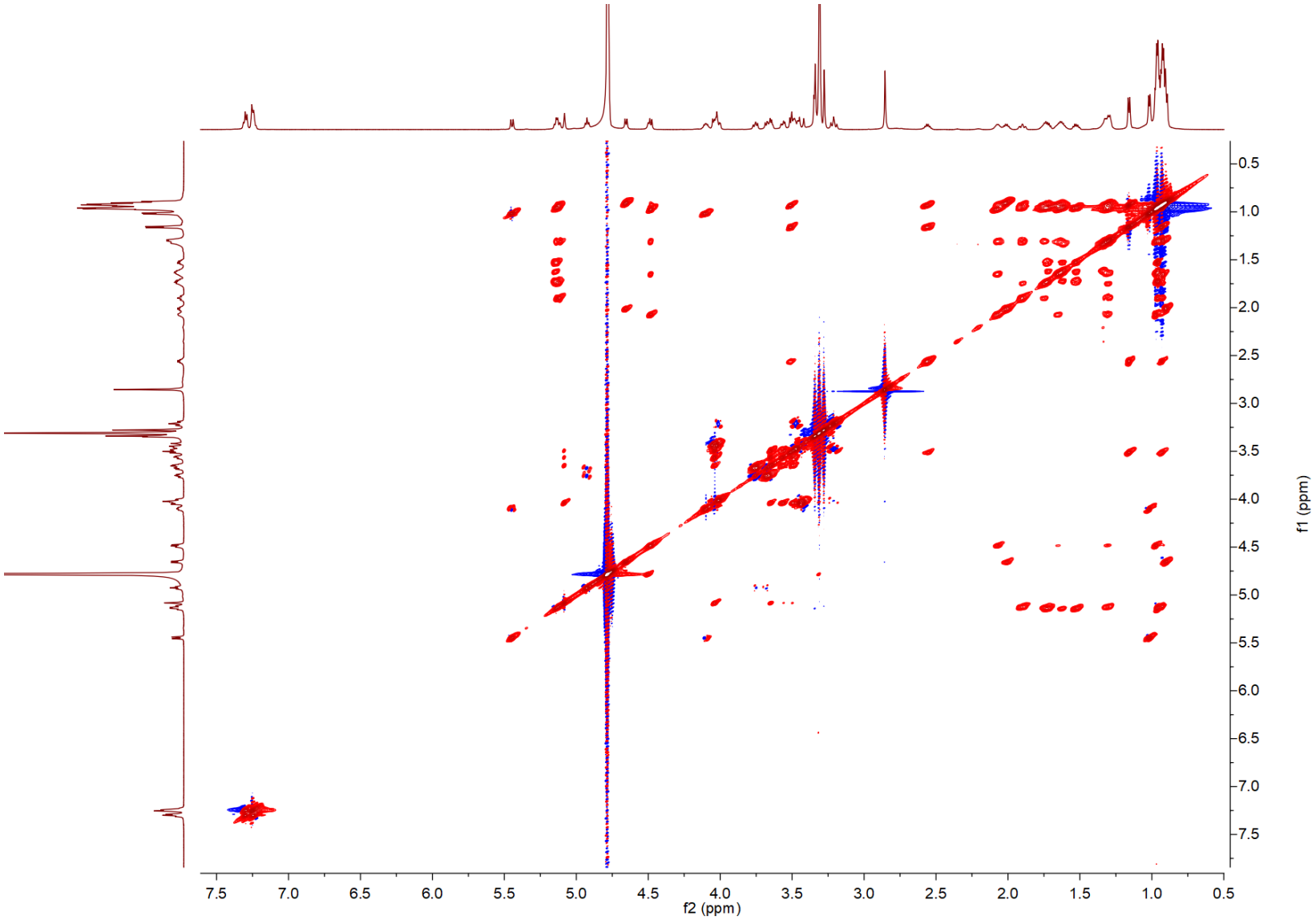

Figure S18.4. ^{1}H-^{1}H TOCSY spectrum of 1 in methanol-d_4

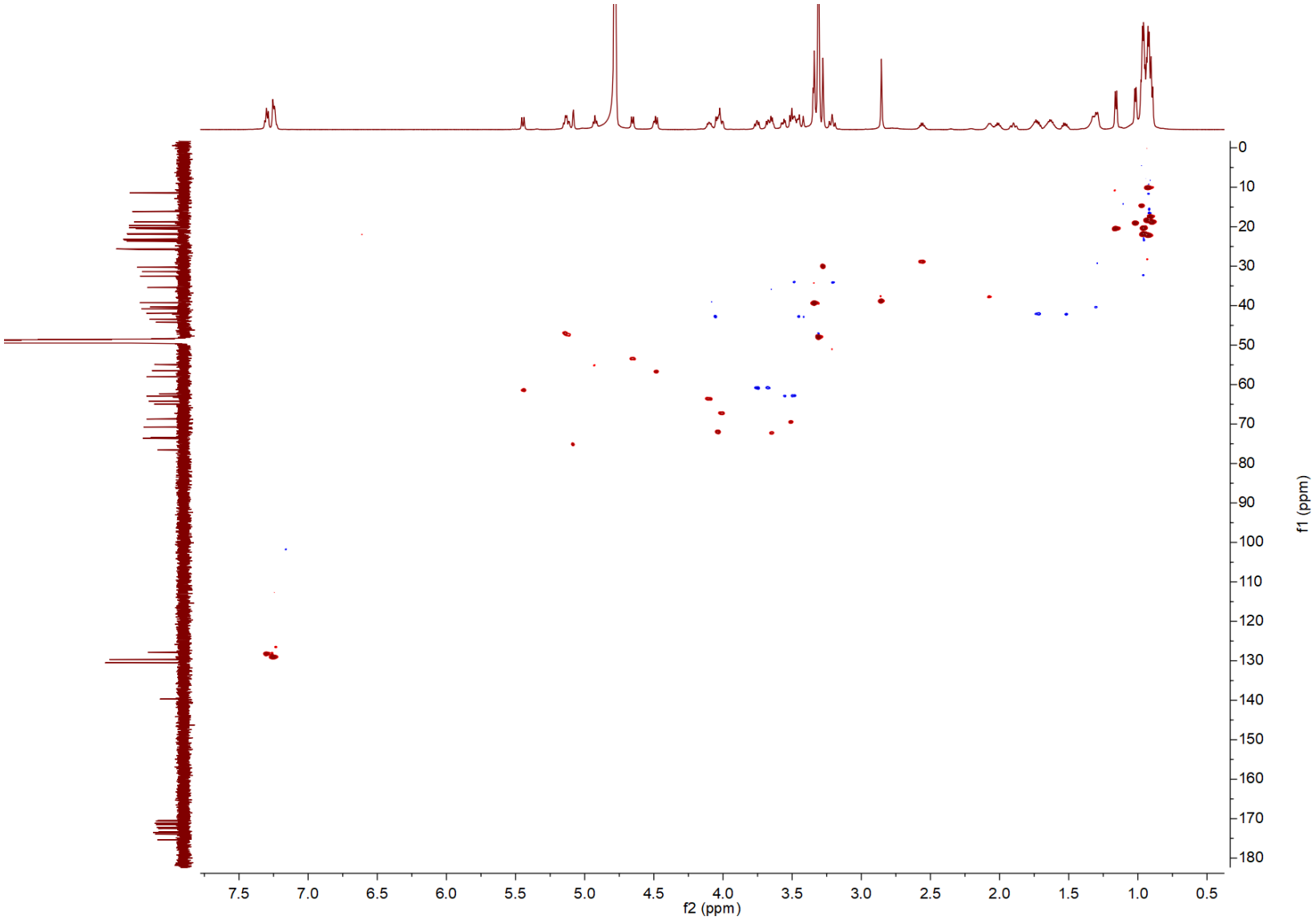

Figure S18.5. HSQC spectrum of 1 in methanol-d_4

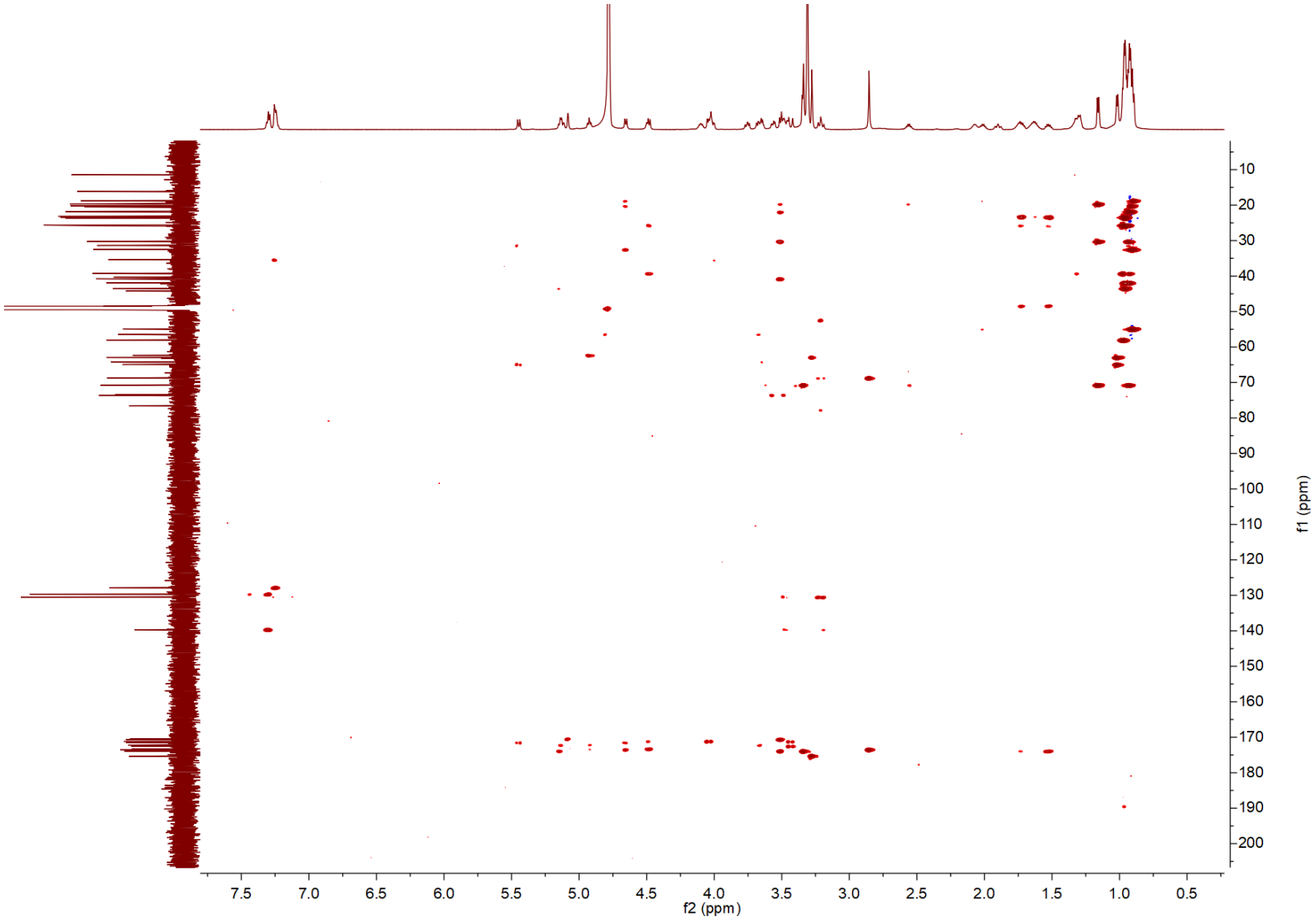

Figure S18.6. HMBC spectrum of 1 in methanol-d_4

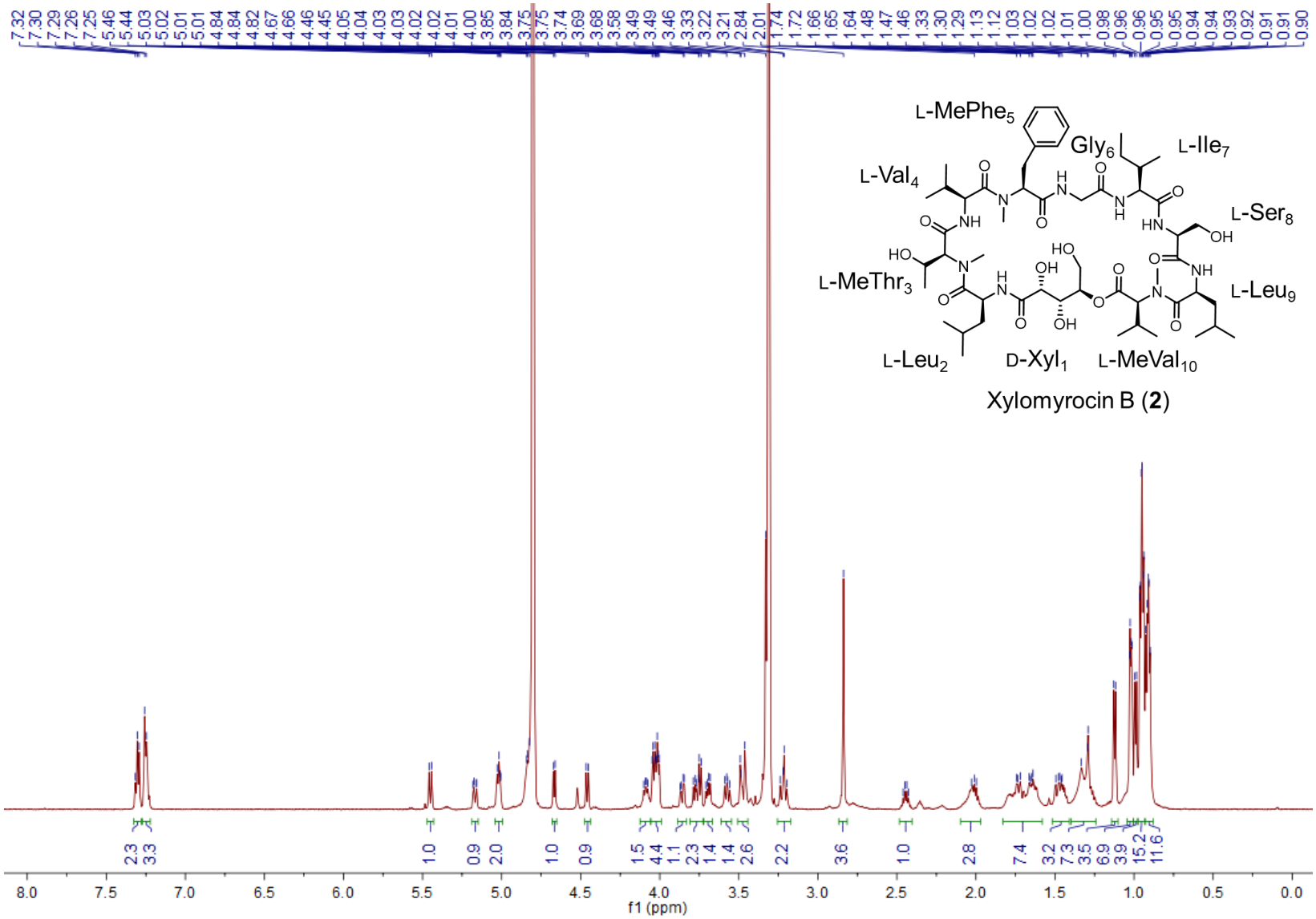

Figure S18.7. ^{1}H NMR spectrum of **2** in methanol-d_4

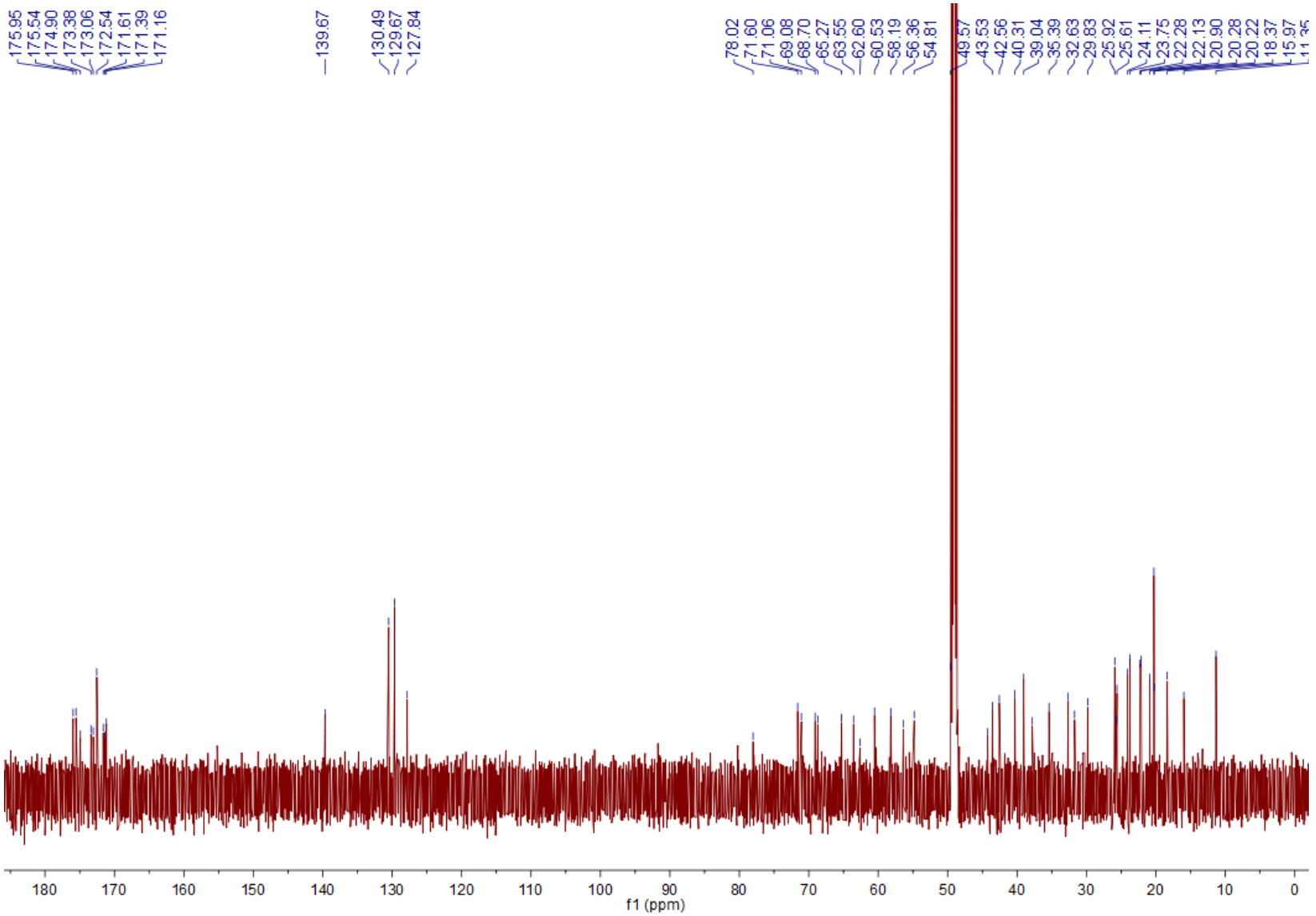

Figure S18.8. ^{13}C NMR spectrum of **2** in methanol-d_4

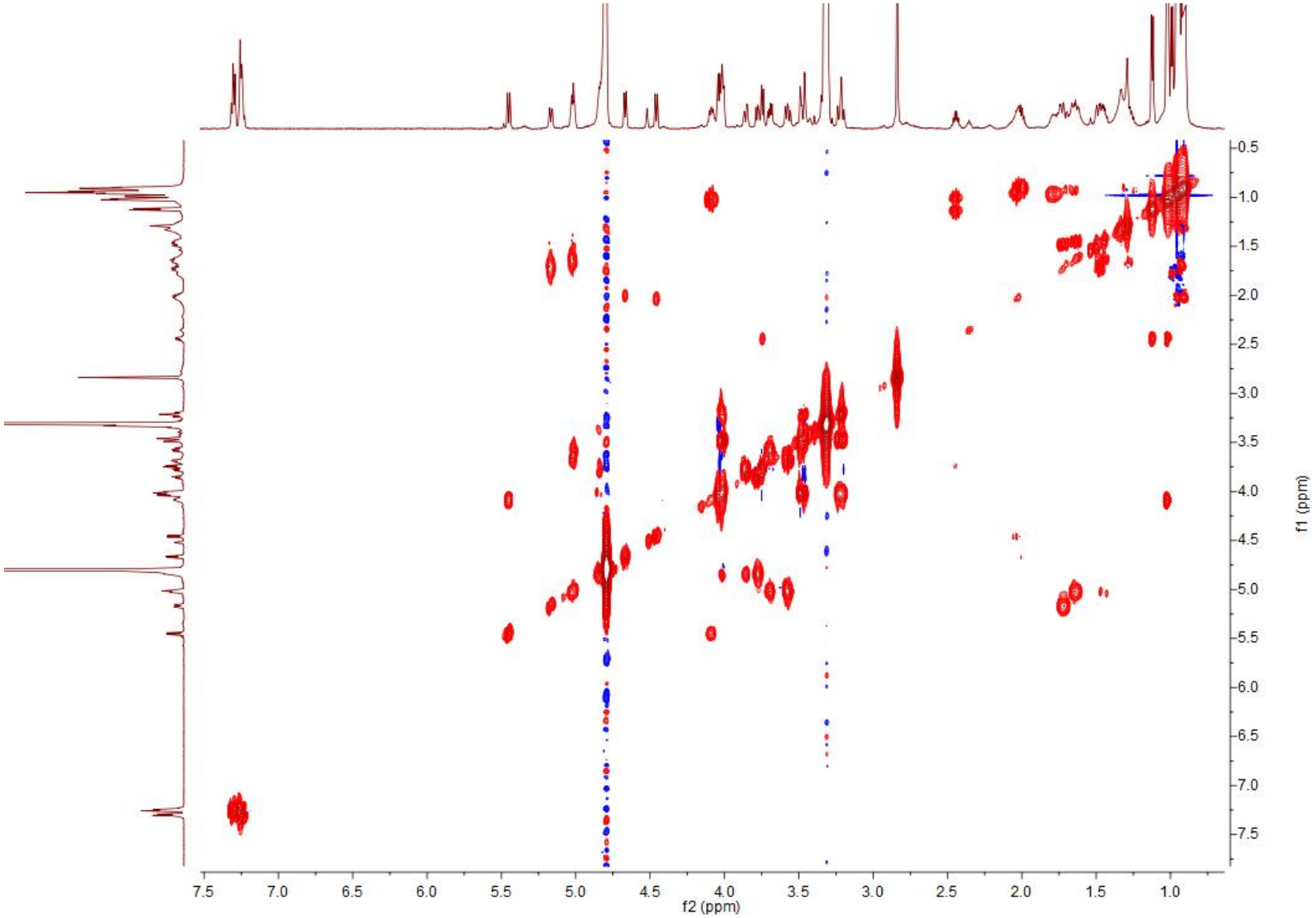

Figure S18.9. ^{1}H-^{1}H COSY spectrum of 2 in methanol-d_4

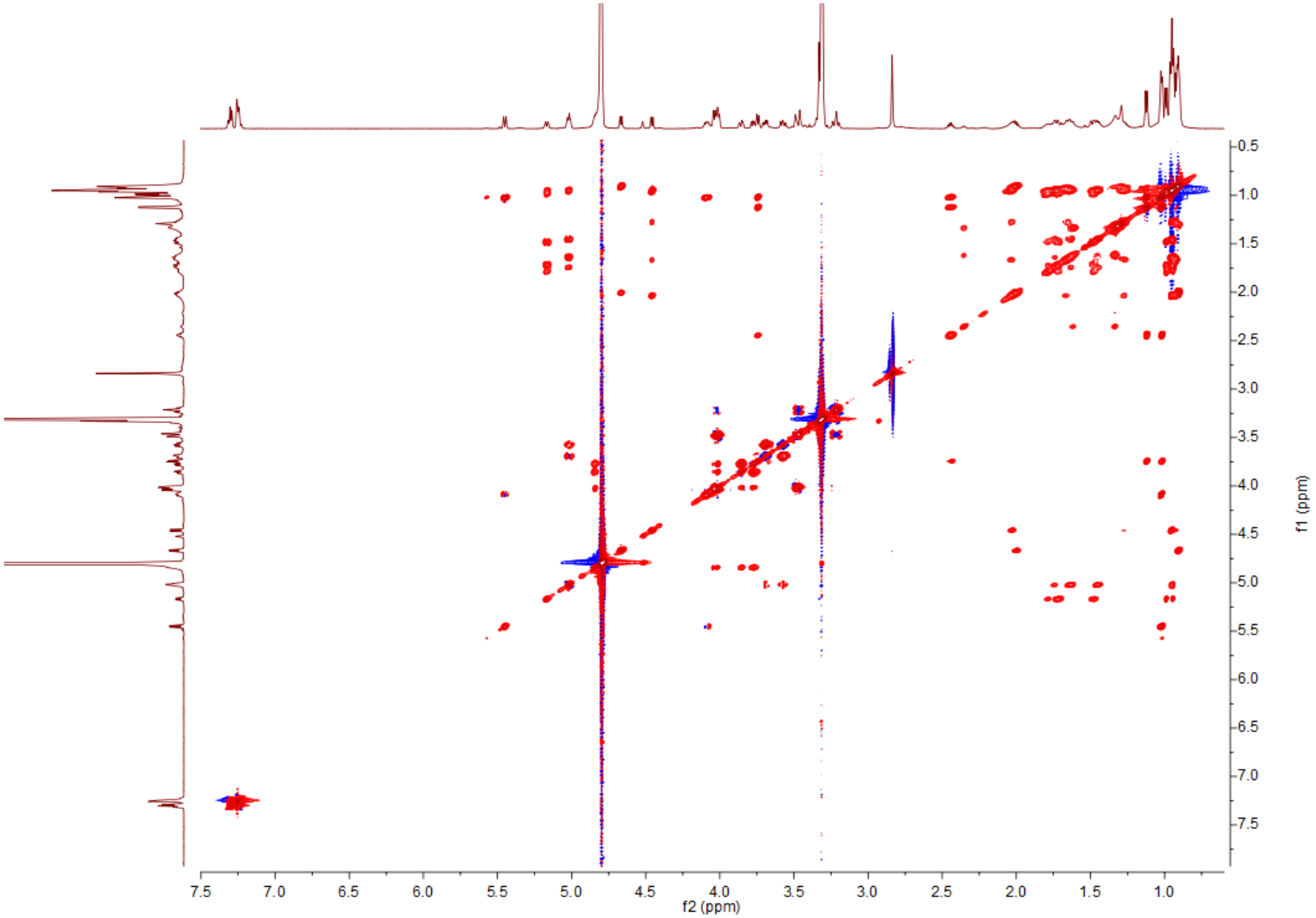

Figure S18.10. ^{1}H-^{1}H TOCSY spectrum of **2** in methanol-d_4

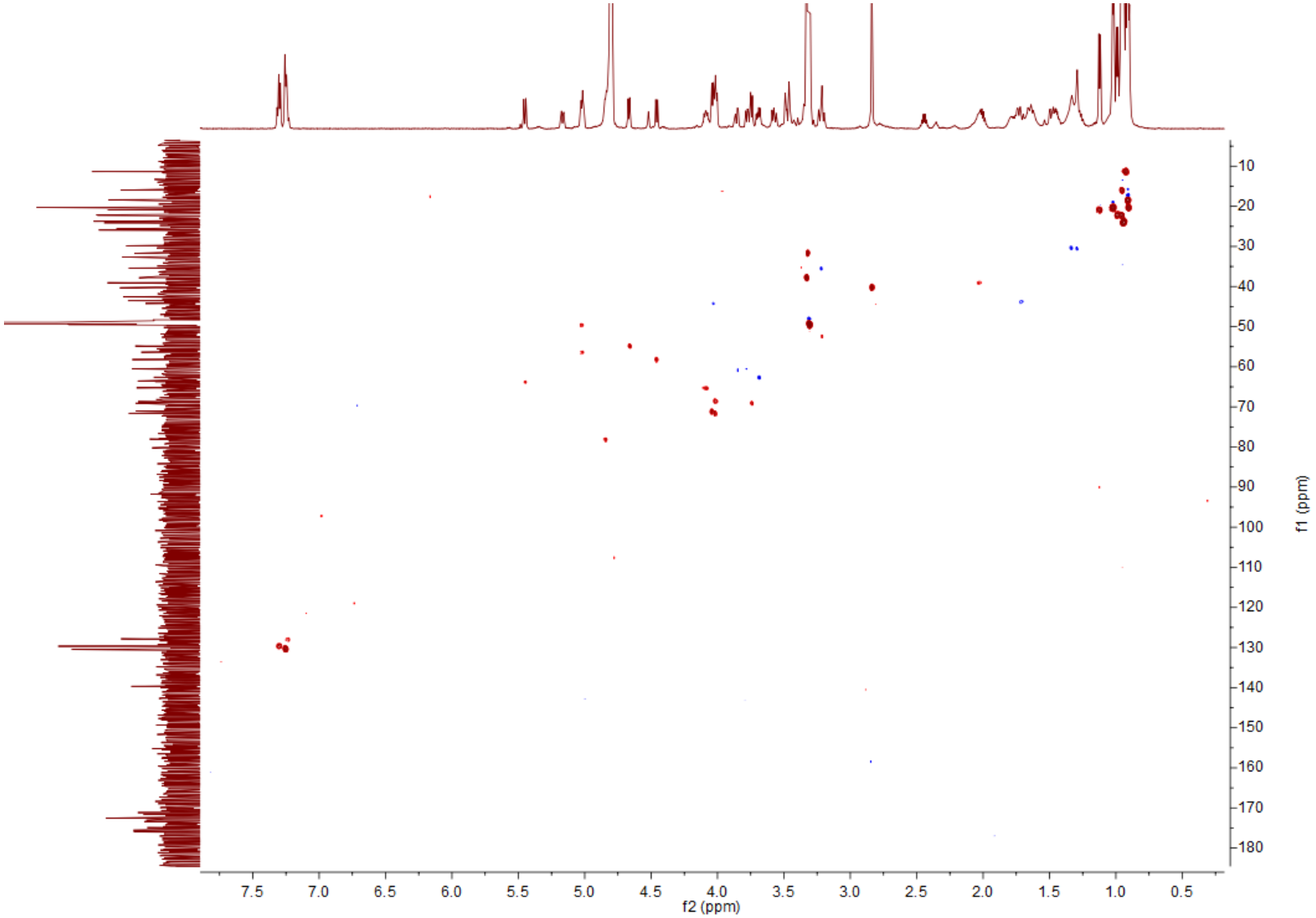

Figure S18.11. HSQC spectrum of 2 in methanol-d_4

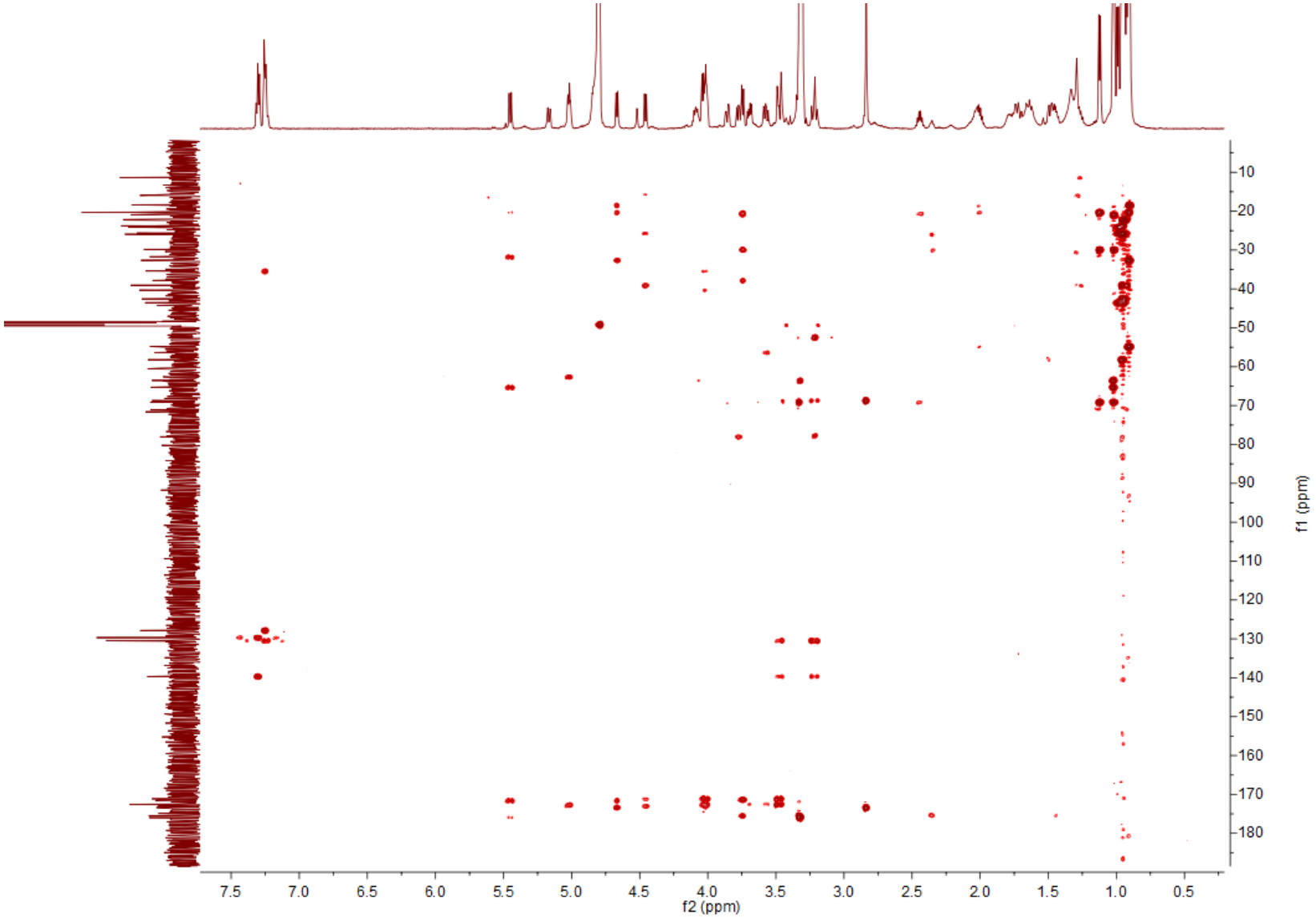

Figure S18.12. HMBC spectrum of 2 in methanol-d_4

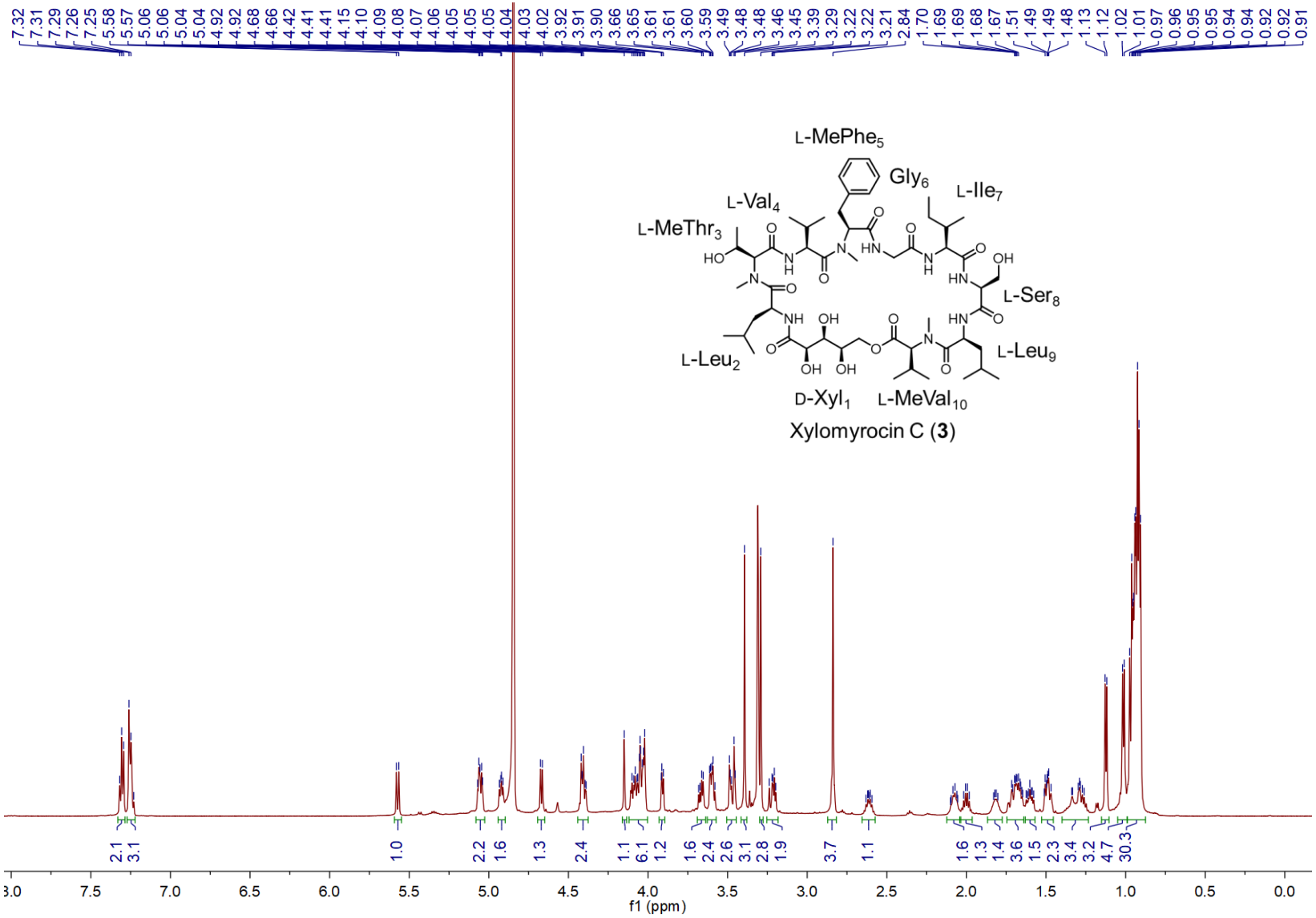

Figure S18.13. ^{1}H NMR spectrum of 3 in methanol-d_4

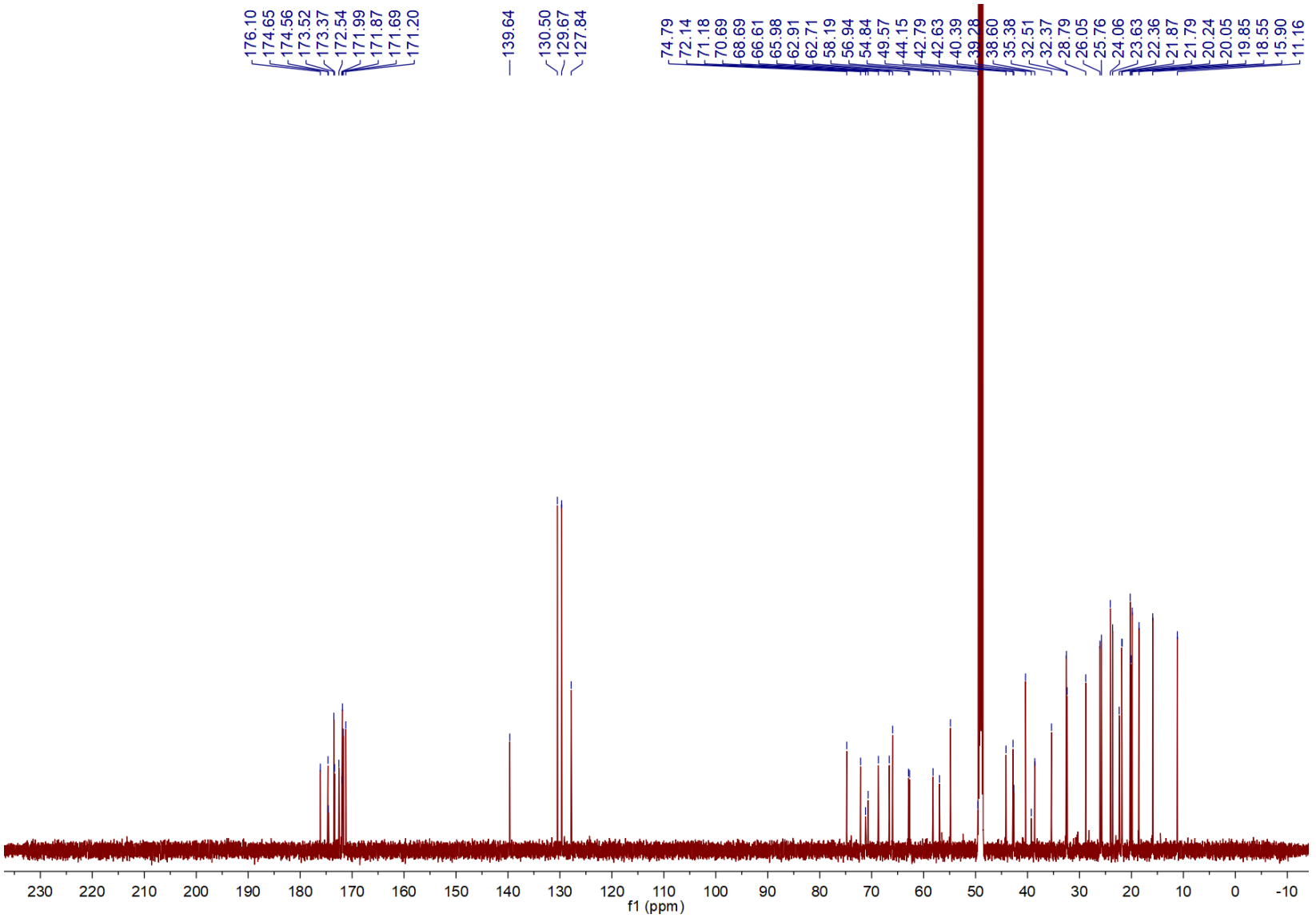

Figure S18.14. ^{13}C NMR spectrum of 3 in methanol-d_4

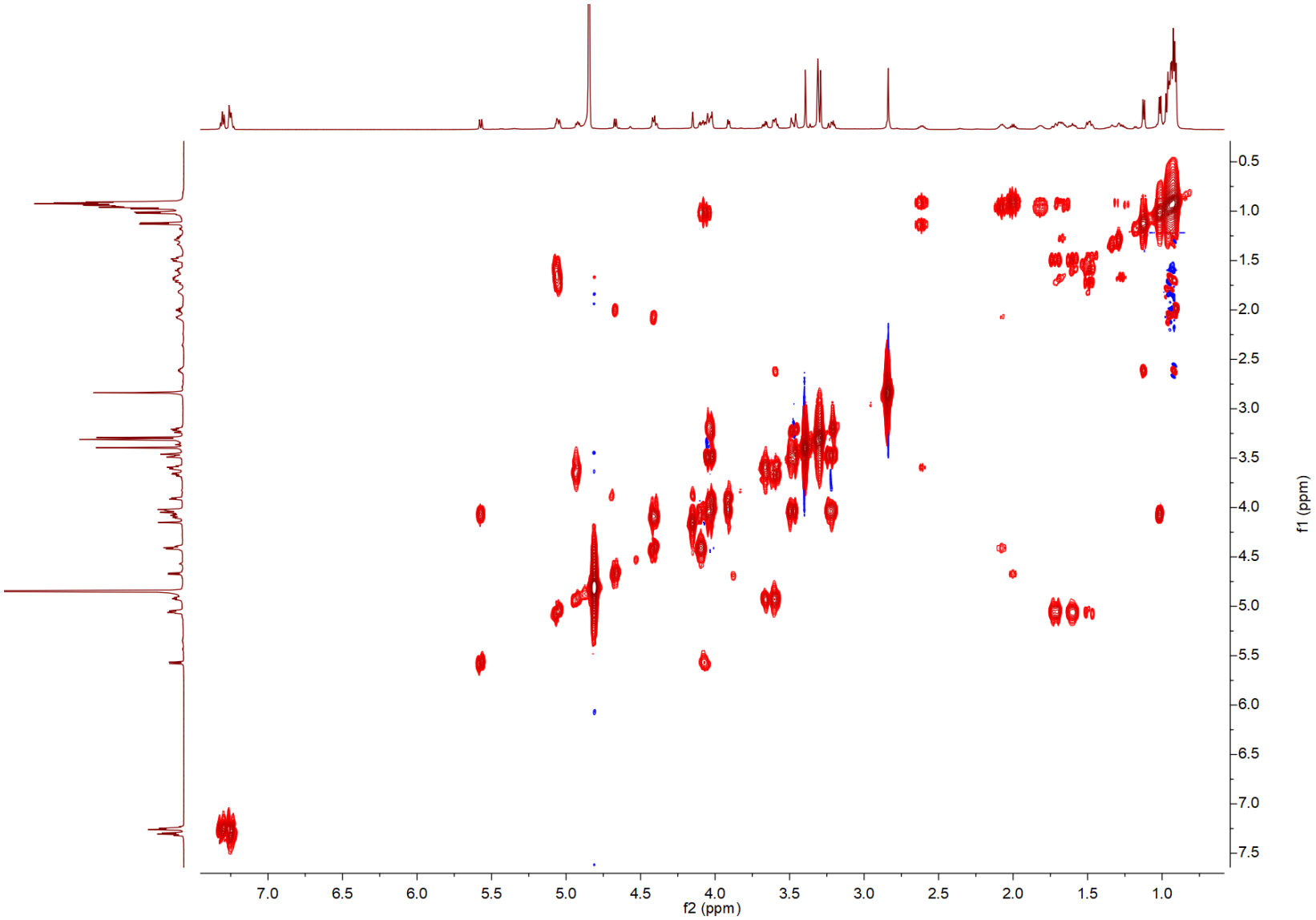

Figure S18.15. ^{1}H-^{1}H COSY spectrum of 3 in methanol-d_4

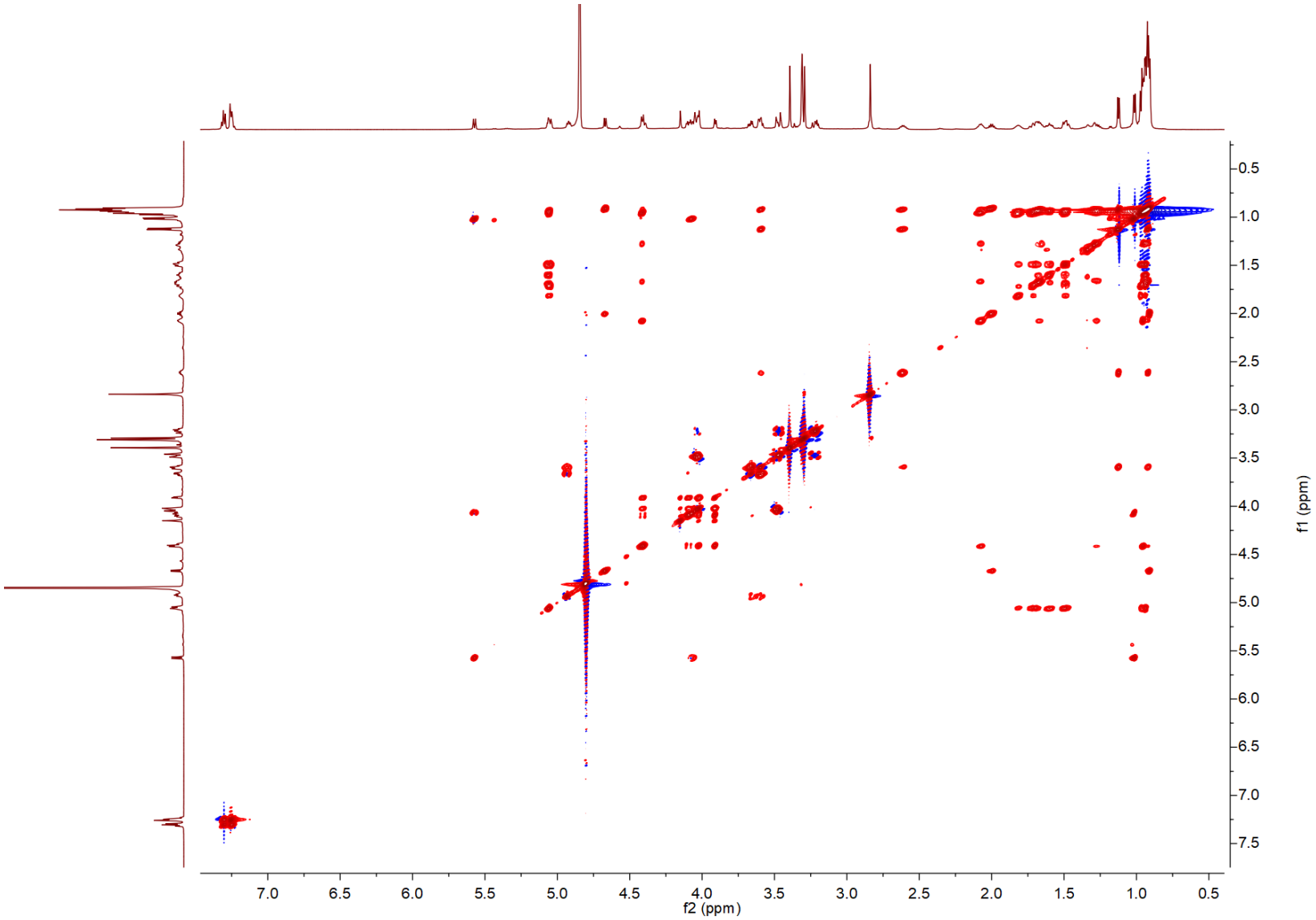

Figure S18.16. ^{1}H-^{1}H TOCSY spectrum of 3 in methanol-d_4

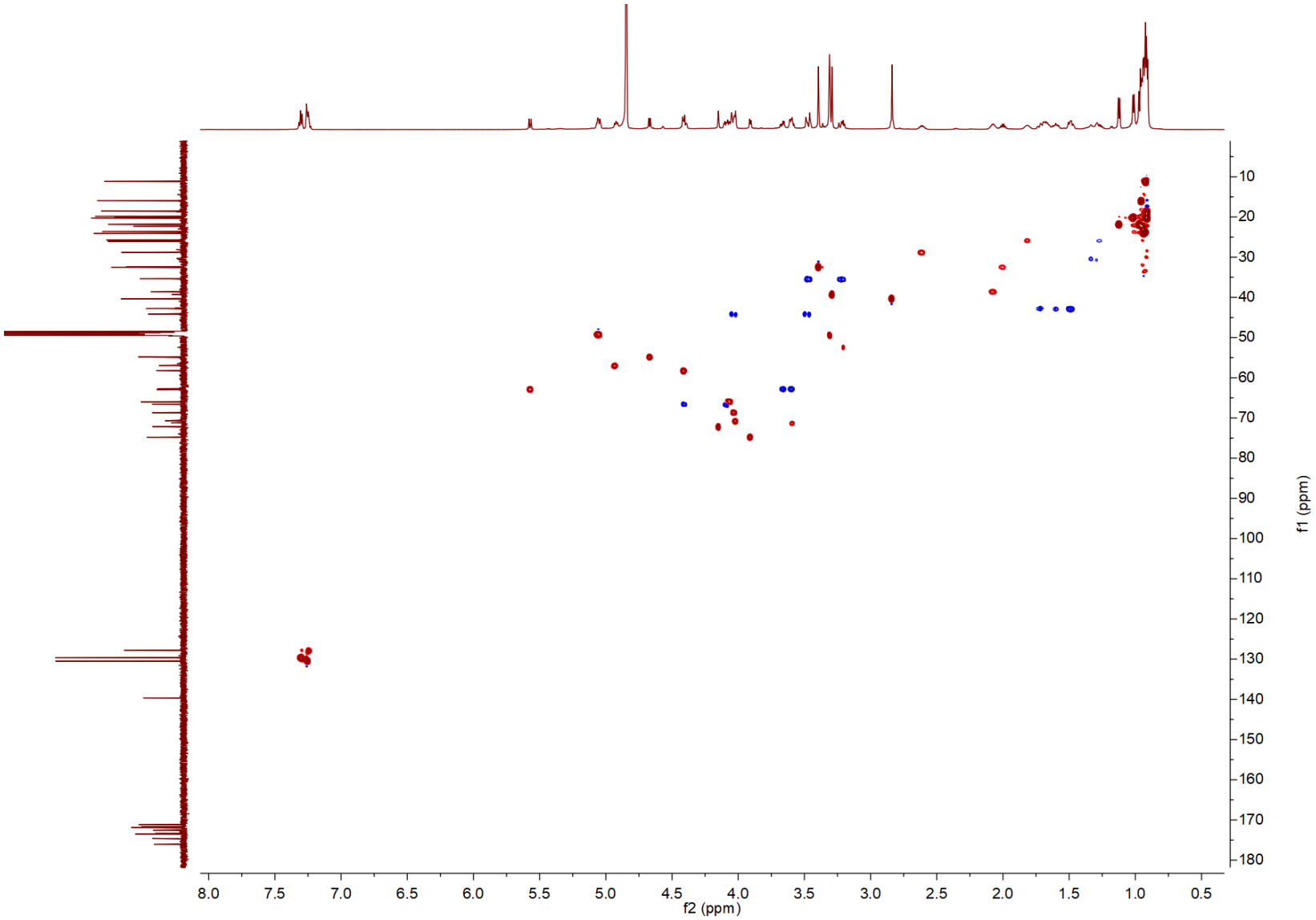

Figure S18.17. HSQC spectrum of 3 in methanol-d_4

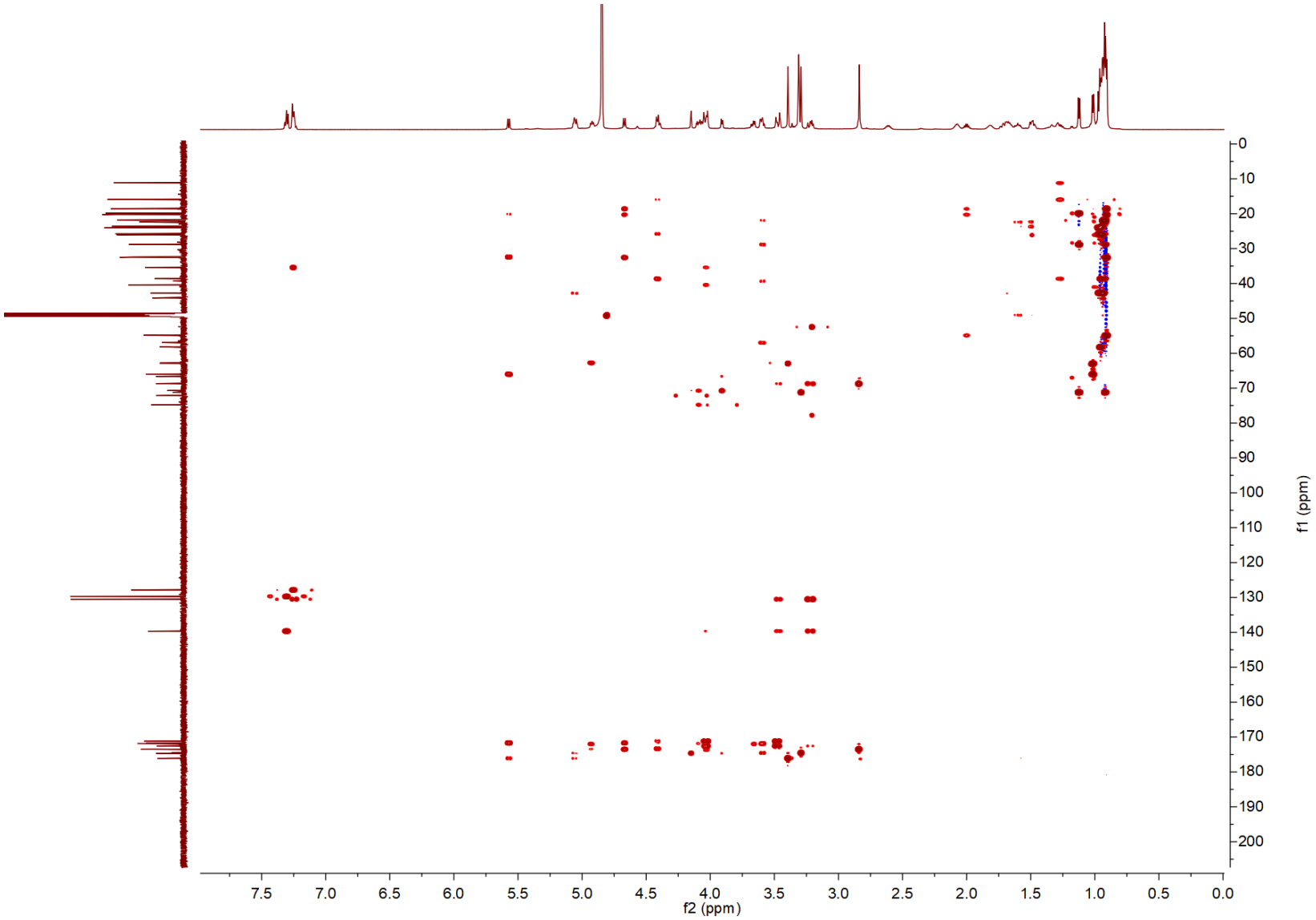

Figure S18.18. HMBC spectrum of 3 in methanol-d_4

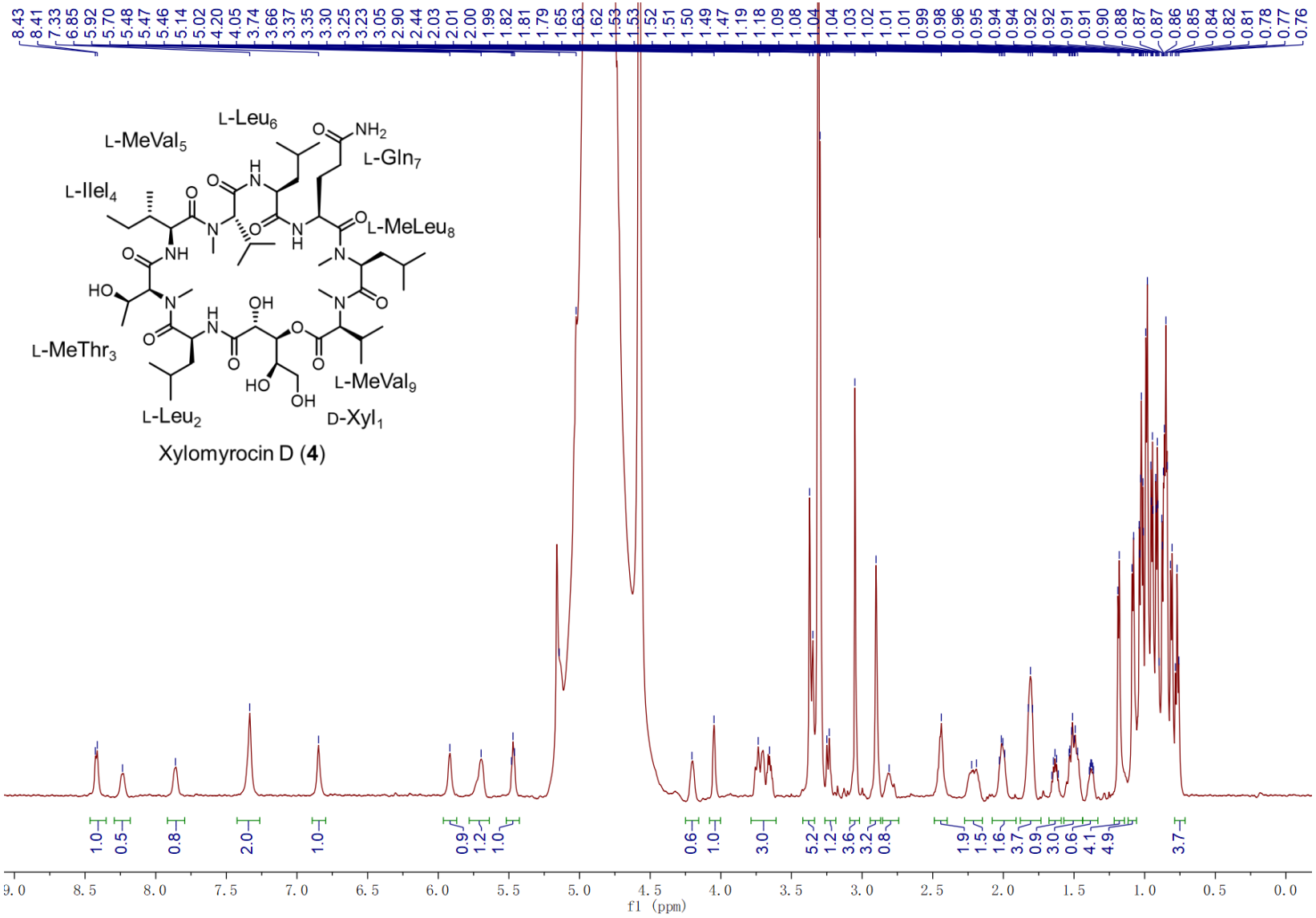

Figure S18.19. ^{1}H NMR spectrum of 4 in CD_3OH

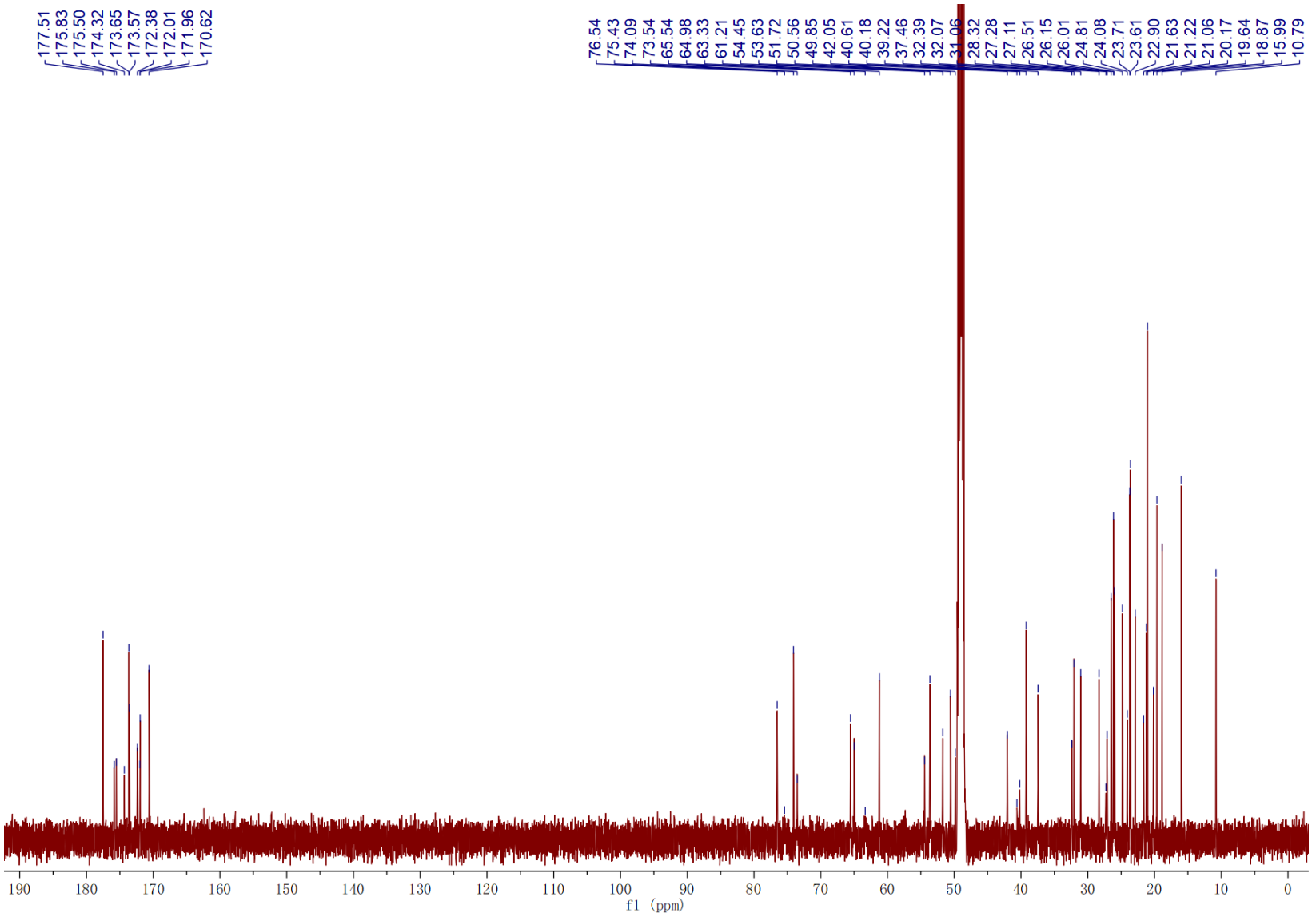

Figure S18.20. ^{13}C NMR spectrum of 4 in CD_3OH

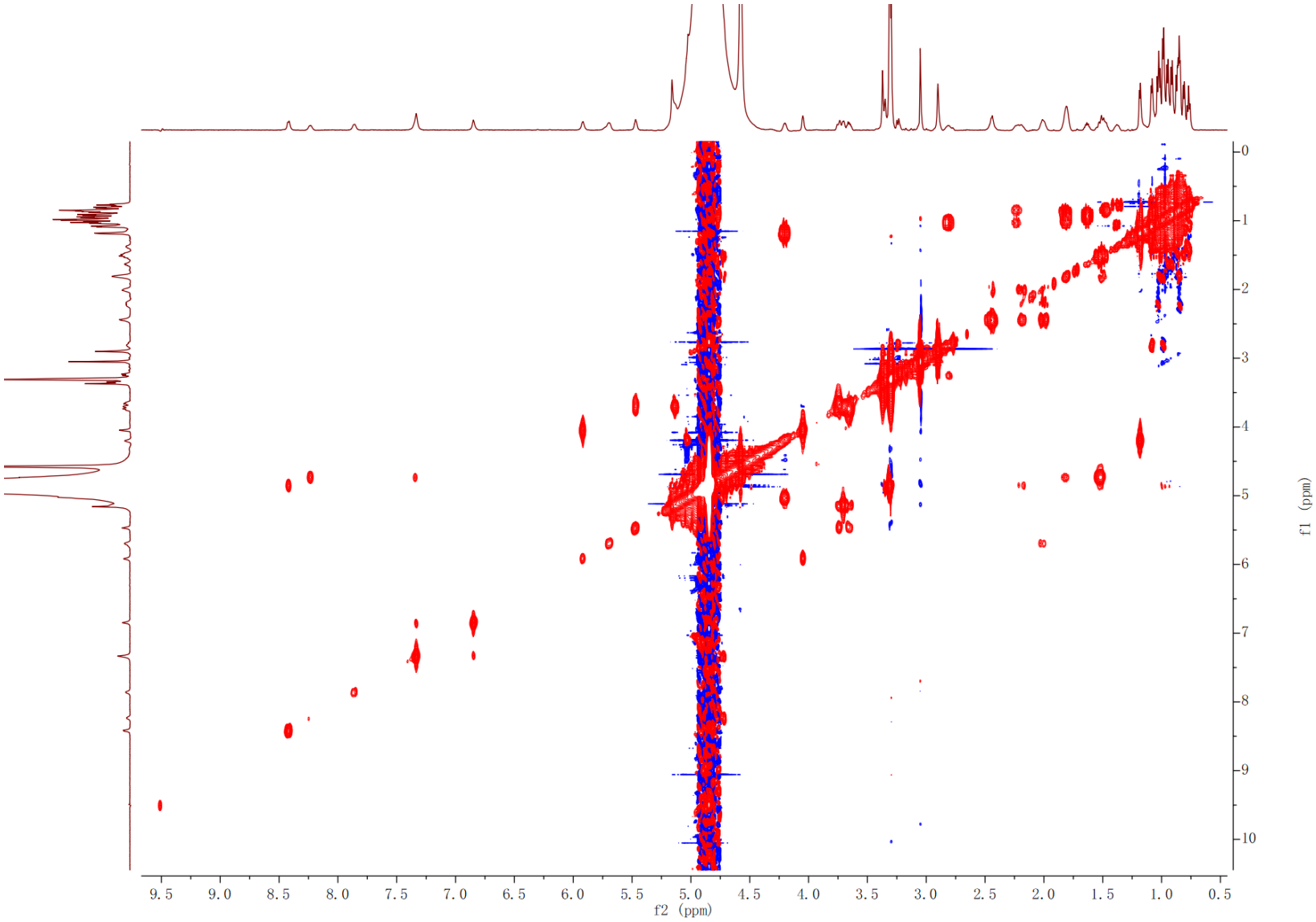

Figure S18.21. ^{1}H-^{1}H COSY spectrum of 4 in CD_3OH

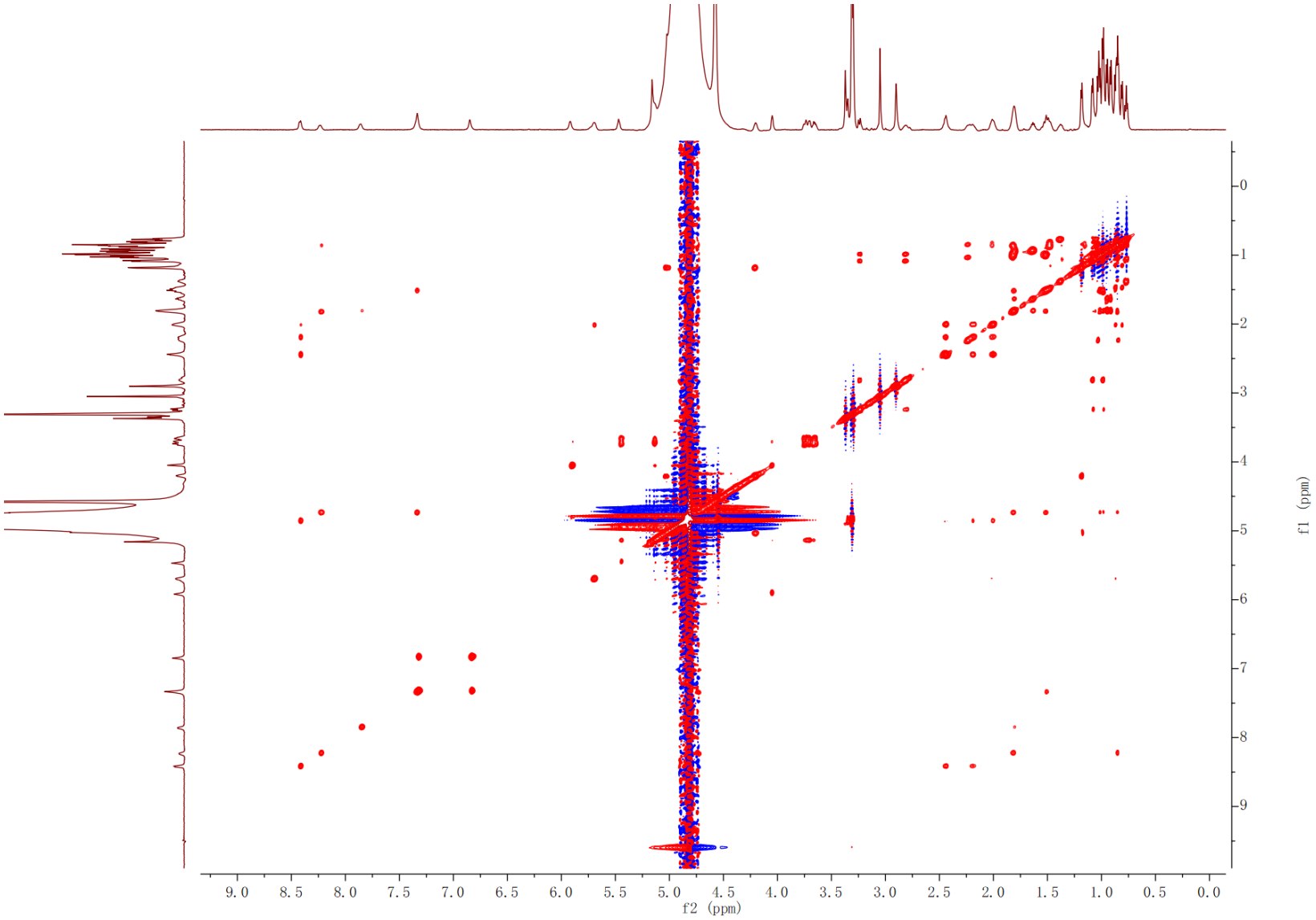

Figure S18.22. ^{1}H-^{1}H TOCSY spectrum of 4 in CD_3OH

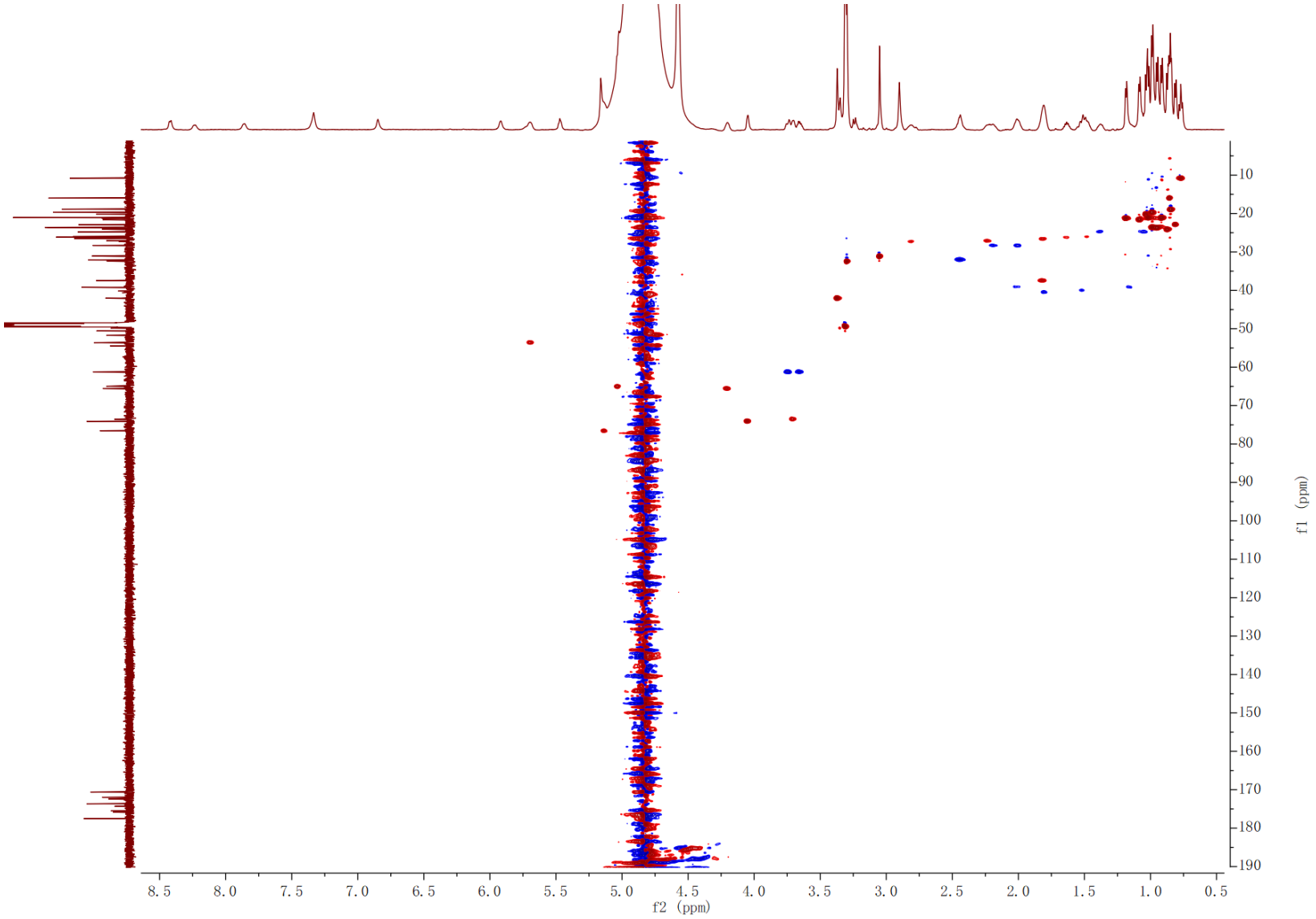

Figure S18.23. HSQC spectrum of 4 in CD_3OH

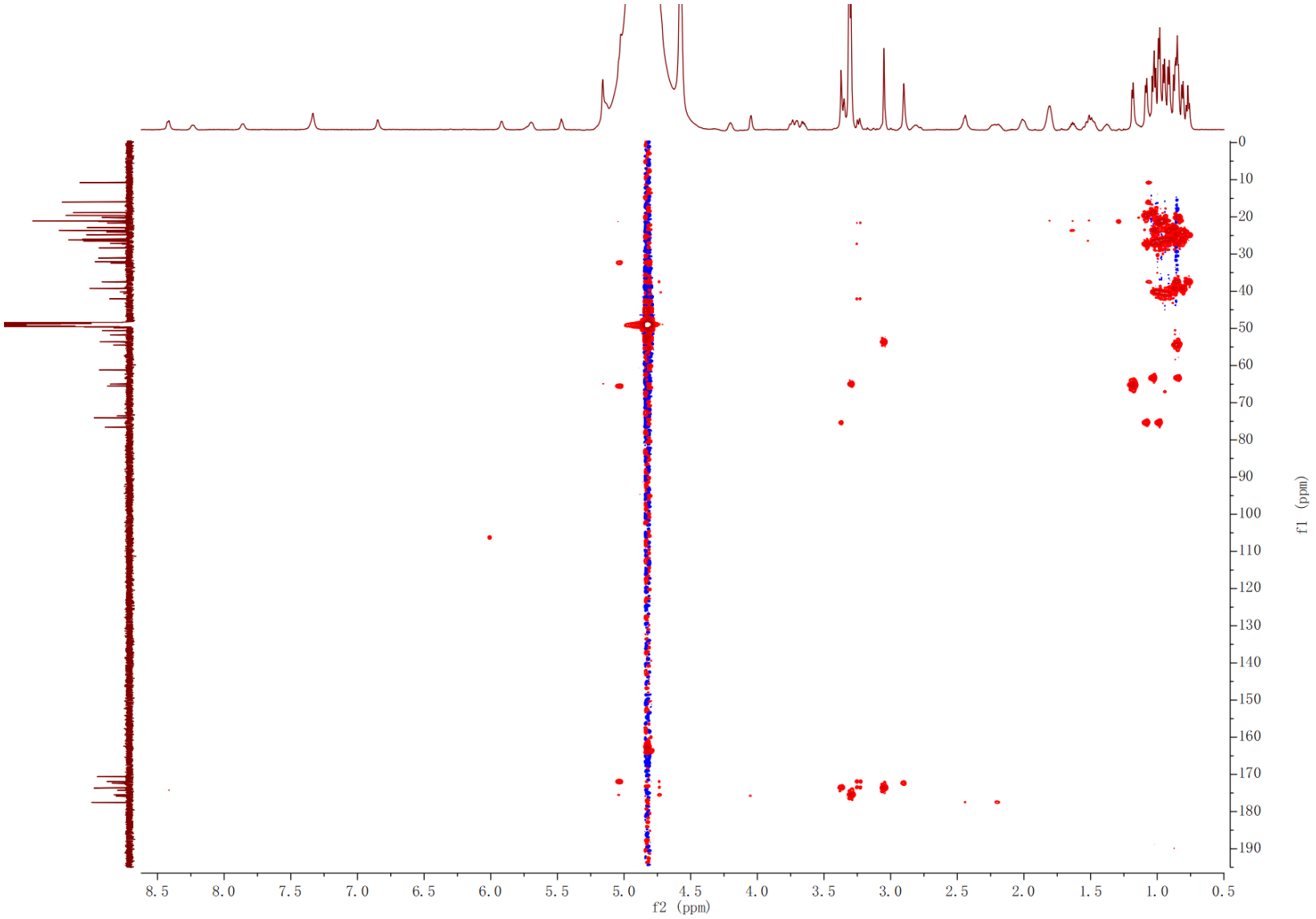

Figure S18.24. HMBC spectrum of 4 in CD_3OH

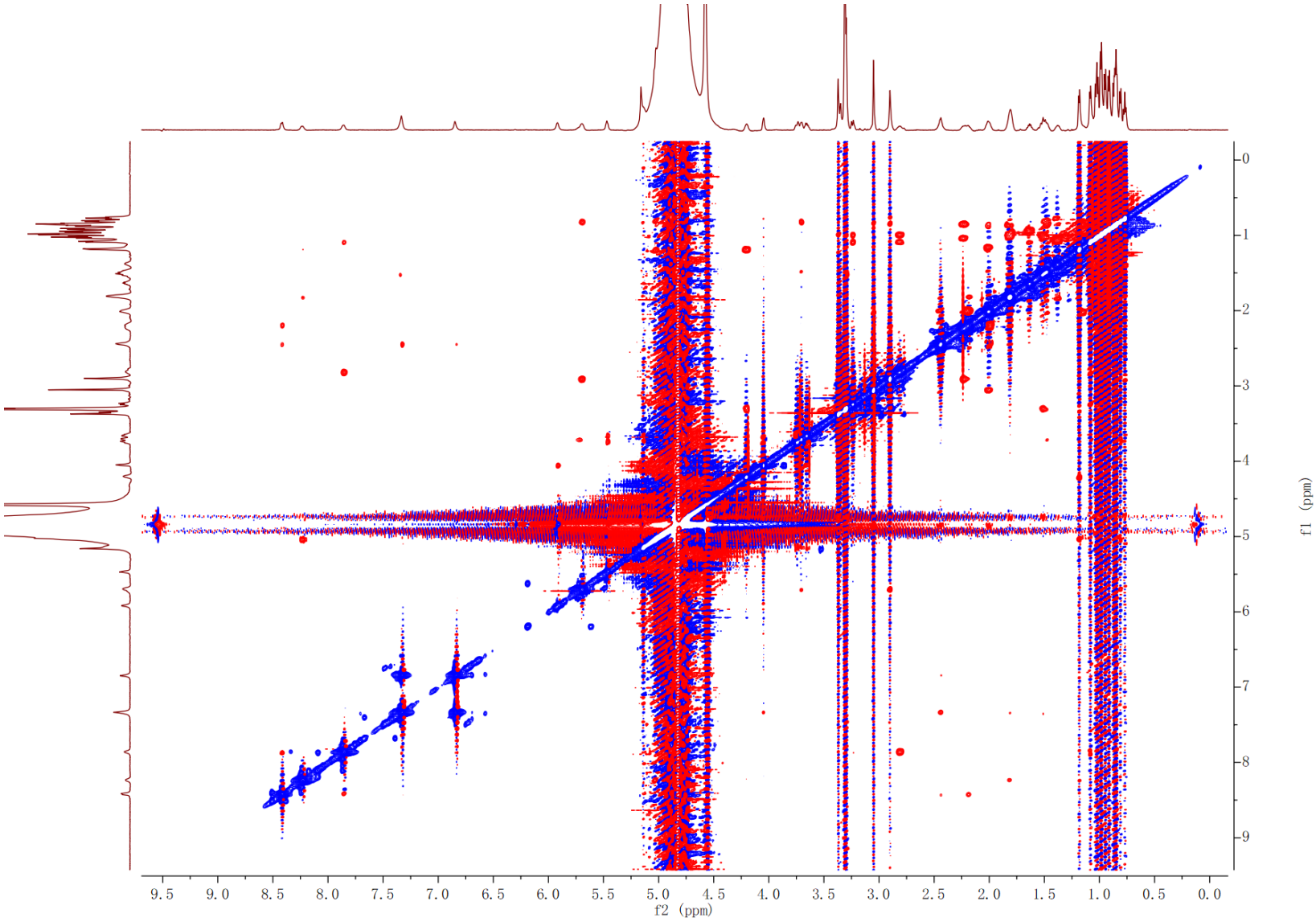

Figure S18.25. ROESY spectrum of 4 in CD_3OH

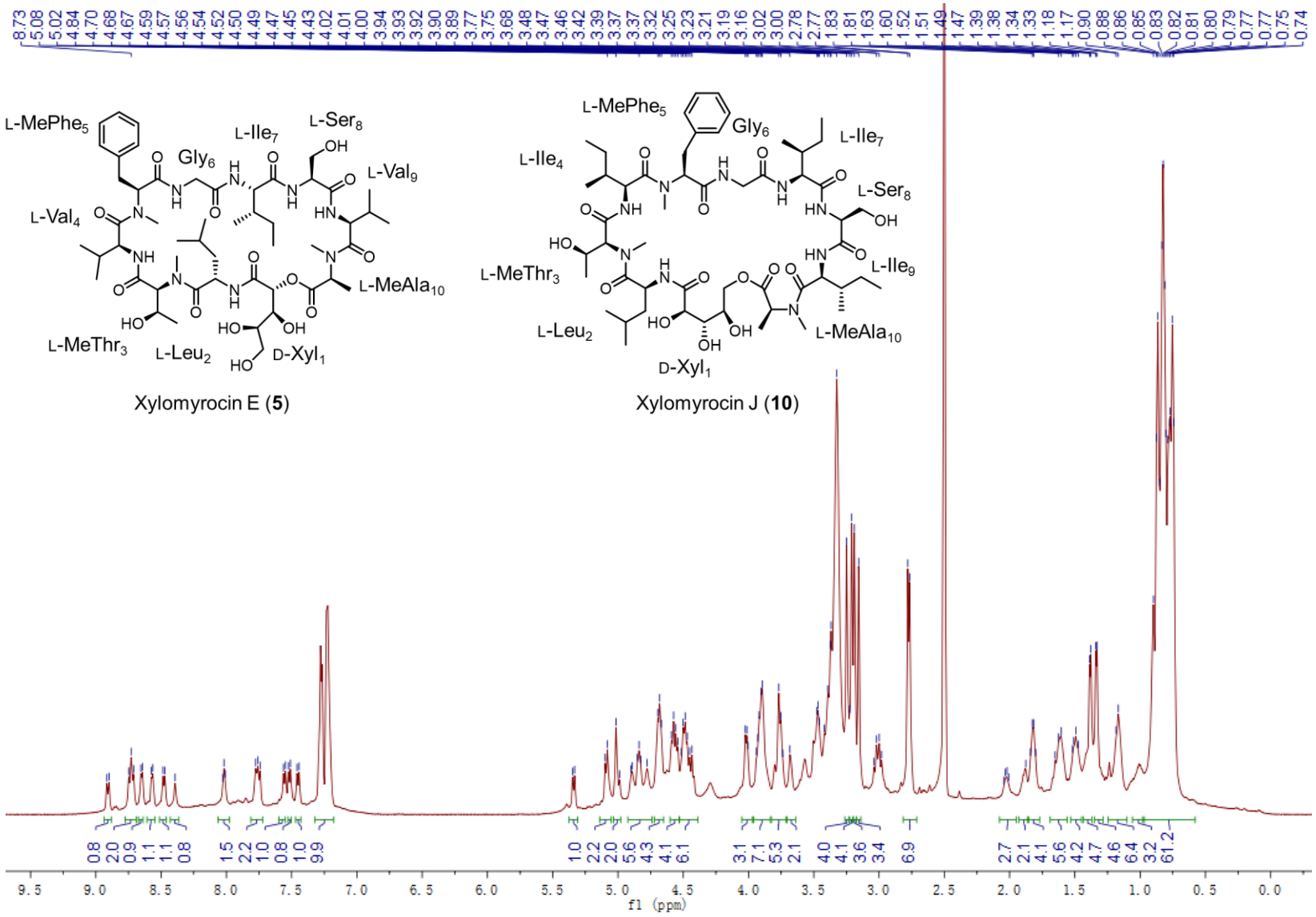

Figure S18.26. ^{1}H NMR spectrum of the mixture of 5 and 10 in DMSO-d_6

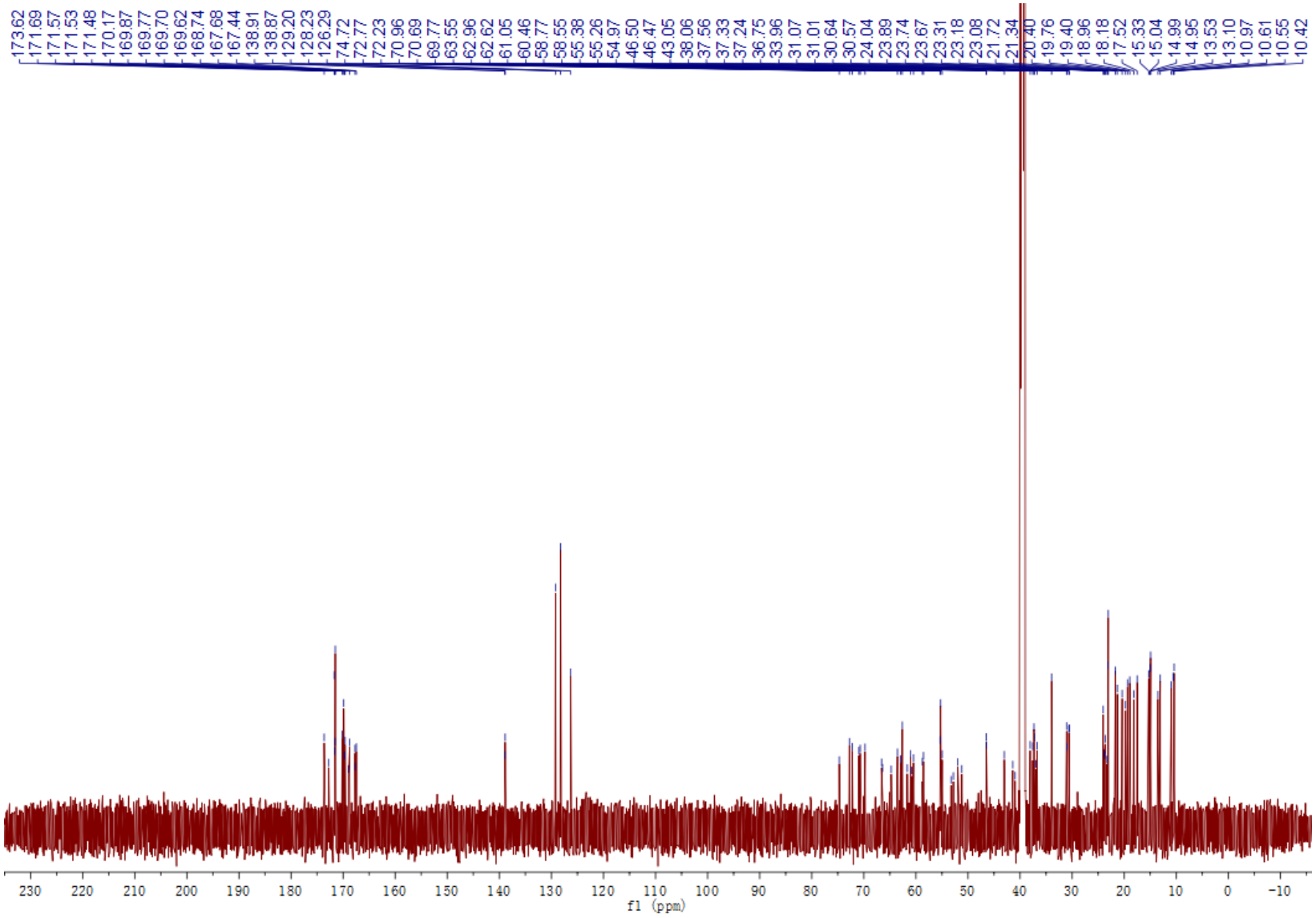

Figure S18.27. ^{13}C NMR spectrum of the mixture of 5 and 10 in DMSO-d_6

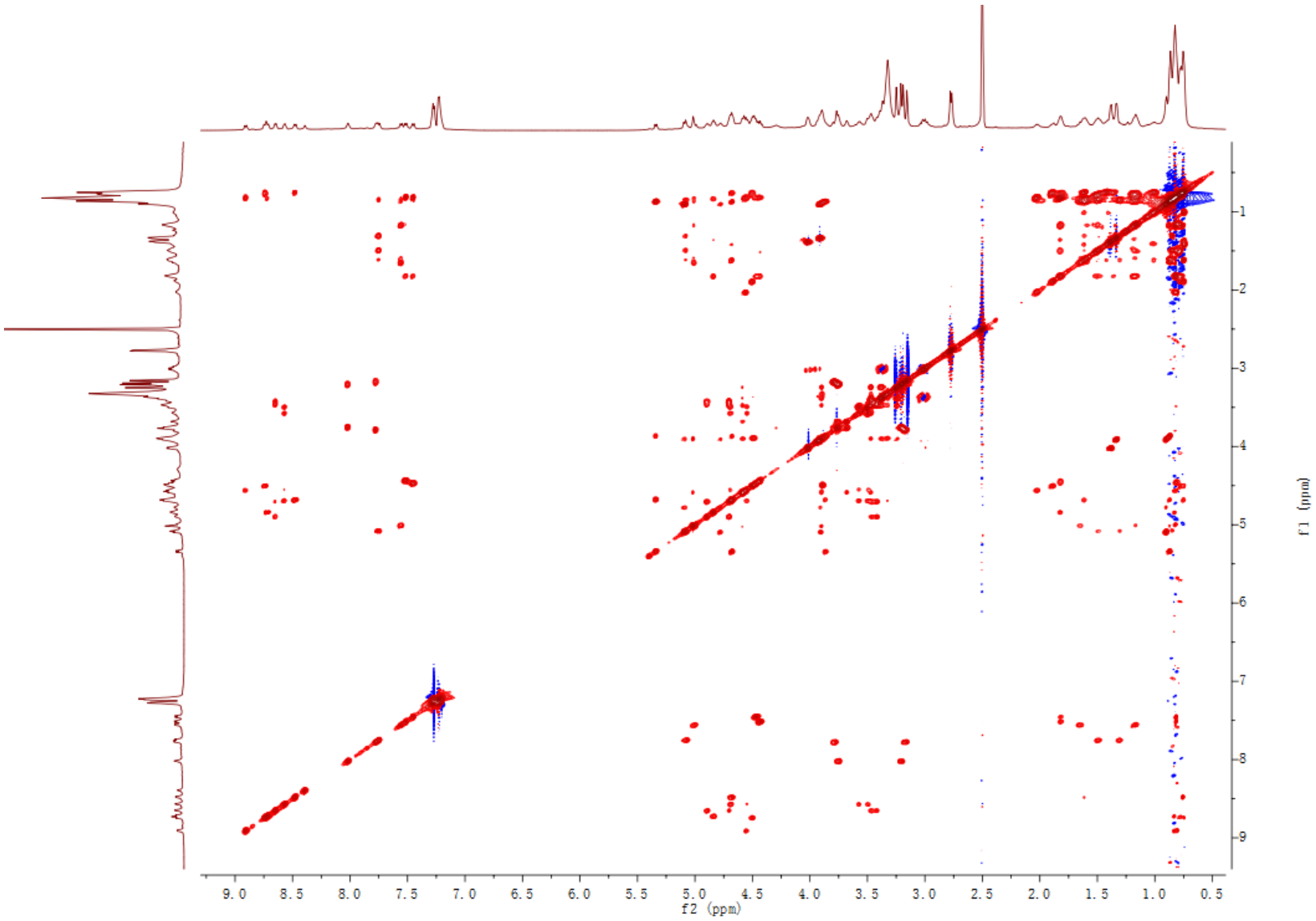

Figure S18.28. ^{1}H-^{1}H TOCSY spectrum of the mixture of 5 and 10 in DMSO-d_6

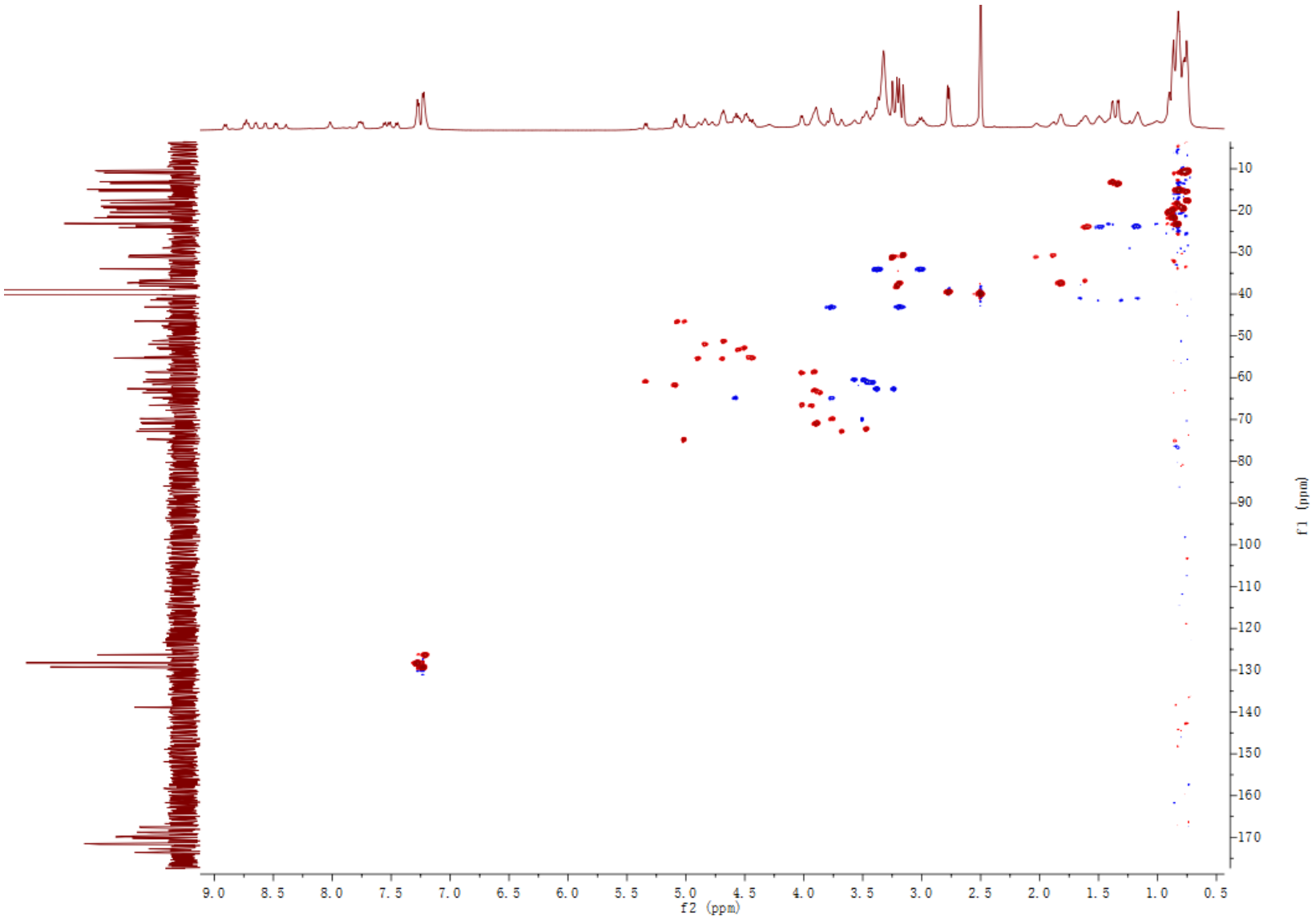

Figure S18.29. HSQC spectrum of the mixture of 5 and 10 in DMSO-d_6

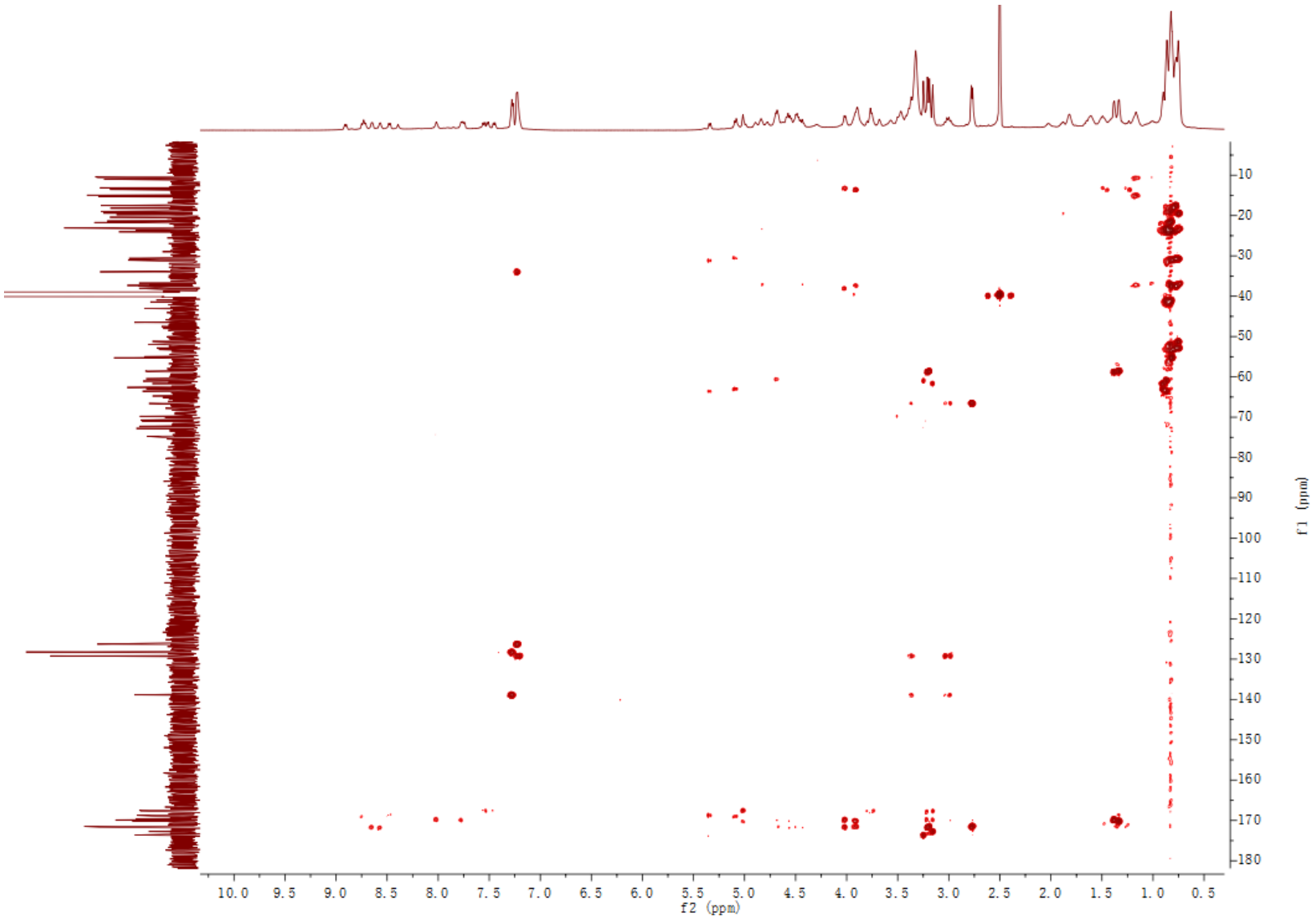

Figure S18.30. HMBC spectrum of the mixture of 5 and 10 in DMSO-d_6

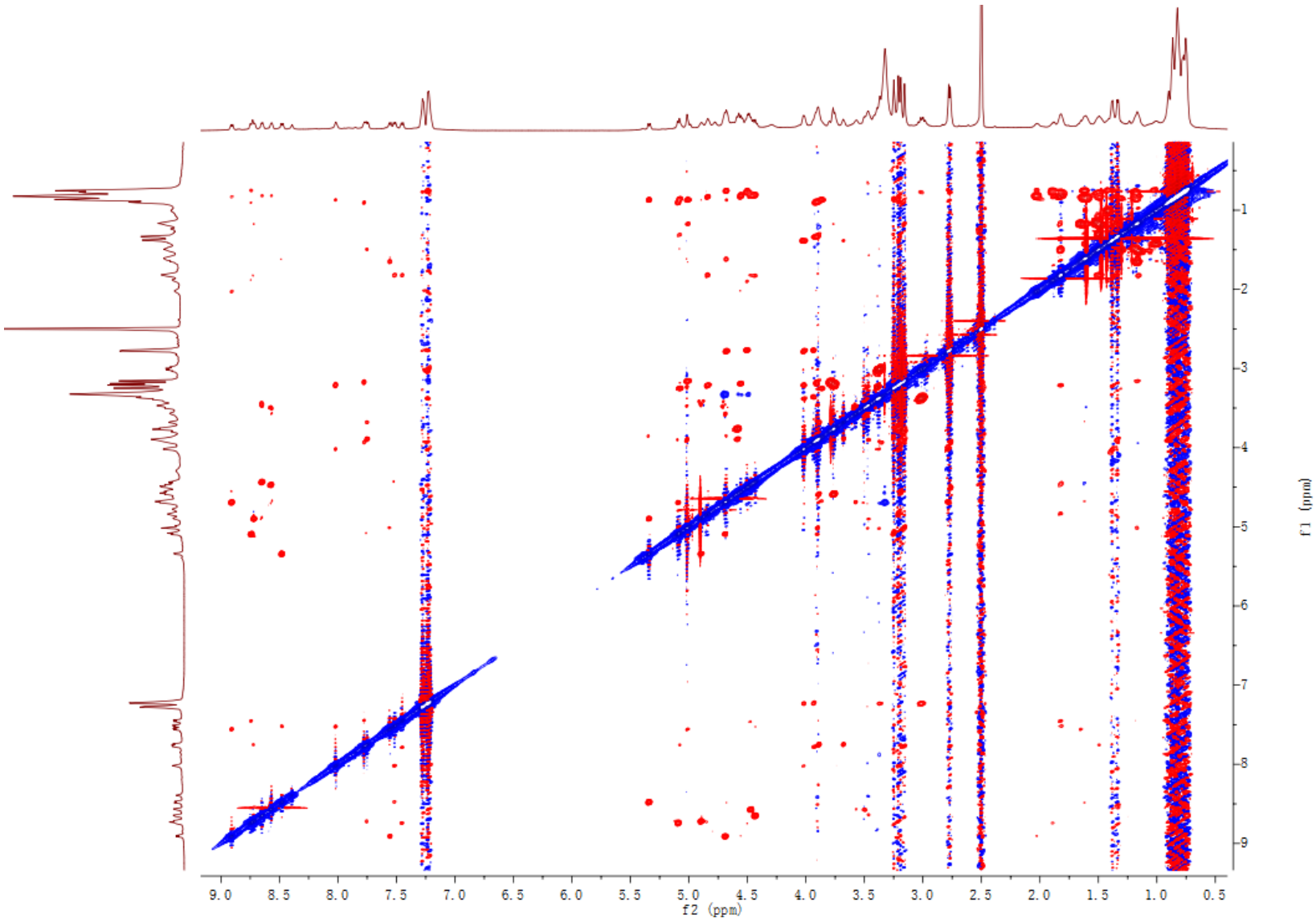

Figure S18.31. ROESY spectrum of the mixture of 5 and 10 in DMSO-d_6

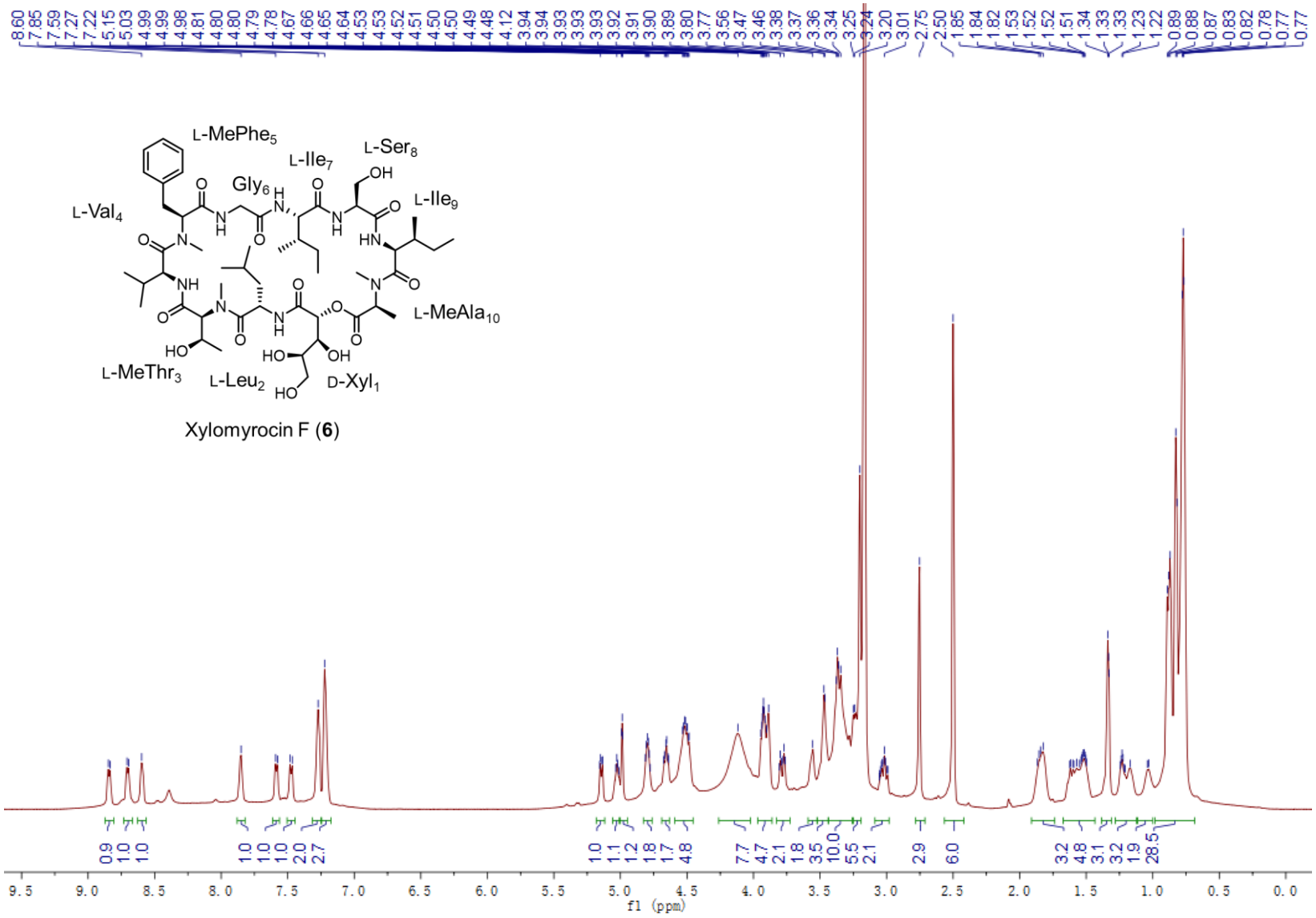

Figure S18.32. ^{1}H NMR spectrum of 6 in DMSO-d_6

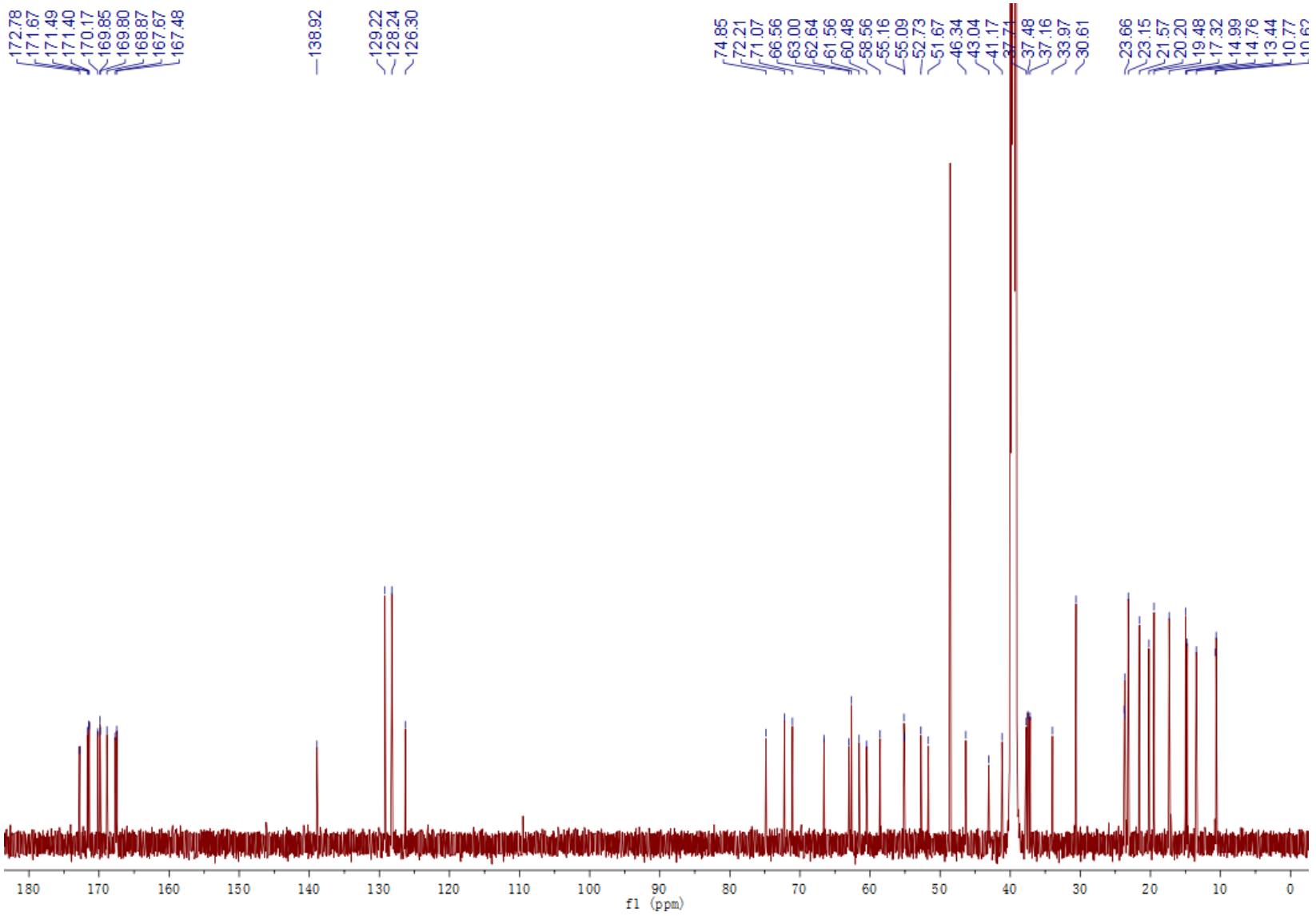

Figure S18.33. ^{13}C NMR spectrum of 6 in DMSO-d_6

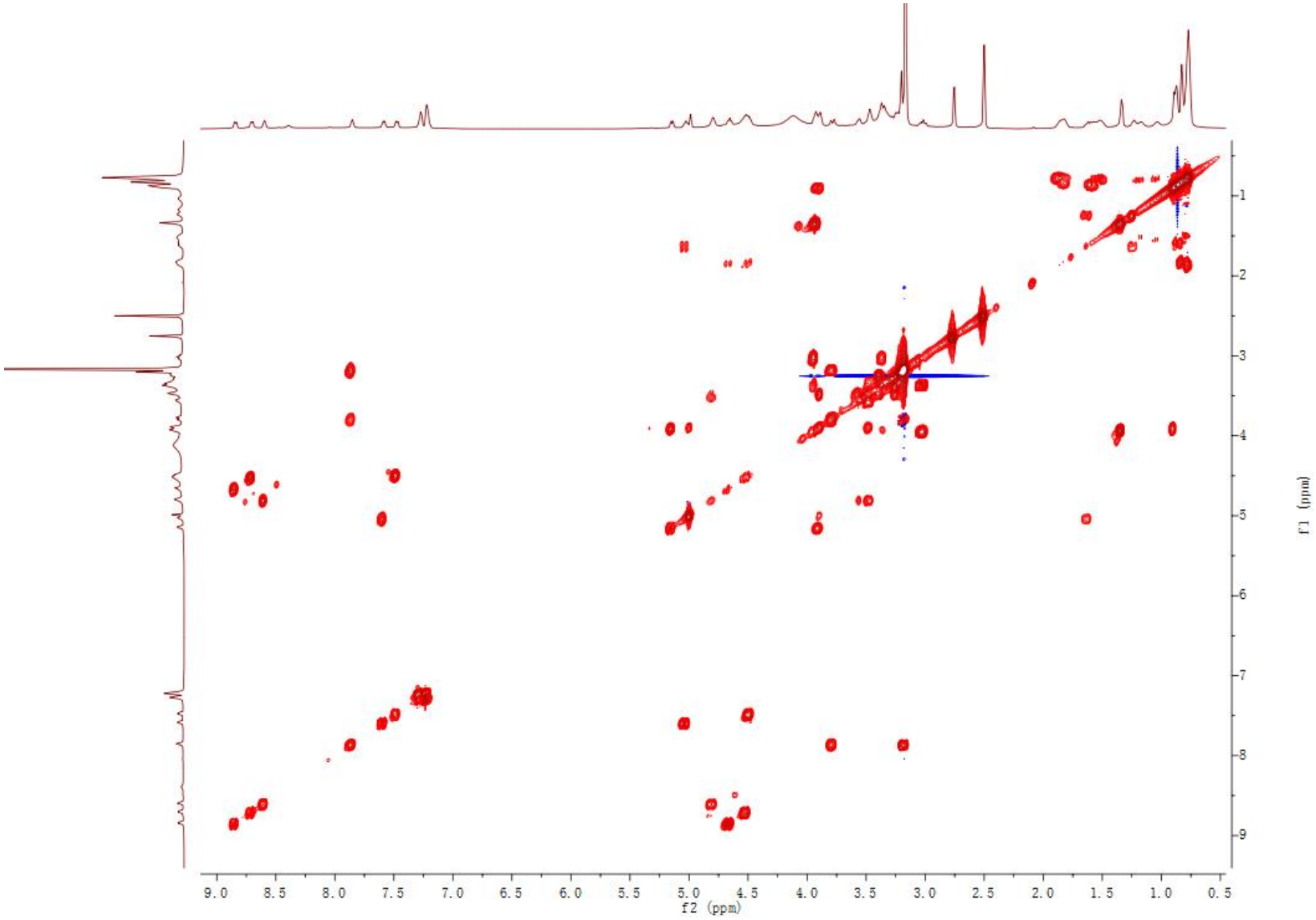

Figure S18.34. ^{1}H-^{1}H COSY spectrum of 6 in DMSO-d_6

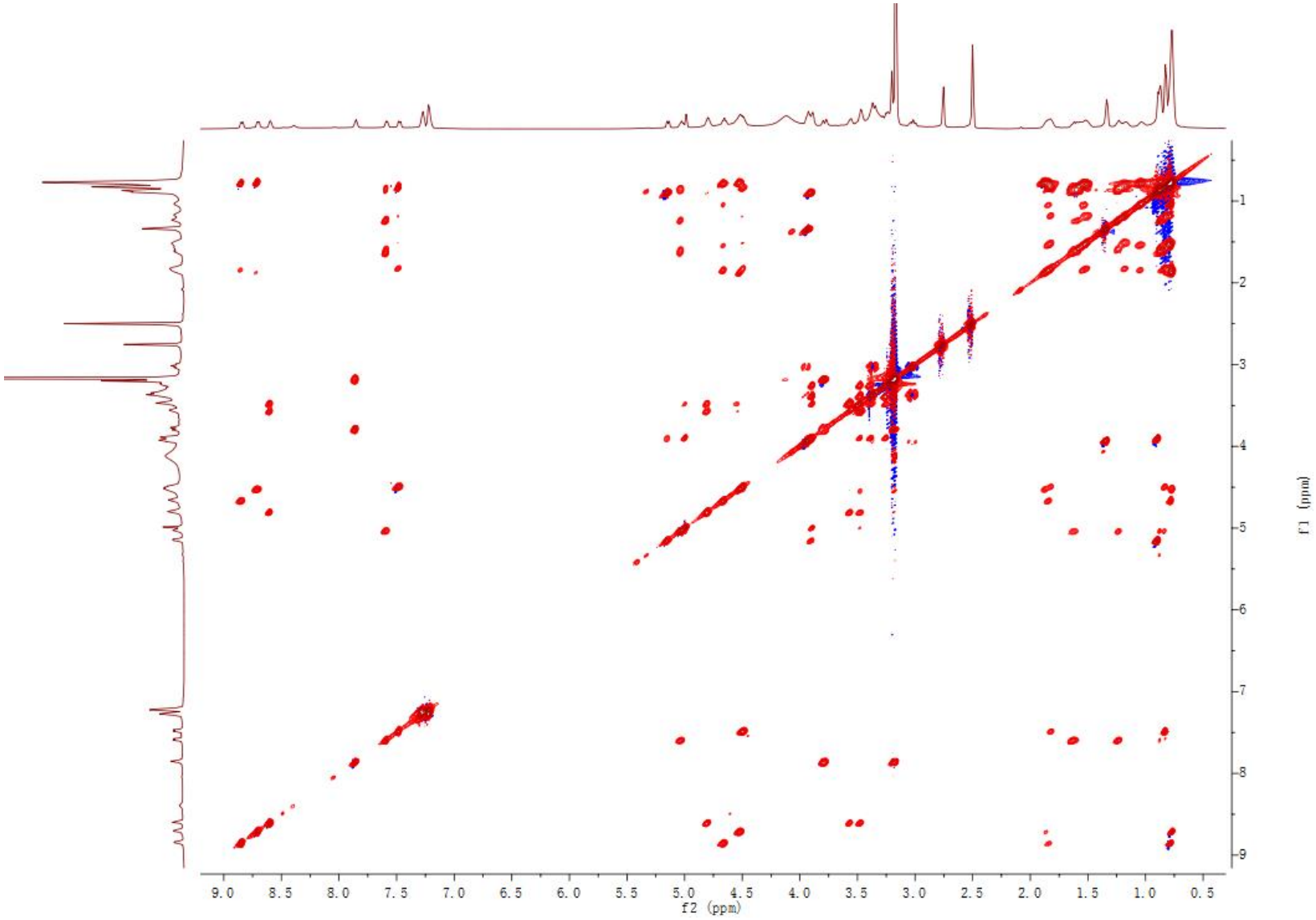

Figure S18.35. ^{1}H-^{1}H TOCSY spectrum of **6** in DMSO-d_6

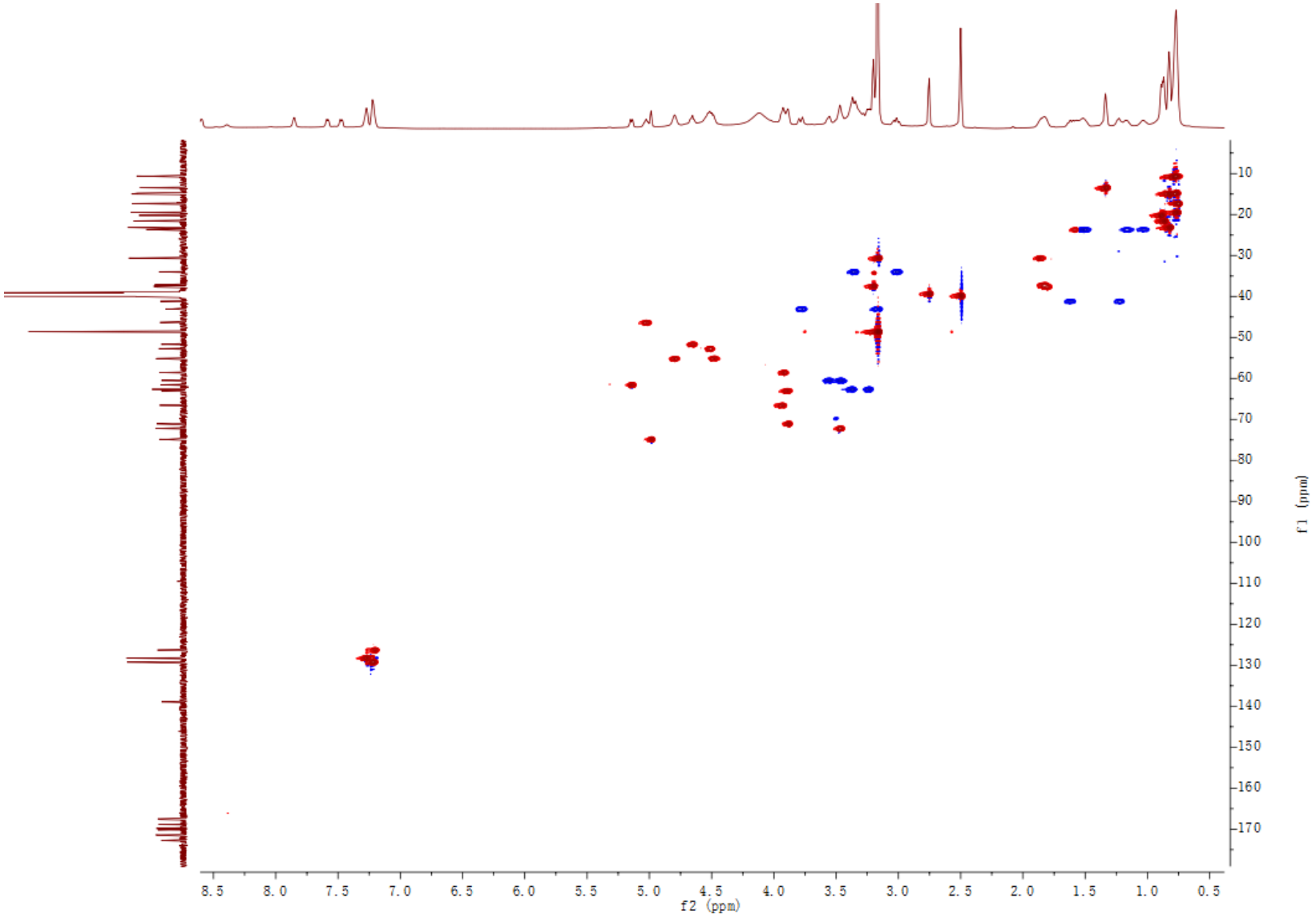

Figure S18.36. HSQC spectrum of 6 in DMSO-d_6

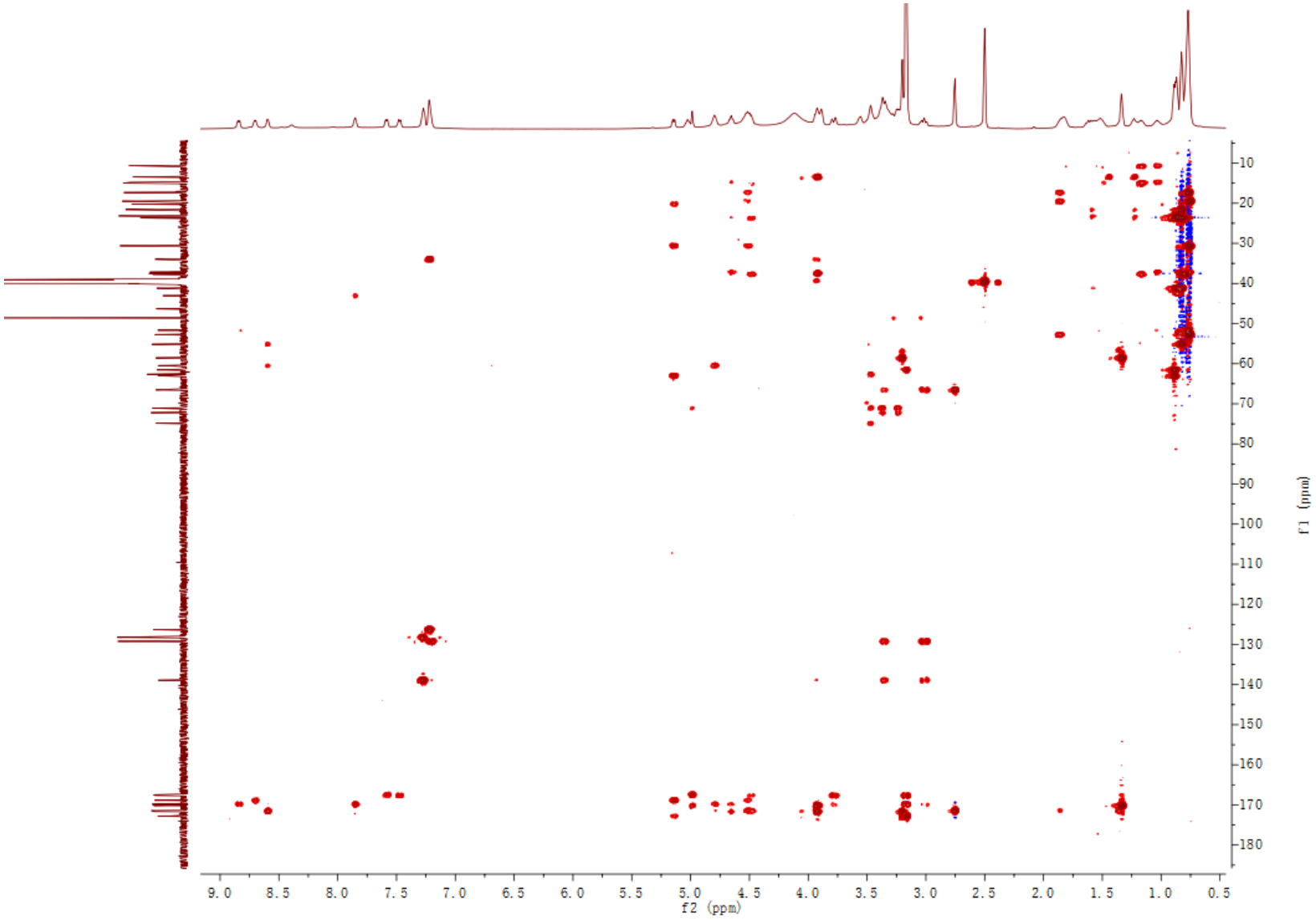

Figure S18.37. HMBC spectrum of 6 in DMSO-d_6

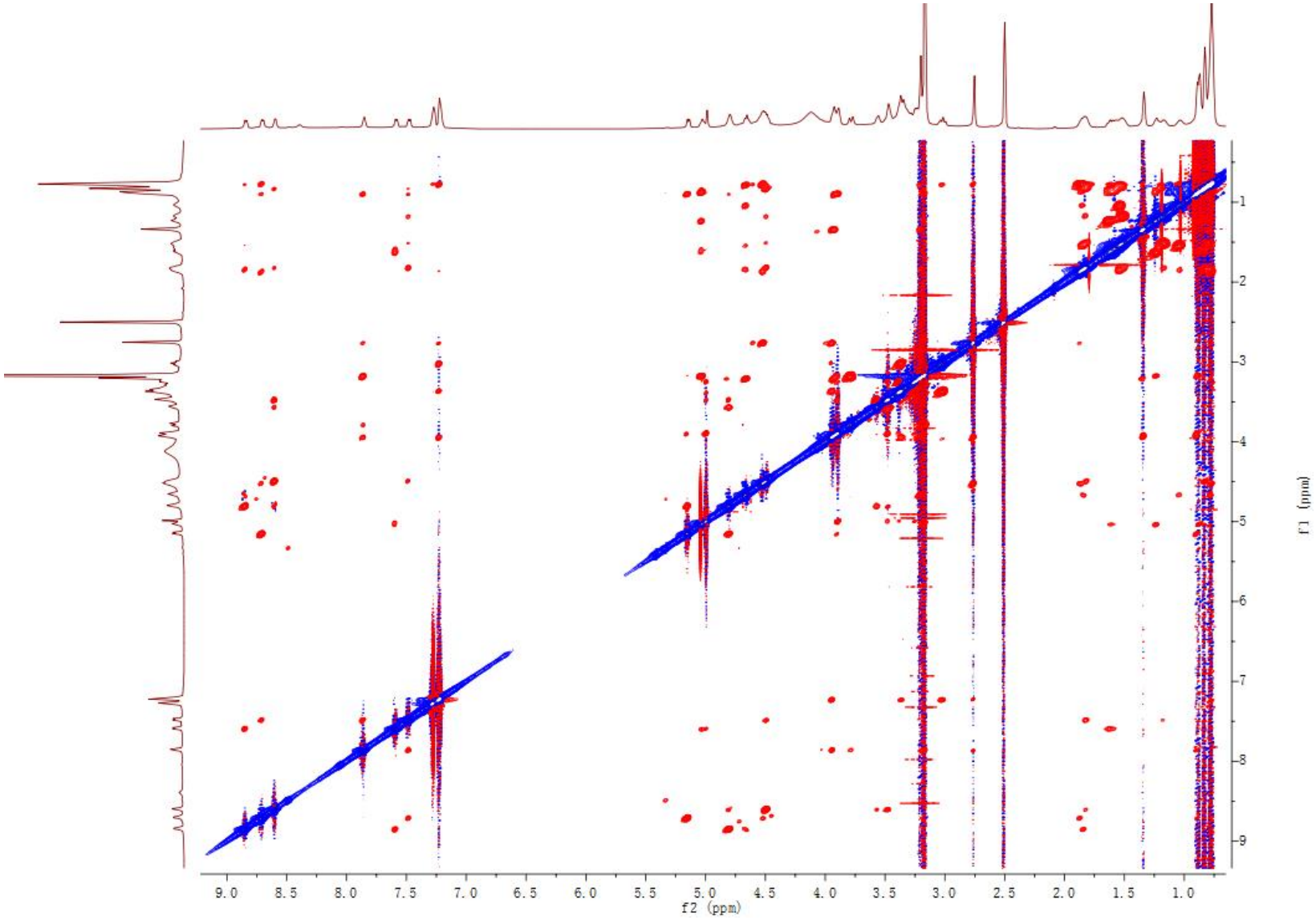

Figure S18.38. ROESY spectrum of 6 in DMSO-d_6

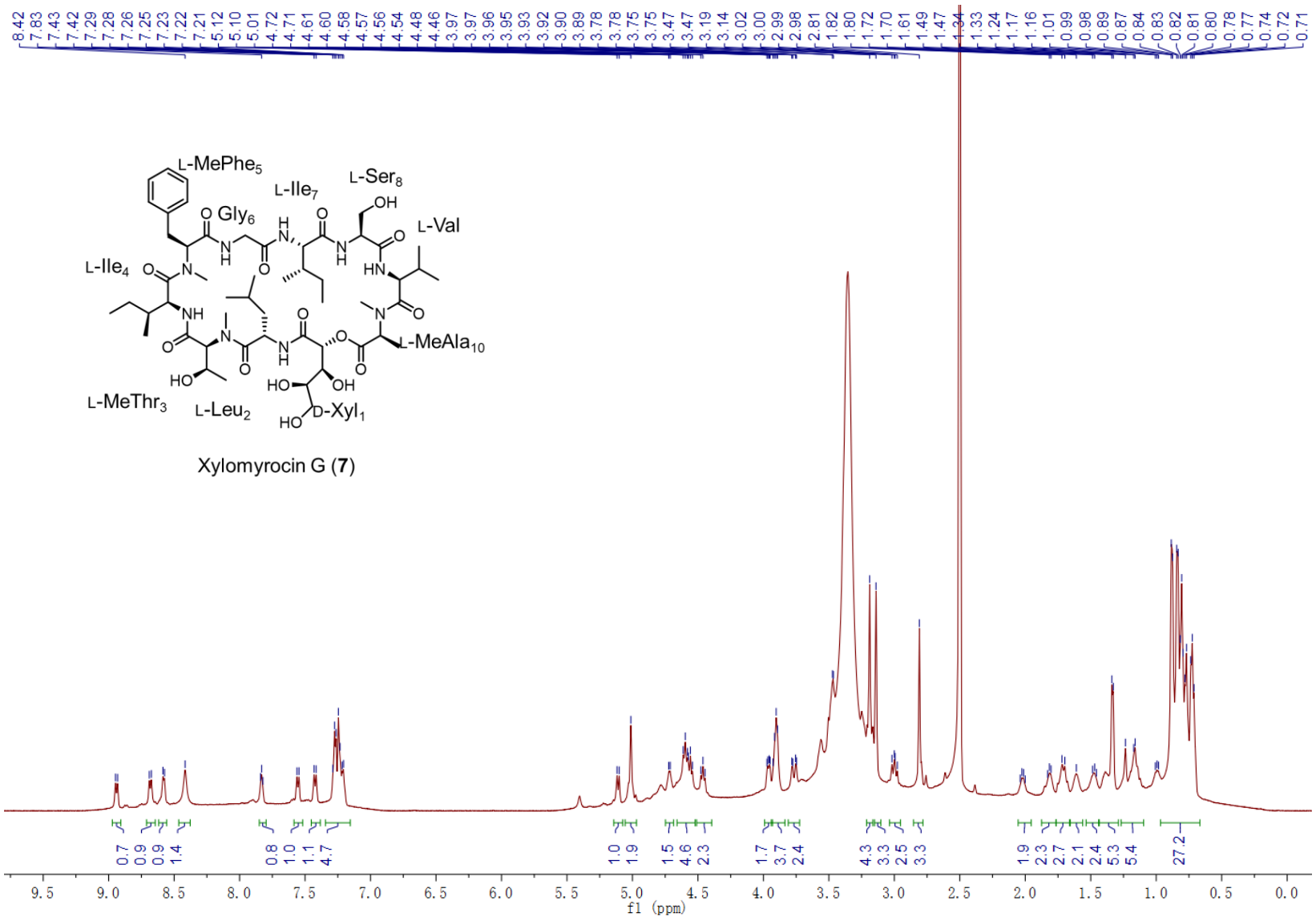

Figure S18.39. ^{1}H NMR spectrum of 7 in DMSO-d_6

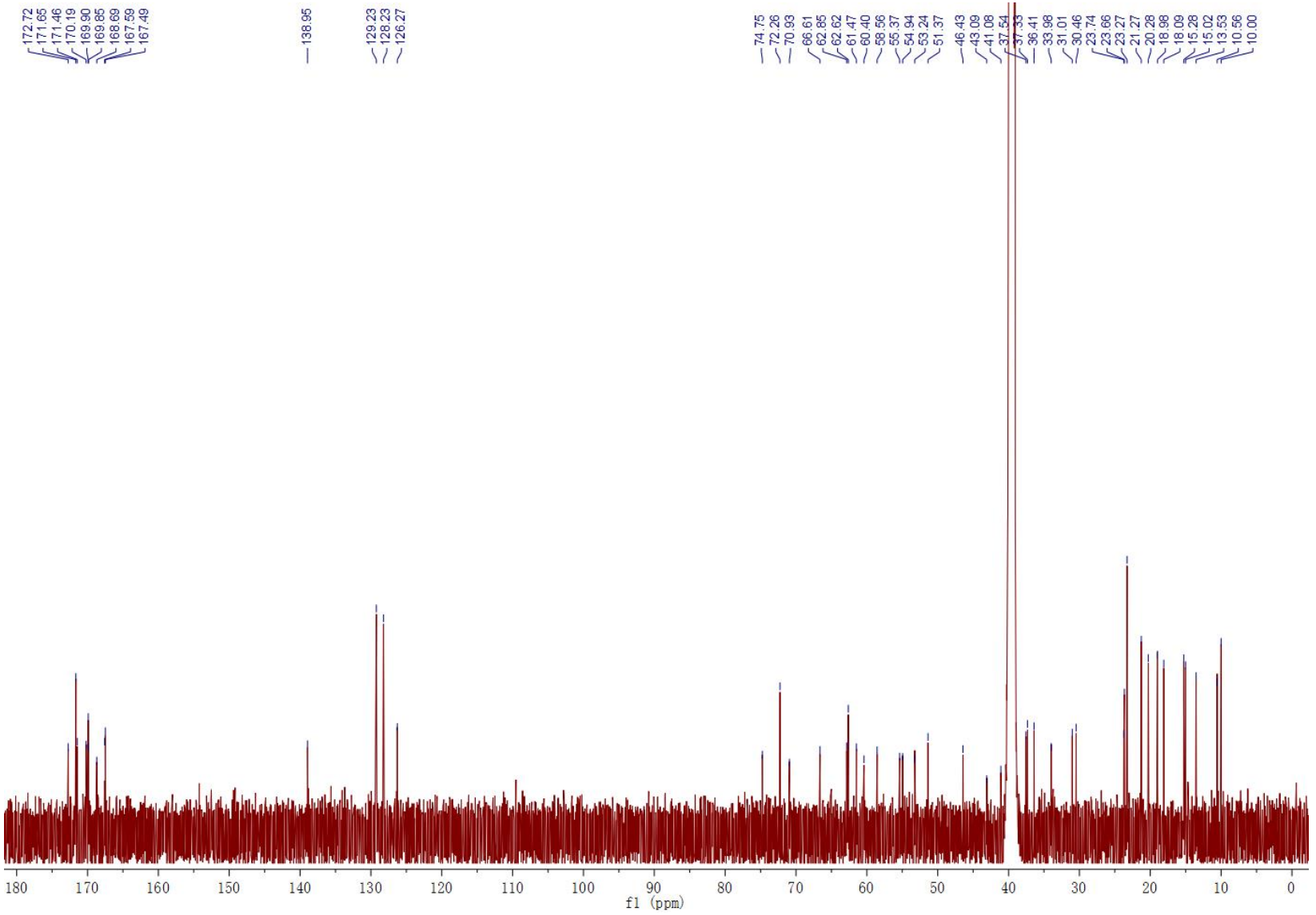

Figure S18.40. ^{13}C NMR spectrum of 7 in DMSO-d_6

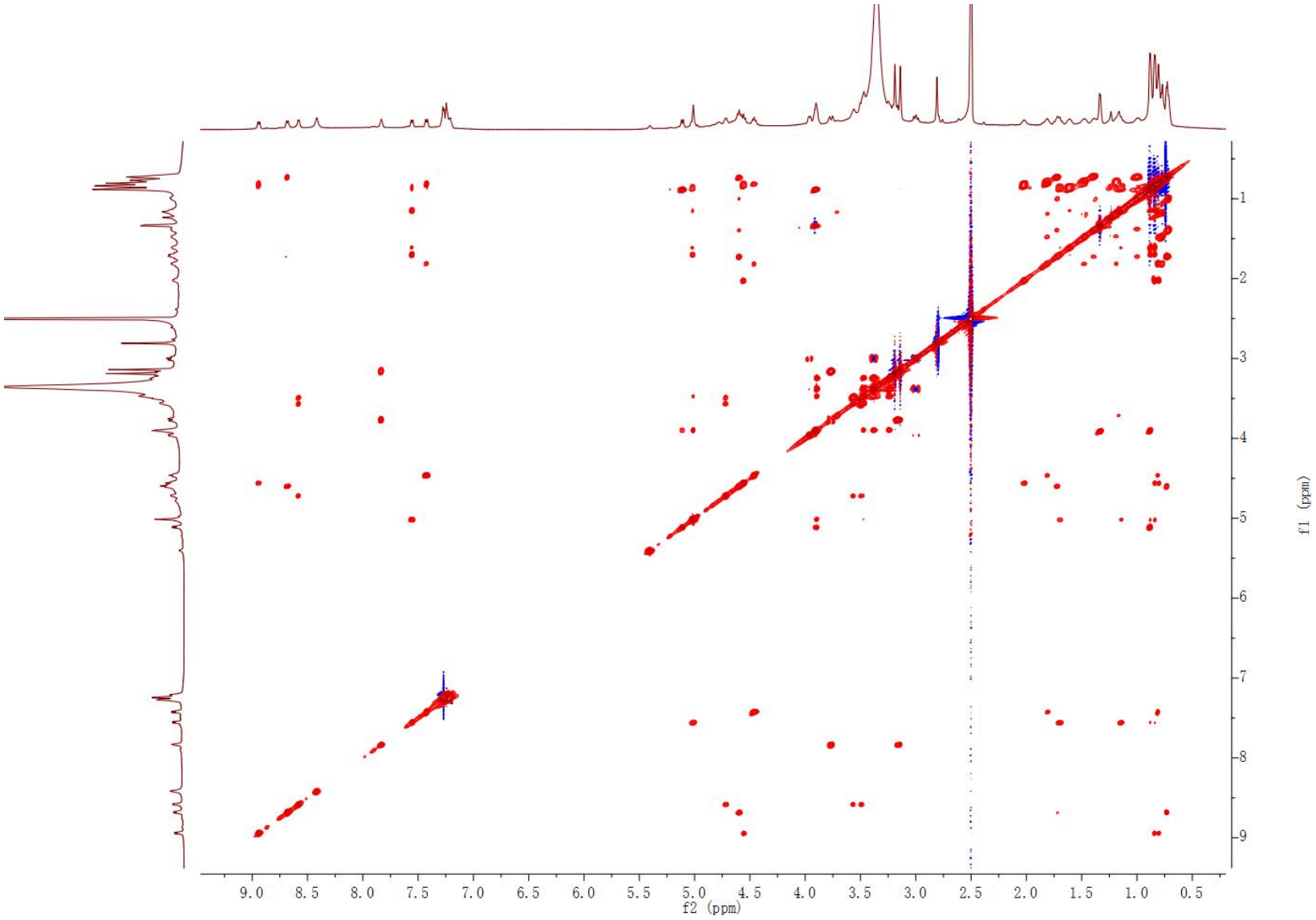

Figure S18.41. ^{1}H-^{1}H TOCSY spectrum of 7 in DMSO-d_6

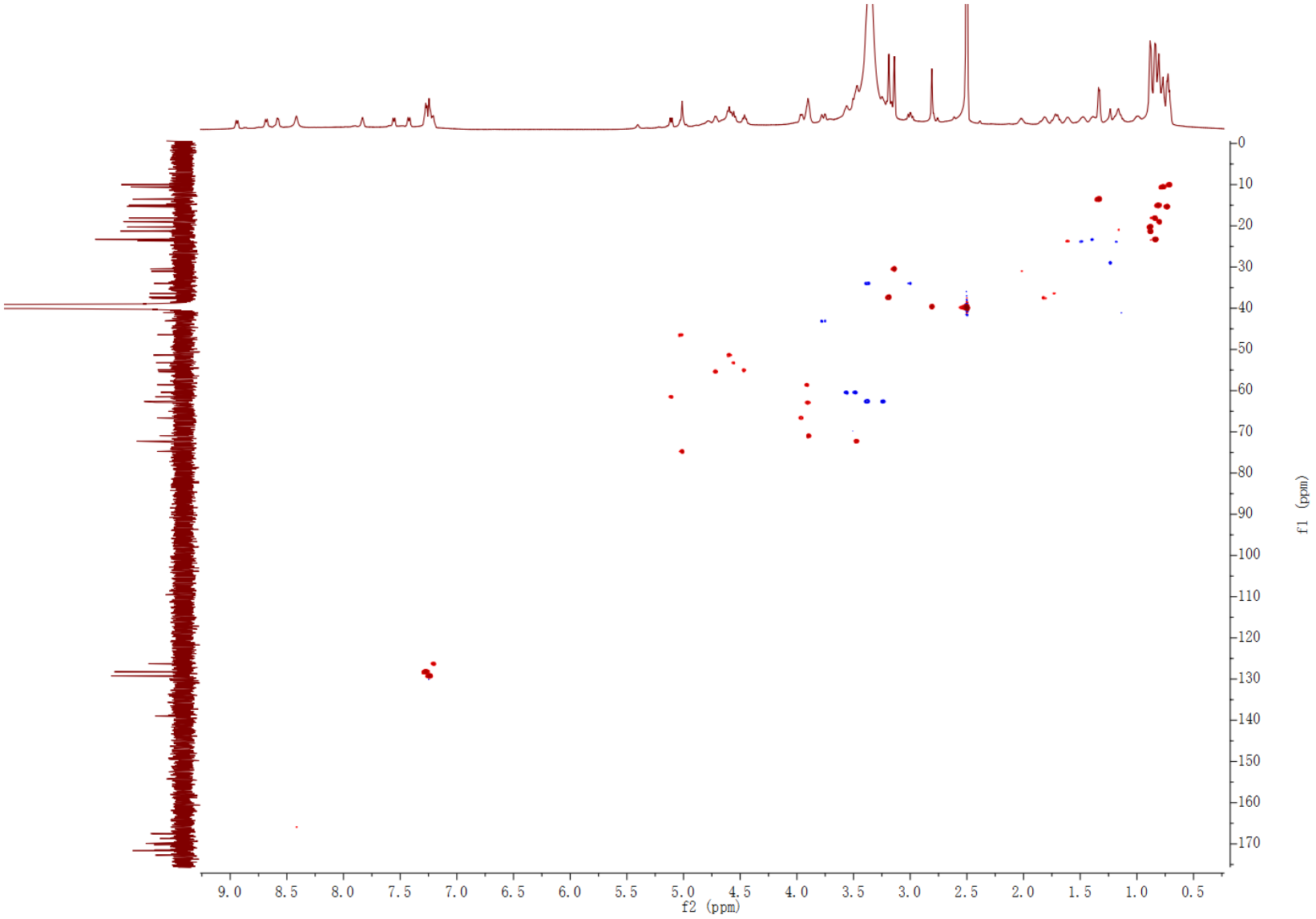

Figure S18.42. HSQC spectrum of 7 in DMSO-d_6

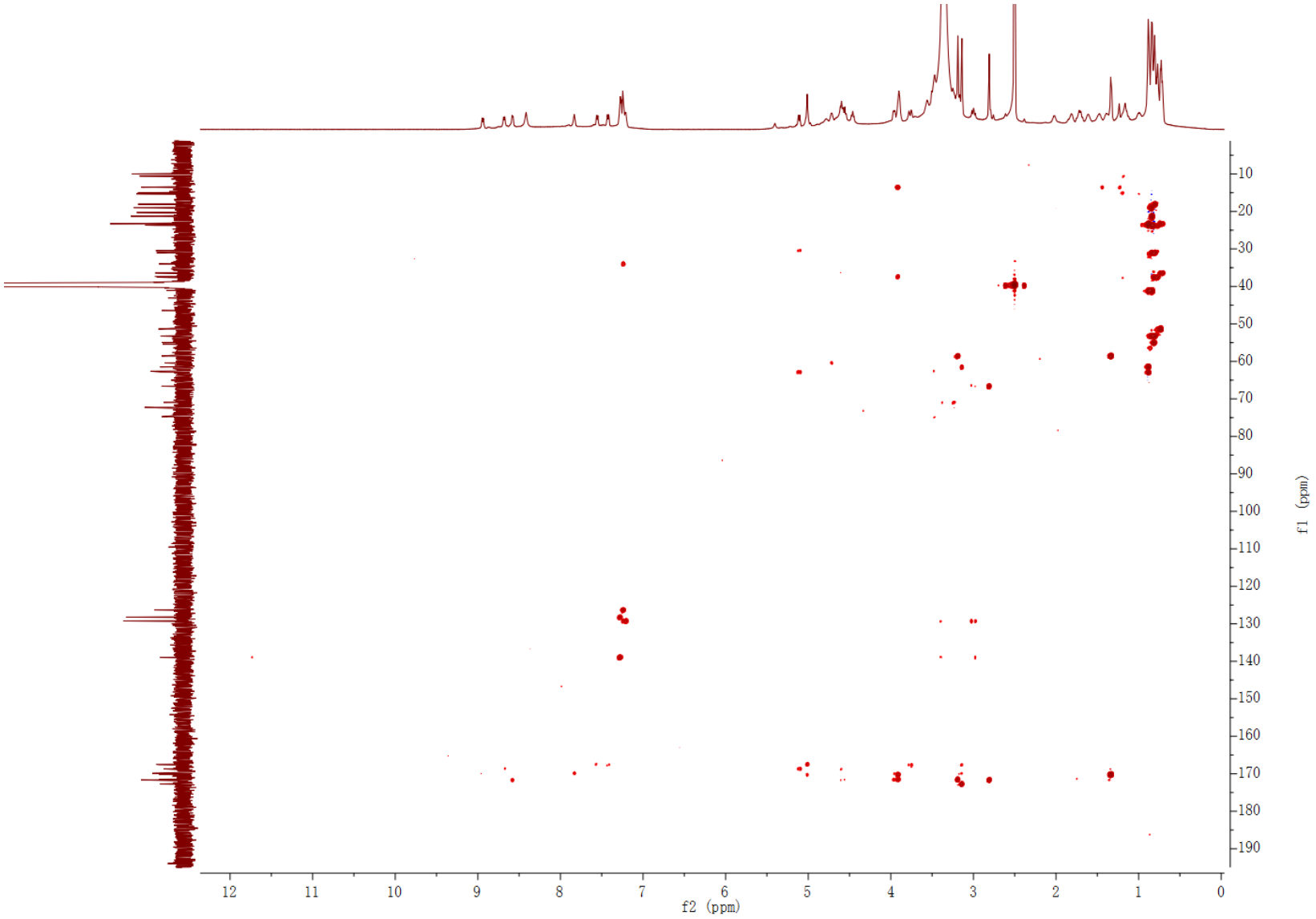

Figure S18.43. HMBC spectrum of 7 in DMSO-d_6

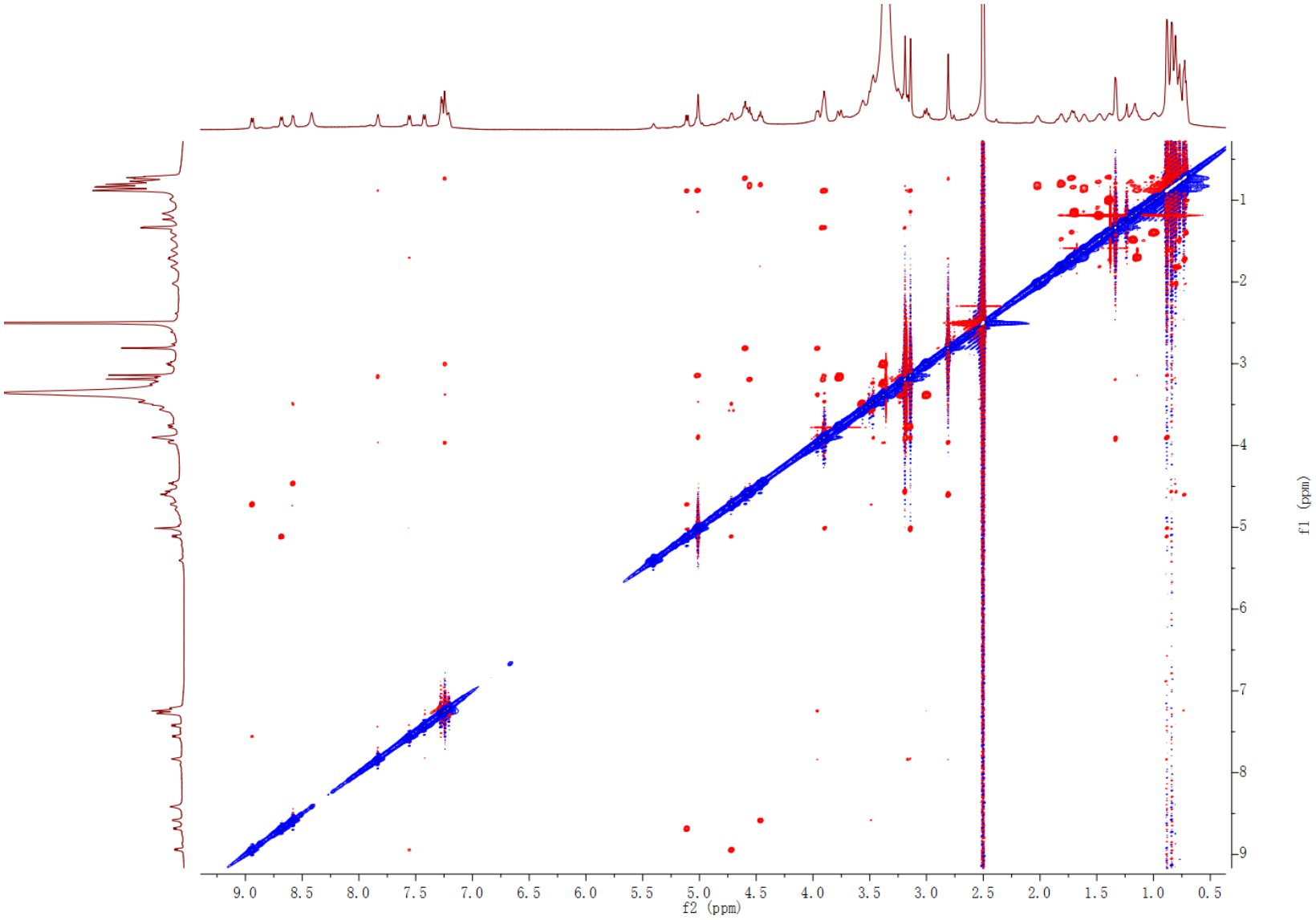

Figure S18.44. ROESY spectrum of 7 in DMSO-d_6

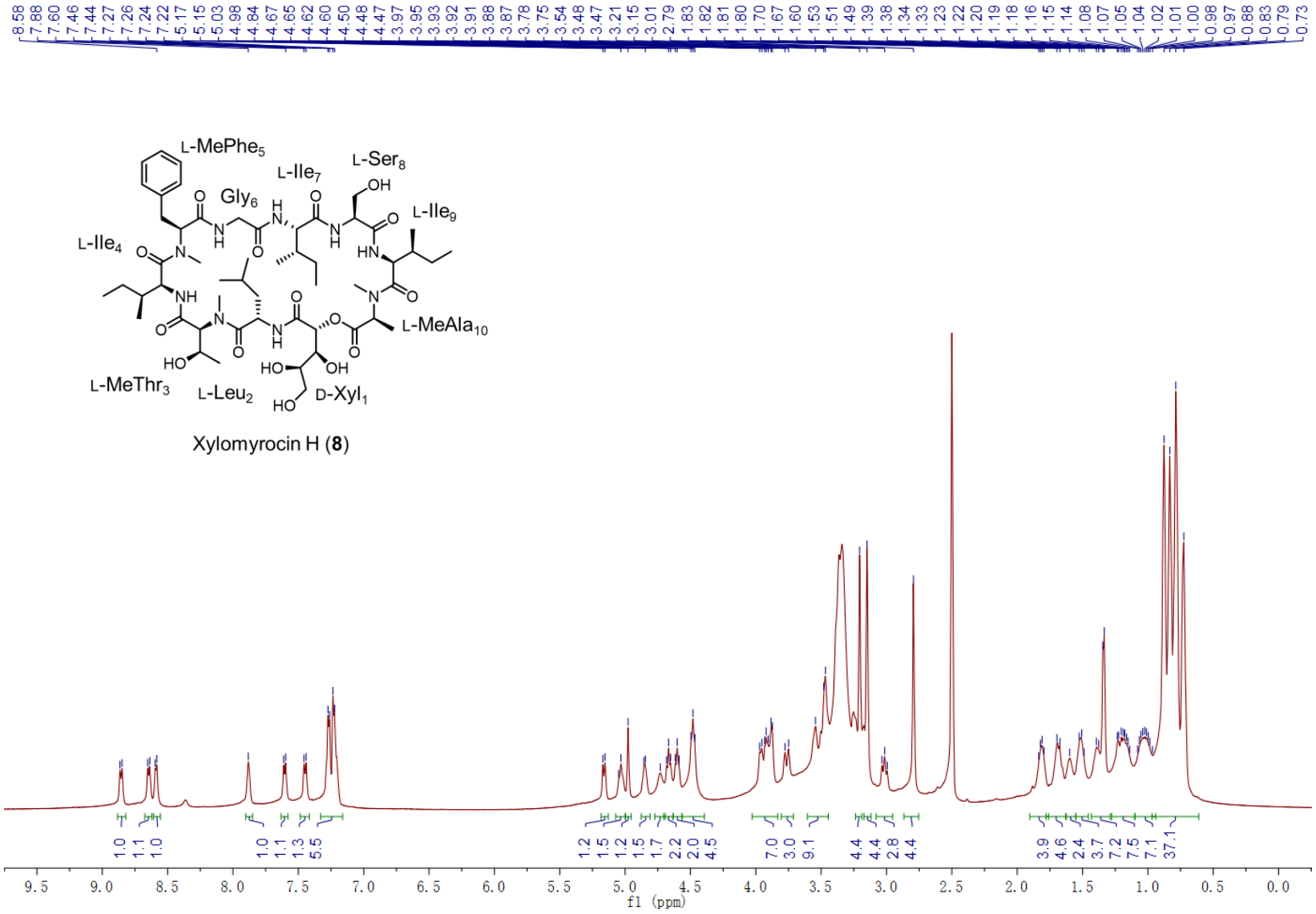

Figure S18.45. ^{1}H NMR spectrum of 8 in DMSO-d_6

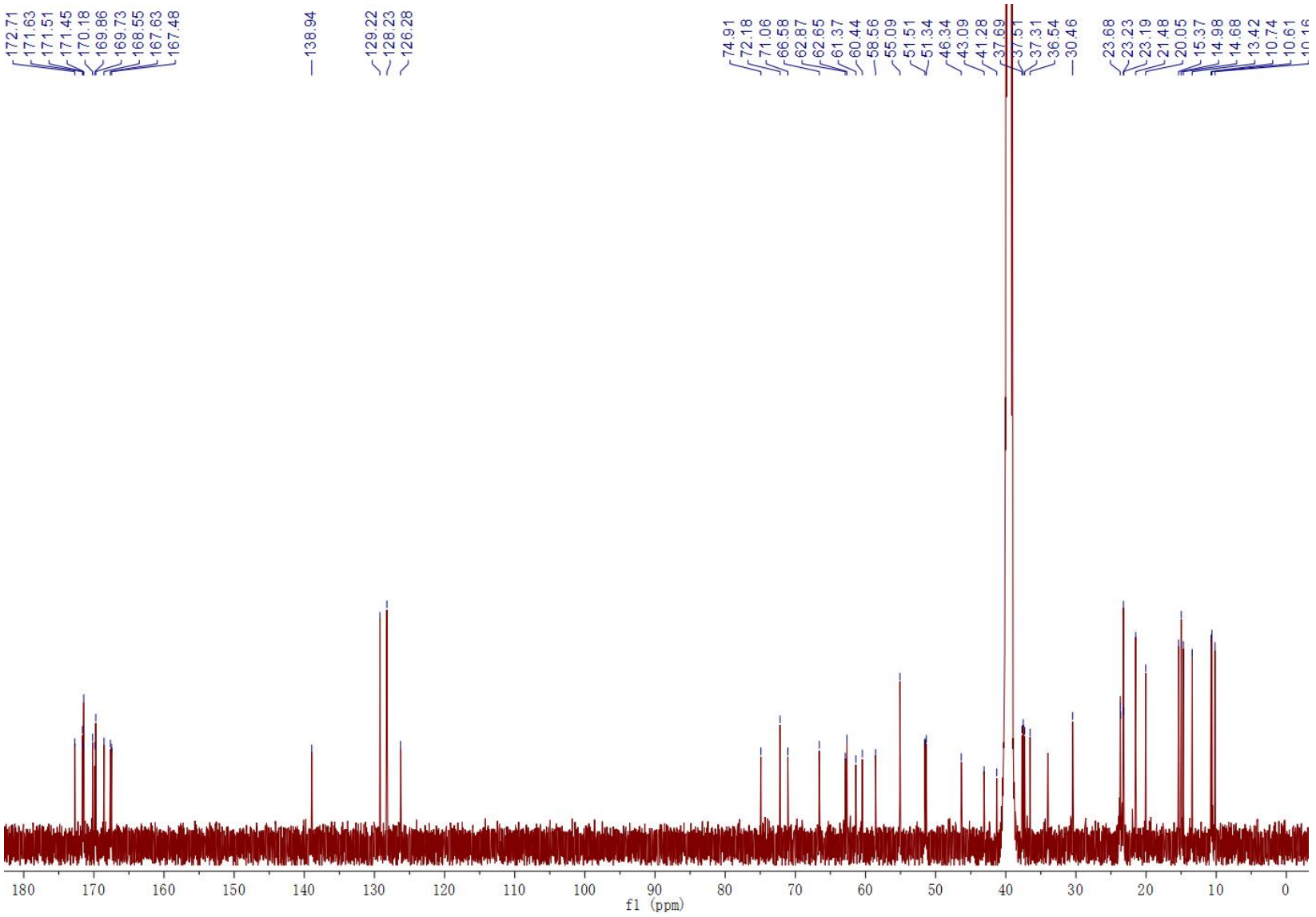

Figure S18.46. ^{13}C NMR spectrum of 8 in DMSO-d_6

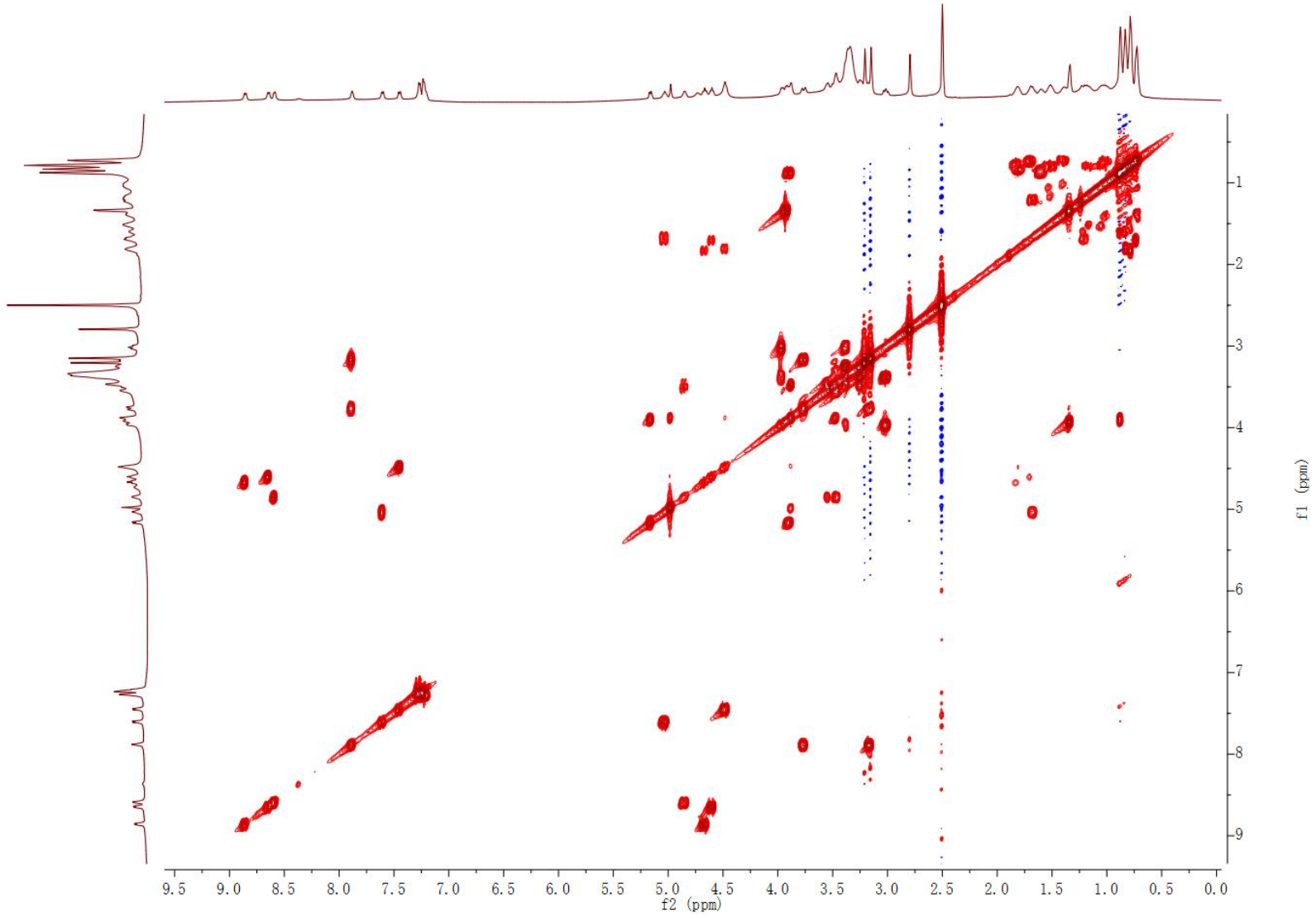

Figure S18.47. ^{1}H-^{1}H COSY spectrum of 8 in DMSO-d_6

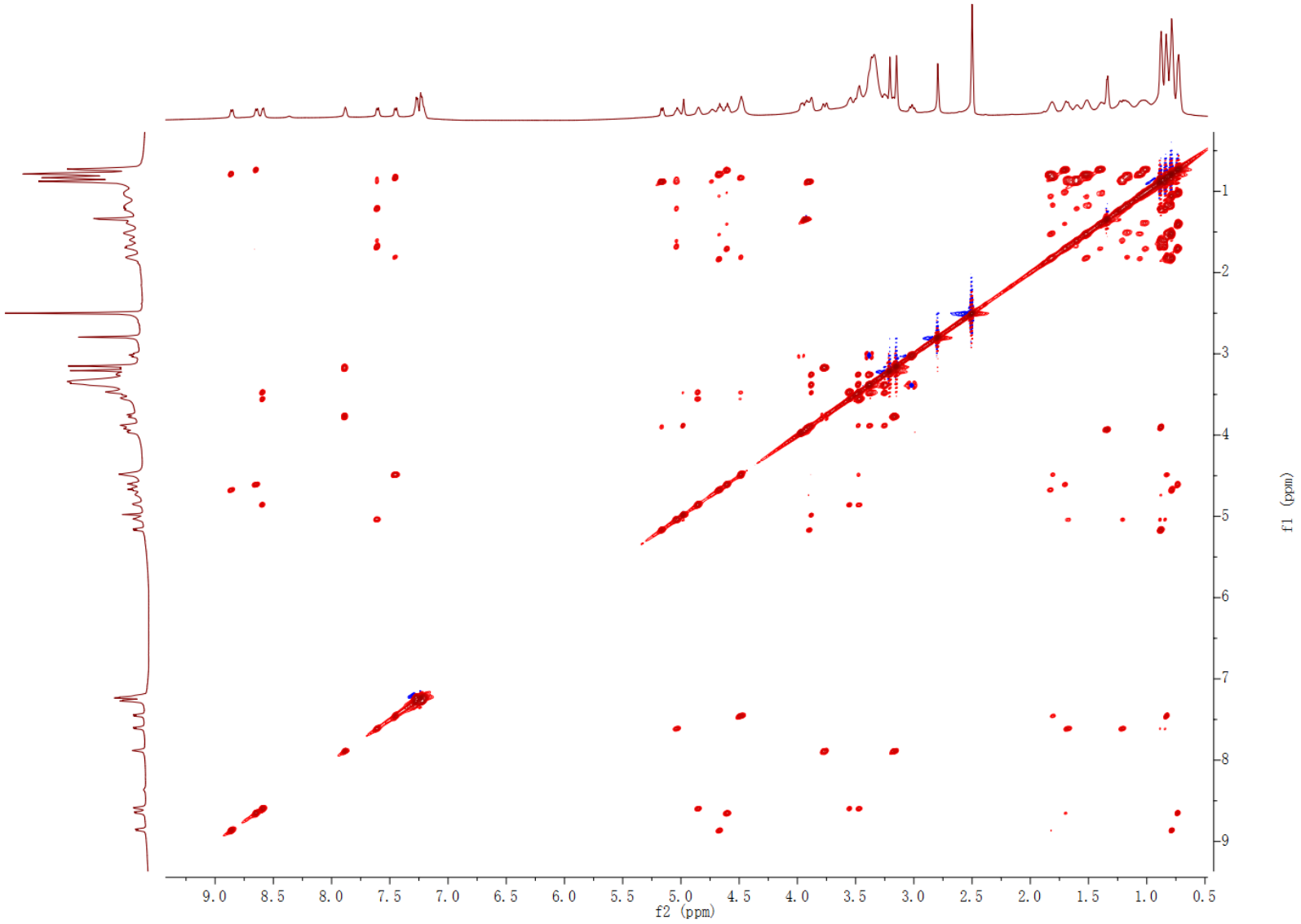

Figure S18.48. ^{1}H-^{1}H TOCSY spectrum of **8** in DMSO-d_6

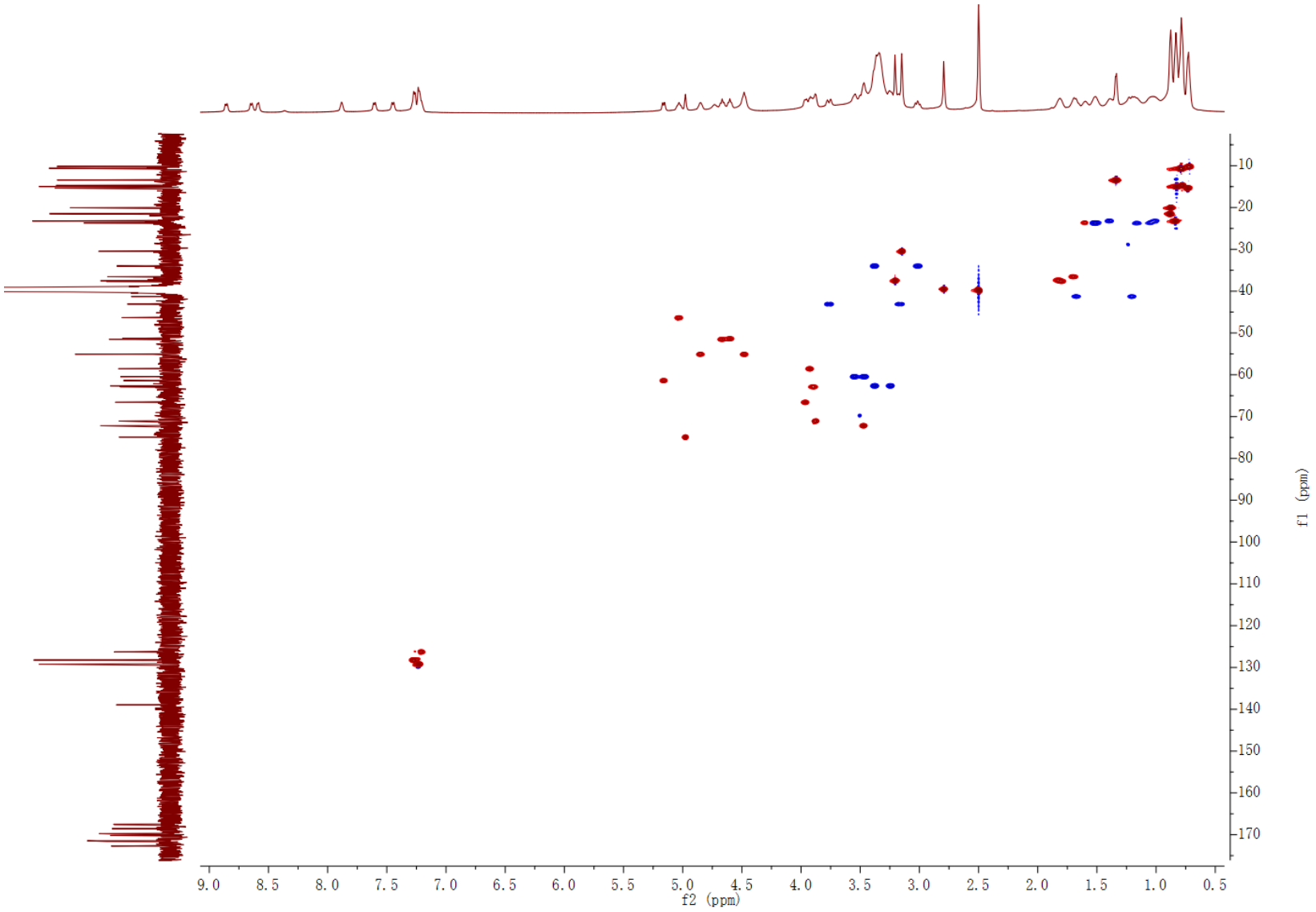

Figure S18.49. HSQC spectrum of 8 in DMSO-d_6

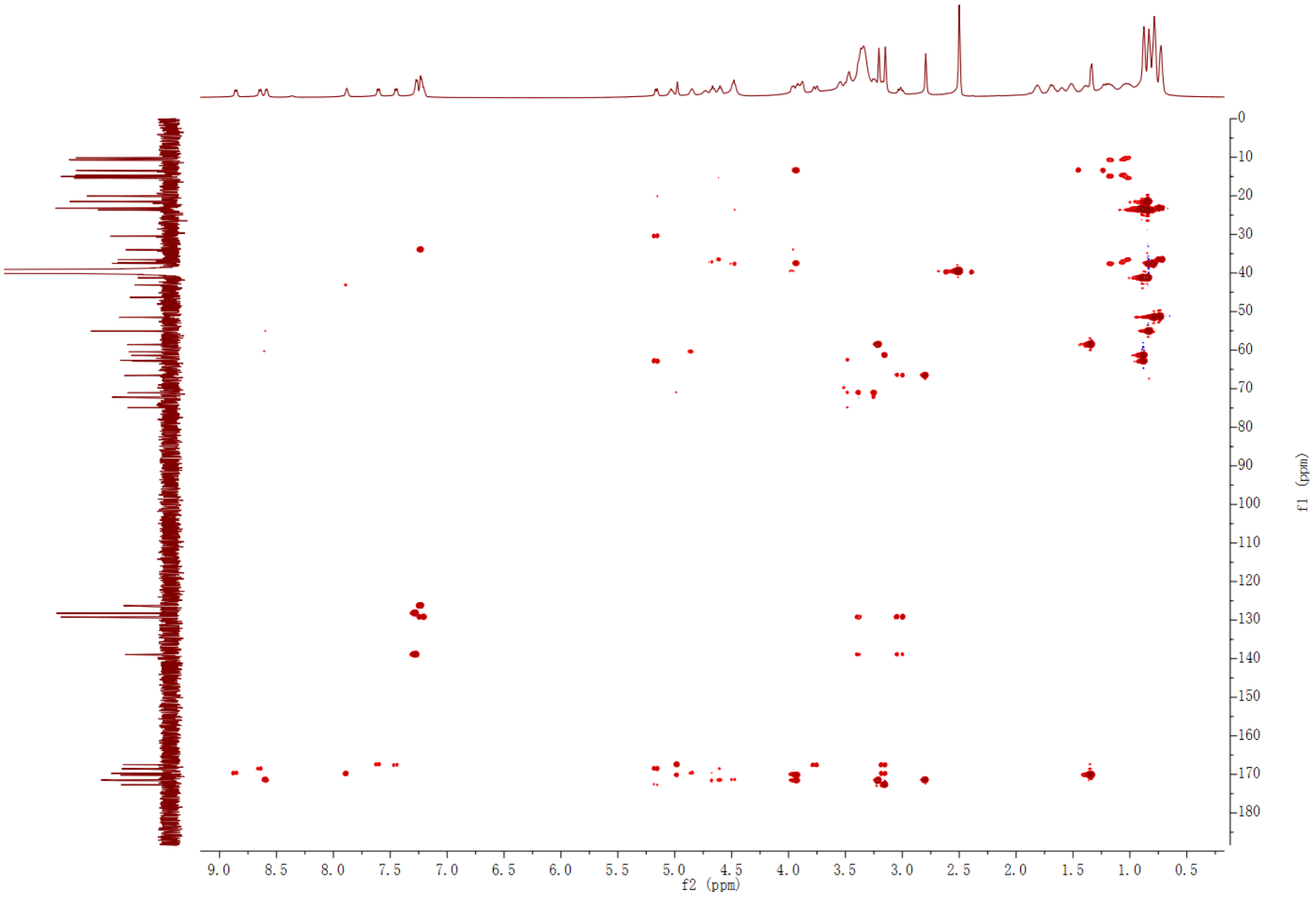

Figure S18.50. HMBC spectrum of 8 in DMSO-d_6

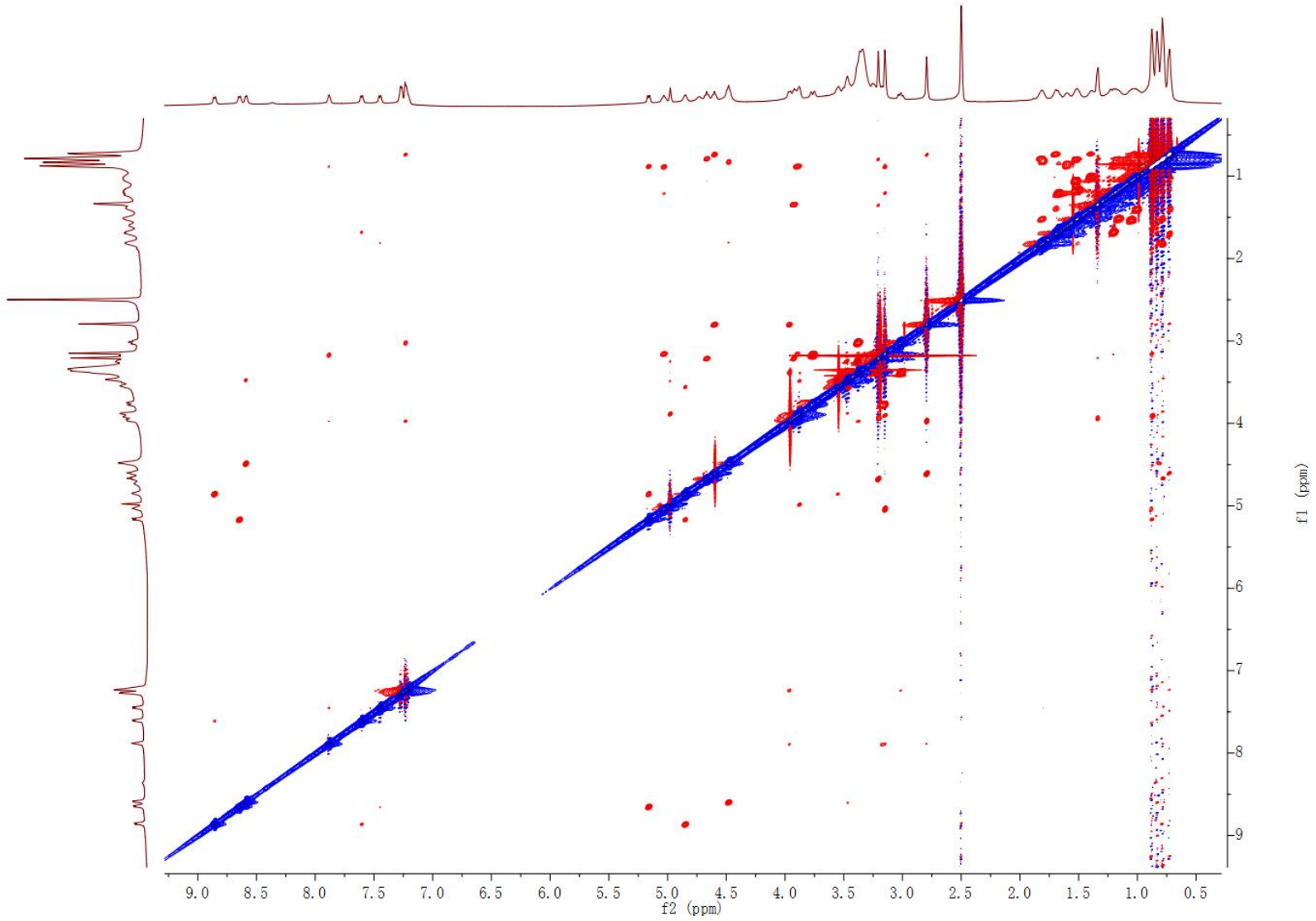

Figure S18.51. ROESY spectrum of 8 in DMSO-d_6

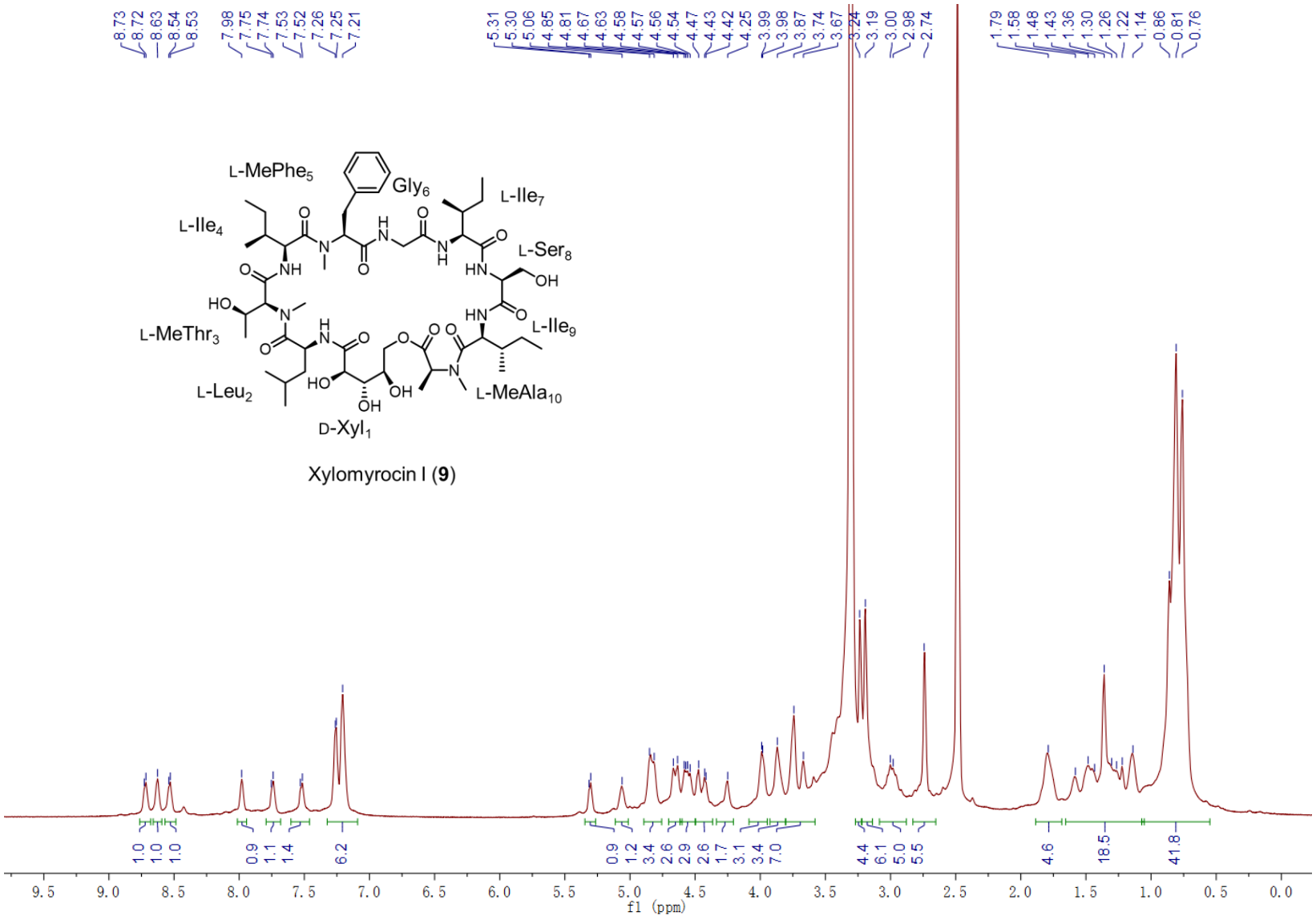

Figure S18.52. ^{1}H NMR spectrum of 9 in DMSO-d_6

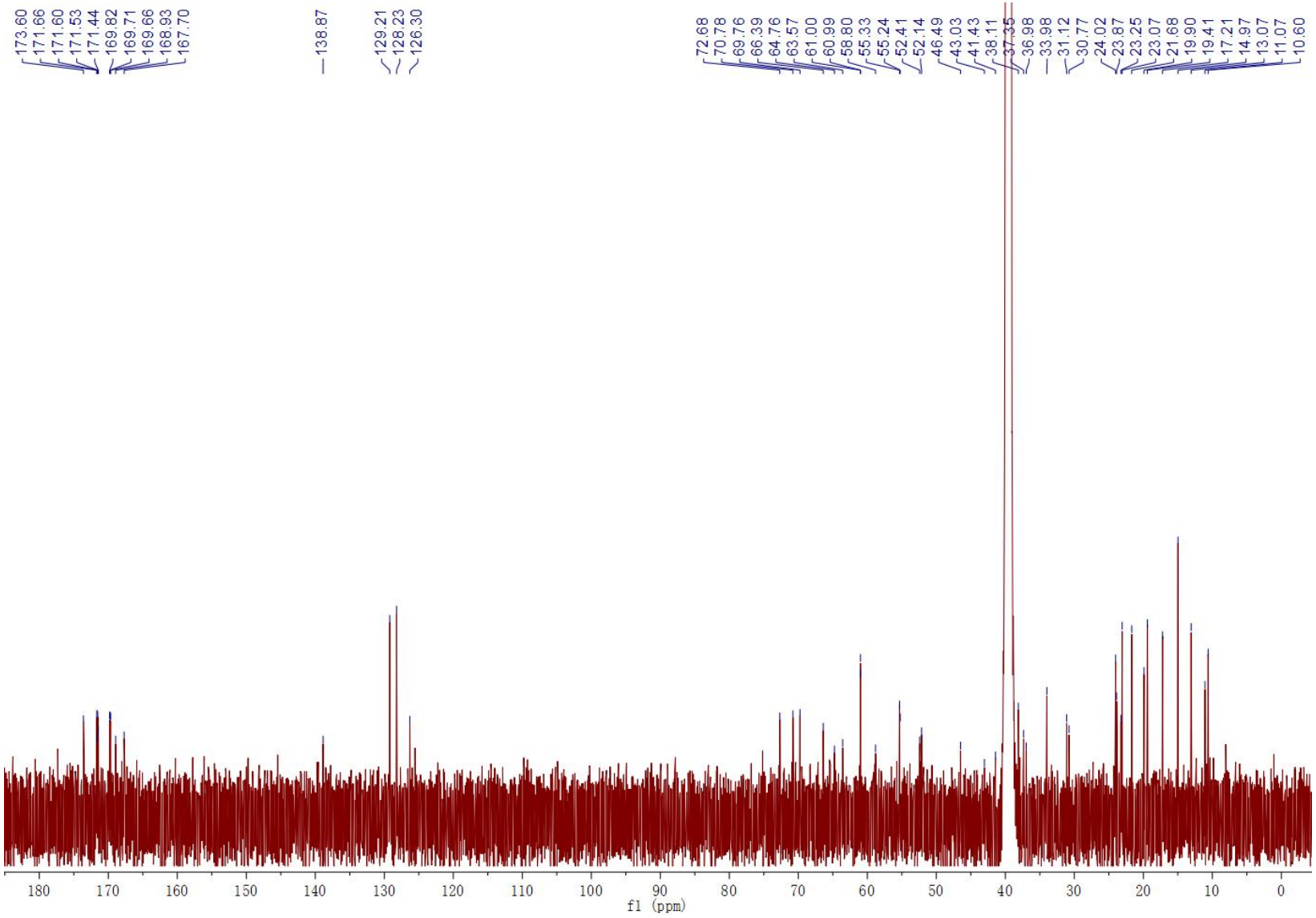

Figure S18.53. ^{13}C NMR spectrum of 9 in DMSO-d_6

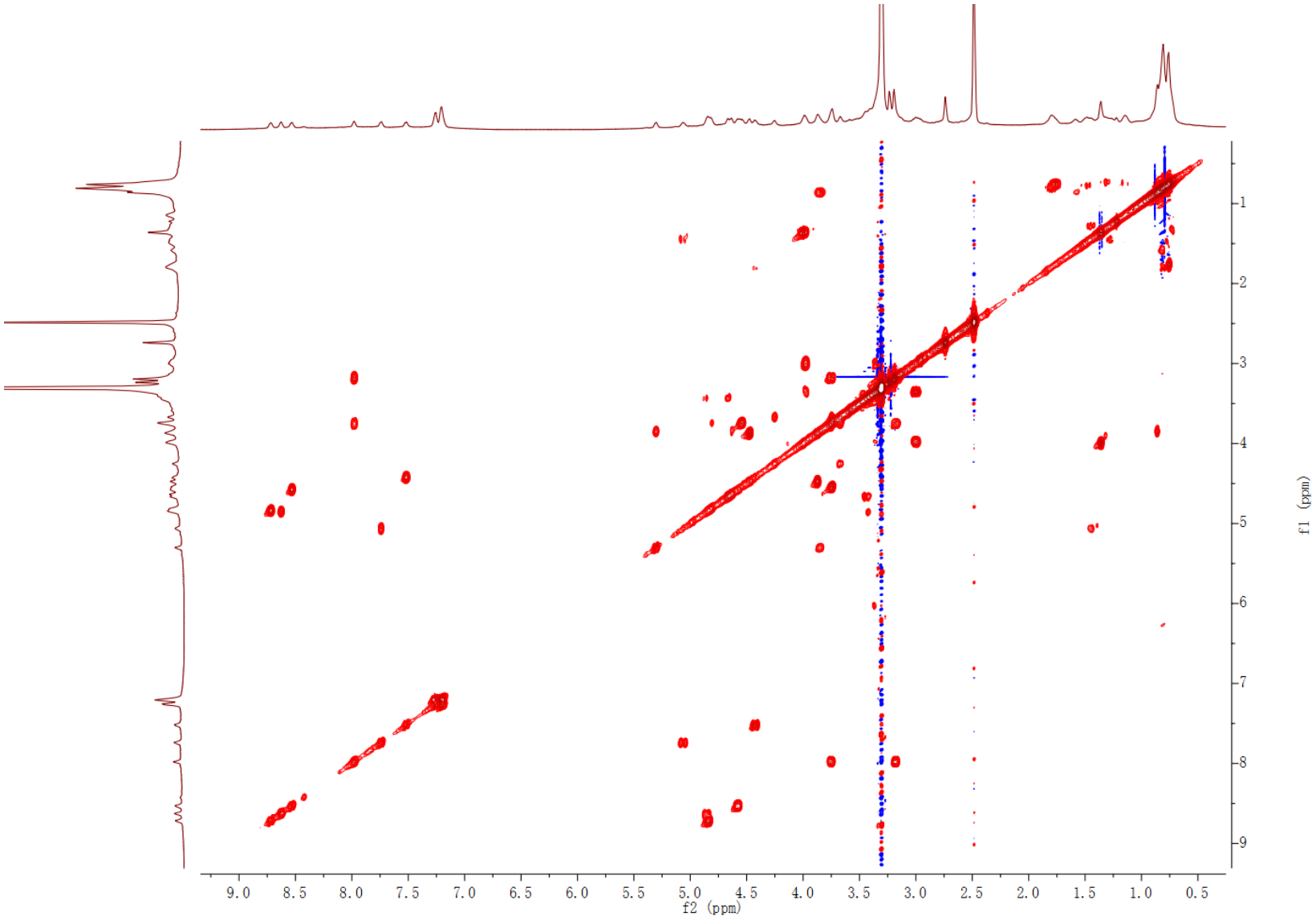

Figure S18.54. ^{1}H-^{1}H COSY spectrum of **9** in DMSO-d_6

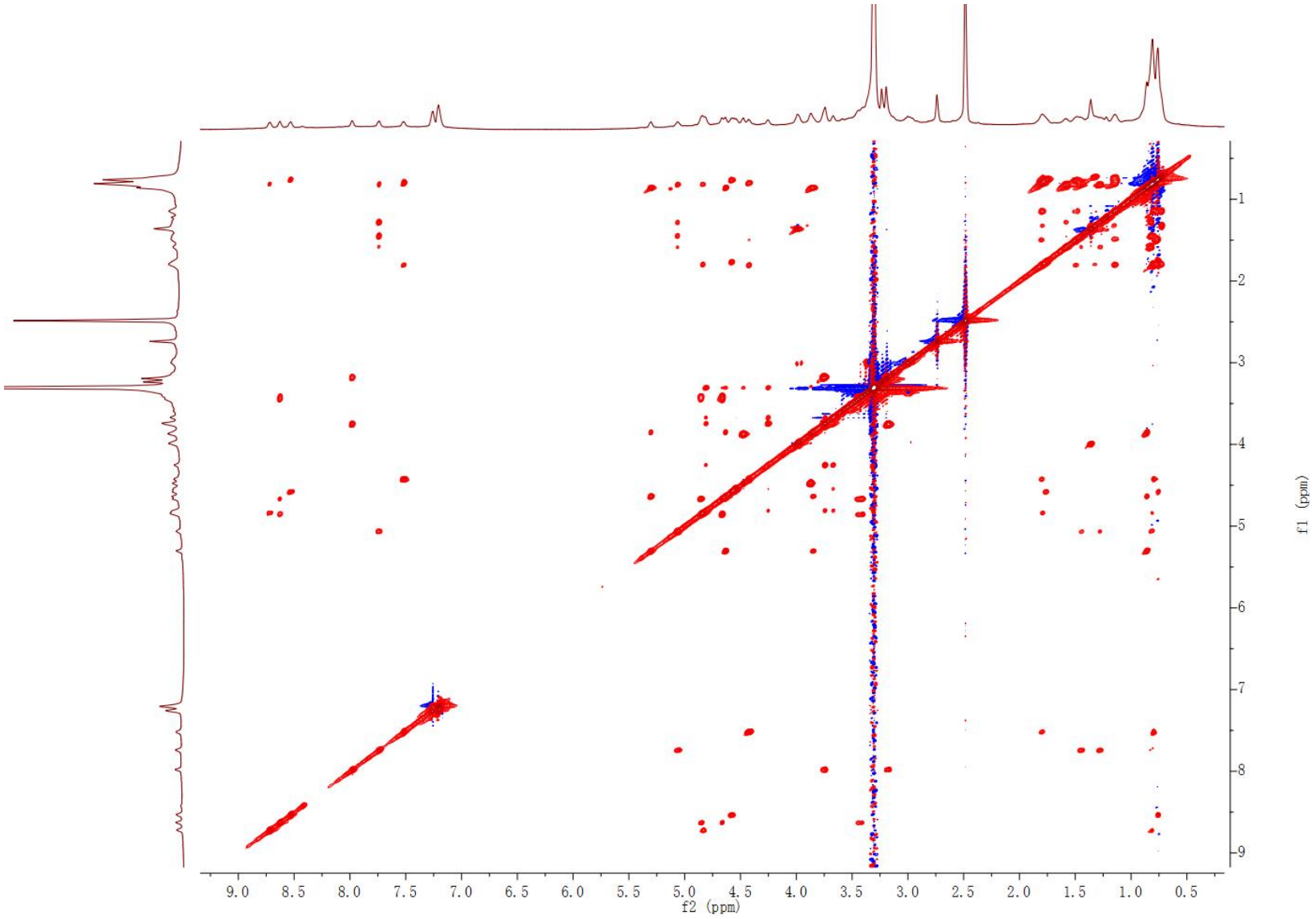

Figure S18.55. ^{1}H-^{1}H TOCSY spectrum of **9** in DMSO-d_6

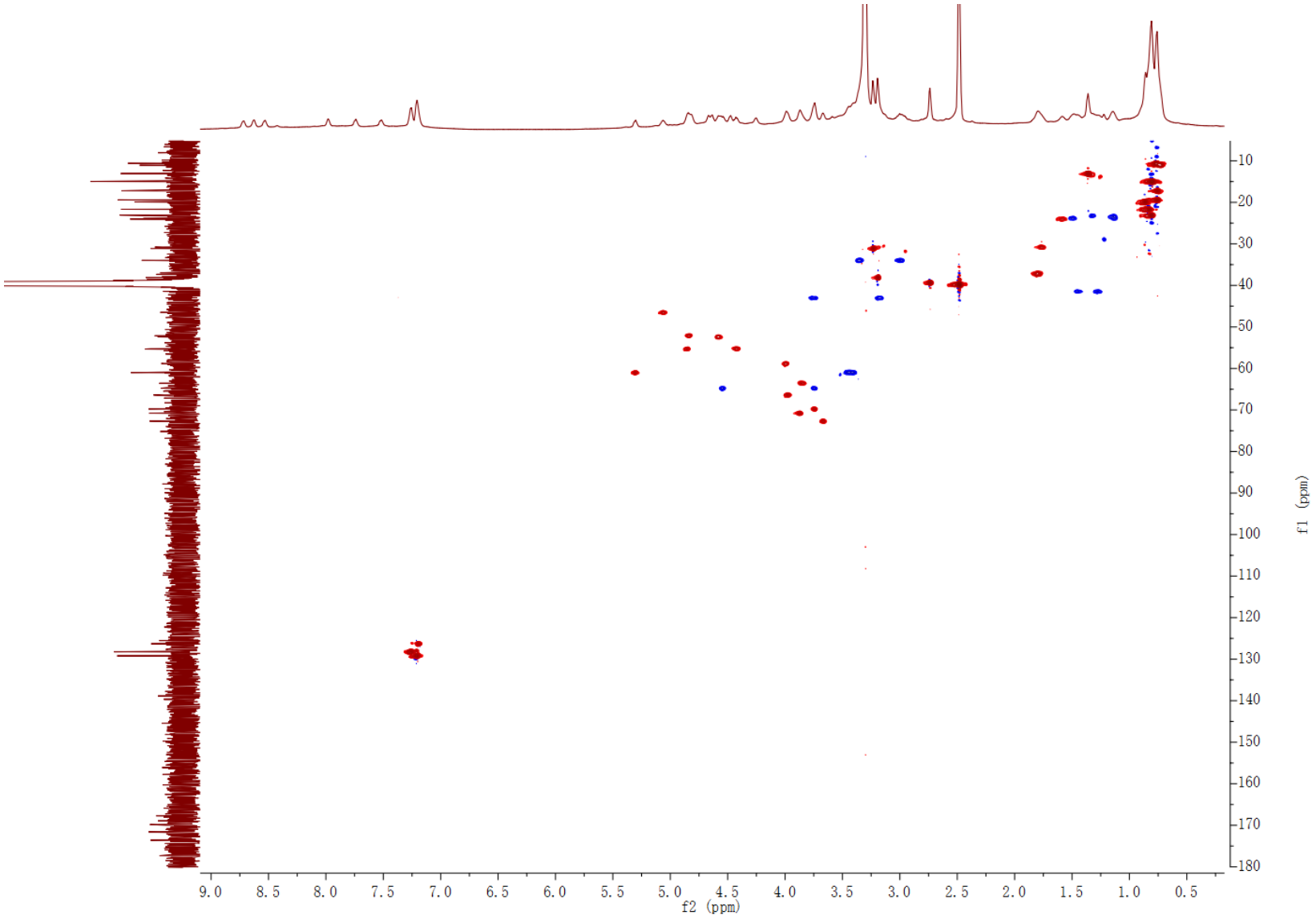

Figure S18.56. HSQC spectrum of 9 in DMSO-d_6

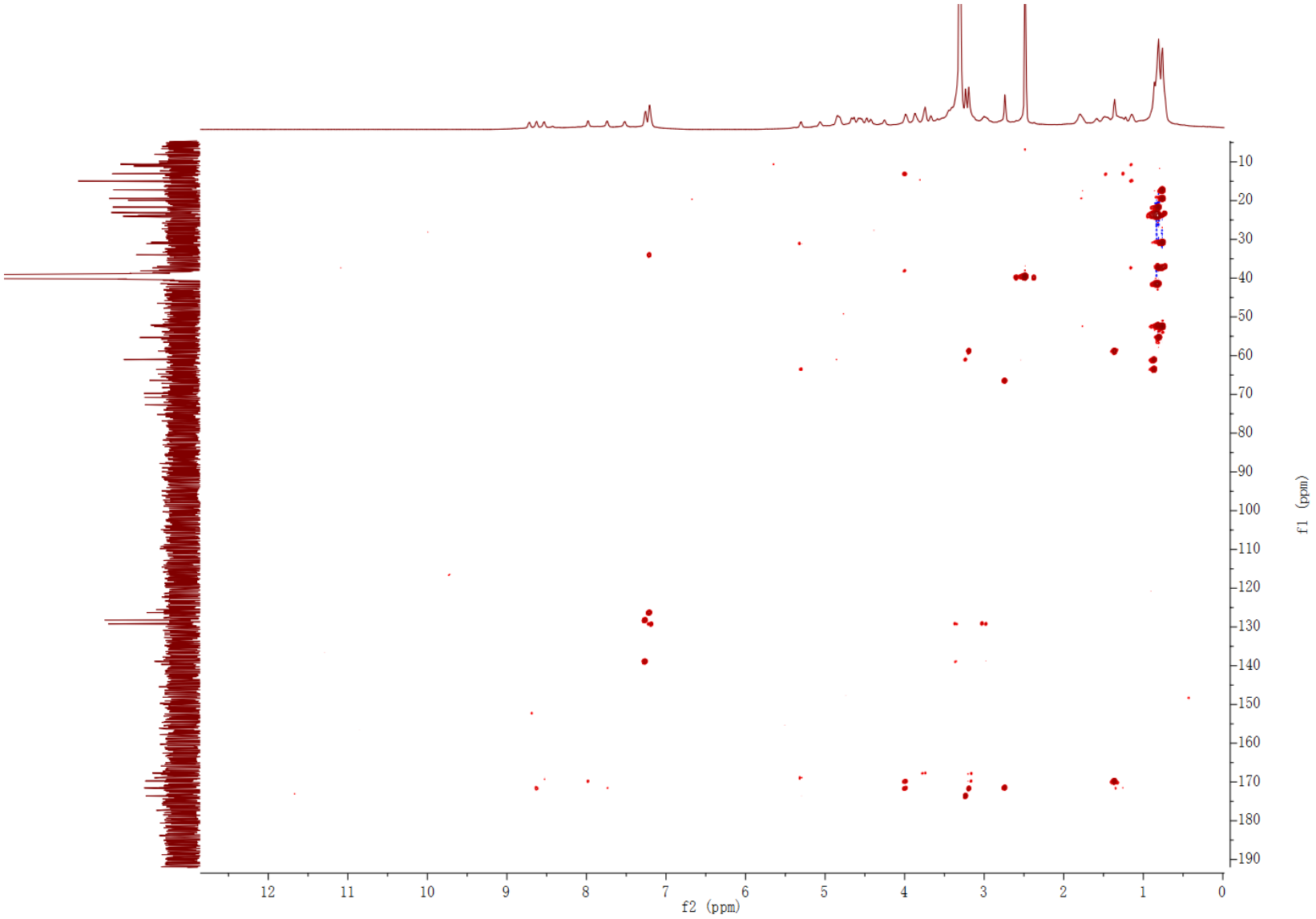

Figure S18.57. HMBC spectrum of 9 in DMSO-d_6

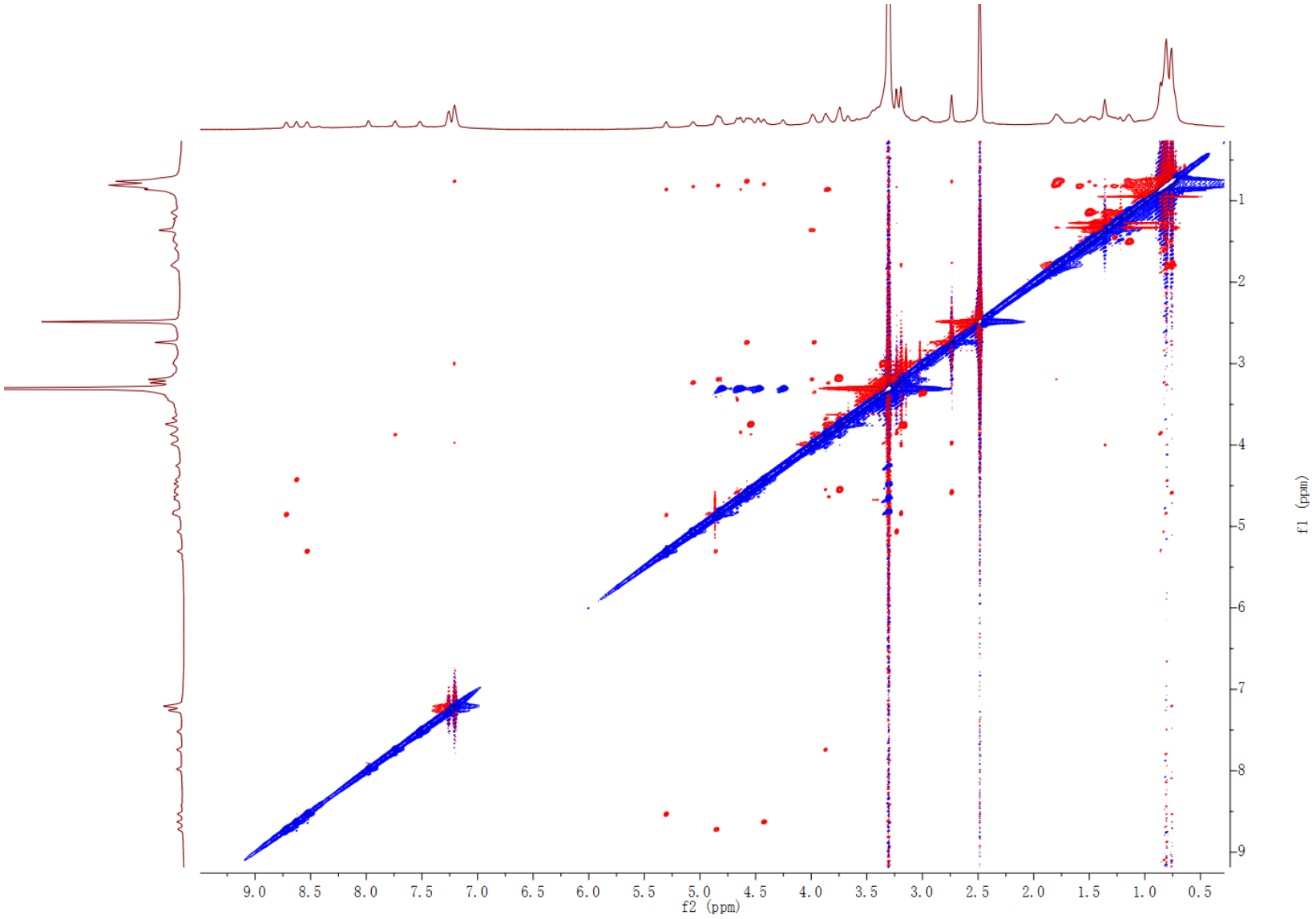

Figure S18.58. ROESY spectrum of 9 in DMSO-d_6

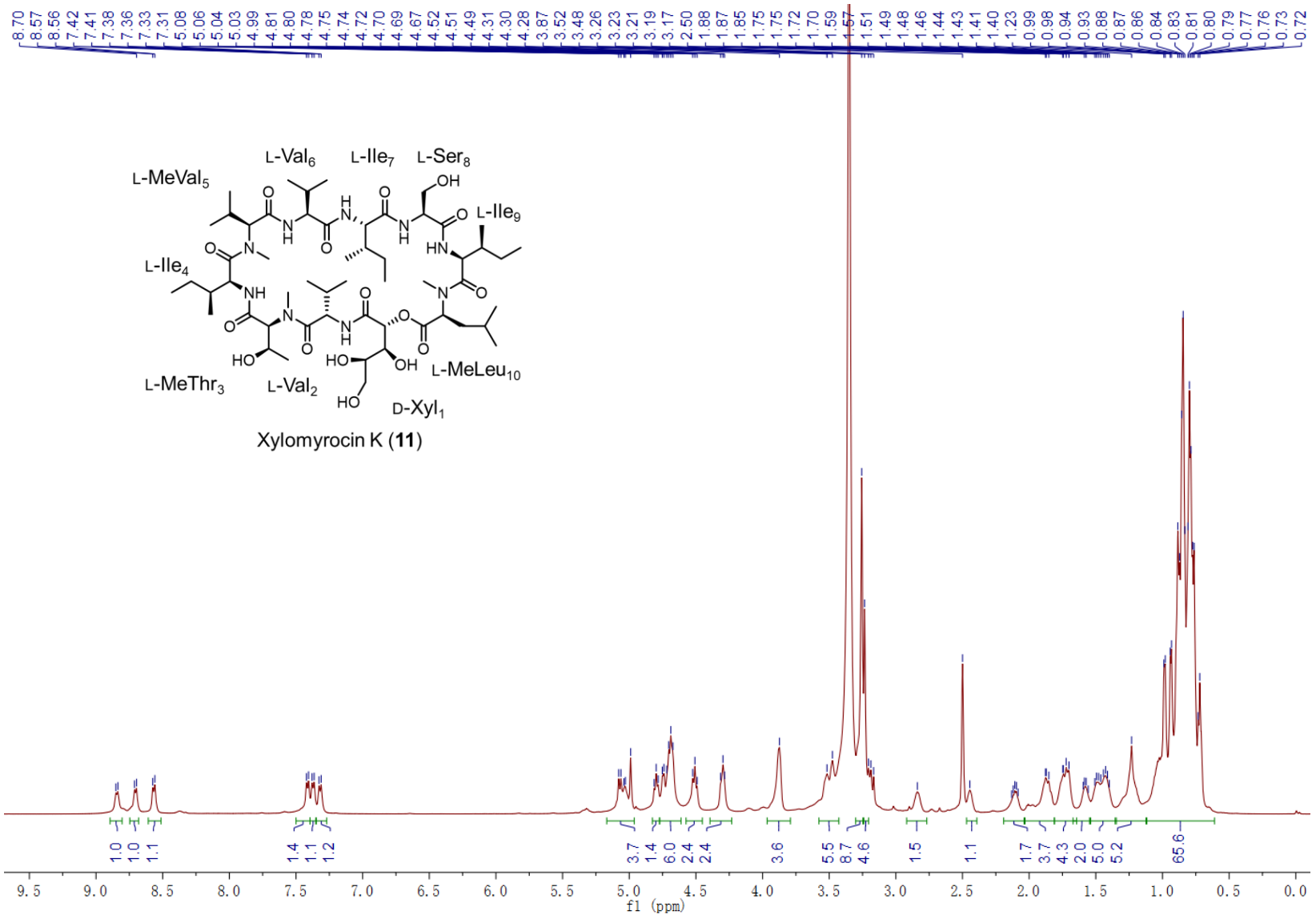

Figure S18.59. ^{1}H NMR spectrum of 11 in DMSO-d_6

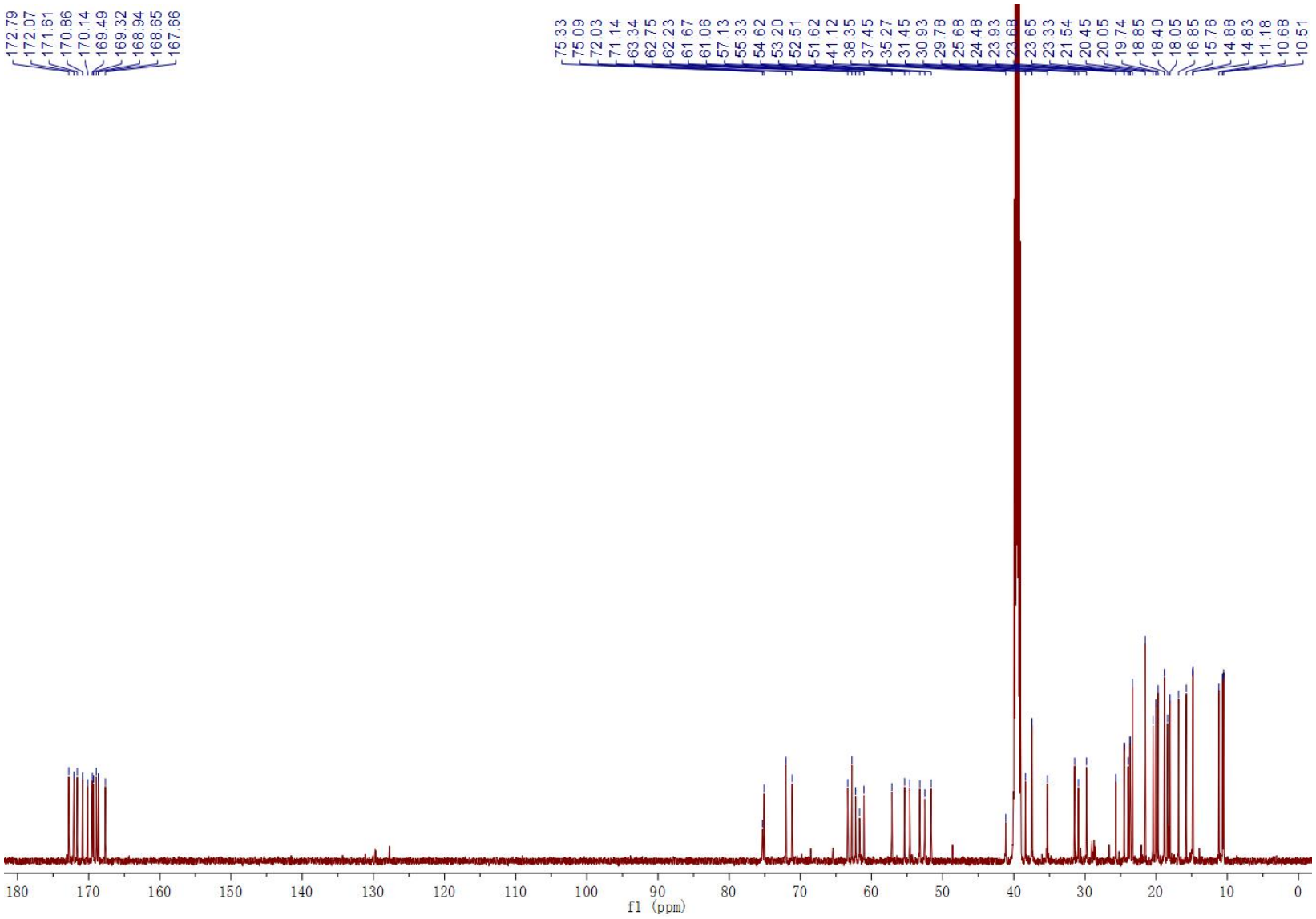

Figure S18.60. ^{13}C NMR spectrum of 11 in DMSO-d_6

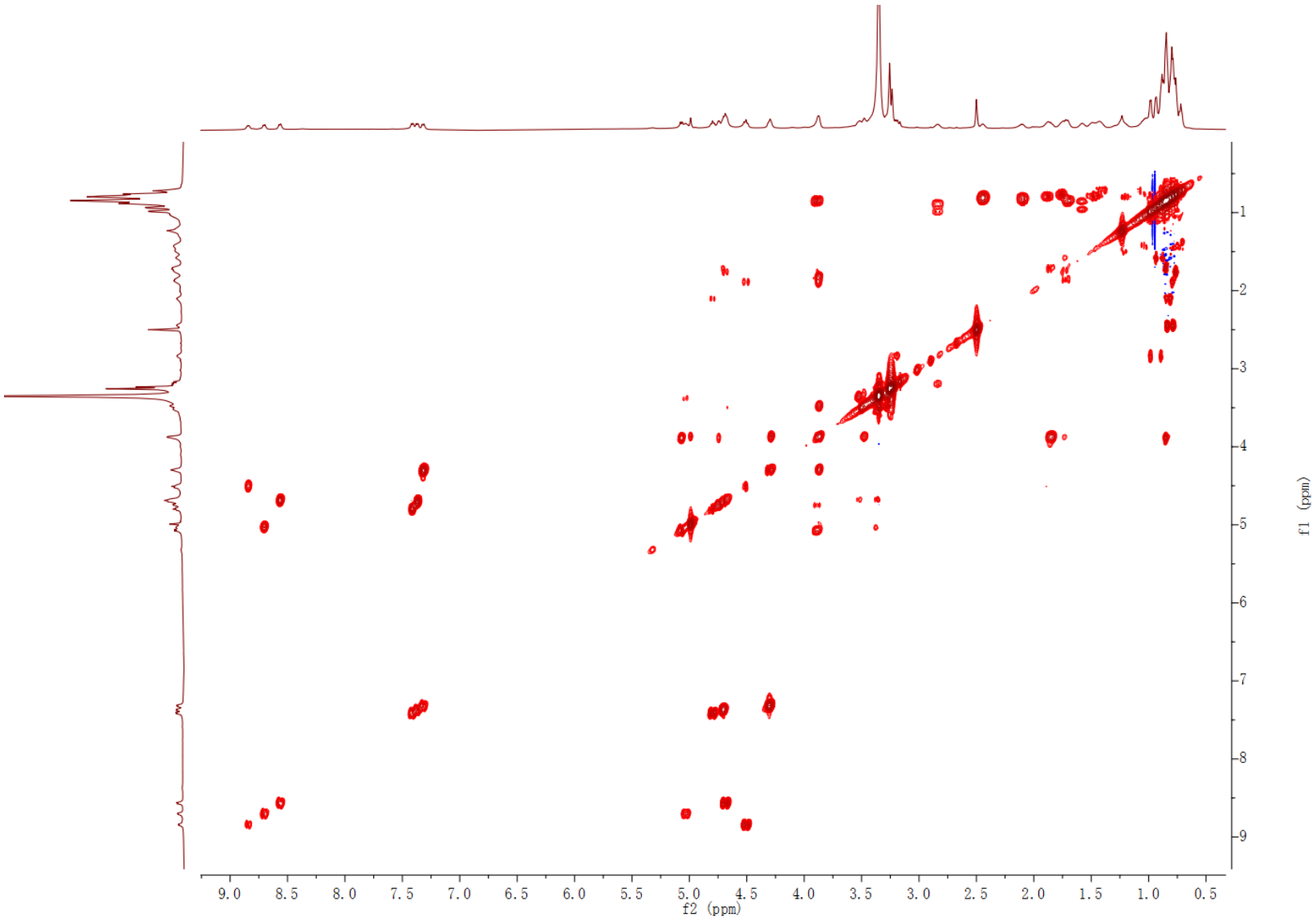

Figure S18.61. ^{1}H-^{1}H COSY spectrum of 11 in DMSO-d_6

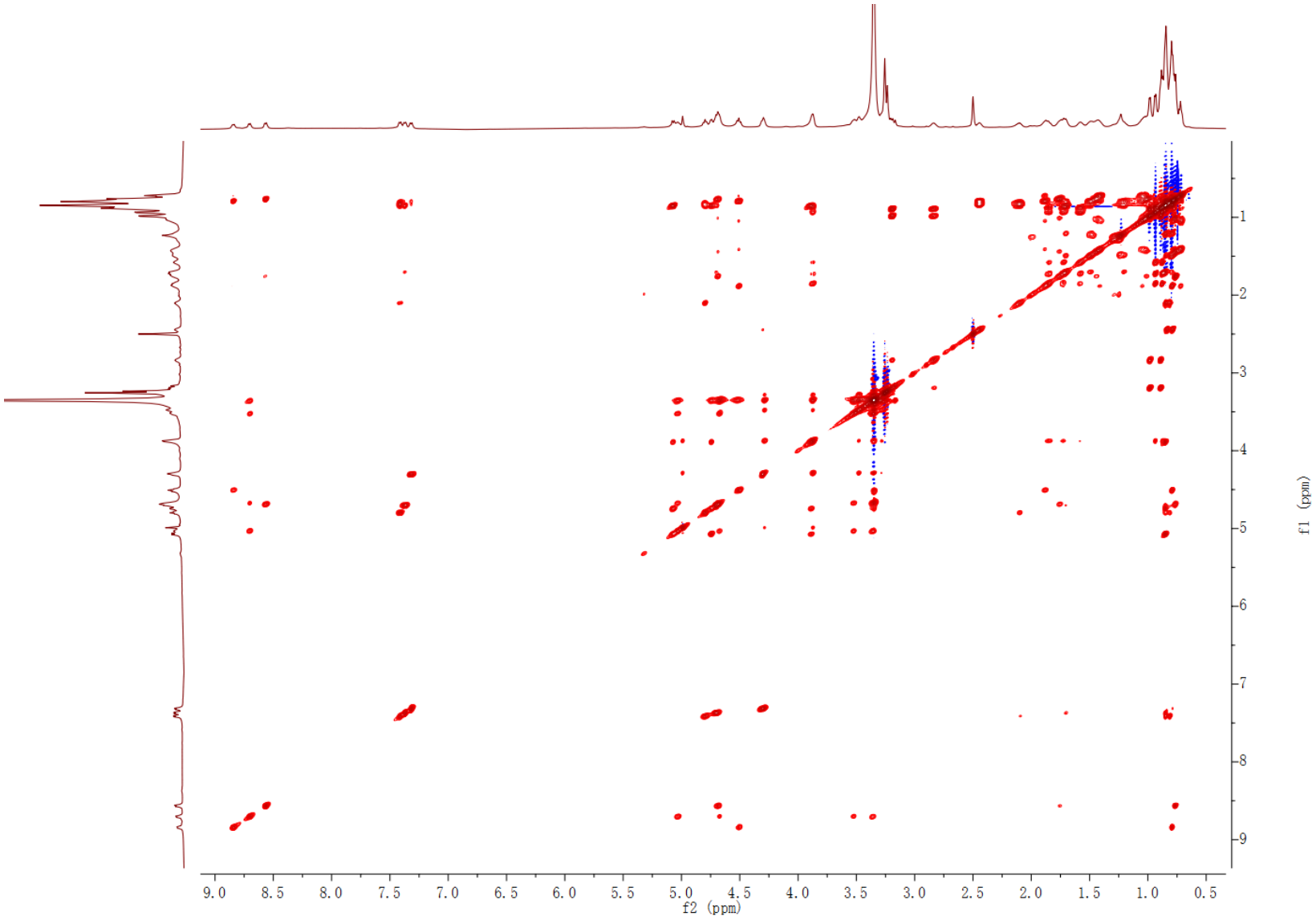

Figure S18.62. ^{1}H-^{1}H TOCSY spectrum of 11 in DMSO-d_6

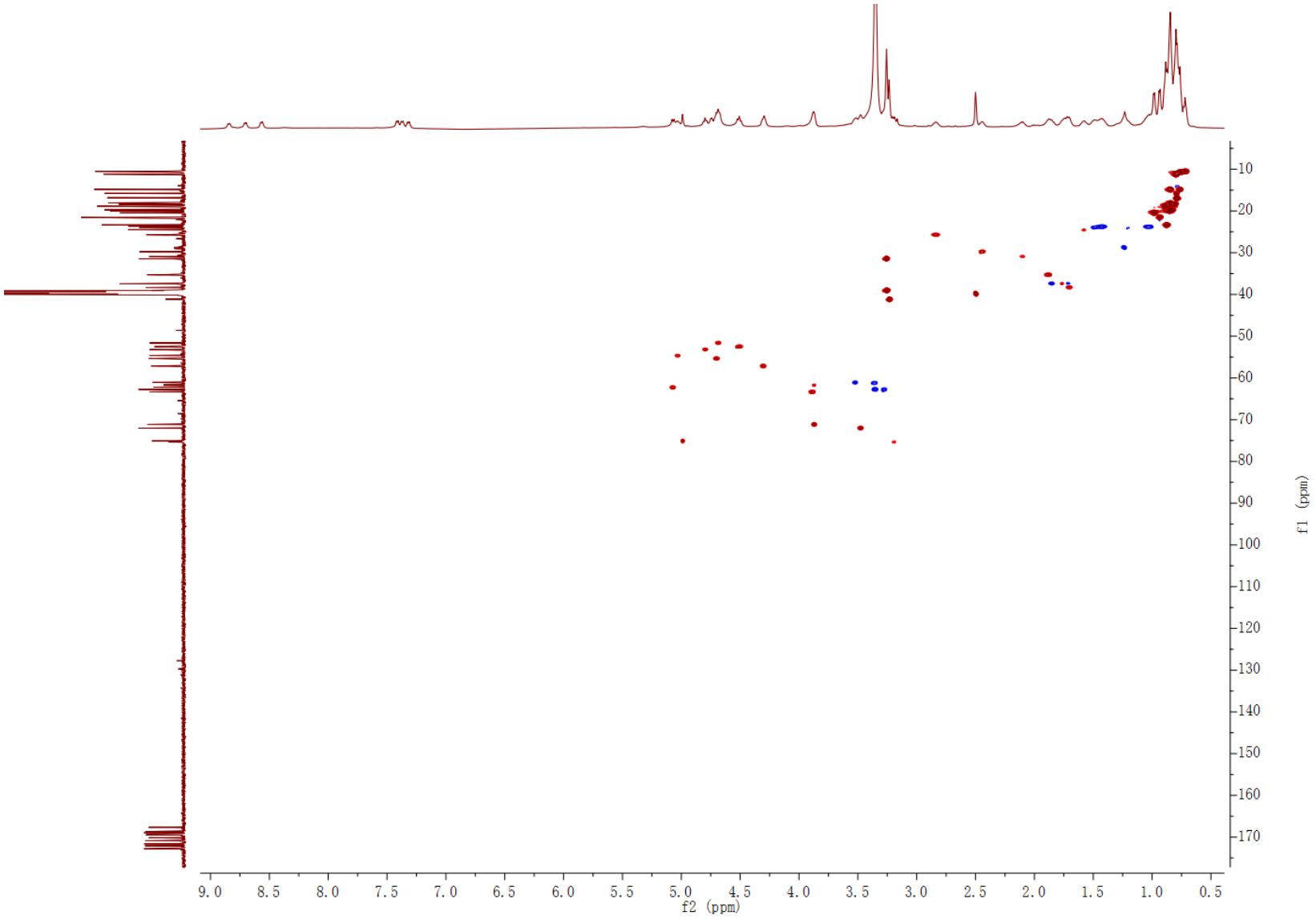

Figure S18.63. HSQC spectrum of 11 in DMSO-d_6

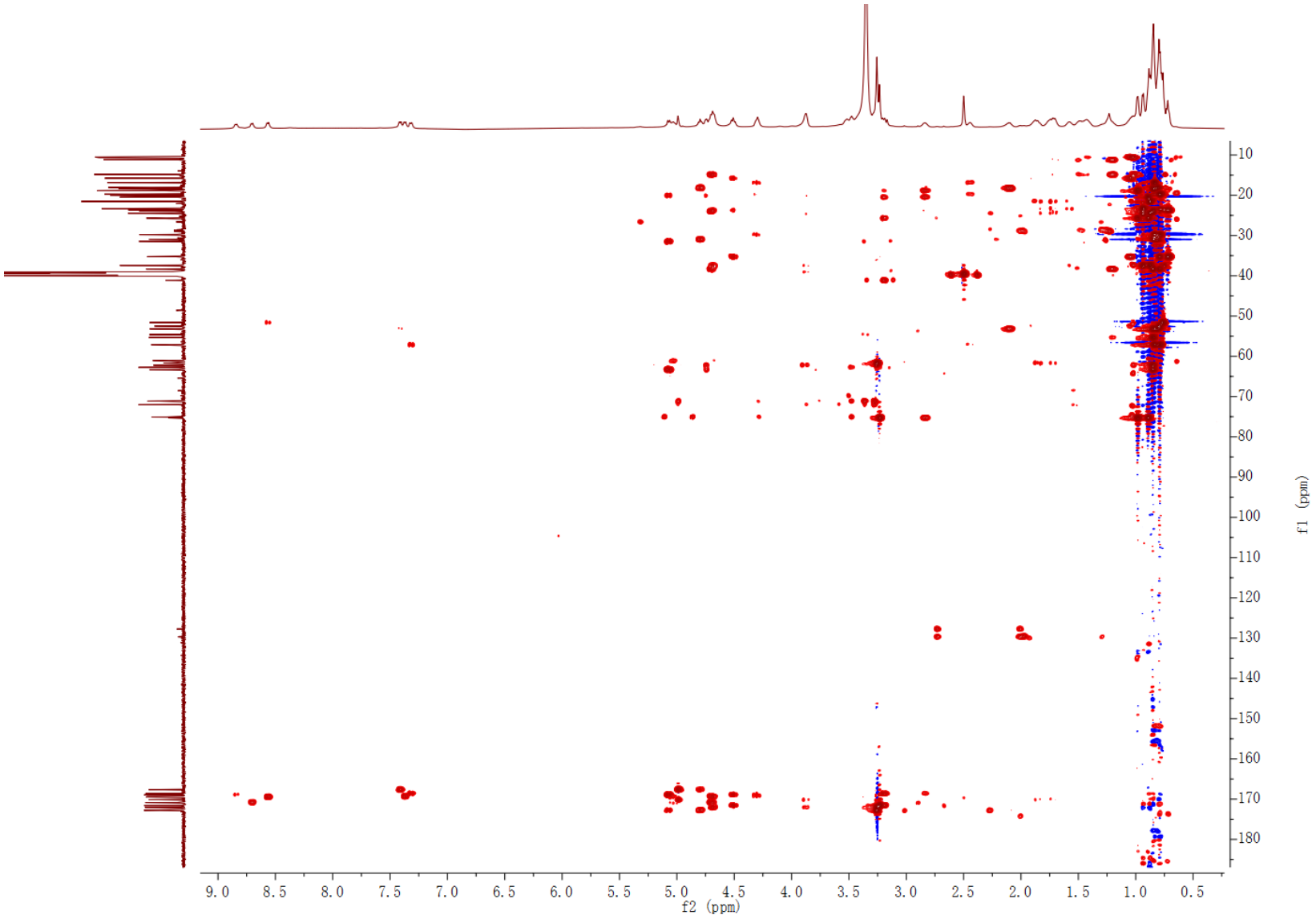

Figure S18.64. HMBC spectrum of 11 in DMSO-d_6

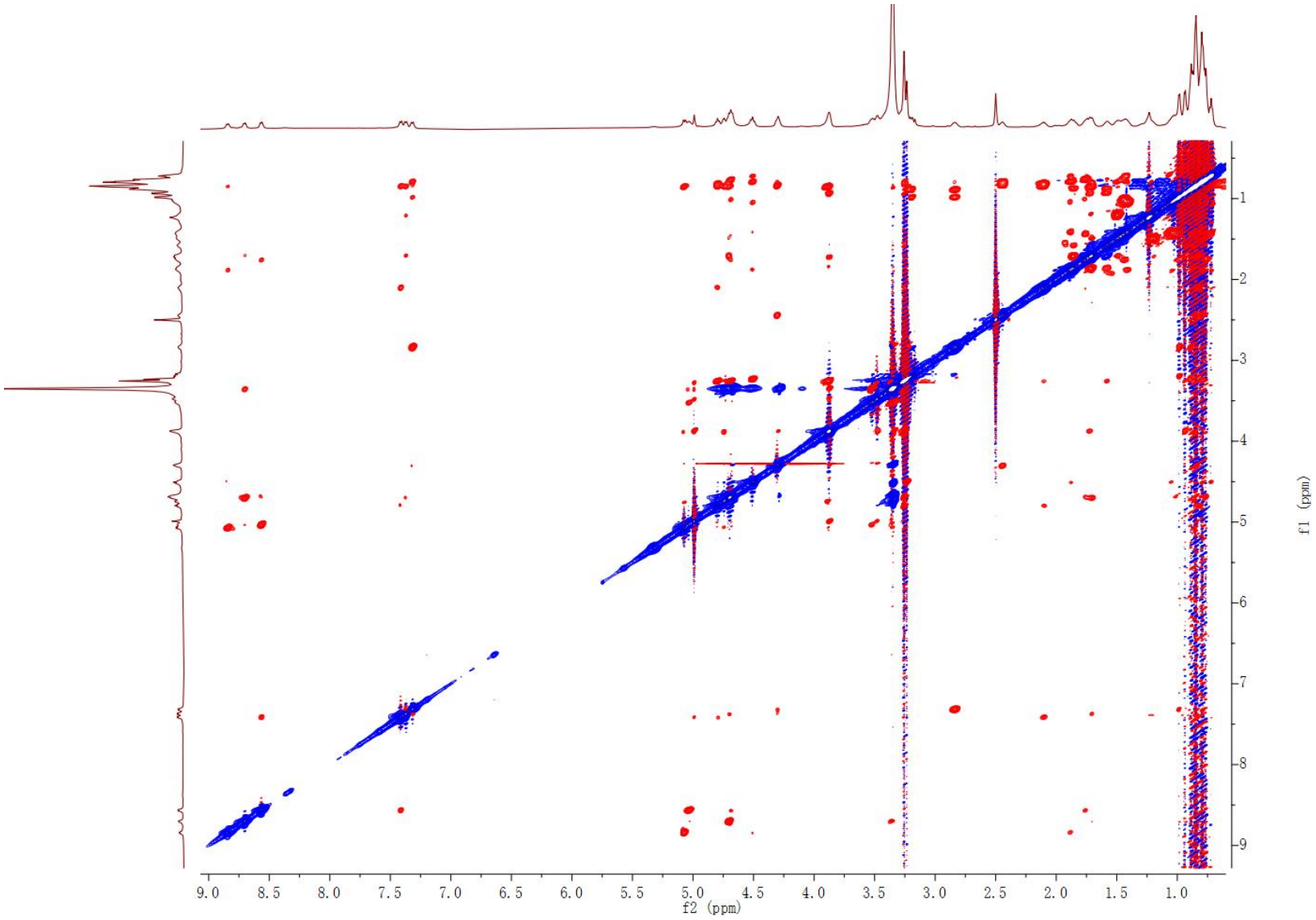

Figure S18.65. ROESY spectrum of 11 in DMSO-d_6

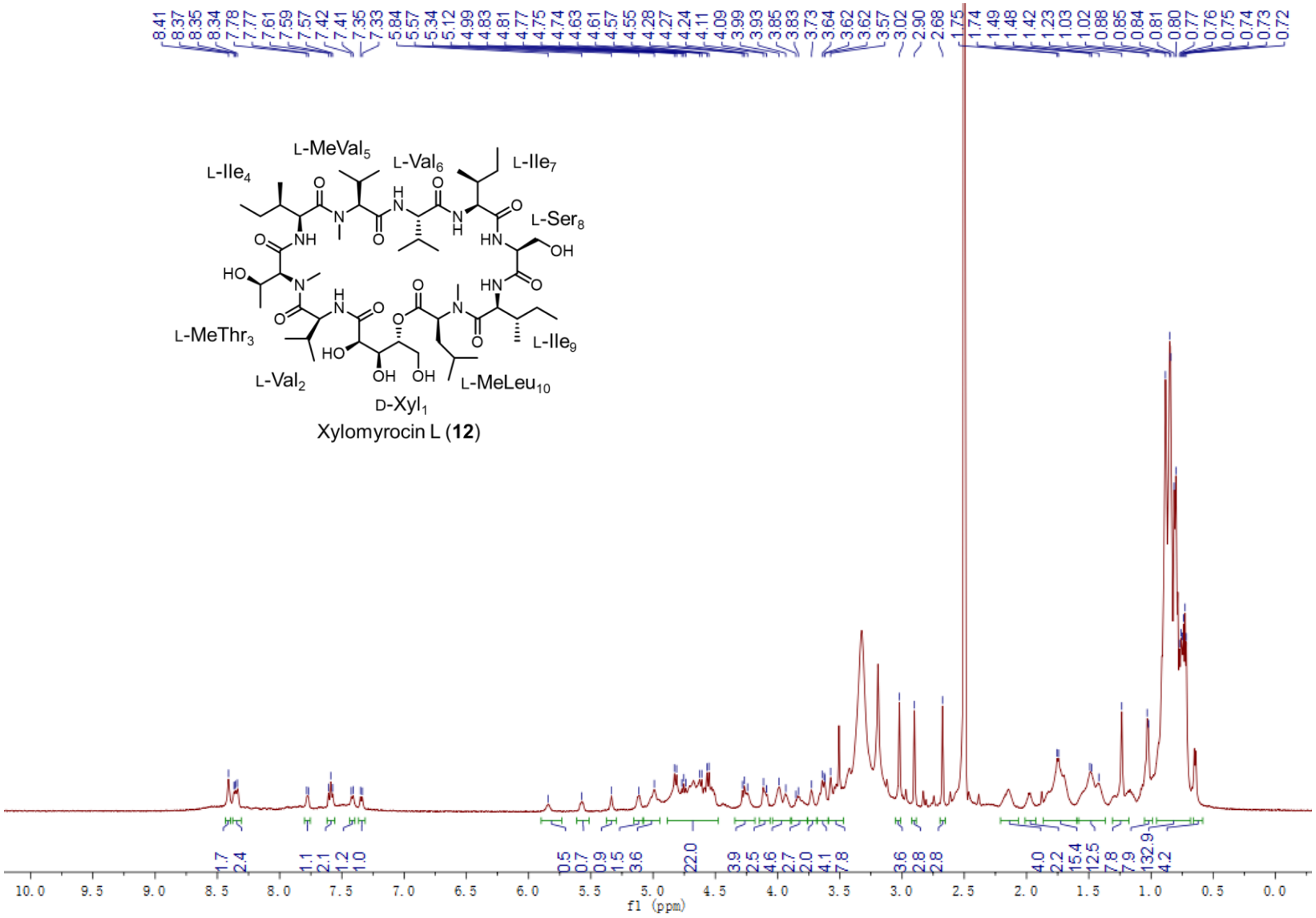

Figure S18.66. ^{1}H NMR spectrum of 12 in DMSO-d_6

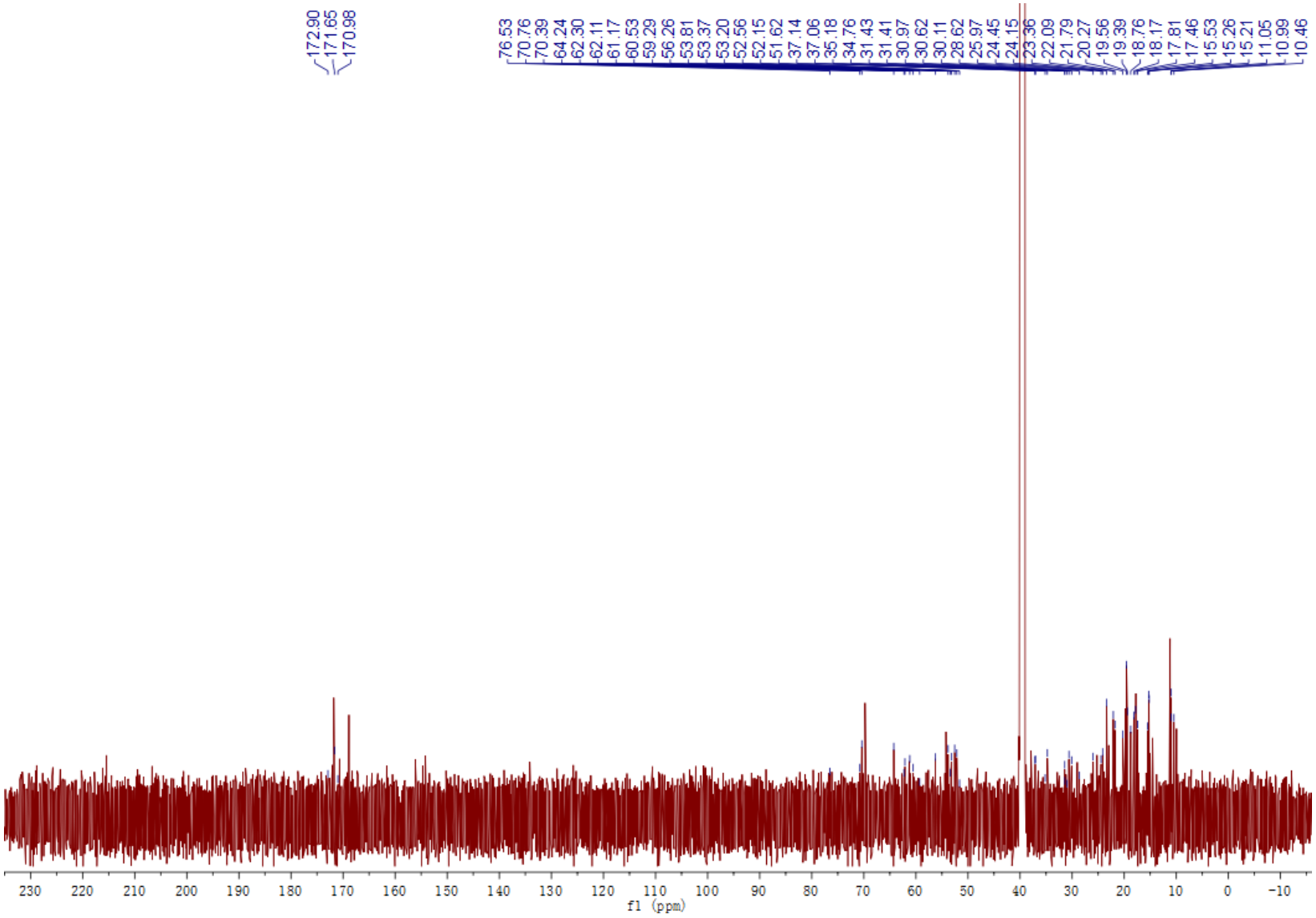

Figure S18.67. ^{13}C NMR spectrum of 12 in DMSO-d_6

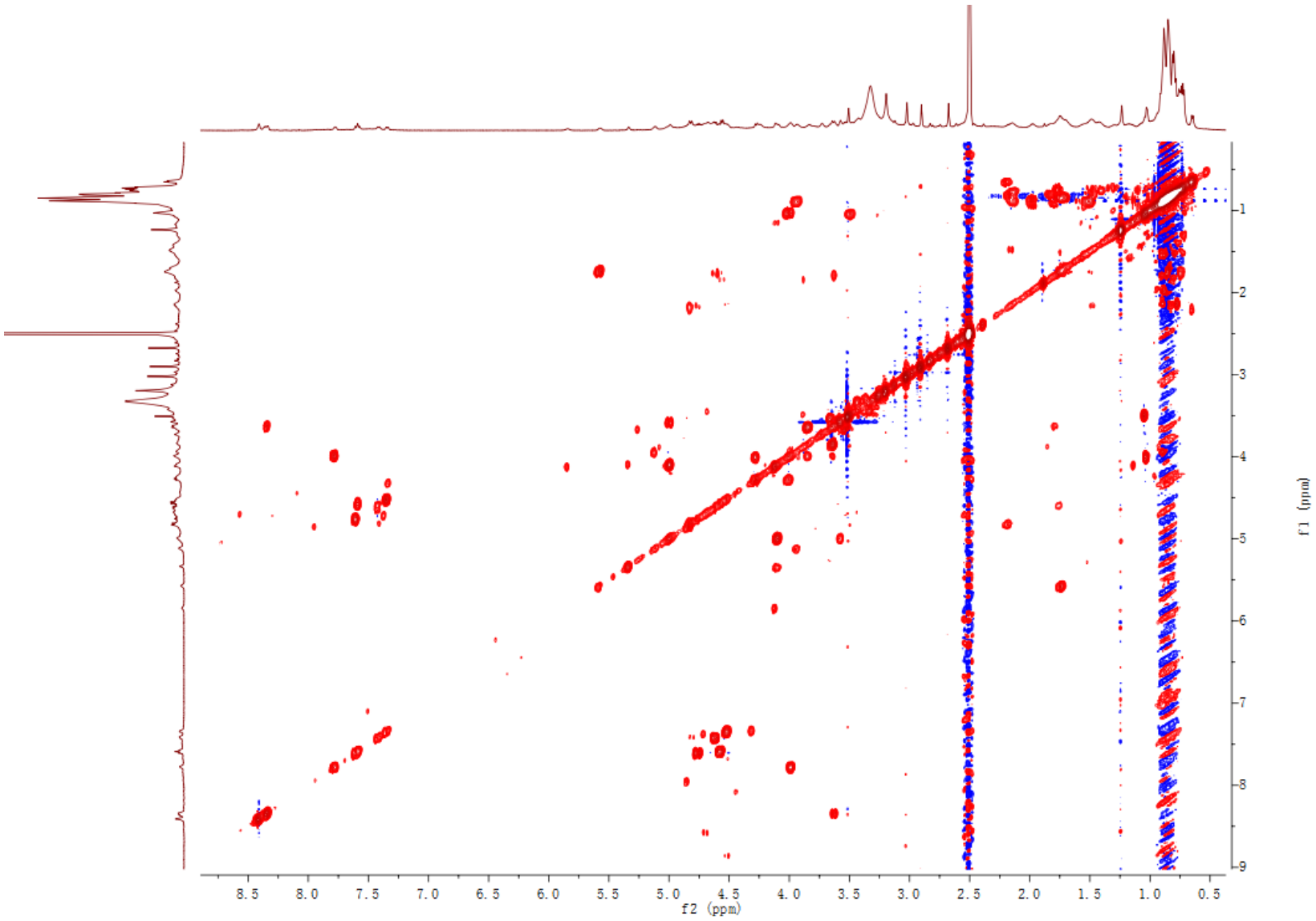

Figure S18.68. ^{1}H-^{1}H COSY spectrum of **12** in DMSO-d_6

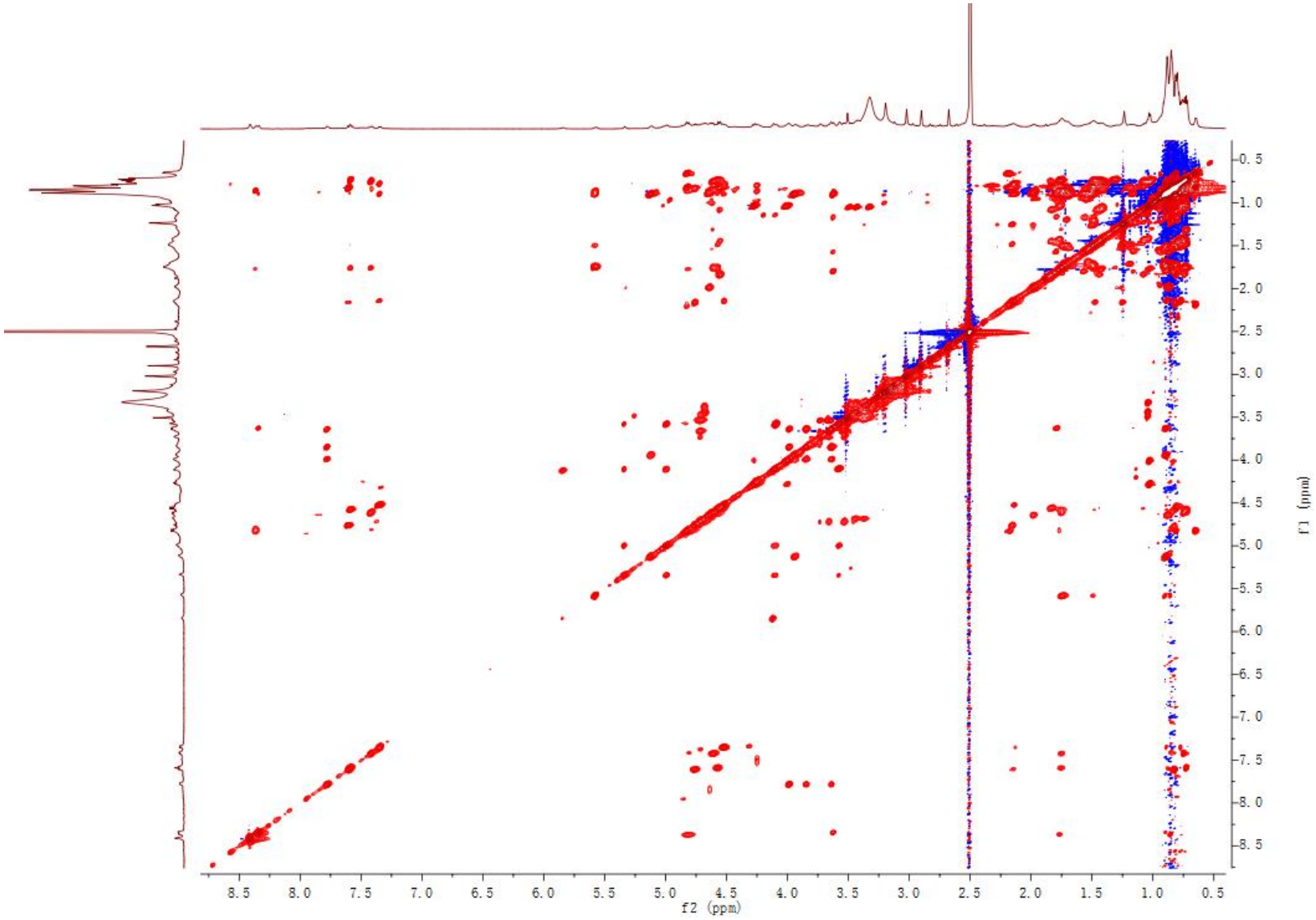

Figure S18.69. ^{1}H-^{1}H TOCSY spectrum of 12 in DMSO-d_6

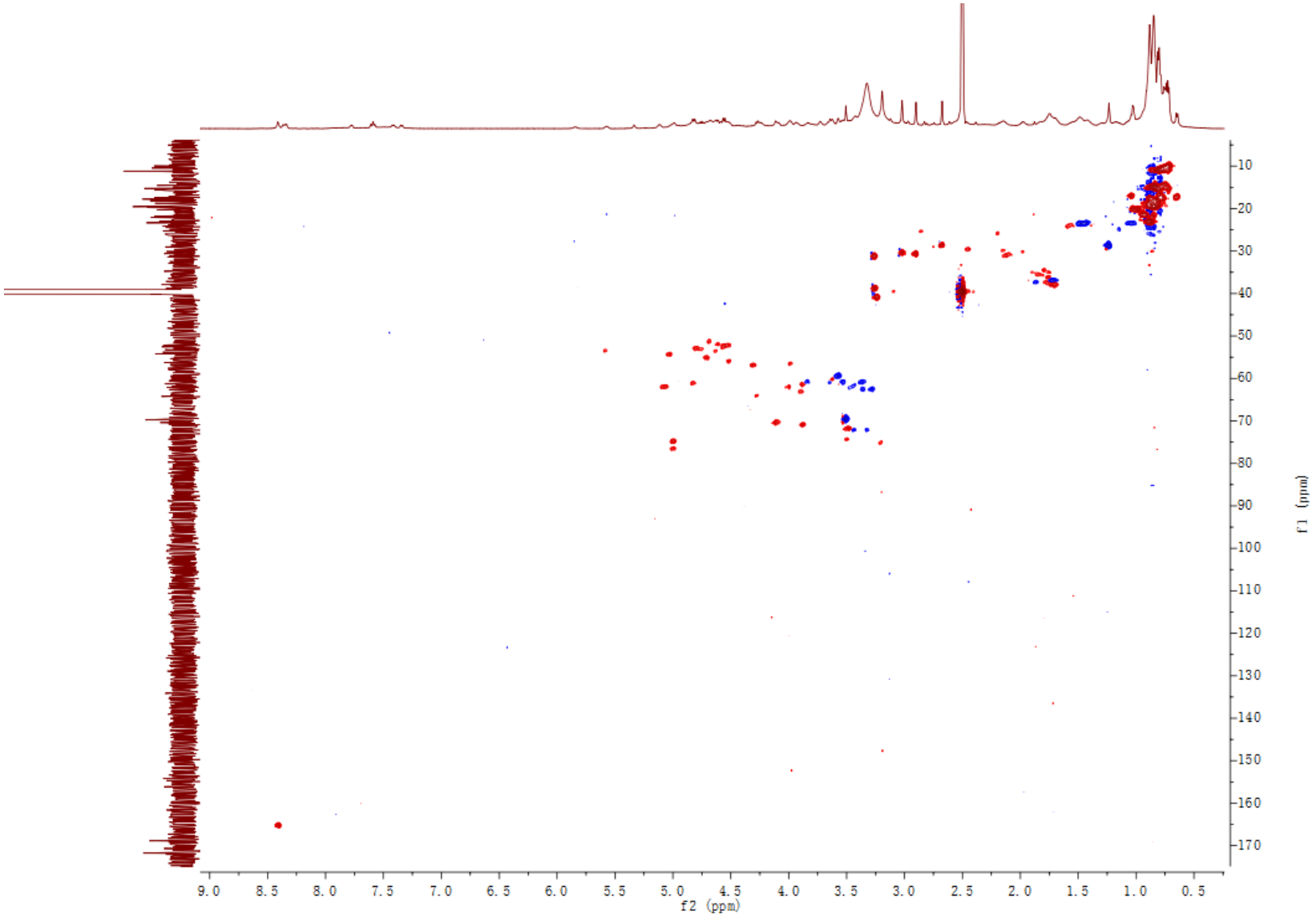

Figure S18.70. HSQC spectrum of 12 in DMSO-d_6

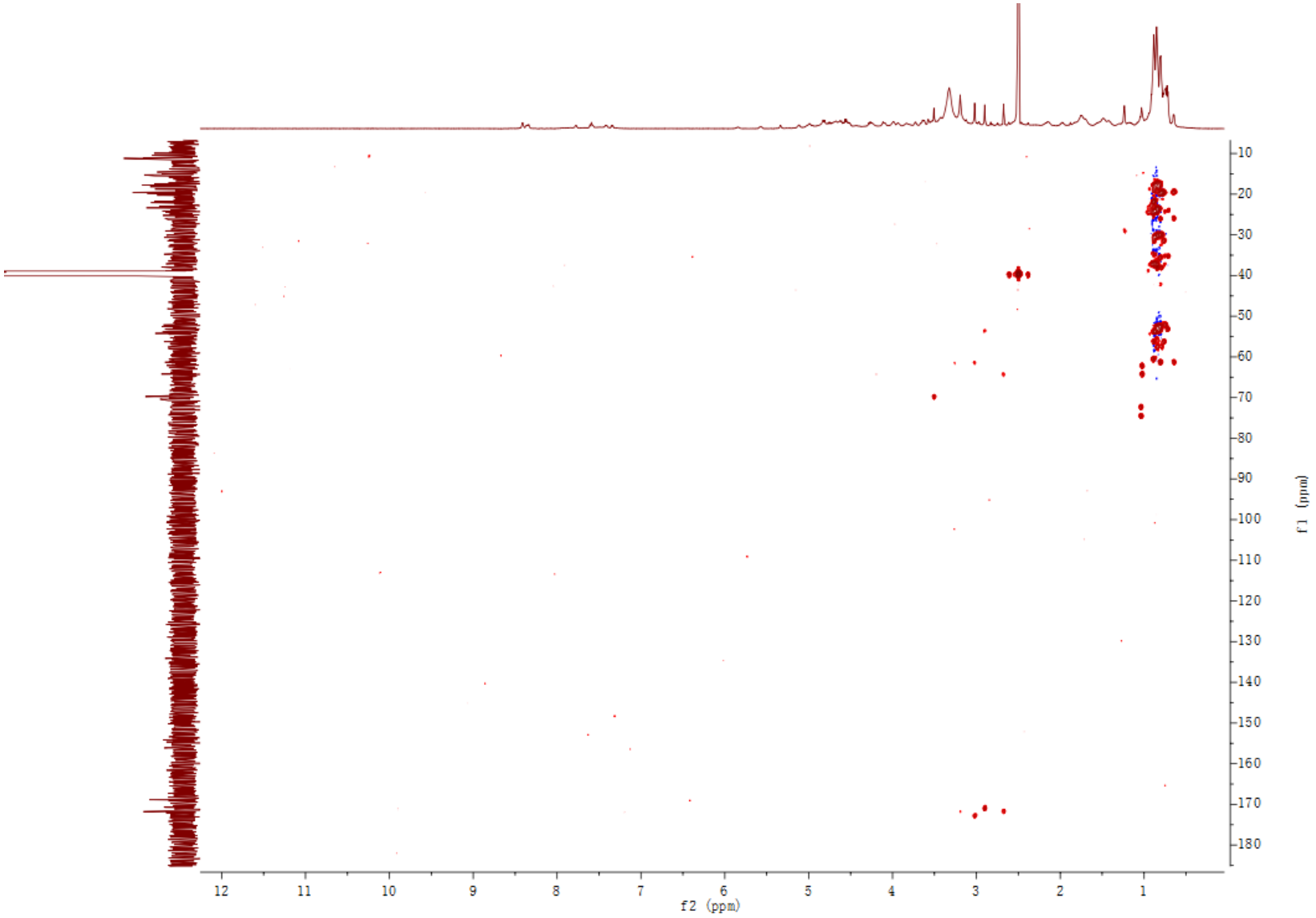

Figure S18.71. HMBC spectrum of 12 in DMSO-d_6

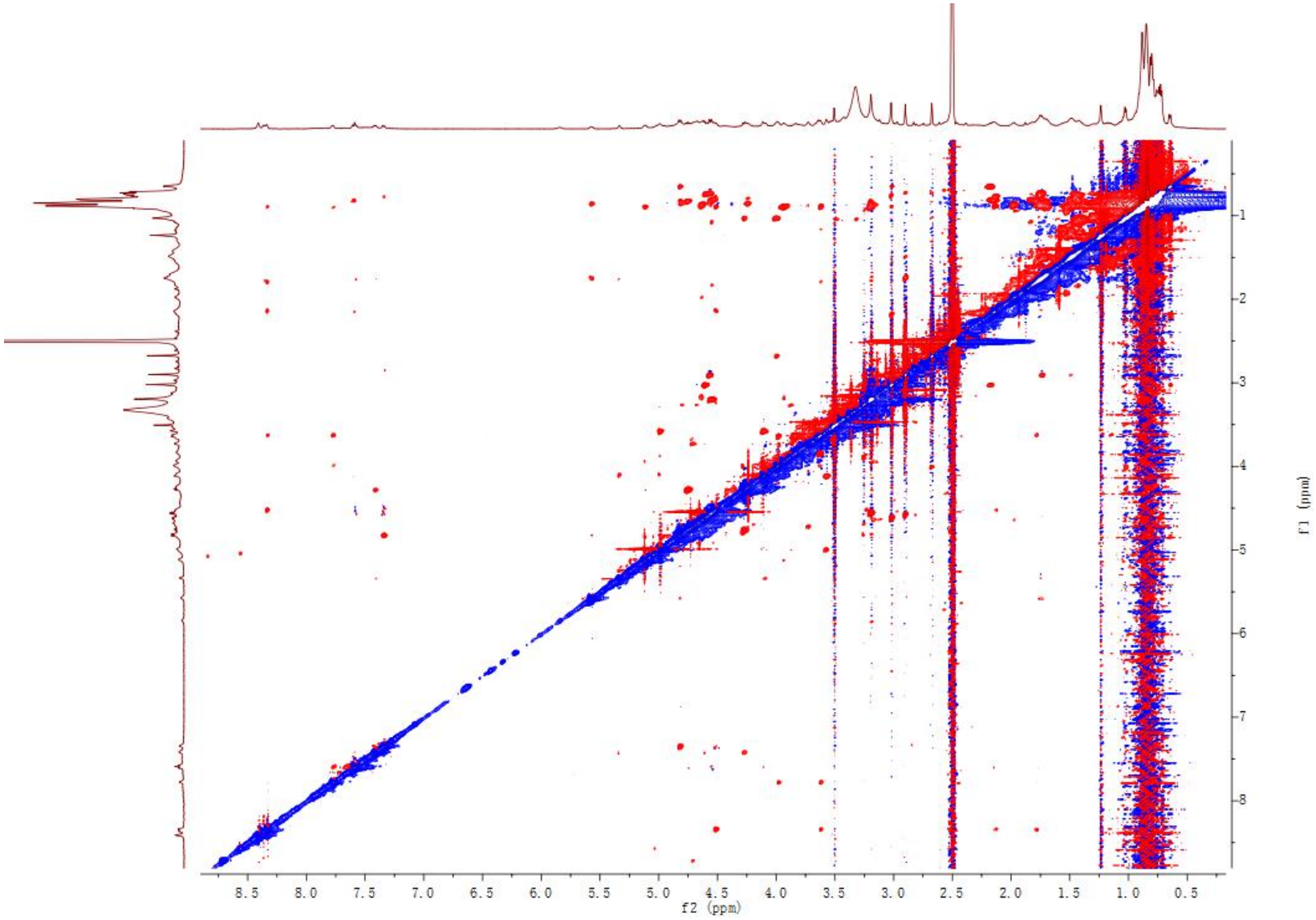

Figure S18.72. ROESY spectrum of 12 in DMSO-d_6

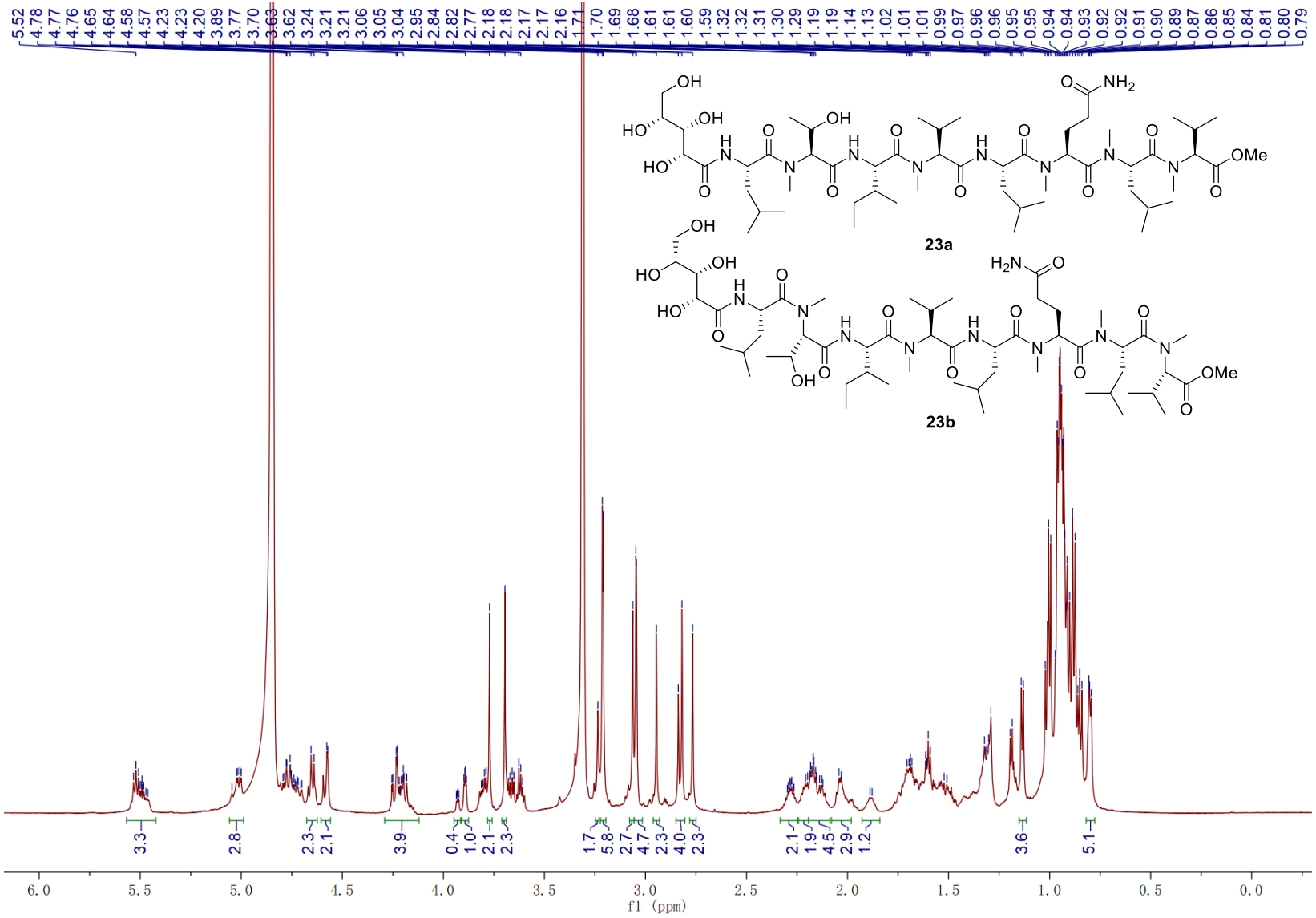

Figure S18.73. ^{1}H NMR spectrum of 23 in methanol-d_4

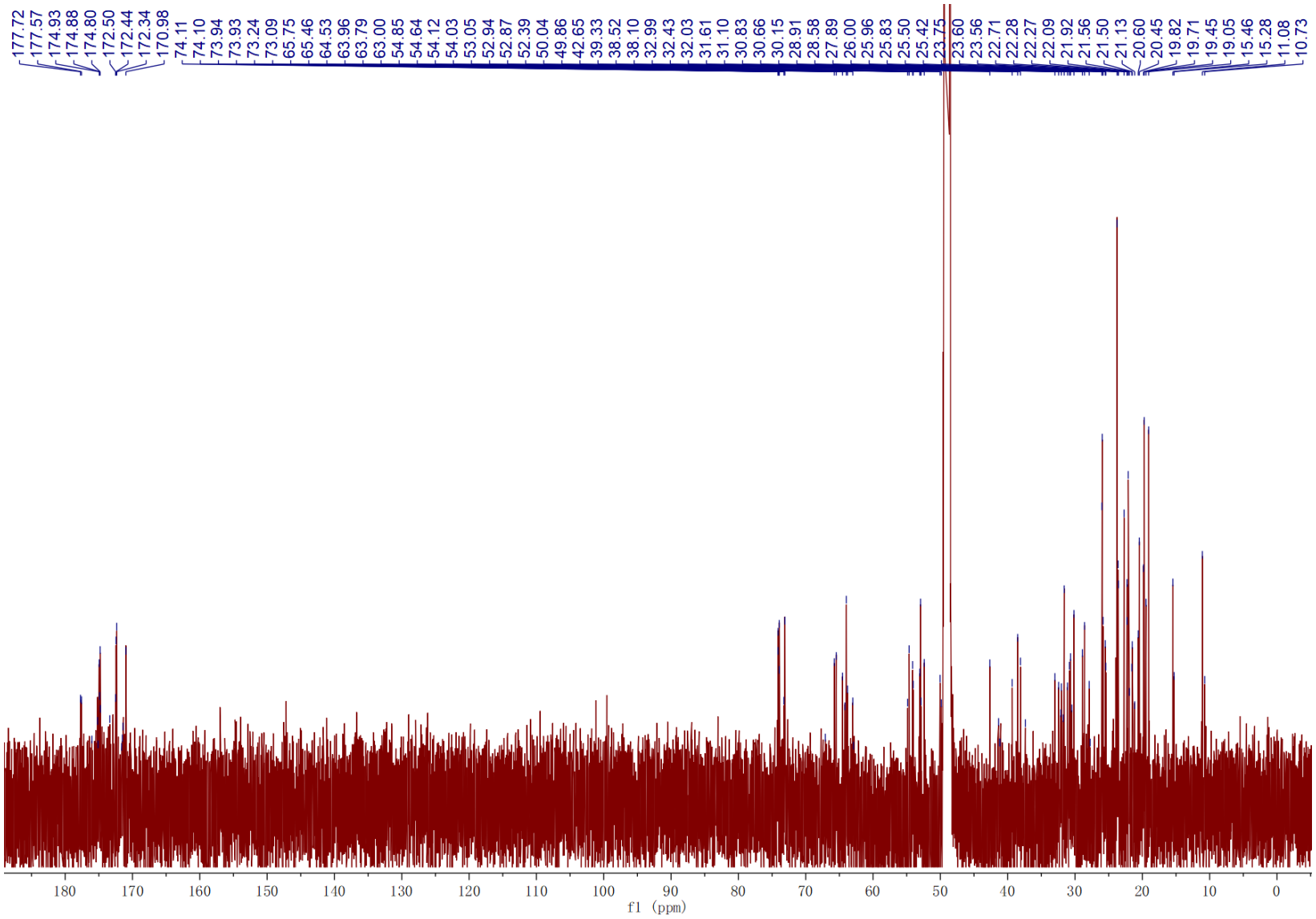

Figure S18.74. ^{13}C NMR spectrum of 23 in methanol-d_4

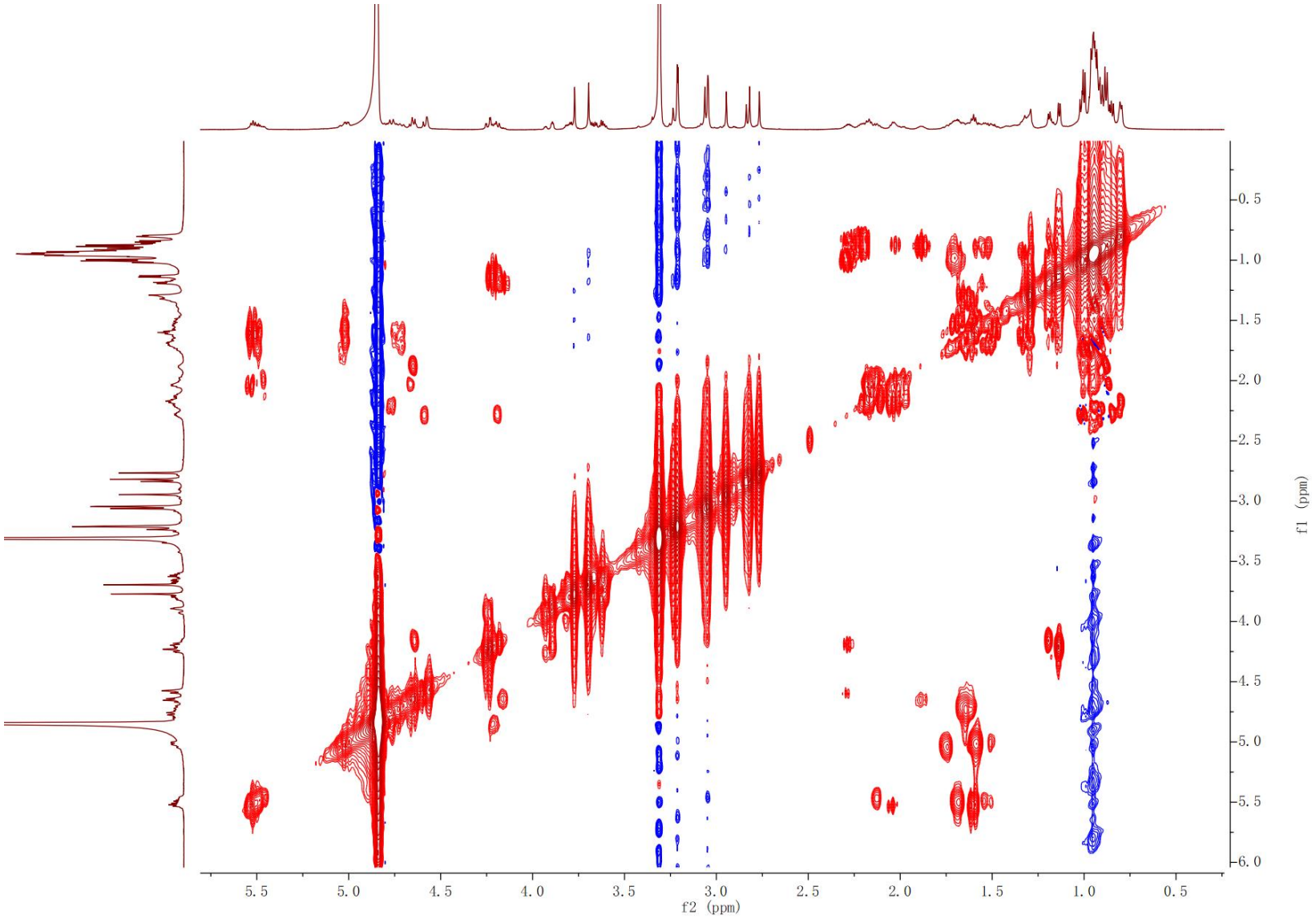

Figure S18.75. ^{1}H-^{1}H COSY spectrum of 23 in methanol-d_4

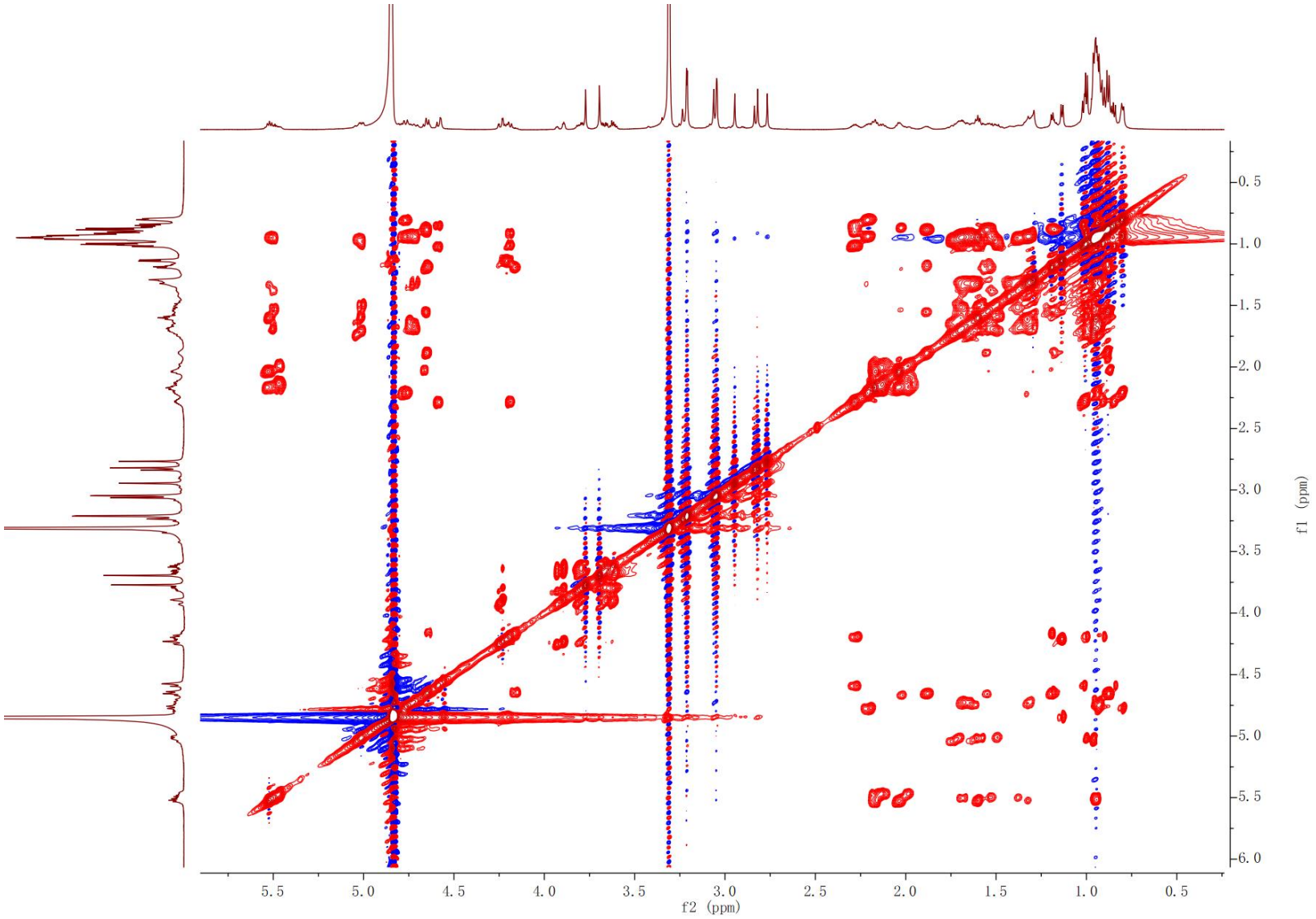

Figure S18.76. ^{1}H-^{1}H TOCSY spectrum of 23 in methanol-d_4

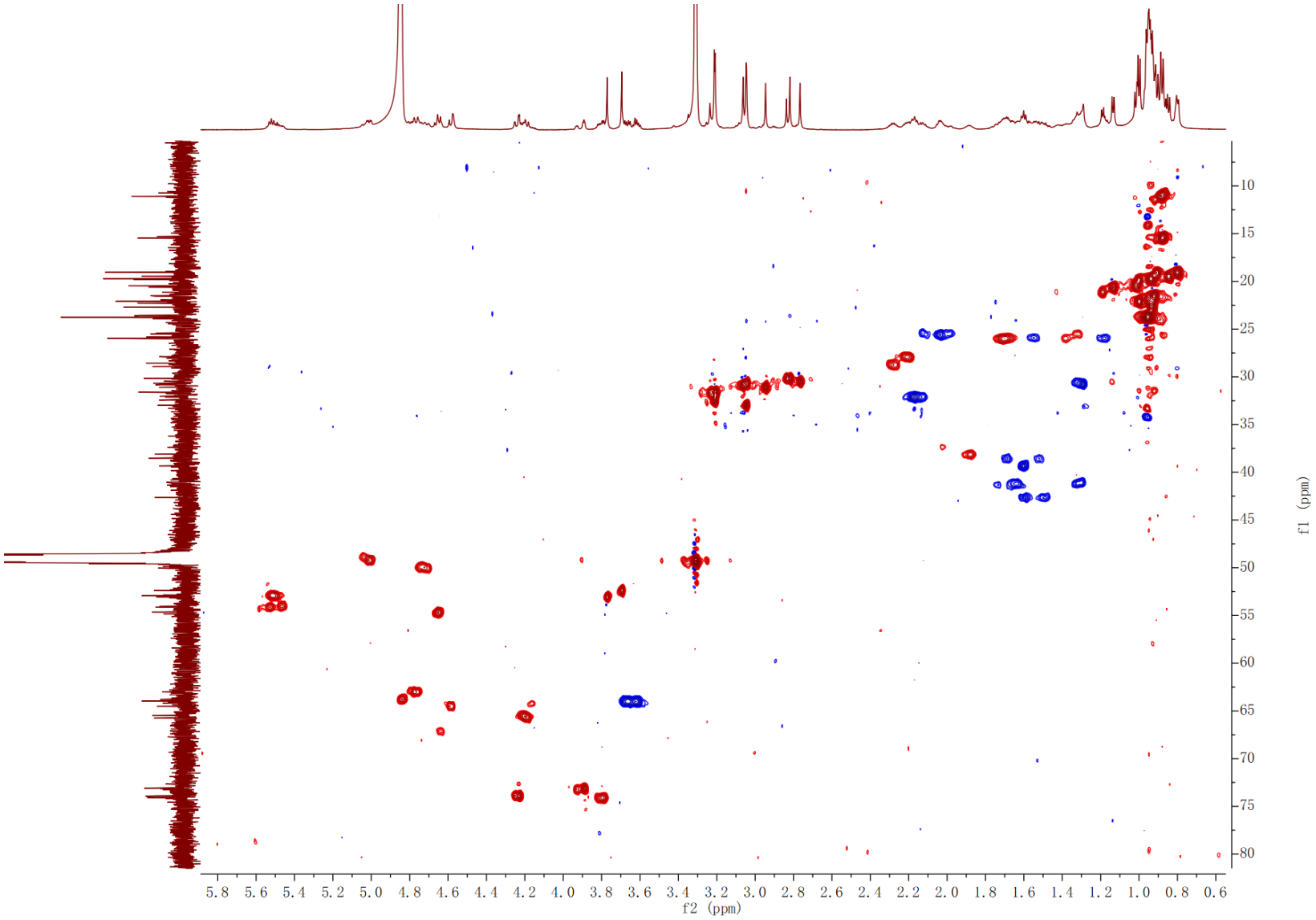

Figure S18.77. HSQC spectrum of 23 in methanol-d_4

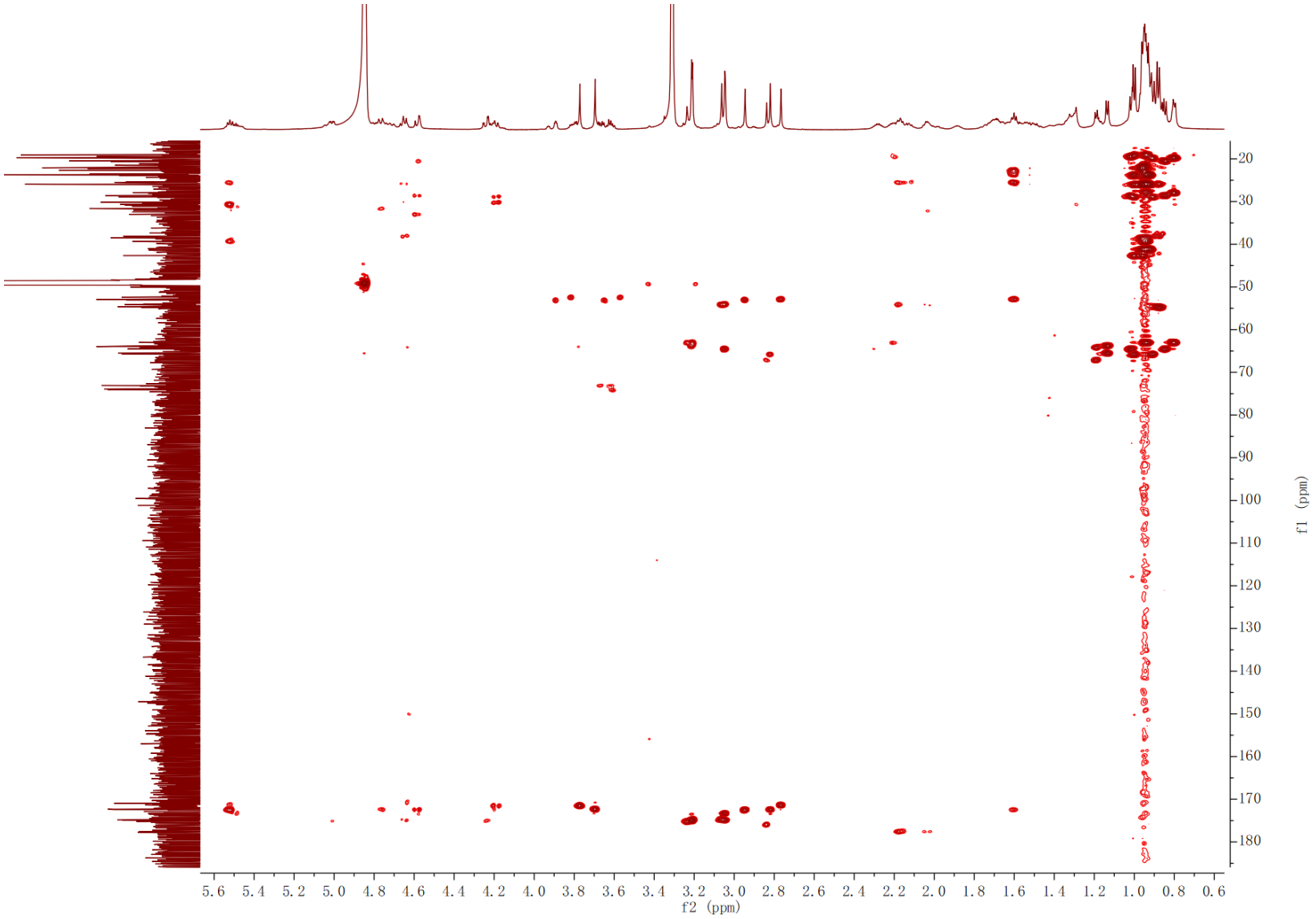

Figure S18.78. HMBC spectrum of 23 in methanol-d_4

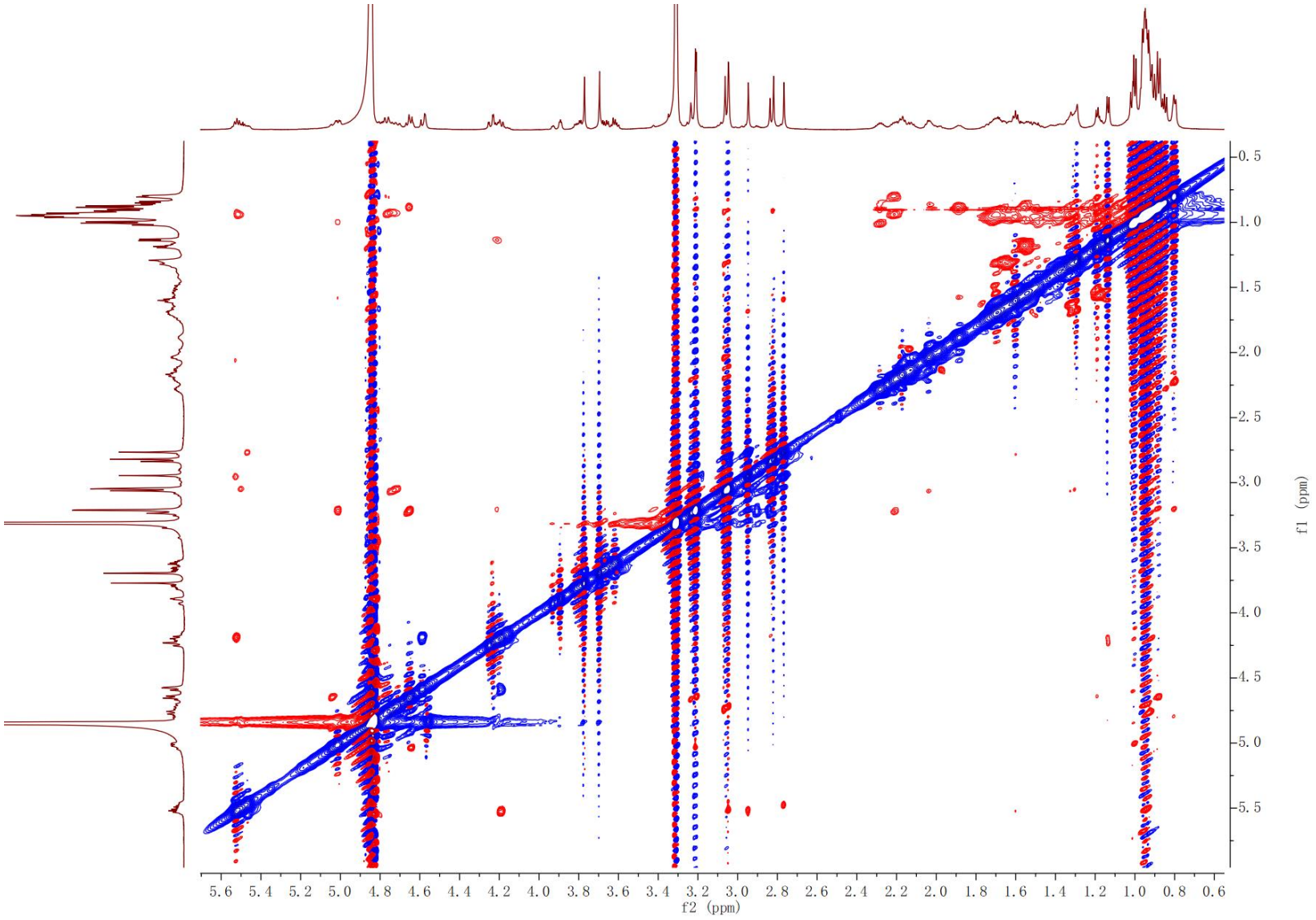

Figure S18.79. ROESY spectrum of 23 in methanol-d_4

4. SI References

1. Wang, M., et al. Sharing and community curation of mass spectrometry data with global natural products social molecular networking. *Nat. Biotechnol.* **34**, 828–837 (2016).

2. Aron, A. T., et al. Reproducible molecular networking of untargeted mass spectrometry data using GNPS. *Nat. Protoc.* **15**, 1954–1991 (2020).

3. Shannon, P., et al. Cytoscape: a software environment for integrated models of biomolecular interaction networks. *Genome Res.* **13**, 2498–2504 (2003).

4. Jansson, P.-E., Kenne, L. & Schweda, E. Nuclear magnetic resonance and conformational studies on monoacetylated methyl D-gluco- and D-galacto-pyranosides. *J. Chem. Soc., Perkin Trans. 1* 377–383 (1987).

5. McEwan, T., McInnes, A. G. & Smith, D. G. ^{1}H- and ^{13}C-N.M.R. spectra of the methyl mono-, di-, and tri-*O*-acetyl-α- and -β-D-xylopyranosides. *Carbohyd. Res.* **104**, 161–168 (1982).

6. Harada, K.-i., et al. A method using LC/MS for determination of absolute configuration of constituent amino acids in peptide--- advanced Marfey's method--- *Tetrahedron Lett.* **36**, 1515–1518 (1995).

7. Sýkora, D., Žáková, L. & Buděšínský, M. High-performance liquid chromatography and nuclear magnetic resonance study of linear tetrapeptides and octapeptides containing *N*-methylated amino acid residues. *J. Chromatogr. A* **1160**, 128–136 (2007).

8. Chatterjee, J., Mierke, D. F. & Kessler, H. Conformational preference and potential templates of *N*-methylated cyclic pentaalanine peptides. *Chem. Eur. J.* **14**, 1508–1517 (2008).

9. Fischer, G. Chemical aspects of peptide bond isomerisation. *Chem. Soc. Rev.* **29**, 119–127 (2000).

10. Dolomanov, O. V., Bourhis, L. J., Gildea, R. J., Howard, J. A. K. & Puschmann, H. OLEX2: a complete structure solution, refinement and analysis program. *J. Appl. Crystallogr.* **42**, 339–341 (2009).

11. Sheldrick, G. M. SHELXT - integrated space-group and crystal-structure determination. *Acta Crystallogr. A Found. Adv.* **A71**, 3–8 (2015).

12. Koren, S., et al. Canu: scalable and accurate long-read assembly via adaptive k-mer weighting and repeat separation. *Genome Res.* **27**, 722–736 (2017).

13. DePristo, M. A., et al. A framework for variation discovery and genotyping using next-generation DNA sequencing data. *Nat. Genet.* **43**, 491–498 (2011).

14. McKenna, A., et al. The genome analysis toolkit: a mapreduce framework for analyzing next-generation DNA sequencing data. *Genome Res.* **20**, 1297–1303 (2010).

15. Boetzer, M., Henkel, C. V., Jansen, H. J., Butler, D. & Pirovano, W. Scaffolding pre-assembled contigs using SSPACE. *Bioinformatics* **27**, 578–579 (2011).

16. English, A. C., et al. Mind the gap: upgrading genomes with Pacific Biosciences RS long-read sequencing technology. *Plos One* **7**, e47768 (2012).

17. Tilburn, J., et al. Transformation by integration in *Aspergillus nidulans*. *Gene* **26**, 205–221 (1983).

18. Smilkstein, M., Sriwilaijaroen, N., Kelly, J. X., Wilairat, P. & Riscoe, M. Simple and inexpensive fluorescence-based technique for high-throughput antimalarial drug screening. *Antimicrob. Agents Chemother.* **48**, 1803–1806 (2004).

19. Onishi, H. R., et al. Antibacterial agents that inhibit lipid A biosynthesis. *Science* **274**, 980–982 (1996).

20. Li, Y., et al. Anti-*Cryptococcus* epipolythiodioxopiperazines from *Podospora australis*. *J*. *Nat*. *Prod*. **79**, 2357–2363 (2016).

21. Blin, K., et al. antiSMASH 5.0: updates to the secondary metabolite genome mining pipeline. *Nucleic Acids Res.* **47**, W81–W87 (2019).

22. Stachelhaus, T., Mootz, H. D. & Marahiel, M. A. The specificity-conferring code of adenylation domains in nonribosomal peptide synthetases. *Chem. Biol.* **6**, 493–505 (1999).

23. Röttig, M., et al. NRPSpredictor2—a web server for predicting NRPS adenylation domain specificity. *Nucleic Acids Res.* **39**, W362–W367 (2011).